Design of a 4D Printing System using Thermal Sensitive Smart Materials and Photoactivated Shape Changing Polymers

A Thesis

Submitted to the Faculty

of

Drexel University

by

Steven Kyle Leist

in partial fulfillment of the

requirements for the degree

of

Doctorate of Philosophy

in

Mechanical Engineering

December 2017

Dedications

For Mom and Dad.

It finally happened. I'm no longer a professional student. Thank you for your limitless love and support.

Acknowledgements

This research and work would not have been possible without the aid and support of many people in my life. First and foremost, I would like to thank my family, especially my parents, Ray and Elaine Leist. From the beginning you have always supported me, no matter the choice. You always made sure I finished what I started, this thesis being one of them. Thank you to Chuck & Kim, John & Kristie, Corey, Matt, Payden, Paxton, Paris, and Alice. Also, thank you to the dog, Rugby, who received his very own PhD in "Being a Good Boy".

A very big thank you to my professor, Dr. Jack Zhou, who allowed me to switch projects and explore this exciting new research. From the start, you have always encouraged the act of seeking and exploring new ideas. I never would have explored the area of light reactive smart materials and 4D printing without you. Thank you for your instruction and guidance throughout my time at Drexel. Thank you also to all the lab members in the Advanced Manufacturing and Design lab.

Thank you to my committee for their time and guidance, Dr. Richard Chiou, Dr. Leo Han, Dr. Frank Ji, Dr. Donggang Yao, and Dr. Ajmal Yousuff. Your technical advice and suggestions helped shape this thesis. Hopefully, the industry of 4D printing and light reactive smart materials will continue to grow.

I would also like to thank Daniel Hagaman from Dr. Ji's chemistry lab. This project could not have been completed without you. Thanks for all of the resources and endless knowledge that aided in this research. I'm honored that we got to work together and bring this exciting new research to light.

Thank you to all my friends at Drexel, Dr. Qudus Hamid, Dr. Jamie Kennedy, Dr. Paul Kim, Ryan Robinson, and Dr. Chengyang Wang. Thanks for the late nights, hangouts, advice, and exchanging of brain power. You made classes fun and the long days seem shorter.

Thank you, Kathie Donahue, for everything you have done for me. You were like a second mother to me and were there for all the times of stress, but you always found a solution.

Thank you to my friends who were smart enough to graduate and get a job, Matt Bechtel, Sanjay Bridges, Rohan Desai, Jon Hansen, Stephanie Lipartito, Jessica Mathew, Kimberly Moy, Eric Tran, Ben Tweddale, Melissa Werlau and George Yan. Without you, I probably would have graduated earlier. Our hangouts and laughter were a necessary ingredient that kept me sane. You guys reminded me that I can have a life outside of the lab.

Finally, thank you to my girlfriend, Jessica Sances. I am very lucky to be with someone who is so caring, supportive, and understanding. Thanks for dealing with all the stress and crazy hours.

Table of Contents

List of Tables

List of Figures

Abstract

Design of a 4D Printing System using Thermal Sensitive Smart Materials and Photoactivated Shape Changing Polymers

Steven K. Leist
Advisor: Jack Zhou, PhD

4D printing is an emerging additive manufacturing technology that combines 3D printing with smart materials. Current 3D printing technology can print objects with a multitude of materials; however, these objects are usually static, geometrically permanent, and not suitable for multi-functional use. The 4D printed objects can change their shape over time when exposed to different external stimuli such as heat, pressure, magnetic fields, or moisture. In this research, heat and light reactive smart materials are explored as a 4D printing materials. Synthetization of a material that actuates when exposed to stimulus can be a very difficult process, and merging that same material with the ability to be 3D printed can be further difficult. A common 3D printing thermoplastic, poly(lactic) acid (PLA), is used as a shape memory material that is 3D printed using a fused deposition machine (FDM) and combined with nylon fabric for the exploration of smart textiles. The research shows that post printed PLA possesses shape memory properties depending on the thickness of the 3D printed material and the activation temperature. PLA can be thermomechanically trained into temporary shapes and return to its original shape when exposed to high temperatures. PLA can be 3D printed onto nylon fabrics for the creation of the smart textiles.

Additionally, a photoisomerable shape changing material is explored because light activation is wireless, controllable, focusable, abundant, causes rapid shape change of the smart material, and induces reversible shape change in the material. This study supports the fundamental research to generate knowledge needed for synthesis of a novel azobenzene shape changing polymer (SCP) and integrating this smart material into objects printed with a 4D printing process

using syringe printing. Multiple versions of azobenzene SCP are synthesized that actuate when exposed to 365 nm and 455 nm light. Two SCPs, MeOABHx and DR1Hx, are selected for the 4D printing research because of their ability to photoisomerize at room temperature and 3D printability. The physical properties of these polymers are characterized, photomechanical bending tests are performed, and the photo-generated stress is measured using a dynamic mechanical analyzer (DMA). The SCPs are deposited onto a passive layer to create bilayer films in order to actuate. The photomechanical efficiency of bilayer films is evaluated depending on the thickness of the passive layer film, type of azobenzene SCP, wavelength of the light source, intensity of the light source, and distance between the light and films.

4D printing can be used to streamline the design and manufacturing process of actuating parts. Complex heavy parts can be removed from actuation systems such as onboard power storage, motors, sensors, and processors by embedding these capabilities into the material themselves. This reduces the amount of required parts, the amount of materials, and reduces the cost of producing these parts. 4D printed products possess the properties of programmability, reaction and adaption to their environment, and automation. Therefore, they can find wider applications including foldable unmanned aerial vehicles, artificial muscles, grippers, biomedical drug delivery systems, stents, and minimally invasive surgeries.

Chapter 1. Introduction and Background

1.1 Additive Manufacturing

Ever since its creation in the 1980s, 3D printing has been on the rise both economically and popularity wise. Many industries have expanded due to 3D printing such as advanced manufacturing, product design (Huang, Liu, Mokasdar, & Hou, 2013) , biomedical applications (Gross, Erkal, Lockwood, Chen, & Spence, 2014) , and hobbyists (Berman, 2012) . This expansion in the different industries is due to growth in the type of printing methods and the different materials used for printing. Currently, 3D printing possesses many different techniques: fused deposition modelling (FDM), stereolithography, selective laser sintering (SLS), syringe printing, bioprinting, and Polyjet printing (Table 1-1). 3D printers are capable of printing very accurate, complex models, made from many different hard and soft materials (plastics, resins, metals, polymers, food, and biomaterials). Decreasing costs in 3D printing technology is providing more people access to this technology, which is creating community of designers, engineers, and hobbyist focused in the additive manufacturing sector. Previously, 3d printers were a tool found in the industrial and academic research areas, but, today, it can be found in secondary schools and homes. 3D modelling software allows users to create custom parts or download premade designs from other users, due to the Internet of Things (IoT), and allow users to print these designs from their personal 3D printers. It is predicted that the 3D printing industry will continue growing and access further industries over the next 10 years (Gebler, Uiterkamp, & Visser, 2014; Kietzmann, Pitt, & Berthon, 2015; Lu, Li, & Tian, 2015; Rayna & Striukova, 2016) .

Table 1- 1. A list of different additive manufacturing methods along with their appropriate materials used in each technique and their accuracy.

Method	Materials	Accuracy
Fused Deposition Modelling (FDM)	Thermoplastics	0.127 mm
Stereolithography (SLA)	Photopolymers	0.05 - 0.15 mm
Selective Laser Sintering (SLS) or Selective Laser Melting (SLM)	Thermoplastics, ceramic powders, metal powders, metal alloys	0.2 - 0.3 mm
Syringe Printing	Biomaterials, biological tissues, food	0.05 - 0.3 mm
Polyjet Printing	Photo polymers	0.1 mm

Currently, 3D printing has many benefits and uses; however, post printed materials retain rigid and static parts that do not possess the ability to actuate or transform shape right off the print bed. Multiple parts must be printed and assembled if a designer wishes to create a moving part such as a hinge or an actuator (Figure 1-1). Post processing of some 3D printed materials can be time consuming and tedious, similar to machined parts. Another limiting factor to 3D printing is the bed size because it restricts the size and number of parts that can be produced in one iteration and does not take full advantage of the print volume. Another opportunity in the area of advanced manufacturing is the design and creation of smart products that react to their environment and external stimuli in order to remove the need for human interaction. Further research into additive manufacturing technology and material development may lead to the creation of new 3D printable materials that possess volumetric and shape changing properties when exposed to different stimuli. These new developments may lead to a new growth of additive manufacturing, simplify the design and building process, reduce the number of resources, and automate materials.

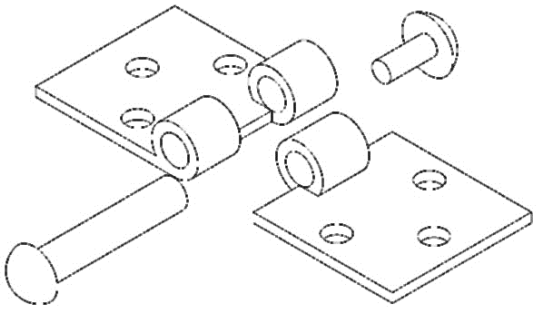

Figure 1- 1. An example of the number of required 3D printed parts for the creation of an actuating hinge.

1.2 Smart Materials

There exists a group of materials that can change their physical properties (color, rigidity, volume, shape) when exposed to different stimuli (temperature, pH levels, magnetic field, moisture, and light) known as smart materials. There are two classes to smart materials: shape memory and shape change. Shape changing materials possess two states that the material switches between when it is exposed to different stimuli. In state 1, typically called the permanent shape, the shape change material is not exposed to any stimuli. The material actuates into an alternate temporary shape, state 2, when the material is exposed to an external stimulus. The temporary shape returns to its original state 1 when the external stimulus is removed (Figure 1-2. (a)). Shape memory materials possesses the ability to be programmed into a temporary shape (Zhao, Qi, & Xie, 2015) . Shape memory materials also possess a permanent shape, state 1. When exposed to an external stimulus, the materials can be mechanically deformed into a temporary shape and fixed in that position. The temporary shape is maintained when the deformed shape is fixed and the stimulus is removed.

Finally, the shape memory material recovers its permanent shape when it is re-exposed to a stimulus (Figure 1-2. (b)).

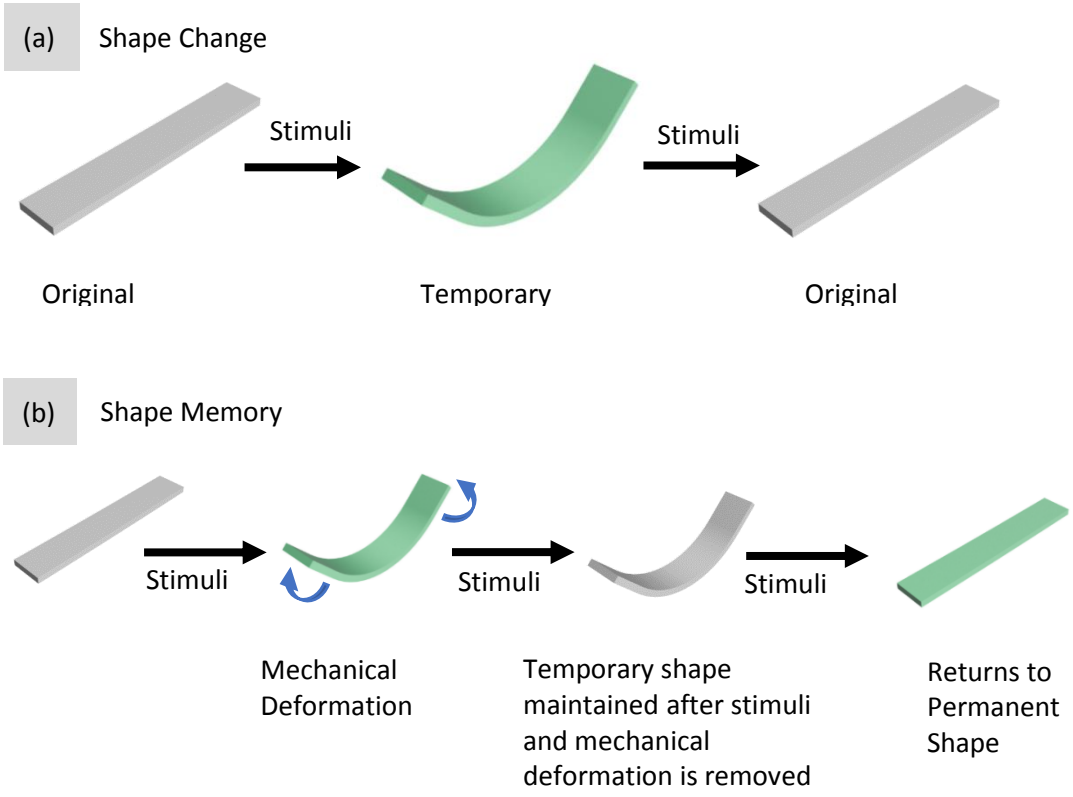

Figure 1- 2. Schematic describing the process of (a) shape changing materials and (b) shape memory materials. (a) Here, shape changing materials possess a switching mechanism that change from state 1 (original shape) to state 2 (temporary shape) when exposed to a stimulus and return to state 1 when the stimulus is removed. (b) In shape memory materials, the material is capable of programming or remembering its temporary shape when exposed to a stimulus and applying a mechanical deformation to that material. The mechanical deformation must be maintained until the stimulus is removed and the material will remember its state 2 (temporary shape). The material returns to state 1 (original shape) when the stimulus is reapplied.

Shape memory alloys (SMAs) are a very popular smart material made from metal alloy that possesses two phases: a low temperature phase (martensite phase) and a high temperature phase

(austenite phase). SMAs can be deformed into custom shapes and return to its original shape when heated, which is called the Shape Memory Effect (SME). The SME is generated when the atomic crystal structure of the SMA converts from one crystalline structure to another. Users can thermomechanically train SMAs to maintain a custom permanent shape. Once the custom shape has been applied, the SMA is annealed above its transition temperature in the austenite phase then cooled (Figure 1-3. (a)). After annealing, the trained SMA is malleable in the martensite phase and can be deformed into different temporary shapes (Figure 1-3. (b)) (Auricchio, Scalet, & Urbano, n.d.; Brinson, Bekker, & Hwang, 1996; Spaggiari, 2013) . The temporary shapes return to its original permanent shape when the SMA is exposed to temperatures above its transition temperature (Figure 1-3. (c) & (d)). Nitinol, a SMA with the composition of nickel and titanium, developed at the Naval Ordinance Lab, has found popularity in the automotive (Jani, Leary, & Subic, 2014) , aerospace (Humbeeck, 1999) , biomedical (Morgan, 2004) , robotics (Cianchetti, Licofonte, Follador, Rogai, & Laschi, 2014; Jani, Leary, Subic, & Gibson, 2013; Laschi & Cianchetti, 2014; Mazzolai, Margheri, Cianchetti, Dario, & Laschi, 2012; Utela, 2008; Wu & Schetky, 2000) , and soft actuation industries (Figure 1-4. (a-c)) (Cianchetti et al., 2014) .

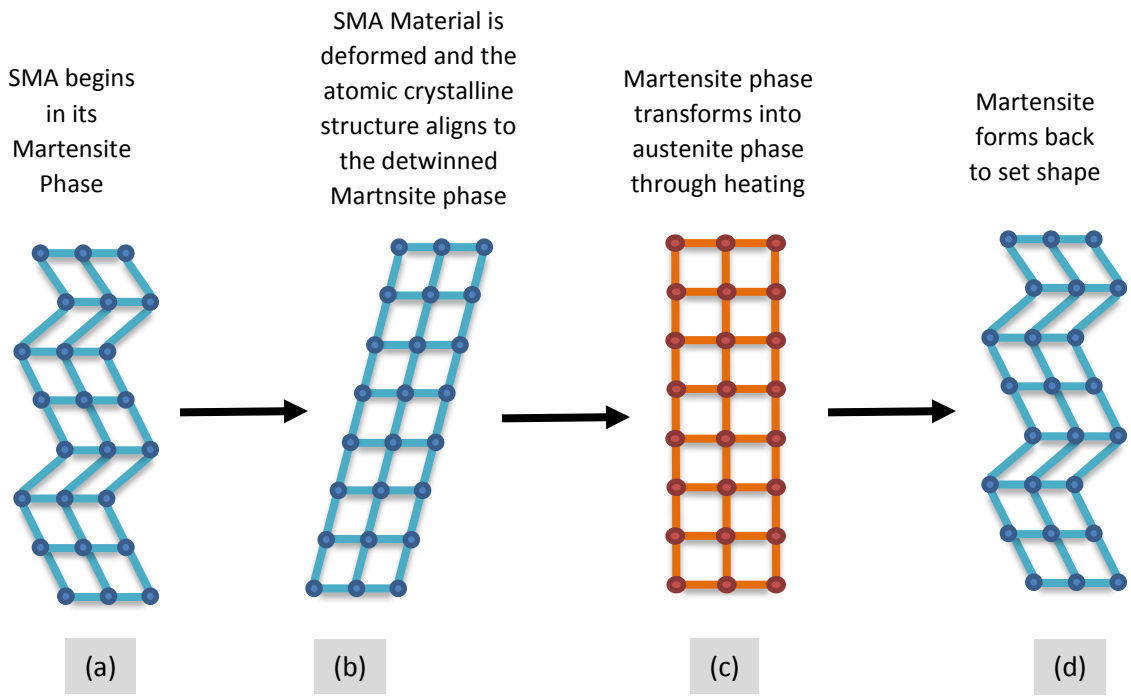

Figure 1- 3. A schematic of the shape memory effect (SME) in a shape memory alloy (SMA) where a material begins in the (a) twinned martensite phase and set shape, (b) the spring is deformed and aligns the crystalline structure into a detwinned martensite phase, (c) the crystalline structure transforms into the austenite phase when heated, and (d) returns to its martensite phase when cooled. *(Leist, Kunkle, Chong, & Zhou, 2015)*

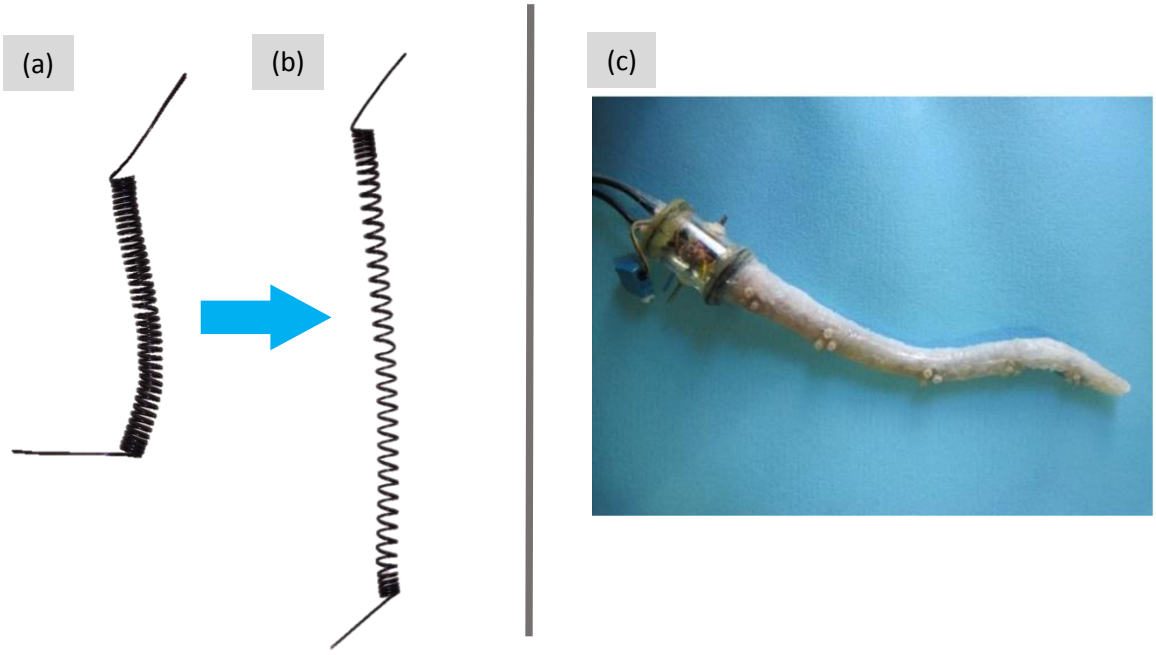

Figure 1- 4. a) An example of a Nitinol SMA wire formed into a spring that begins in its permanent compressed state then b) stretched to its temporary extended state. c) A bioinspired robotic tentacle that uses shape memory alloy (SMA) springs for actuation. *(Cianchetti et al., 2014)* . Adapted with permission from Actuators, 3(3), pp. 226-244 under MDPI.

Other classes of smart materials that are gaining popularity are shape memory polymers (SMPs) and shape changing polymers (SCPs). These smart materials possess the ability to actuate when exposed to external energies such as heat (Figure 1-5) (Srivastava, Chester, Ames, & Anand, 2010; Yang et al., 2014; Zarek et al., 2016) , pressure (Ramuz, Tee, Tok, & Bao, 2012; Tee, Wang, Allen, & Bao, 2012) , water (Yang, Huang, Li, & Li, 2006) , pH-levels (Qiu & Park, 2012) , magnetism (Leng, Lan, Liu, & Du, 2011; Zhao, Behl, & Lendlein, 2012) , or light (Habault, Zhang, & Zhao, 2013; Lendlein, Jiang, Jünger, & Langer, 2005; White, 2012; Zhang, Zhou, Liu, & Liu, 2014) . SCP may allow for the creation of products that automatically react to their environment without the need for heavy, expensive, and complex electronic actuation systems (Leist & Zhou, 2016) . SCPs could streamline self-actuating structures by disregarding the need for onboard power systems, sensors, processors, and motors. Another group of smart materials,

called self-healing materials (SHMs), that possess the ability to react to external stimulus and repair themselves may demonstrate effectiveness for devices exposed to extreme environments such as extreme heat, cold, pressure, and friction (M. D. Hager, Bode, Weber, & Schubert, 2015; M. Hager, Greil, Leyens, van der Zwaag, & Schubert, 2010) . Smart polymers tend to be easier to process in bulk when compared to alloys. Smart polymers do possess drawbacks when compared to SMAs such as low strength, low moduli, and low operating temperatures; however, they are cheaper, possess high strain recovery, low density, biocompatibility, and biodegradability (Khoo et al., 2015) .

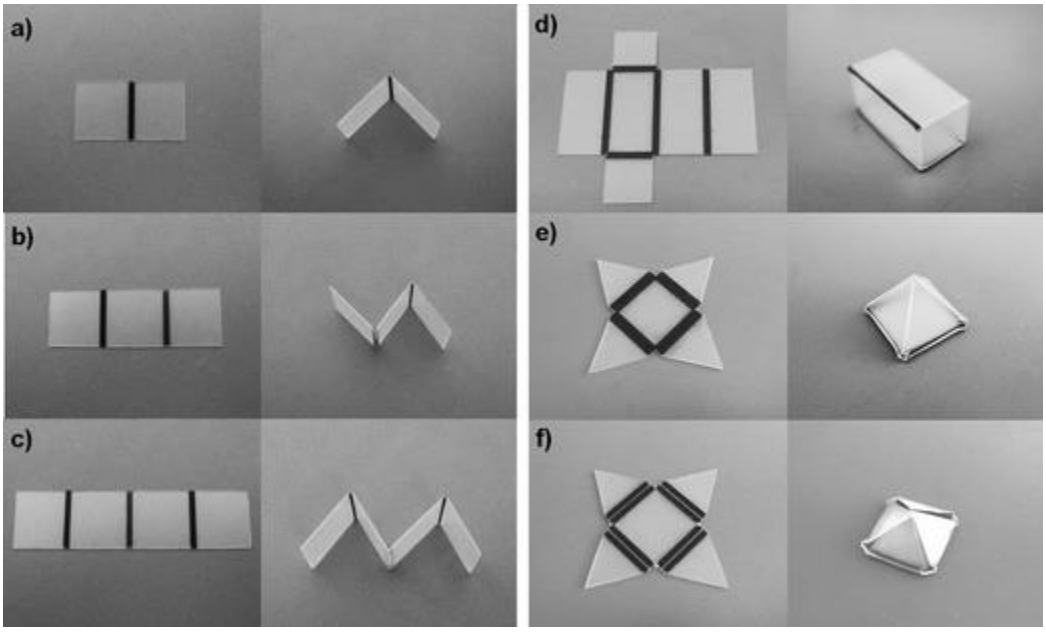

Figure 1- 5. Self-folding of a polystyrene sheet with black ink lines inkjet printed onto the surface that act like hinges when exposed to light *(Liu, Boyles, Genzer, & Dickey, 2011)* . Adapted with permission from Soft Matter, 8(6), under Royal Society of Chemistry.

1.3 Polylactic Acid (PLA)

Polylactic Acid (PLA) is a semicrystalline thermoplastic that retains a combination of crystalline and amorphous structures. PLA is a commonly used FDM printing material that possesses a fairly low glass transition temperature (T_g) around 58-60°C and a melting temperature (T_m) between 150-220°C. A permanent shape can be fixed using PLA because it possesses an ordered crystalline structure below its T_g (Figure 1-6. (a)). Temporary shapes can be created from the material when stress is applied above T_g and maintained when the material is cooled (Figure 1-6. (b)). The stored strain energy can be released as the polymer chains are unconstrained when heating above the switch temperature, T_g or T_m (Figure 1-6. (c)). After shape training, this means that as the temperature increases above PLA's T_g, the polymer chains exhibit greater mobility that allows for shape recovery back to its permanent shape (Berg, McBride, Wang, & Bowman, 2014; Liu, Qin, & Mather, 2007).

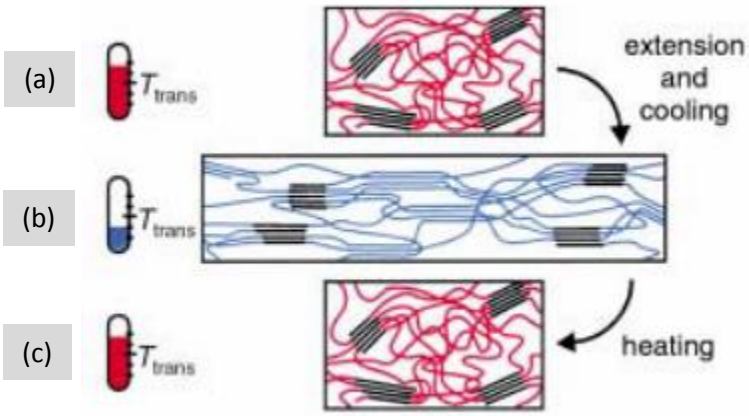

Figure 1- 6. A schematic highlighting the shape memory effect of Polylactic acid (PLA) when thermally activated. (a) Here, T_{trans} represents the glass transition temperature (T_g) of the material and allows for the switching segments to become flexible and deformed elastically. (b) The material can be fixed into a temporary shape when cooled below its T_{trans} and (c) return to its original (permanent) shape when reheated. *(Lendlein, Kelch, Lendlein, & Kelch, 2002)* . Adapted with

permission from Angewandte Chemie International Edition, 2002, 41, pp. 2040, under John Wiley and Sons.

In previous studies, the shape memory properties of PLA have been reported; however, there is limited research in the shape memory properties of PLA post 3D printing (Srivastava, Chester, Ames, & Anand, 2010; WG Yang et al., 2014; Zarek et al., 2016) . Typically, these PLA samples are blended with other polymers, such as polyurethane, to improve the shape recovery ratio and lower the T_g of the sample, but this may affect the mechanical strength of the material. Recently, research has been performed on 3D printed PLA that tests the shape changing properties of the material. Internal strain is generated when PLA is printed onto the 3D printer's substrate (Figure 1-7. (a)). The internal strain is released when the material is removed from the substrate and heated above its T_g (Figure 1-7. (b) (Q. Zhang, Yan, Zhang, & Hu, 2015) . Also, researchers found that the PLA can be 3D printed onto paper to create a composite that can transform shape when exposed to hot and cool temperatures due to the difference in the coefficient of thermal expansion between the PLA and paper (Figure 1-7. (c-d)) (Q. Zhang, Zhang, & Hu, 2016) . The researchers showed that the materials exhibit shape memory capabilities, but the results have not been quantified. The research discussed in this thesis investigates and quantifies the shape memory properties of 3D printed PLA and its effects when combined with nylon textiles.

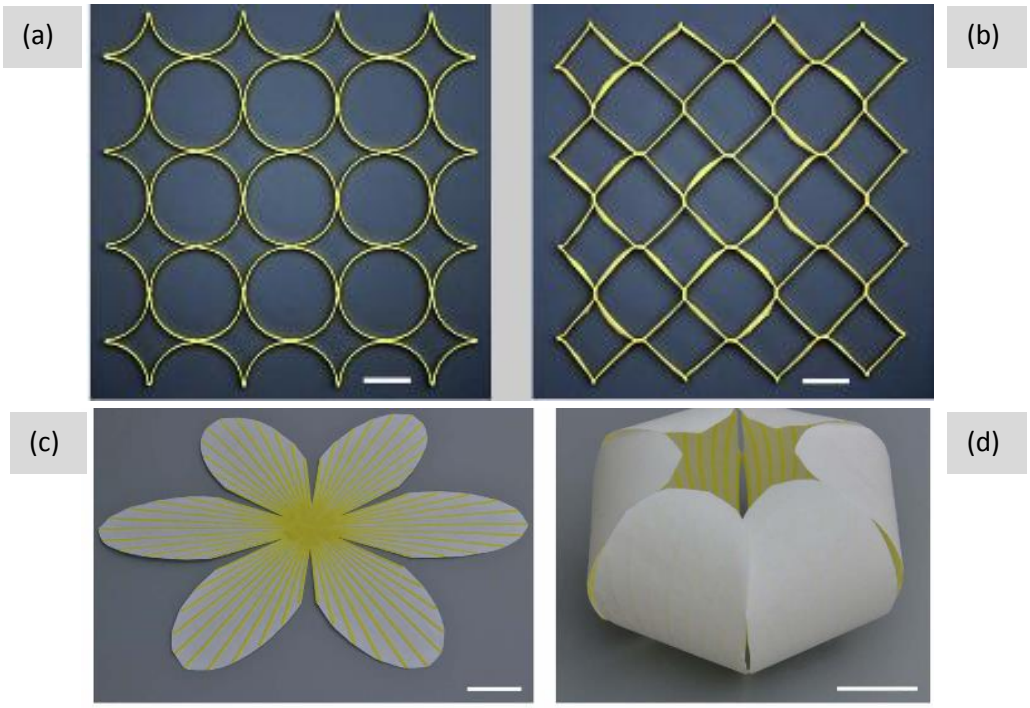

Figure 1- 7. Examples of the shape changing properties of 3D printed PLA when printed in a) a 2D circular lattice that b) transforms into square lattice when heated (Q. Zhang et al., 2015) . c) Initial 3D printed PLA onto paper that d) curls when heated and cooled (Q. Zhang et al., 2016) .

1.4 Azobenzene

There are many different photochromophores such as spiropyranes, stilbenes, and diarylethenes, but azobenzene seems to be the most researched chromophore due to its simple and unique ability for reversible photoisomerization (Ercole, Davis, & Evans, 2009) . Here, photoisomerization is defined as a molecule transforming into a different molecule of different geometry when exposed to light, but maintaining the same elements and atoms. Azobenzene is a photochromic compound that possesses the property to photoisomerize when exposed to different wavelengths of light. During UV light irradiation, azobenzene is capable of changing shape from a

straight *trans*-state that measures at 9Å to a bent *cis*-state that measures at 5.5 Å (Qin et al., 2015) (Figure 1-8). This process is called *trans-cis* isomerization. Azobenzene also possesses a *cis-trans* isomerization. During this process, azobenzene will transform back to its *trans*-state when it is exposed to a visible light wavelength in the *cis*-state. The cis-trans isomerization is capable of thermally relaxing from the *cis*-state to the *trans*-state because the *cis* isomer is very unstable when compared to the *trans* isomer (Garcia-Amorós & Velasco, 2012) . This property may add the two different activation methods, heat and light energy, to an azobenzene SCP. Typically, the molecular photoisomerization translates to a color change in the materials; however, this molecular deformation can be translated to macro-scale deformation if azobenzene is combined with certain polymer matrices to form light reactive or photoactive SMPs or SCPs (Barrett, Mamiya, Yager, & Ikeda, 2007; Lee, Tabiryan, Bunning, & White, 2011; Milam, O'Malley, Kim, Golovaty, & Kyu, 2010; Wen, Zhang, Weng, & Hu, 2014) . Azobenzene exhibits one of the fastest photoisomerization reactions, which occurs in picoseconds or nanoseconds under optimal conditions (Ikeda & Tsutsumi, 1995) . In some cases, one wavelength of light can activate motion in the material and reverse that same motion; this provides different opportunities and applications for an azobenzene SCP (2010; Mahimwalla, Yager, Mamiya, & Shishido, 2012; Tabiryan, Serak, Dai, & Bunning, 2005; White, Serak, Tabiryan, Vaia, & Bunning, 2008; White, Tabiryan, et al., 2008) .

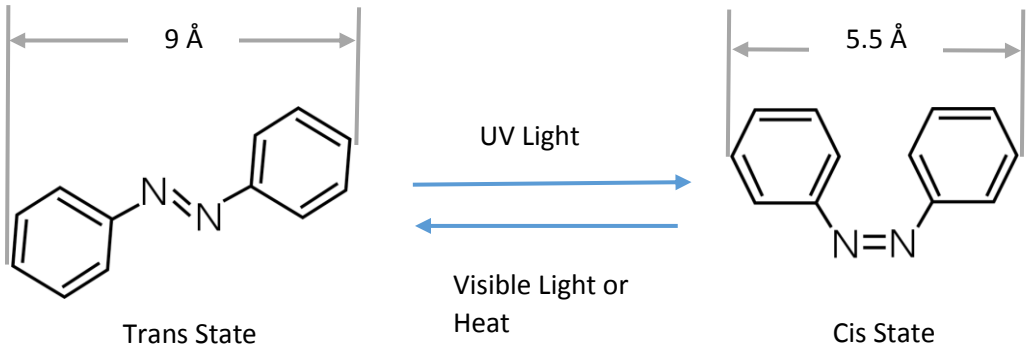

Figure 1- 8. Schematic of Azobenzene *trans-cis* transformation when exposed to UV light and its transformation to *cis-trans* when exposed to visible light or heat. The length of the azobenzene molecule transforms from 9 Å in the straight *trans* state to 5.5 Å in the bent cis state.

Most azobenzene SMPs and SCPs are grouped into a category called liquid crystal. Liquid crystal polymers (LCPs) refers to materials that possess molecules with specific orientations and positions (White & Broer, 2015) . These molecules can organize themselves into different mesophases of nematic, smectic, chiral, and isotropic phases. Nematic phases possess mesogens that are organized in the same direction along the long axis, but they do not display positional order (Figure 1-9. (a)). Mesophases possess chemical compounds that retain liquid crystalline properties, called mesogens. Smectic phases possess mesogens with order in a single direction along the long axis and positional order (Figure 1-9. (b)). Chiral phases possess mesogens that display a twisting property (Figure 1-9. (c)). Isotropic phases possess no order and display randomness of the mesogens with in the liquid-crystalline state (Figure 1-9. (d)). These phases are important to the photomechanical response of azobenzene smart polymers. The azobenzene's mesophase begins in the nematic phase because the rod-shaped trans-state azobenzene moieties are orientated in the same direction as the LCP. The transformation into the cis-state causes disorder within the LCP network when exposed to UV light and causes a volume change within the material.

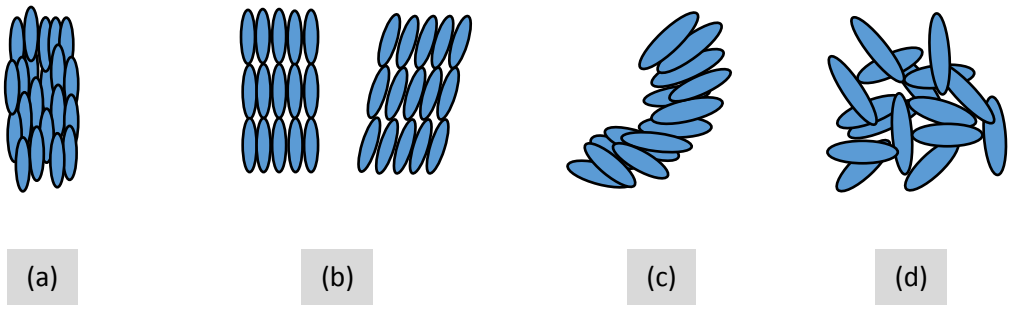

Figure 1- 9. The structure of different mesophases for liquid crystalline polymers: a) nematic, b) smectic, c) chiral, and d) isotropic.

Depending on the chemical composition and the cross-linking of the material, the type of liquid crystalline material can be referred to as an LCP, liquid crystalline network (LCN), or liquid crystalline elastomer (LCE). LCPs include the mesogen in the backbone (main-chain) of the polymer and exhibit almost no change in molecular order when exposed to stimuli (Figure 1-10. (a)). LCNs form crosslinks between the polymer's backbone and the mesogen, which can lead to small disruption in molecular order when exposed to stimuli (Figure 1-10. (b)). LCEs possess a combination of crosslinking between polymer backbones, but the mesogens are located on the side-chains of the polymer backbone or within the polymer backbone itself (Figure 1-10. (c)). LCEs display very large molecular order changes when exposed to external stimuli (White & Broer, 2015) . For the purpose of this research, the area of SCPs and side-chain azobenzene moieties are explored due to their larger order of deformation when compared to the other liquid crystalline materials.

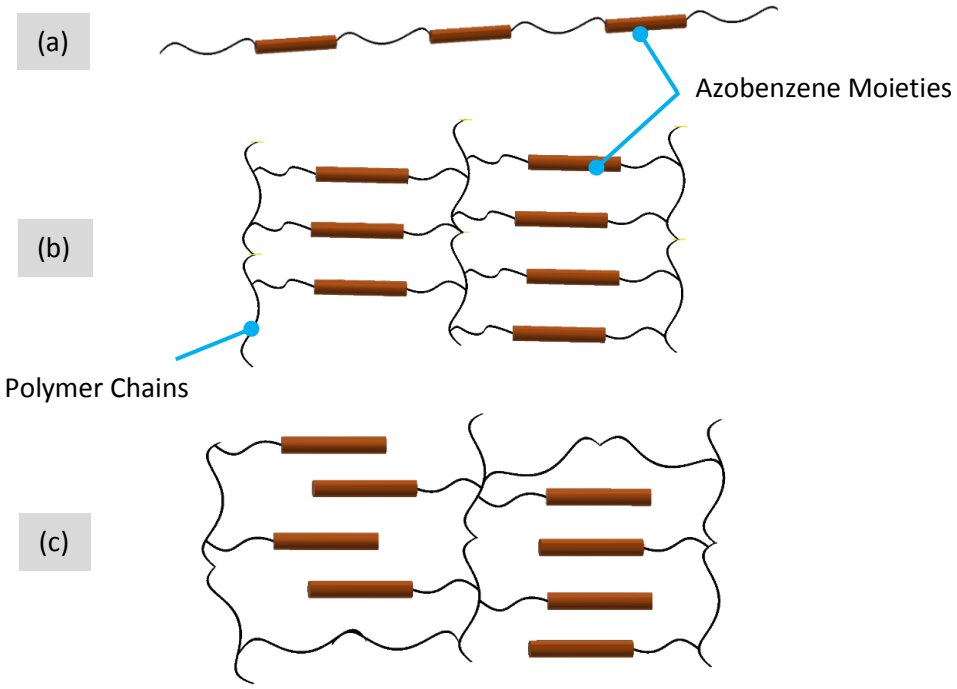

Figure 1- 10. Examples of the different structures of a) liquid crystalline polymers (LCPs), b) liquid crystalline networks (LCNs) shows the mesogens crosslinked to the main-chain polymer, and c) liquid crystalline elastomers (LCEs) can be attached to the main-chain or side-chain of the polymer.

Azobenzene smart materials are a unique group because they possess both shape changing and shape memory capabilities. Most research is focused on azobenzene SCPs because of their abilities to switch between two different shapes in UV and visible light. Researchers have shown that azobenzene SCPs are capable of being photo-fixed into customizable shapes using light (K. Lee, Koerner, et al., 2011a) . TJ White and his associates heated their SCP above 120°C (above its T_g) and deformed the material into a hook shape. The material is lowered to room temperature and continues to hold its hook shape. When a beam of linear 442 nm polarized light is directed on the SCP, the hook unbends to a straight shape. The SCP maintains its straight shape even when the light is turned off. Next, circular 442 nm polarized light is directed on the SCP and makes the SCP transform into the hook shape. This characteristic can be observed because the long polymer

network chains thermally relax to a more stable state when heated above their T_g (Figure 1-11) (Barrett, Mamiya, Yager, & Ikeda, 2007; Lee, Tabiryan, Bunning, & White, 2011; Milam, O'Malley, Kim, Golovaty, & Kyu, 2010; Wen, Zhang, Weng, & Hu, 2014).

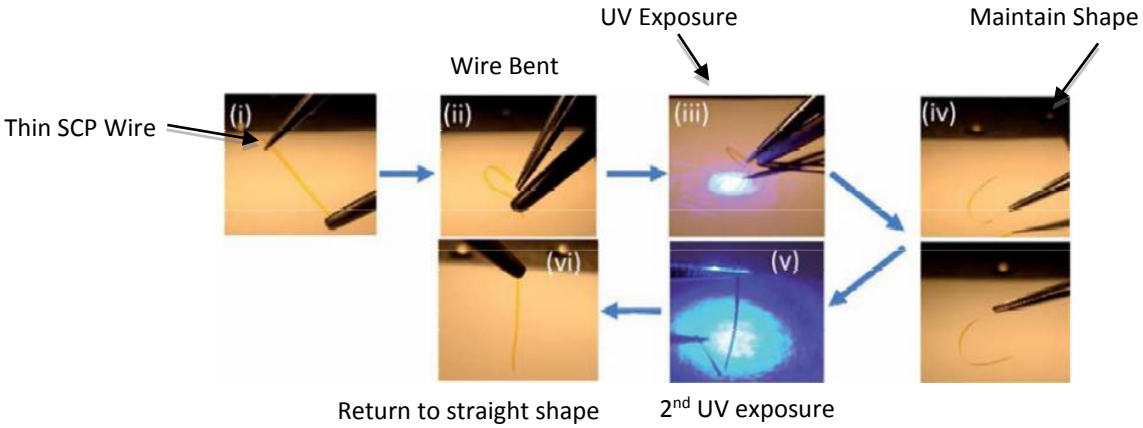

Figure 1- 11. SCP mechanically deformed (i, ii) and exposed to light (iii) that maintains deformed shape after light is removed (iv). The SCP returns to its straight shape when it is exposed to light again (v, vi) *(Lee, Koerner, Vaia, Bunning, & White, 2011a)* . Adapted with permission from Soft Matter, 7(9), pp. 4320, under the Royal Society of Chemistry.

Overall, azobenzene possesses many unique characteristics that appeal to different SMP and SCP applications. Many researchers have managed to combine azobenzene films with flexible films for photoactivated applications in actuators, artificial muscles, surface relief gratings (SRG) (Saphiannikova & Toshchevikov, 2010), and sensors. *Van Oosten et al.* have created artificial photo-driven cilia for micro mixing (van Oosten, Bastiaansen, & Broer, 2009). Cheng and his team created a photo-driven microrobot by stretching and laminating a photo responsive material on top of a polyethylene (PE) sheet (Cheng, Yin, Zhang, Yen, & Yu, 2010). Other researchers used similar methodology of combining a photo responsive material on top of a PE film to create a light driven motor (Yamada et al., 2008). This area of research has a lot of potential for creating material systems that can be activated by light and perform different functions depending on the users'

desires. Additive Manufacturing (AM) of these materials may allow for more complicated designs of light driven actuators and motors. AM would also allow for researchers to create precise and highly detailed photoactivated 3D structures instead of flat sheets, which have only been demonstrated in past research.

1.5 4D Printing

There have been many advances in the area of additive manufacturing by 3D printing smart materials that react to external stimuli, which has led to the development of an exciting new technology. 4D printing is defined as using 3D printing technology to print smart materials that can actuate and change shape over time when exposed to external stimuli right off the print bed (Figure 1-12). Traditional rigid 3D printing materials (acrylonitrile butadiene styrene (ABS), polylactic acid (PLA), polyvinyl alcohol (PVA), photo-resins, and photopolymers) can be printed in combination with the smart materials due to multi-material printing. This allows specific regions of the 3D printed product to be specified as smart material or rigid material with the help of 3D printing techniques, 3D modelling software, and the additive manufacturing machines.

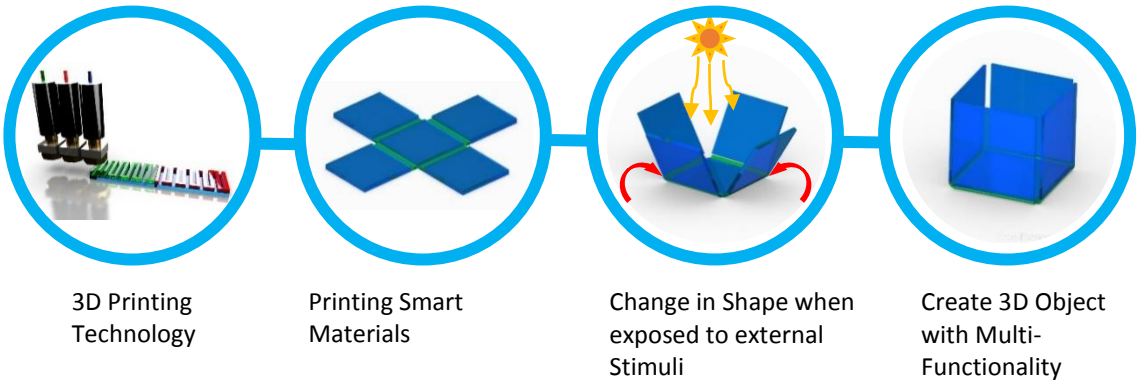

Figure 1- 12. Diagram of the 4D printing process that combines 3D printing and smart materials to create products that react to external stimuli. *(Leist, Gao, Chiou, & Zhou, 2017) (Leist et al., 2017)*

At the helm of 4D printing research is Skylar Tibbits (MIT), the head of the Self-Assembly Lab (SAL). Tibbits led to the development of 4D printing by creating dynamic objects that combined 3D printing technology and moisture reactive smart materials. Skylar Tibbits uses a polymer that can expand 150% when exposed to water (hygroscopic) as his smart material. A rigid plastic is printed at specific geometries and angles that prevents the hygroscopic material from expanding in certain directions and induce bending (Figure 13). This 4D printing method can be used to print 1D strands that transform into 2D or 3D objects (Figure 1-14. (a)), printed in flat 2D plates that transform into 3D objects (Figure 1-14. (b) & (c)), or combined with different rigid materials such as wood to create dynamic objects (Figure 1-14. (d)). Skylar's 4D printing methodology requires a very specific activation environment. The water activation seems like a very effective activation method; however, it displays one-way shape change and can be quite slow. It has not been confirmed if their method is reversible. Users may be limited by the amount of water required to shape change the object. Skylar's 4D material requires full submersion; a user would require a large surface area or volume to transform a flat plate into a 3D box for example. Another

design limitation is time-controlled activation of the smart material. Users are unable to transform specific areas of the material, or turn the transformation on and off. Skylar's 4D printing is effective in very specific applications that require the entire system to react to moisture, but there is inherently no control in the activation method.

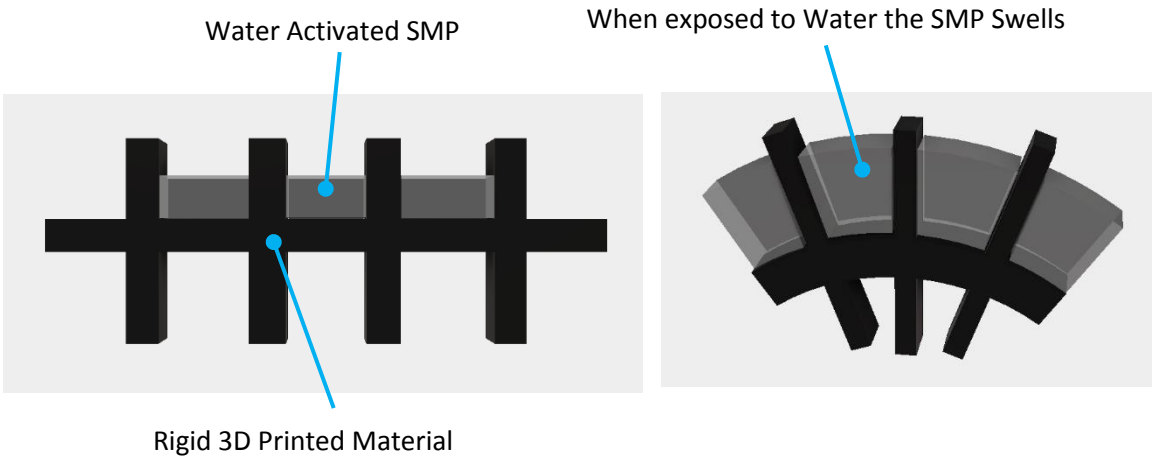

Figure 1- 13. Schematic displaying the water activation 4D printing, whereby a hygroscopic material swells when exposed to moisture and exerts stress on a rigid material to induce bending.

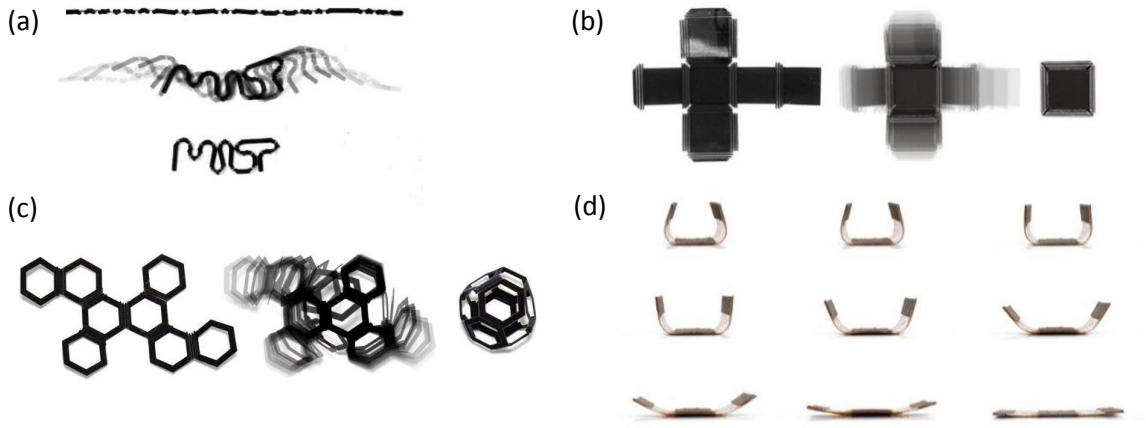

Figure 1- 14. a) A 3D printed 1D strand that transforms into the letters "MIT" when exposed to water. b) Flat 2D plate folding into a cube when submerged in water. Adapted with permission from Architectural Design, pp. 119-120 under the John Wiley and Sons License c) 3D printed 2D flat object that transforms into a 3D Octahedron. Adapted with permission from Self-Assembly Lab, "4D Printing: Self-Folding Truncated Octahedron", Self-Assembly Lab, Stratasys ltd., and Autodesk Inc. d) Fused deposition modelling (FDM) printed wood based material that folds when submerged in water. Adapted with permission from Self-Assembly Lab, "Programmable Wood", Self-Assembly Lab, C. Guberan, E. Demaine, Autodesk Inc., and Institute of Computational Design, University of Stuttgart.

Recently, researchers at Harvard's School of Engineering and Applied Sciences (SEAS) have created a 4D printing system inspired by biomimetics (Gladman, Matsumoto, Nuzzo, Mahadevan, & Lewis, 2016) . The smart material is a biocompatible hydrogel composite ink composed of stiff cellulose fibrils that are embedded in a soft acrylamide matrix and swells when submerged in water. The fibrils act as stiff strands that creates anisotropic swelling within the soft matrix, similar to the cell wall swelling found in plants (Burgert & Fratzl, 2009) . The material is 3D printed at ambient temperature and physically crosslinked using UV polymerization. The anisotropic orientation is created when the composite ink is extruded through the 3D printer nozzle and causes shear alignment of the fibrils. The composite ink swells along the longitudinal direction

of the 3D printed filament or in the direction of the printing path. The bending can be controlled when the material is 3D printed in a bilayer architecture.

Researchers found that there is no observable actuation if a flat 2D pattern is 3D printed using the composite ink without the fibrils; however, when the fibrils are included in the ink then twisting or bending can be observed. The researchers were able to create the printing path using 3D modelling software and simulate the bending mechanics of the component. Different printing path geometries are 3D printed such as spirals, grid, and combination of spirals and grid patterns that produced negative Gaussian curvature, positive Gaussian curvature, and a combination of positive and negative Gaussian curvature, respectively. Orientation of the print path (90^{o} and 45^{o}) induces different shapes such as cylindrical curving and twisting if the bilayer is printed in a grid pattern (Figure 1-15). After printing, the product can be submerged in water and take minutes to transform; however, this shape change is not reversible. The 4D printed hygroscopic parts can display dual shape change when it is exposed to different temperatures of water (50^{o}F or cold water) by adding temperature sensitive poly(N-isopropylacrylamide).

SEAS 4D printing system provides a method of creating 3D printed parts that change shape in water immersion using only a single material. Their modelling and simulation program allow designers to create products that can actuate and change shape based on material and printing properties: strand diameter, spacing between printing paths, and pathway orientation. The technique opens up the possibilities for 4D printing to access the biomedical market because of the biocompatible material. Cells could be seeded into more complex scaffold designs, better strategies for drug delivery systems, and improvement of minimally invasive medical devices.

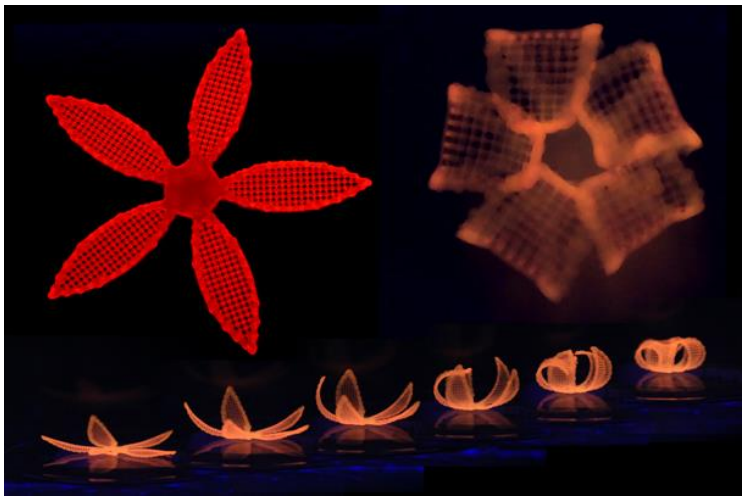

Figure 1- 15. Folding behavior of a 4D printed water activated hydrogel composite that displays different folding behaviors depending on the geometry of the 3D printed path *(Gladman et al., 2016)* Adapted by permission from Nature Materials, Vol. 15(4), pp. 416 under the Nature Publishing Group License

Hygroscopic 4D printing shows how objects can react intelligently to their environment without the need for human interaction. Intelligent sensors or structures could be deployed in extreme environments that prove difficult for human investigation such as space exploration, deep sea exploration, or within the human body. The hygroscopic polymers can be made of soft materials that may prove useful when handling biological substance such as tissue, organs, or live flora and fauna. Self-assembly shelters, structures, and barriers could be deployed in areas of natural disasters to protect victims and refugees. These accommodations can be transferred in compacted flat shapes to take advantage of the shipping volume, then transform into their ultimate form at their final destination, taking advantage of the extreme environment conditions.

Qe and his coworkers produced a 3D printable smart material, called printed active composite (PAC), capable of changing shape due to heating the PAC above its T_g. The researchers have been able to create many complex designs by printing hinges infused with the PAC combined

with rigid materials. However, one of the main issues with the PAC heat activated material is that it requires an applied stress combined with temperatures above T_g in order to change shape (Figure 16. (a) & (b)). Researchers also discovered that the direction of the PAC filament produces different bending features such as curling, spiraling, or repeated sinusoidal curvature (Figure 1-17. (a) & (b)). The addition of stress complicates the procedure of shape change because temperature is not the only external energy required. The process is not truly wireless because it requires an outside source to provide stress on the object while applying temperatures above T_g. The shape change seems to be one-way and only repeatable if the stress and heat training process is repeated (Ge et al., 2016; Ge, Dunn, Qi, & Dunn, 2014) . The temperature-stress procedure is very useful for one-way assembly or one-way disassembly, but not very useful in a fully automated and reversible actuation system.

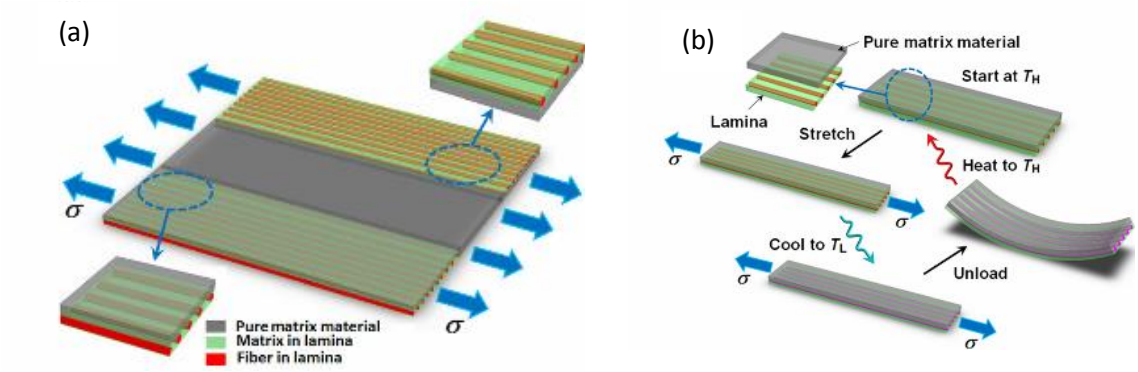

Figure 1- 16. (a) The printed active composite (PAC) construction made up of a top layer of elastomeric material and a bottom layer of a combination of glassy polymer and elastomeric matrix material. (b) The process of activating the PAC by heating the material, applying a load to the material, allowing it to cool, and releasing the stress to allow the material to bend. Reheating the PAC induces the material to return to its original flat shape. Adapted with permission from Applied Physics Letters, 103(13), pp. 3-4 under the AIP Publishing LLC License.

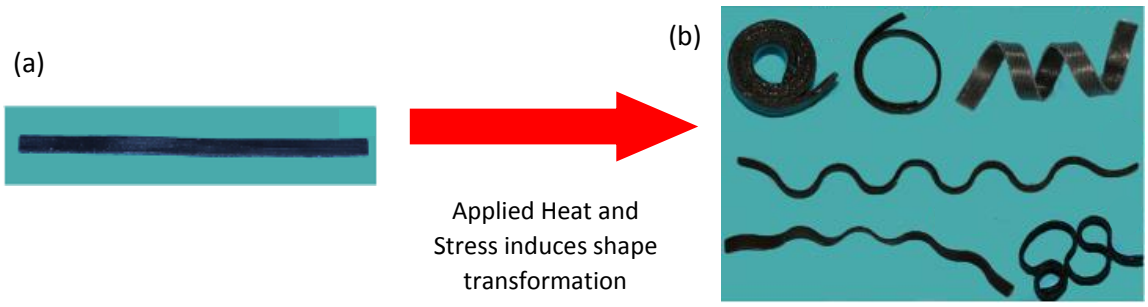

Figure 1- 17. (a) Initial printed flat shape of the printed active composite (PAC) without heat training. (b) Different geometries and shapes can be induced such as curling, bending, twisting, and waves depending on the PAC fiber orientation when the material is exposed to heat and stress. *(Ge, Qi, & Dunn, 2013)*

Smart materials play an important role in the development of 4D printing research. Many different smart materials exist and are in development; however, many of them cannot be 3D printed. It should be noted that smart materials that do not possess the ability for shape change are still important to 3D printing research. Materials that have the ability to change color, hardness, or transparency would prove important to camouflage technology, sensors, detection of foreign substances, and biomedical applications (Lendlein, 2010; Zhao et al., 2012) . Additional activation techniques in 4D printing will become further accessible as more smart materials are investigated.

1.6 Research Tasks and Approaches

The main objective of this research is to investigate a printable azobenzene SCP or thermosensitive SMP that allows for the possibility of creating customizable designs with higher

accuracy and precision for the manufacturing of actuators that react to light or heat. 3D printing allows different patterns and surface designs to be created that may generate different motions and shapes in smart materials. Skylar Tibbits established that by printing materials in different patterns they could make two flat plates with different dimensions bend with different curvatures (Raviv et al., 2014; Tibbits & Cheung, 2012; Tibbits, 2014) . A light activated 3D printable material would be beneficial because its activation method is wireless, the device requires no onboard batteries, no wires, and no moving parts. Removing excess components reduces the weight of the final product. This would reduce production, shipping costs, and waste because there would be less need to seek outside production to make extra components; all of their actuators could be 3D printed. The development and use of smart polymers may also lead to more biocompatible, biodegradable, and recyclable materials that can be used as cheaper biomedical devices and reduce the number of surgeries for patients.

Our proposed 4D printing system would print flexible actuators that could perform as arms, joints, and grippers. Initially, thermosensitive shape memory materials will be tested in the 4D printing system. The shape memory properties of the post printed thermosensitive smart materials will be evaluated. Next, the thermosensitive material will be 3D printed onto textiles to explore the area of smart textiles. Along with heat reactive shape memory materials, light reactive shape changing materials will be investigated. A study into the background and synthesis of azobenzene SCPs will be performed to evaluate the 3D printability and shape changing properties of azobenzene materials. Next, different azobenzene materials will be evaluated for use as a 4D printed actuator. The actuators are designed to bend bi-directionally depending on the location of the azobenzene SCP on the film. The azobenzene SCP material will be printed with a plastic material that would act as the structure of the actuators and help them maintain their shape. 3D printing allows specific areas of the product to be strictly photoactive polymer, only specific areas

will change shape if light is directed on the entire product. This means 3D shapes can be created from layer-by-layer printed shapes. This project presents a unique and innovative technology that benefits researchers in the areas of additive manufacturing, smart materials, and 4D printing. Heat reactive 4D printing materials will be a great introduction into the realm of 4D printing research, but light activated actuators could expand applications in product design, advanced manufacturing processes, automotive industry, aviation, medical devices, and space technology.

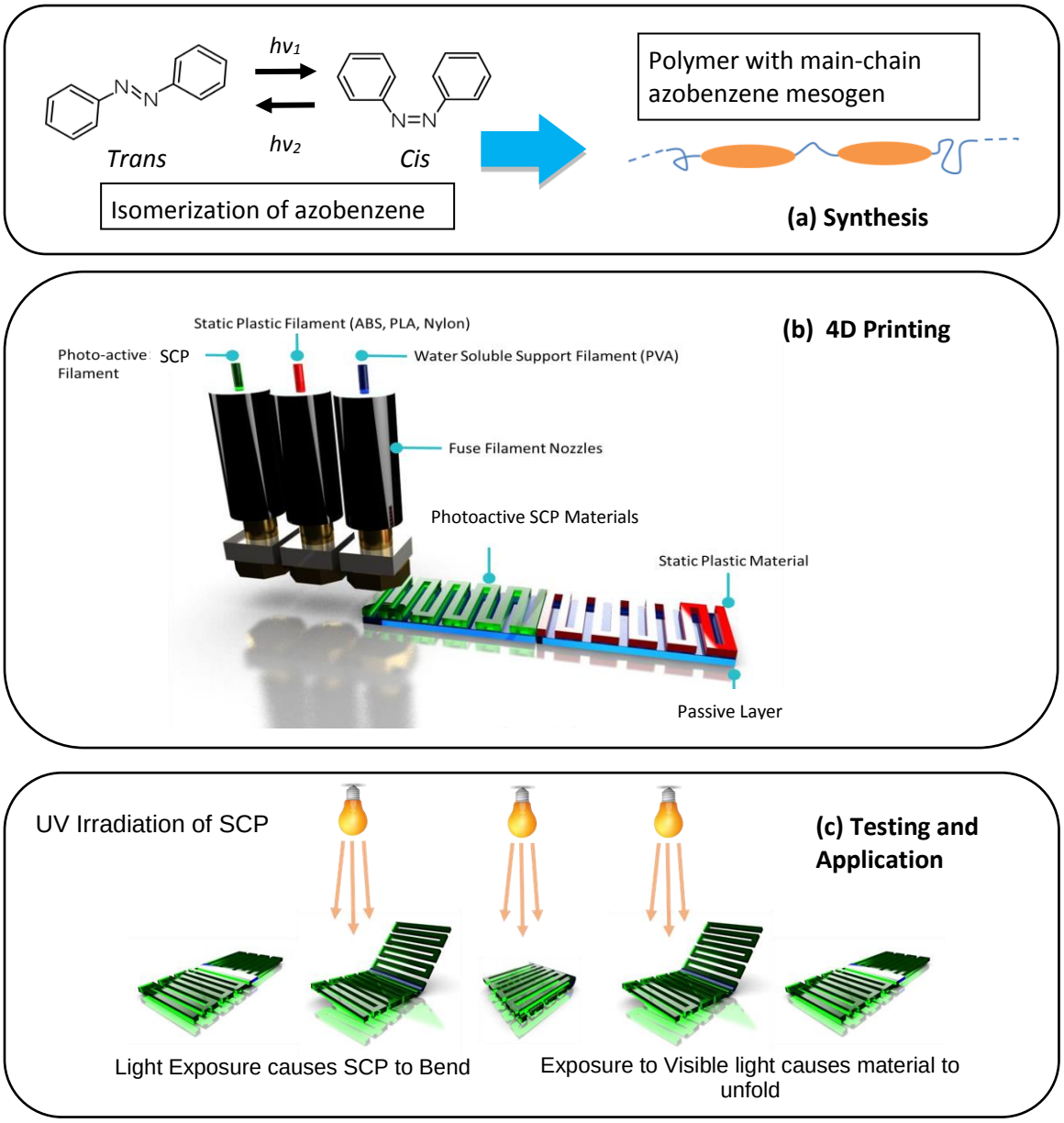

Figure 1- 18. (a) Azobenzene isomerization from trans-isomer (straight state) to cis-isomer (bent state) when exposed to light or heat and the proposed main-chain azobenzene AMP. (b) The 4D printing methodology of the azobenzene SCP using a multi-nozzle printer. (c) Photo activation of the azobenzene SCP bending and unbending when exposed to UV light.

1.7 Thesis Overview

An overview of the work presented in this thesis is displayed in Figure 1-18. The research commenced from testing thermosensitive 4D printed material and its combination with textiles. Next, the research transitions to the design and synthesis of azobenzene SCPs that can be used in 3D printers and possess shape changing properties (Figure 1-18. (a)). After synthesis, 4D printing of the SCPs is tested (Figure 1-18. (b)). Then photomechanical testing and applications of the 4D printed photoisomerable SCPs are investigated (Figure 1-18. (c)). The outline of this thesis is as follows:

Chapter 2 presents the examination into a current 3D printing material that can be used as a heat reactive 4D printing material. The shape memory properties of post printed Polylactic acid (PLA) is investigated. Currently, the shape recovery properties of post printed PLA have not been reported. Different designs and thicknesses of PLA are 3D printed and thermomechanically programmed into custom temporary shapes. Next, the shape recovery of those shapes are recorded and analyzed. Finally, PLA is 3D printed onto nylon material to test the concept of 4D printed smart textiles.

Chapter 3 presents the investigation into a light reactive shape changing polymer to be used as a 4D printing material. Initially, the viability of synthesizing a photoisomerable polymer that can be 3D printed and possess shape changing properties is investigated, namely, azobenzene SCPs. The azobenzene SCP is tested in the 4D printing system and different designs are printed. Characterization of the synthesized material will be performed to evaluate the properties of the material and determine if these properties can be altered for creation of another photoisomerable material. Photomechanical bending tests will be performed on the photoisomerable materials to determine their photomechanical efficiency.

Chapter 4 presents an investigation into the design and applications of the photoisomerable 4D printed materials. The photomechanical tests provide insight on the potentials and limitations of the 4D printed photoisomerable components. Different designs of the photoisomerable will be 4D printed that can change shape when exposed to different stimuli, actuate, and investigate if the designs can complete tasks.

Chapter 5 and 6 presents the summary of work, conclusions, and future work for this project.

Chapter 2. Investigate the shape memory properties of 4D Printed Polylactic Acid (PLA) and its combination with Nylon Materials for the creation of Smart Textiles

2.1 A Synopsis of Smart Materials, Shape Memory Polymers, and introduction into Smart Textiles

The textile industry has been displaying increasing interest into adaptable materials and technological state-of-the-art textiles. Shape memory materials (SMM) are materials that sense a change in temperature in their environment and change their physical properties, such as a change in shape. One method of creating smart textiles is combining yarns with SMAs or with SMPs to create smart woven textiles fabrics (Figure 2-1) (Chan Vili, 2007) . These smart woven textiles would have potential use for interior applications that require minimal human interaction. The materials sense and react to the environment's temperature that causes the materials to expand or contract. As an example, a smart fabric being used as window blinds could expand and lower when exposed to sun. Thus reducing the amount of sunlight in a room. Although this is an exciting new technology, the processing and manufacturing of the smart woven textiles proves to be difficult.

Figure 2- 1. Smart woven textile honeycomb yarn in a contracted state *(Chan Vili, 2007)* .

Typically, SMPs used in smart textile research are polyurethanes and polyurethane blends (Polypropylene, Nylon-12, and poly(lactic) acid) (Ahmad, Luo, & Miraftab, 2016; Hu, Meng, Li, & Ibekwe, 2012; Jing, Mi, Peng, & Turng, 2015; Stylios & Wan, 2007) . The concept has of combining smart textiles with 3D printing is a recent one. A 3D printer capable of printing soft fabrics (wools) and being combined with typical FDM plastics was created; however, the shape memory properties were not explored (Hudson, 2014) . One solution is to look at current 3D printable materials and determine if they can be combined with textiles in order to create 3D printed smart textiles. Poly(lactic) Acid (PLA) is a common FDM material that possesses shape changing and shape memory properties. As previously discussed, it has been shown that FDM printed PLA possess shape changing properties (Q. Zhang et al., 2015, 2016) . This property is caused by the strain generated during the 3D printing process when contracted strain is generated within the PLA with higher printing speeds (Figure 2-2. (a) & (b)). Thus, the material shrinks when exposed to temperatures above its T_g, causing the shape change (Figure 2-3. (a) & (b)). It was also discovered that PLA could be 3D printed onto materials with different coefficient of thermal expansion, such as paper, and create light weight 3D structures from 2D sheets using the thermal stimulus shape

change (Figure 2-4. (a-e)). Researchers found that this methodology could be used for pattern transformation in heat shrinkable materials and simplify the manufacturing process of shape memory materials suited for microstructures.

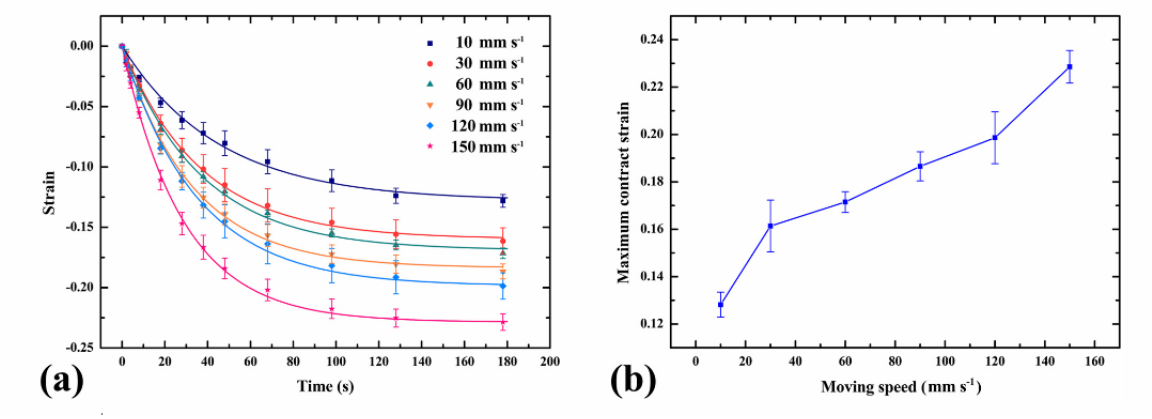

Figure 2- 2. (a) Maximum contraction strains for PLA 3D printed at different building speeds and their theoretical curves. (b) The maximum contraction strain of the post printed PLA after it has been heated. *(Q. Zhang et al., 2015)*

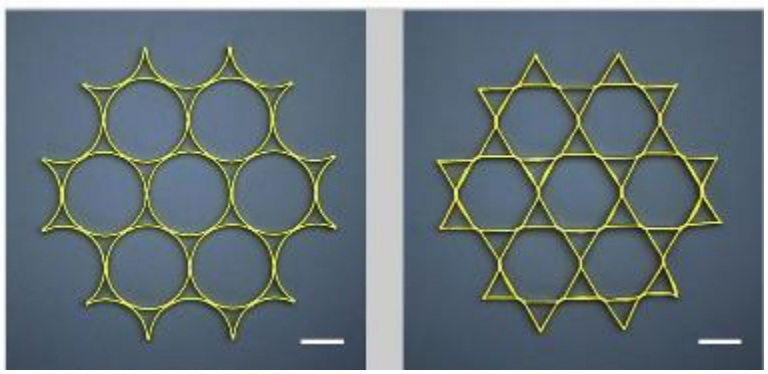

Figure 2- 3. (a) Initial 2D pattern of the thinly printed PLA material that (b) transform into a hexagonal shape from a circular shape when heated. Scale bar represents 12 mm. *(Q. Zhang et al., 2015)*

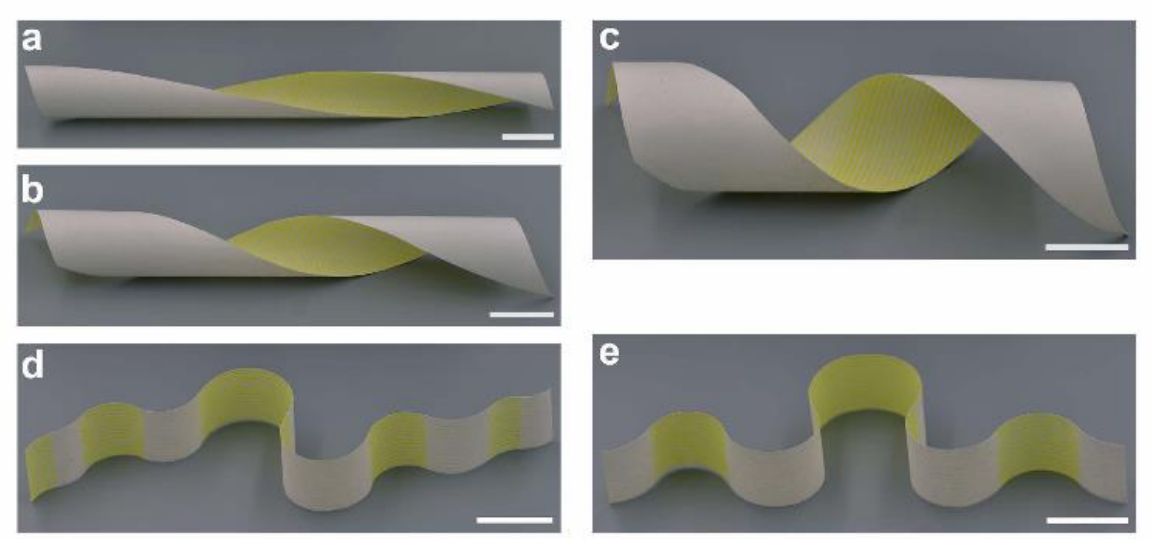

Figure 2- 4. (a-c) Different spiral 3D structures after PLA is 3D printed onto paper with different printing angles. (d-e) Different curvatures of PLA on paper after it is printed in specific sections. Scale bar represents 20 mm. *(Q. Zhang et al., 2016)*

The purpose of this project is to combine the two discussed researches together, then investigate the potential of a common fused deposition modeling (FDM) material, PLA, for use in 4D printing and the concept of combining PLA with nylon fabric for the creation of smart textiles. PLA possesses thermal shape memory behavior and maintains these abilities when combined with nylon fabric that can be thermomechanically trained into temporary shapes and return to their permanent 3D printed shapes when heated.

2.2 Exploring the concept of 4D printed PLA and testing the thermal shape fixing properties of post printed PLA

Although there has been extensive research into the shape memory properties of PLA, little research on the shape memory properties of PLA post 3D printing has been reported. The shape

memory properties of PLA due to its thickness of the films, the temperature of the programming, and the length of time for the programming have been studied; however, these properties have not been identified for 3D printed structures. In this research, multiple designs were 3D printed to test the concept of 4D printing using PLA (Figure 2-5. (a-d)) and the shape memory/programming properties were quantified.

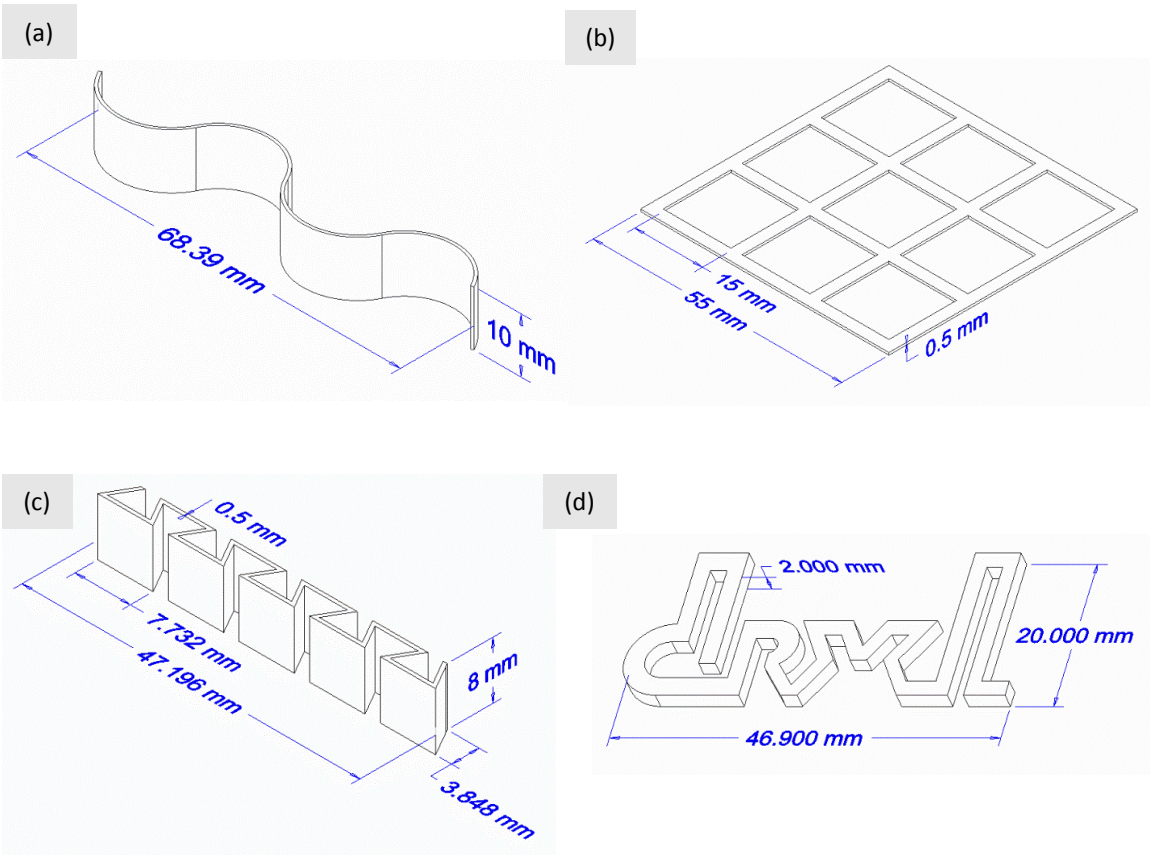

Figure 2- 5. The dimensions, printing orientation, and 3D models of a (a) spline, (b) grid, (c) arm, and (d) "drxl" shapes that were used as the samples for the 3D printing and shape memory tests. (Leist et al., 2017)

In order to understand the relationships between the printing properties of the PLA and the shape fixing properties, we 3D printed different thicknesses of PLA cantilevers ranging from 800 μm, 1000 μm, and 1200 μm. The material used in the printer was 1.75 mm in diameter PLA filament from Flashforge. The PLA possessed a glass transition temperature (T_g) around 58-60°C and a melting temperature (T_m) at 150-220°C (Jing et al., 2015; Martin & Avérous, 2001) . During printing, a permanent shape was established because the ordered crystalline structure of PLA is printed above its T_m and cooled to room temperature (below its T_g). During the programming stage, temporary shapes could be created when a stress was applied to the PLA when it was heated above its T_g, fixed in that position, and maintained that stress/strain as the material cooled. The stress was removed once the material fully cooled to room temperature and the temporary shape was maintained.

Cyclic mechanical tests were performed to quantify the shape memory of the post printed PLA. During these tests, the strain fixity rate (R_f) was calculated (Behl & Lendlein, 2007) . R_f measures the materials' ability to hold a temporary shape after it has been programmed (Eq. 1). During each number of cycles (N), the applied mechanical strain (ε_m) and the temporary strain after fixing, ($\varepsilon_u(N)$) are used to calculate R_f. However, during out experiments we measured the final bending angle of the cantilever (θ_f) compared to the bending angle during programming or shape fixing (θ_f) (Eq. 2).

$$\boldsymbol{R_f = \frac{\varepsilon_f(N)}{\varepsilon_m}\, x\, 100\%} \qquad \textbf{(Eq. 1)}$$

$$\boldsymbol{R_f = \frac{\theta_f(N)}{\theta_m}\, x\, 100\%} \qquad \textbf{(Eq. 2)}$$

2.2.1 Concepts of 4D Printed PLA

Different designs and concepts were 3D printed to test the shape memory capabilities of PLA. A spline with four curves, 68.39 mm in length, 10 mm wide, and a thickness of 0.50 mm was 3D printed on the Flashforge Pro 3D printer. The designs were placed into a pool of water at 70°C for 60 seconds and compressed within the water. After the spline was compressed, it is removed from the pool and allowed to cool to room temperature, which caused the compressed spline to harden (Figure 2-6. (a)). The spline maintained its temporary compressed shape under T_g. The compressed spline quickly expands back to its original shape once it is returned to the 70°C pool of water (Figure 2-6. (b)). Alternate designs of PLA 4D printing were tested using the same method. In other examples, a 3D printed "arm" can be bent in the user's desired direction and return to the permanent straight shape (Figure 2-6. (c)- (d)). In another test, a "drxl" logo can be compressed or extended when heated and return to the "drxl" symbol when heated above its transition temperature, (Figure 2-7. (a)-(c)). All models tested, take seconds to return to their permanent shapes when heated above their T_g.

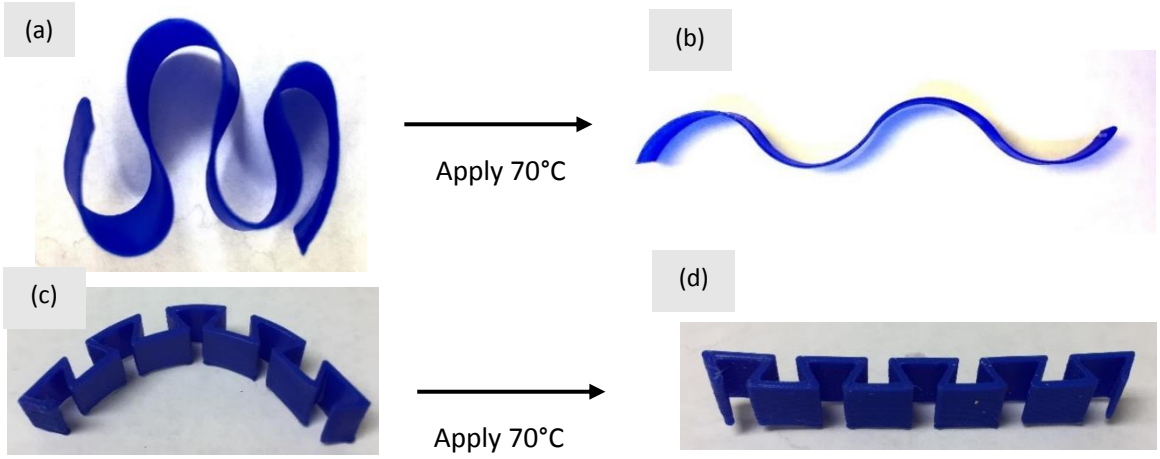

Figure 2- 6. (a) Temporary compressed shape of a four-curved spline after it has been heated to 70°C and then cooled to room temperature. (b) The compressed spline extends to its permanent shape after it is reheated to 70°C. Similar process is used for (c) an arm that can be bent when heated then cooled to room temperature and (d) return to its permanent straight shape when reheated to 70°C. *(Leist et al., 2017)*

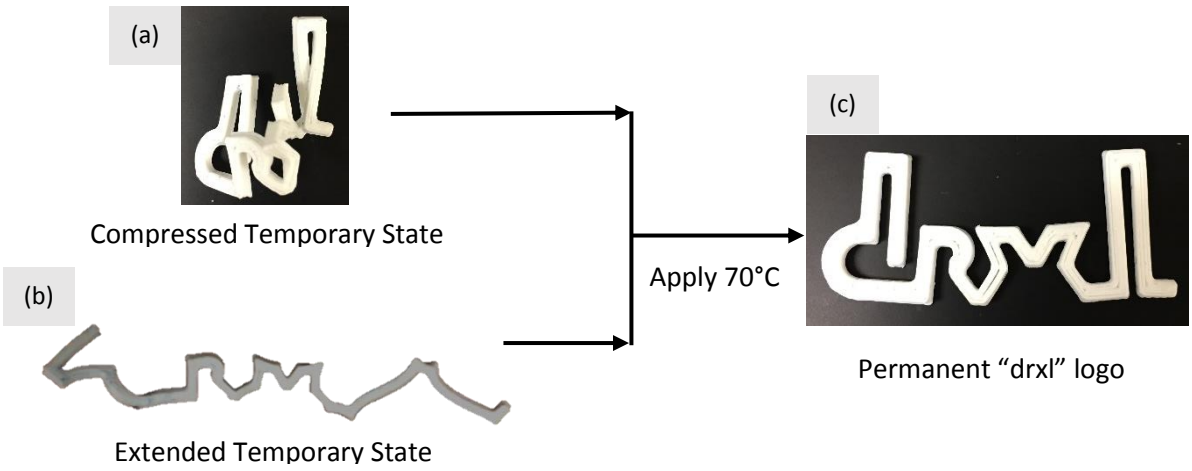

Figure 2- 7. (a) A compressed "drxl" logo after it has been heated above its glass transition temperature (70°C) then cooled and (b) an extended "drxl" logo that is cooled. (c) Both shapes can return to the permanent "drxl" shape when reheated to 70°C. *(Leist et al., 2017)*

2.2.2 Testing the Shape Fixing of PLA

Cantilevers with dimensions of 10 mm in width, 40 mm in length, and with different thicknesses were 3D printed for testing the shape memory repeatability of the PLA (Figure 2-8. (a)). The printer properties were set to 100 mm/s, the print bed temperature was set to 60°C, and the nozzle temperature was set to 230°C. Three different thicknesses of the samples ranging from 800μm, 1000μm, and 1200μm were prepared for the heat activation test. The tests were divided into two sections. The first testing section was the shape memory bending experiment and in the second section the deformed samples' shape recovery under the activation of hot water was recorded. The cantilever is heat treated at 65~70°C and bent at a 90° angle. Once bent, the cantilever is removed from the heat and cooled to room temperature, where it maintains its bent shape (Figure 2-8. (b)). The original bending angle, α, of each sample were measured to record the initial bending angle. Twelve "L" shaped samples were prepared for each thickness. Throughout the shape fixing tests, all samples maintained 100% of their temporary 90° shape. During the second testing section, the expected final unbending result is shown in figure 2-8. (c) and the unbending angle, α', is recorded over time, which will be discussed in the next sections.

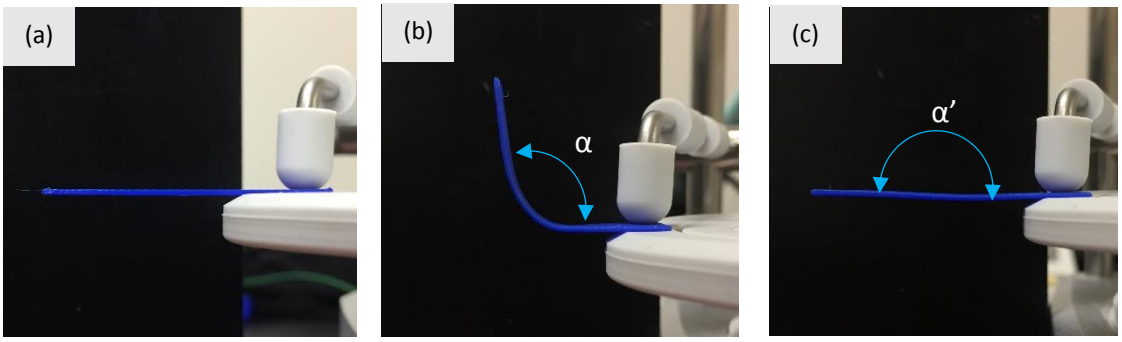

Figure 2- 8. A 3D printed PLA cantilever used to test its shape fixing and shape memory behavior. (a) The original PLA cantilever is printed at 0° or 180°. (b) The cantilever is placed into a pool of 70°C water and fixed at a 90° angle (α) then cooled to T_g. (c) The cantilever is returned to the heated water and the bending angle (α') is recorded. *(Leist et al., 2017)*

2.2.3 Outcomes

The outcomes of this research are a combination of proof-of-concept of the shape fixing capabilities and ability to quantify the shape fixing capabilities of post printed PLA. The research showed that the shape fixing was unaffected by the different thicknesses of PLA; however, this would change with different fixing temperatures and different fixing times. The settings that were ideal for attaining 100% shape fixity were determined for PLA cantilevers of smaller thicknesses ranging from 800µm, 1000µm, and 1200µm. The cantilevers were capable of being fixed to 100% fixity when exposed to water at 70°C for 2 minutes due to the thinness of our 3D printed cantilevers. However, programming temperatures would have to be increased for designs with thicker bodies and more volume to maintain 100% shape fixity. It has been presented that shape fixing was capable for objects that were fixed in tension (Fig 2-7. (a)) or compression (Figure 2-7. (b)) and both were capable of recovering majority of its permanent shape (Figure 2-7. c)). The research has shown that different mechanisms can be designed for different applications such as a spline that can act as

spring, components that can fold into compact shapes for easy packaging, or joints that can bend in specified directions depending on their programming shape.

2.3 Investigating the shape recovery rate of the 3D printed objects when it is printed at different thicknesses and exposed to different temperatures.

2.3.1 Quantifying the Shape Memory and Shape Recovery of Smart Materials

In order to quantify the shape memory and shape recovery properties of the smart materials, cyclic mechanical tests were performed to calculate the recovery rate in relation to the fixed bending angle (R_b) of the PLA cantilevers. A thermomechanical bending test was performed for calculating the recovery rate according to the recovery bending angle of the different thickness 3D printed cantilevers. All of the cantilevers discussed in this research were 3D printed in a flat (0°, 180°) orientation. During the programing stage, the cantilever was bent at an initial angle (θ_i) above the material's T_g and cooled to room temperature. Next, the cantilever was reheated, above T_g, during the shape recovery process and the bending angle (θ_f) is recorded until it reaches a final bending angle. A video analysis software called Tracker was used to track the angular position of the cantilever. The shape recovery according to the bending angle is calculated using a ratio between temporary fixed angle and the bending angles (Eq. 3). It should be noted that this equation will be used for chapter 3, photoisomerable 4D printing, during the bending analysis of the azobenzene SCP.

$$R_b = \frac{(\theta_i - \theta_f)}{\theta_i} \quad \textbf{(Eq. 3)}$$

2.3.2 Results

The position angle of an 800 µm, 1000 µm, and 1200 µm thick cantilever beam that unbends when exposed to three different temperatures of water was recorded for 45-60 seconds to assess the shape recovery efficiency of 3D printed PLA. First, the beams were tested in 65°C water, which showed the bending position angle and the bending speed decreases with increasing PLA thickness. Next, the different thicknesses of the PLA beams were exposed to 75°C water; the results demonstrated similar trends to 65°C data. Increasing thickness of cantilevers resulted in decreased angle position; however, bending times were similar for 800 µm and 1000 µm thickness. Finally, the unbending position angle of different thickness PLA cantilevers were tested in 85°C water.

In this research, a testing system was prepared as shown in figure 2-9. This system included a moving table, which moved along vertical z-direction connected to a holder with two binder clippers at each end. One end of the holder is fixed by a binder clipper to the moving table and the "L" shape sample is attached to the other end of holder by the second binder clip. The temperature of water in the beaker was kept at a specific value by a hot plate. The cantilever is returned to different temperatures of water (65°C, 75°C, and 85°C) in figure 2-9 (b) and recorded until it stopped bending in figure 2-9, (c). It can be seen that the cantilever attempted to return to its original permanent straight shape. A digital camera was employed to record the unbending process and the video was exported to Tracker for analysis. The same process was repeated four times in each case of 65°C, 75°C and 85°C heated water and for all three different thicknesses of the PLA samples.

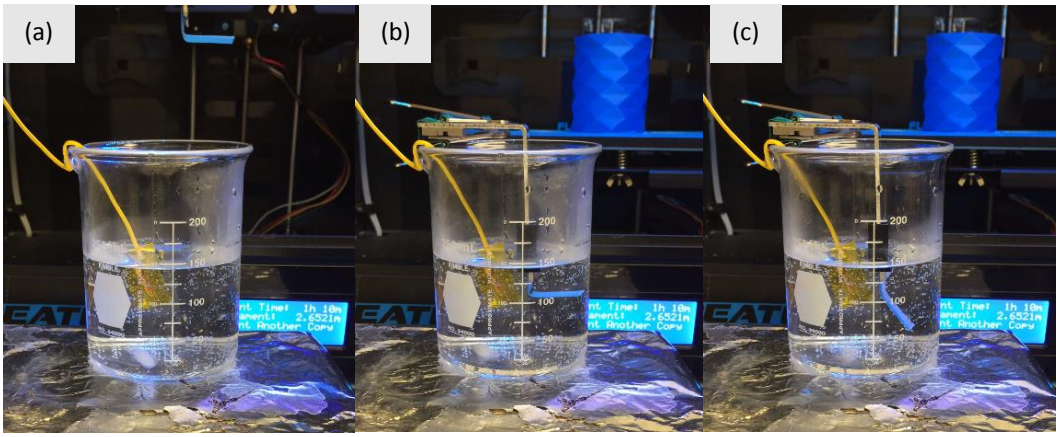

Figure 2- 9. Experimental setup of heating activation test. (a) Before cantilever immersion in hot water. (b) Cantilever begins unbending from 90º after immersion in hot water. (c) The final bending angle of cantilever after submersion in hot water for three minutes. *(Leist et al., 2017)*

2.3.3 Outcomes

The exposure to different environmental temperatures and the different material thickness added different outcomes to the shape recovery efficiency. As expected, the results display a trend of increasing average bending angle for all thicknesses as the temperature increased (Figure 2-10). The rate of bending is substantial in higher temperatures, since it takes less than 10 seconds for the cantilevers to reach their final bending position. However, it can be seen that the cantilevers never reach 100% shape recovery. Figure 2-11 displays a trend of decreasing average bending angle for all temperatures as the thickness increased. Overall, higher temperatures and thinner 3D printed PLA materials are most desired for fast reacting smart materials and higher chance to return to its original permanent shape.

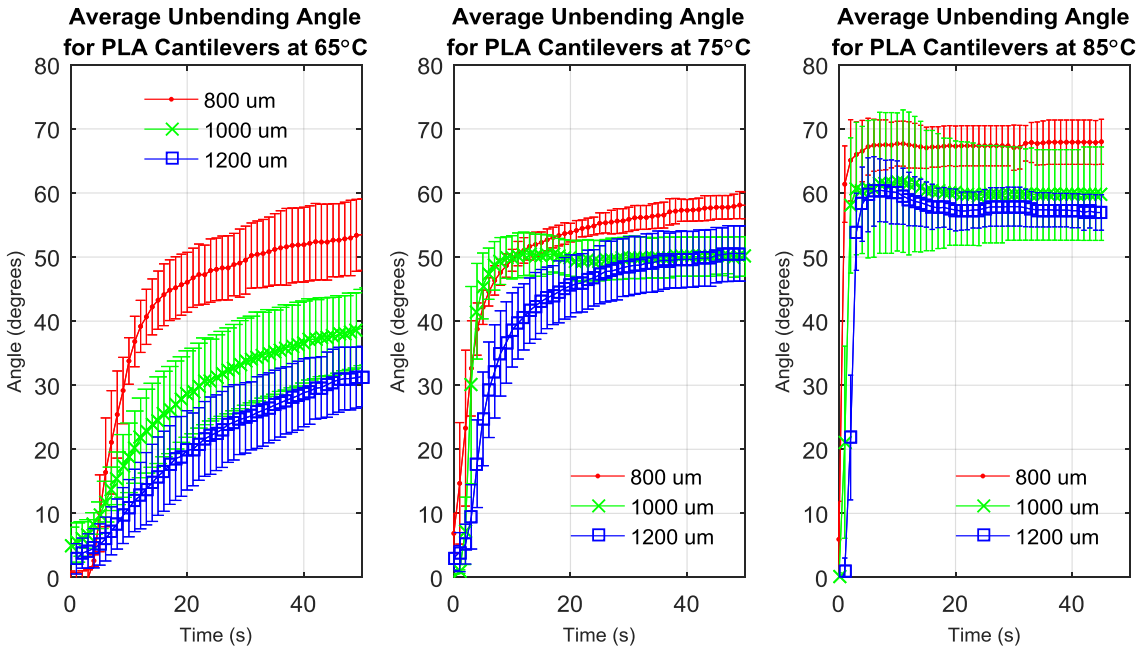

Figure 2- 10. The average angle of unbending for 800 µm, 1000 µm, 1200 µm PLA cantilevers exposed to 65°C, 75°C, and 85°C water. *(Leist et al., 2017)*

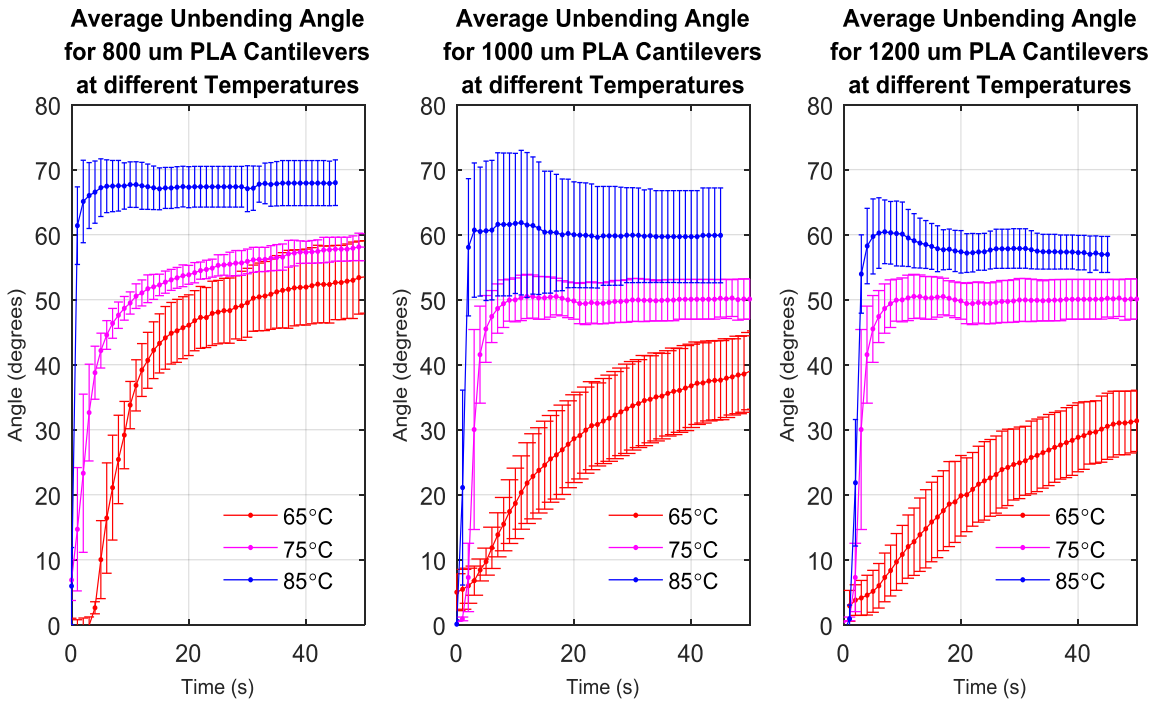

Figure 2- 11. The average angle of unbending for 800 µm, 1000 µm, 1200 µm PLA cantilevers exposed to 65°C, 75°C, and 85°C water. *(Leist et al., 2017)*

During testing, the final bending angle never returned to its 100% final bending position. However, a thinner cantilever and a higher temperature had the highest percent of shape recovery at 75.54% for an 800 µm thick cantilever at 85°C. An increasing cantilever thickness and lower transition temperature displayed lower percentage of shape recovery at 42.92% for a 1200 µm thick cantilever at 65°C. A trend of increasing shape recovery can be observed for increasing temperature and decreasing sample thickness (Figure 2-12). The materials not reaching 100% shape recovery may be due to the increased stress and strain during the programming stage, which may have caused necking in the material. Increasing the programming temperature may reduce the amount of crystallization within the material by allowing the polymer chains of PLA to slide pass each other

easier. This may reduce the stress and strain on the material during shape fixing, and increase its shape recovery efficiency.

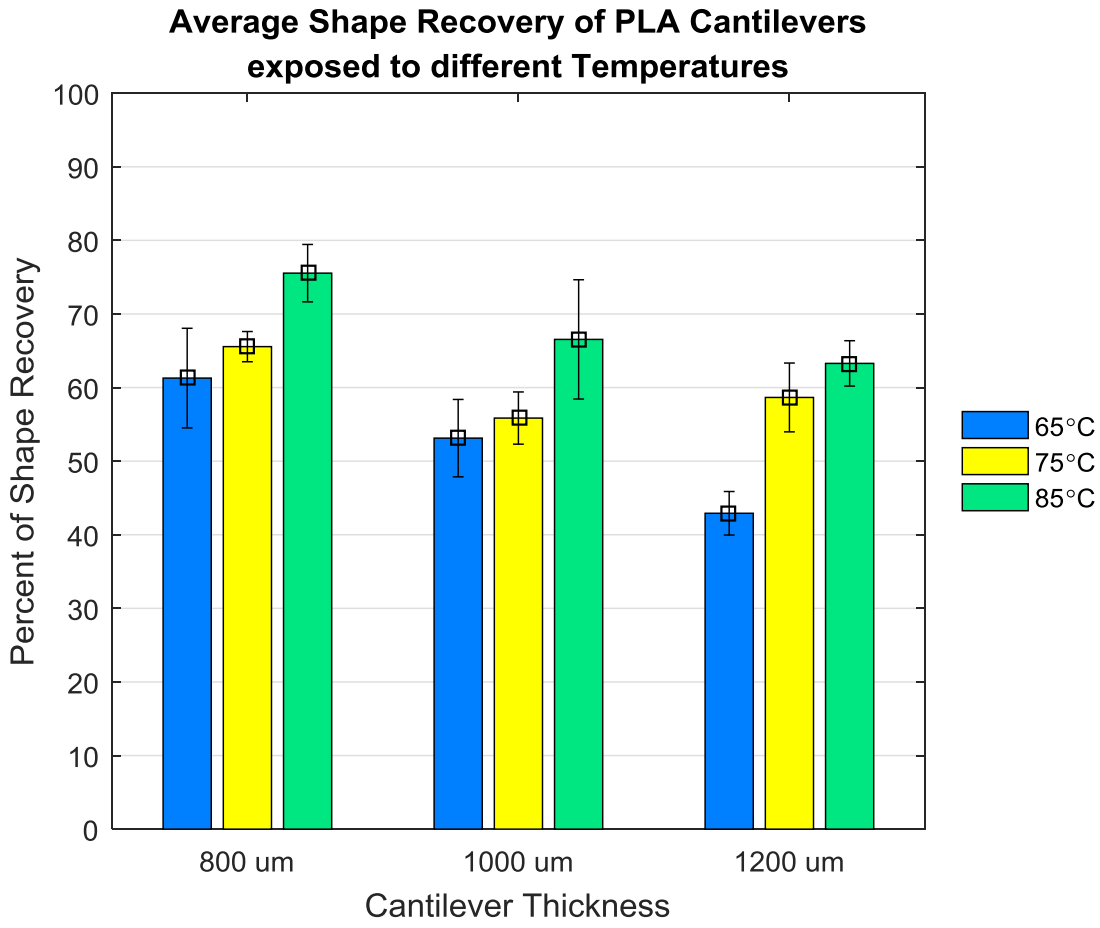

Figure 2- 12. The average percent of shape recovery for different cantilever thicknesses (800 µm, 1000 µm, 1200 µm) at different temperatures (65°C, 75°C, 85°C). *(Leist et al., 2017)*

The outcomes of this research provide knowledge about the shape recovering properties of 3D printed PLA according to the material's thickness and temperature of the recovery environment. The research showed that material thickness affects the shape recovery time and final percentage

of shape recovery. Components with different thicknesses could be designed to possess different bending rates or different final bending angles. These properties may prove to be important for a process called sequential folding, where design of the actuating hinges is important for creating 3D objects from 2D objects to prevent moving parts from interfering with each other(Barrett, Mamiya, Yager, & Ikeda, 2007; K. Lee, Tabiryan, Bunning, & White, 2011; Milam, O'Malley, Kim, Golovaty, & Kyu, 2010; Wen, Zhang, Weng, & Hu, 2014) . Although, the materials did not retain 100% recovery, they could be improved with higher programming temperatures or recovery temperatures, or the materials would be blended with another polymer that is more flexible, such as thermoplastic polyurethane (TPU). Multi-material shape memory effect should be tested for combinations of PLA with other current 3D printable materials (nylon, ABS, and PVA). In the future, development of materials with lower T_g may have suitable applications in the biomedical industries if their activation temperatures are closer to body temperature (37°C), which would allow for the automated reaction of biomedical devices when they are placed in the body. The use of polymers instead of metals within the body may allow for these materials to degrade and replace the structure of the product with the cells of the individual, instead of requiring future surgeries to replace to remove or replace the metallic biomedical instruments.

2.4 Investigating the shape memory properties of 3D printed PLA when combined with textiles.

2.4.1 Experimental Setup for PLA combined with Nylon Materials

Since PLA possesses shape memory properties, the possibility to combine these properties with textiles is explored. A third experiment investigates the concept of PLA material 3D printed on top of nylon fabric to test the shape memory effect and its potential to be a smart textile. Two

types of 4D printing were explored in this objective. During the first test, the PLA material is the only material used during the process and 3D printed directly onto the print bed. Next, The PLA material is 3D printed onto the nylon fabric in a second experiment (Figure 2-13). The nylon fabric used for the textile printing is Solid Power Mesh Fabric Nylon Spandex made up of 90% nylon and 10% spandex. The nylon fabric is cut into 40 mm x 40 mm squares and measures at 0.26 mm in thickness. Double sided tape is placed onto the print bed and the cut nylon fabric is placed onto the tape for better adhesion to the build plate. Finally, the .STL file is uploaded to the 3D printing software (Simplify 3D) and the part is 3D printed onto the nylon fabric. The printing speed is set to 100 mm/s, the bed temperature is set to room temperature, and the nozzle temperature is set to 230°C for all test prints.

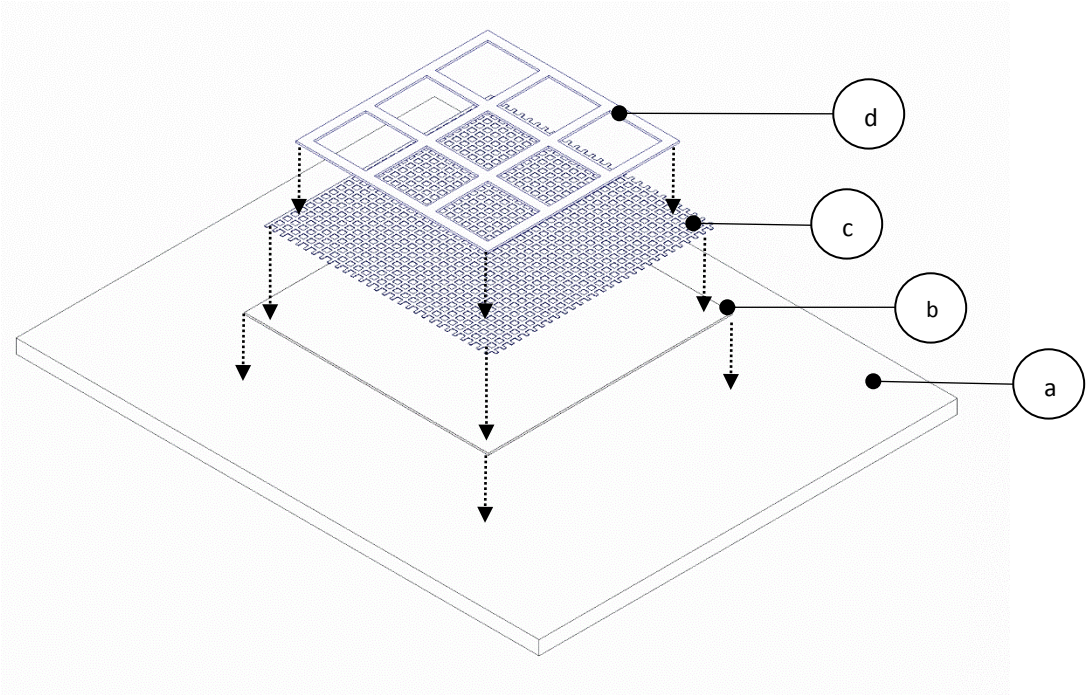

Figure 2- 13. A schematic of the textile 4D printing process, which displays the (a) print bed, (b) the double-sided tape placed onto the print bed, (c) the nylon stretch fabric placed onto the double-sided tape, and (d) the grid model 3D printed onto the nylon fabric. *(Leist et al., 2017)*

2.4.2 Results

A grid structure that was 3D printed onto the nylon material was placed into heated water at 70°C and rolled into a cylinder. Once the materials was rolled into the desired shape, the component was removed from the heated pool and allowed to cool to room temperature. At room temperature, the material remains stiff and maintains its temporary cylindrical shape; however, the cylinder unravels to the permanent flat shape when the cylinder is returned to the heated water above its T_g at 70~80°C (Figure 2-14. (a)-(c)).

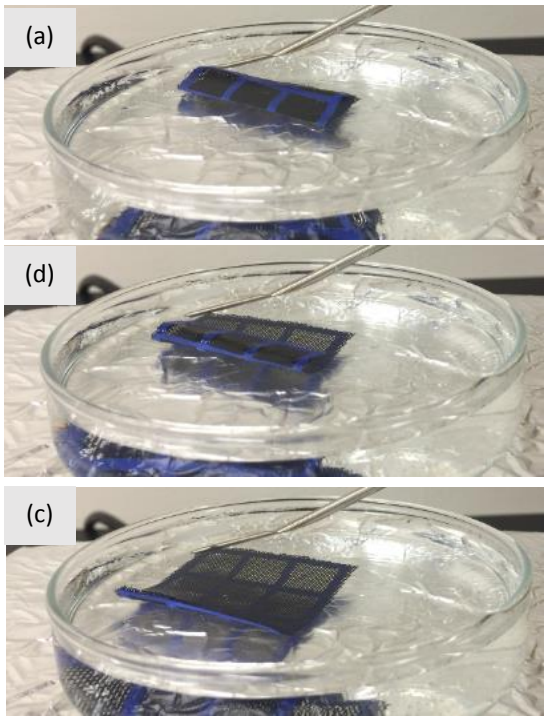

Figure 2- 14. A PLA and nylon fabric combo is heated to 70°C and rolled into a cylinder then cooled. (a-c) The PLA nylon cylinder unfolds into its permanent flat shape when reheated in the 70°C pool of water. *(Leist et al., 2017)*

Next, the nylon fabric with a grid made from PLA 3D printed onto its surface was used for the concept of encapsulation and release of an object when exposed to heated environments. In this case, a magnetic stir bar was placed in the center of the fabric (Figure 2-15. (a)), but the PLA fabric combination cannot be wrapped around the stir bar due to it being stiff at temperatures under 60°C. The PLA fabric and stir bar were submerged into 70°C water for 60 seconds. The corners of the fabric were wrapped around the stir bar and the entire piece is removed from the heated water. The material cools to room temperature and becomes stiff, ensnaring the stir bar (Figure 2-15. (b)). The PLA fabric mesh is returned to the 70°C water in order to release the stir bar (Figure 2-15. (c)).

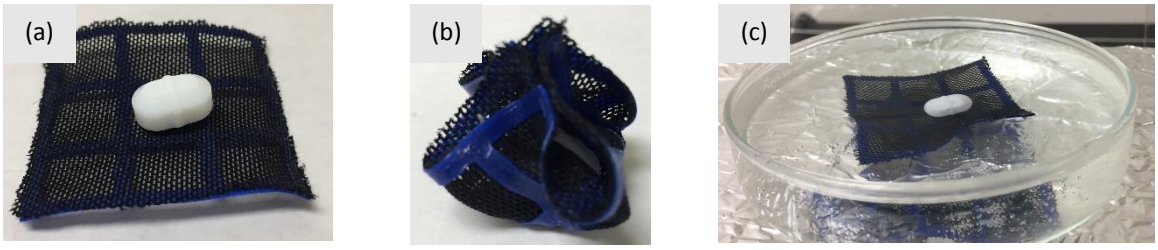

Figure 2- 15. An example of using smart textiles for encapsulation applications. (a) A magnetic stir bar is placed in the center of the PLA nylon fabric. (b) The PLA nylon fabric is heated to 70°C and encapsulates the stir bar, then removed from the heated water to cool to room temperature and able to maintain its shape. (c) The PLA nylon fabric unravels and releases the stir bar when the PLA nylon fabric is returned to the heated bath. *(Leist et al., 2017)*

2.4.3 Outcomes

The concept of smart materials combined with nylon textiles displays the possibility of using smart textiles for encapsulation and controlled release in response to its surrounding environment. The nylon fabric in the experiments serves more as a structure and non-active material, while the PLA serves as the smart material. The research presents a proof-of-concept of 4D printed smart textiles and their future applications. It is observed that the smart textiles could be modified into custom shapes and 2D flat textiles could be transformed into temporary 3D objects that maintain those shapes at room temperature. This may be promising for clothing that reacts to extreme environments and release products that may protect the wearers from dangerous environments. Also, the combination of smart materials with non-reactive textiles as structural materials reduces the need for additional 3D printing material, which may be more expensive.

The shape changing smart textiles could be used for aesthetic reasons or compact packing of supplies and unfolding at their final destination. The combination of textiles with smart materials may allow wearers of clothing to customize and mold clothes to their personal designs and body types. This development could lead to clothing that reacts with the surrounding environment or to the wearer's body temperature. The same piece of clothing could be used for insulating the wearer or ventilating them. Smart textiles may find uses in the biomedical field. Smart fabrics that can be infused with medicine can be used for different biomedical applications that mold to different body parts and persons with different body types. This applications would be ideal for burn victims or patients that have suffered bone fractures, where the materials can be soft when applied to the patient then harden after the medical procedure. The removal of the cast or skin prove to be easier than current methods by reheating to the smart material above its T_g to soften it and allow for unraveling.

Chapter 3. Design, Synthesis, and Testing of a Photoactive Shape Change Polymer

3.1 The Study of Azobenzene and Azobenzene Shape Changing Polymers

Azobenzene based polymers have been heavily researched due to their properties for fast and fully reversible photoisomerization. Azobenzene is considered a photochromic molecule because the *trans* and *cis* spectra (effective absorption spectrum) can change depending on the intensity of the light. There are two main theories for the isomerization movement of the azobenzene compound. The first theory postulates that the isomerization follows a rotational movement about the N-N bond. The second theory postulates that the isomerization follows an inversion movement about the N-N. However, the relaxation back to the cis-state can follow the rotation or the inversion movement through photochemical activation depending on the type of chromophore. A rotational relaxation isomerization can be induced through thermal activation. Theoretically, both cases are possible, but the inversion theory is preferred because the inversion movement requires less free volume in rigid matrices for movement when compared to rotational movement (Mahimwalla et al., 2012) .

Typically, the azobenzene SCPs and SMPs are in thin film form, but the thin films can possess different motions depending on the dye, the polymer structure, crystallinity, and light activation source. In some cases, the films can expand or contract when exposed to light depending on the main-chains that are attached to the chromophores (Bublitz et al., 2000) . It has been shown that the direction of bending can be controlled by the direction of light and the polarity of the light source (Ercole et al., 2009) . Some azobenzene SCPs can be activated using UV light or visible light (White & Broer, 2015; K. Lee et al., 2012; White, 2012) . Researchers performed

photomechanical testing on a polydomain azobenzene LCN testing the shape changing properties and shape memory properties of the cantilever films that measured at 5 mm by 1 mm. The researchers used a 100 mW/cm^2, 442 nm visible light and a 50 mW/cm^2, 375 nm laser for the photoactivation. In the first test, the visible light was polarized parallel to the cantilever film's long axis, which causes the film to bend 21° towards the light source and maintain its position. However, the cantilever switches to bending in the reverse direction by 22° when the polarized light is changed to perpendicular of the cantilever's long axis (Figure 3-1. (a)). It should be noted that this procedure displays a technique of optical fixing that can hold its temporary shape for months, but irradiating the sample with unpolarized or circular polarized 442 nm light will force the material to return to its original shape (K. Lee, Tabiryan, et al., 2011) . A second test was performed using a UV laser on the cantilever azobenzene material. This test displayed different actuation reactions where the cantilever quickly bends at a large angle similar to the 442 nm tests, but then returns to its initial position with prolong exposure to UV light (Figure 3-1. (b)). It can be seen that UV light provided a faster reaction than the visible light, but visible light maintains its final bending position (Figure 3-1. (c)). This may be useful for applications that require different actuation methods for different tasks, but using the same material.

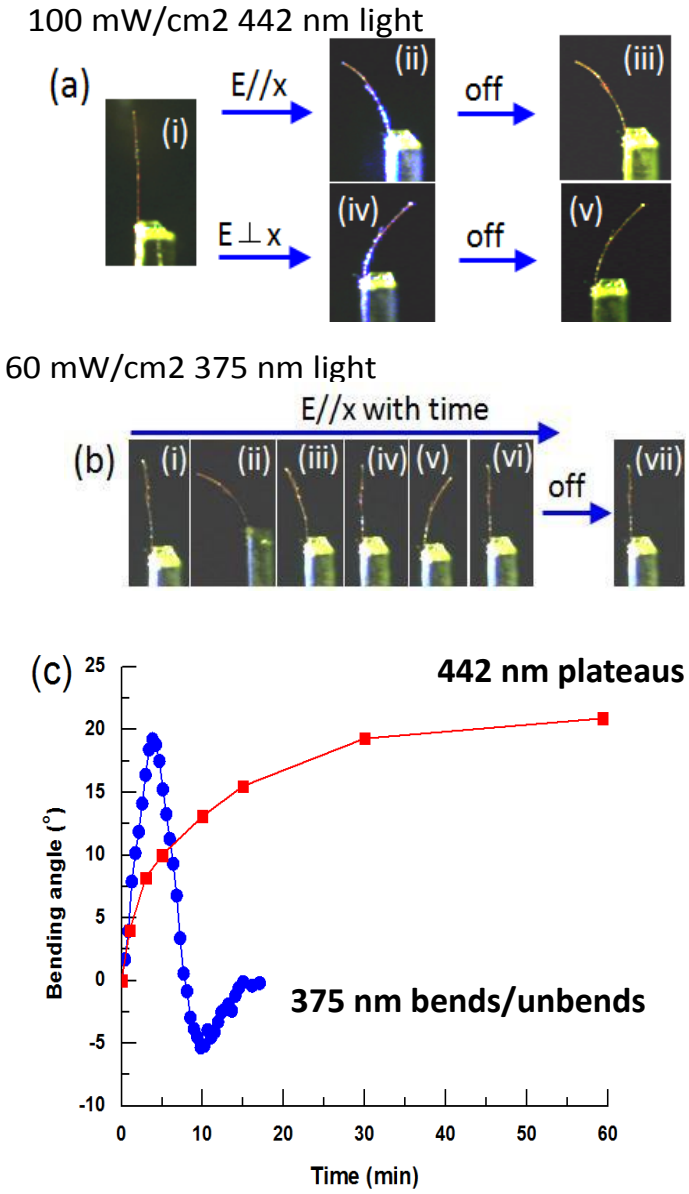

Figure 3- 1. (a) A polydomain azobenzene LCN cantilever exposed to visible 100 mW/cm^2 442 nm that is polarized along the long axis of the film and causes the film to bend towards the light source (i-iii). The same film is exposed to the same visible source, but with the polarization perpendicular to the long axis that causes the film to bend away from the light source (i, iv, v). (b) The azobenzene LCN cantilever exposed to a 60 mW/cm^2 375 nm UV laser causes the film to bend quickly towards the light source, but then return to its original shape after prolong exposure to the UV light. (c) A plot of the bending angle of the azobenzene cantilever exposed to different light sources, which shows the different actuation motions according to the UV or visible blue light sources (K. Lee,

Tabiryan, et al., 2011). Adapted with permission from the Journal of Materials Chemistry, 22(2), pp. 694, under the Royal Society of Chemistry.

The objective of the azobenzene research presents the design and synthesis of an azobenzene photoactive SCP that can be 3D printed and change shape when exposed to different wavelengths of light. After synthesis of a photoactive polymer, the material's properties are characterized and the possibility of using the materials for 4D printing is evaluated. Next, the photomechanical properties are tested for different activation approaches. After photomechanical testing, different designs for light activated 4D printing are explored and tested for different applications and tasks.

3.2 Study the feasibility of creating a poly (silyl ether) containing a main-chain and side-chain azobenzene moiety

3.2.1 Previous Research into Azobenzene Shape Changing Polymers

Most of the developed azobenzene SCPs are in laminate or thin film form. There are different methods for creating the azobenzene SCPs. One method, users have to spin coat the SCP onto the passive film, combine the materials with an adhesive, cure the polymer, and then cut the shapes out of the film if researchers desire to create an actuator or gripper. Another method, usuers have to create a mold in the shape of the desired final product, pour the azobenzene polymer into the mold, cure the polymer, and extract it from the mold. This methodology is limited to the skill of the user and possesses many areas for error. In our proposed research, azobenzene film is laminated with an elastomer or rigid material to act as a structure for the component by using 3D printing methods. The process of cutting different shapes and combining it with different materials

to create structures can be merged into a precise and intelligent digital manufacturing process with additive manufacturing. Our research hopes to streamline the design and manufacturability of light reactive SCPs through the use of 3D printing systems.

We propose to use 4D printing technology to design and create flexible actuators that change shape due to light exposure. 4D printing should expand the area of design for light activated flexible actuators. Users can use 3D modeling software to create designs of their actuators then print them in the same day. If the prototype requires changes, users can easily modify the part on the software and reprint the prototype. This process will save on waste and money by taking advantage of 3D printing's precise and detailed printing techniques. Currently, the most common and cheapest 3D printers are FDM and syringe printers. Converting the azobenzene SCP to a solution that can be used in syringe printers would allow easier access to the 4D printing technology. Although, it may be possible to use an azobenzene SCP in Polyjet printers, our group decided against it because the equipment tends to be expensive and the UV curing of the polymer may affect the photoisomerization of the azobenzene. Polyjet printers use photopolymers and disperse them through inkjet heads that are cured under UV light. The UV curing in the Polyjet printing process limits the types of azobenzene dyes that can used in our research and may interfere with the photoisomerization of azobenzene.

Poly(silyl ether) LCP materials will be synthesized, characterized, and studied to understand the factors that influence their final properties with the assistance of Dr. Frank Ji's Lab (Chemistry Department). As discussed previously, a promising candidate for applications, such as flexible actuators and artificial muscles, is a class of materials known as SCPs (S. Huang, Liu, Mokasdar, & Hou, 2013) . Our SCPs are comprised of a lightly crosslinked polymeric elastomer portion and a liquid crystalline (LC) portion, which will be synthesized in the main chain of the polymer (Figure 3-2). The materials possess the unique property change shape reversibly upon

exposure to external stimuli (temperature, light, and electric field). SCPs that change their shape upon exposure to light contain a photosensitive dye as the mesogen in the LC portion of the polymer matrix. The most common dyes used in this type of SCPs are azobenzene-based dyes, which are used in this research.

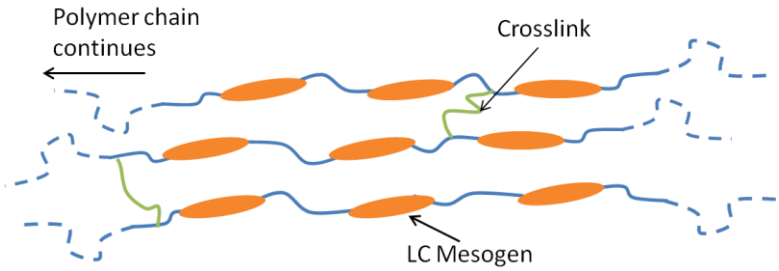

Figure 3- 2. SCP network (blue and green lines) with LC mesogens (orange ovals) in the main-chain. Used with permission from Dr. Frank Ji's Lab, Chemistry Department, Drexel University.

The polymer chains in azobenzene (azo) SCPs retain an extended conformation and a degree of anisotropy of the chain because of the dye molecules' uniform alignment before light irradiation. The amount of anisotropy of the chains changes from system-to-system because it depends on the overall SCP construction. When the azo SCP is irradiated with UV light, the azo dye absorbs light and undergoes its *trans-cis* isomerization. This isomerization induces an isothermal phase change from an initially ordered LC phase (Figure 3-3. (a)) to a disordered isotropic phase, where the mesogens are no longer aligned and the polymer chains adopt a random coil conformation (Figure 3-3. (b)). This large scale macromolecular motion is responsible for the shape change in LCEs and other SCPs (Y. Lee, Lee, Hwang, Lee, & Cho, 2015; Mao et al., 2015; K. Yu, Ritchie, Mao, Dunn, & Qi, 2015) . The original shape can be recovered by irradiating the SCP with a different wavelength of light (visible) to induce the *cis-trans* isomerization of the azo

molecule. Since the *cis-trans* isomerization can be induced by both heat and light, heating the LCE above its T_g is another technique to recover the polymer's original shape.

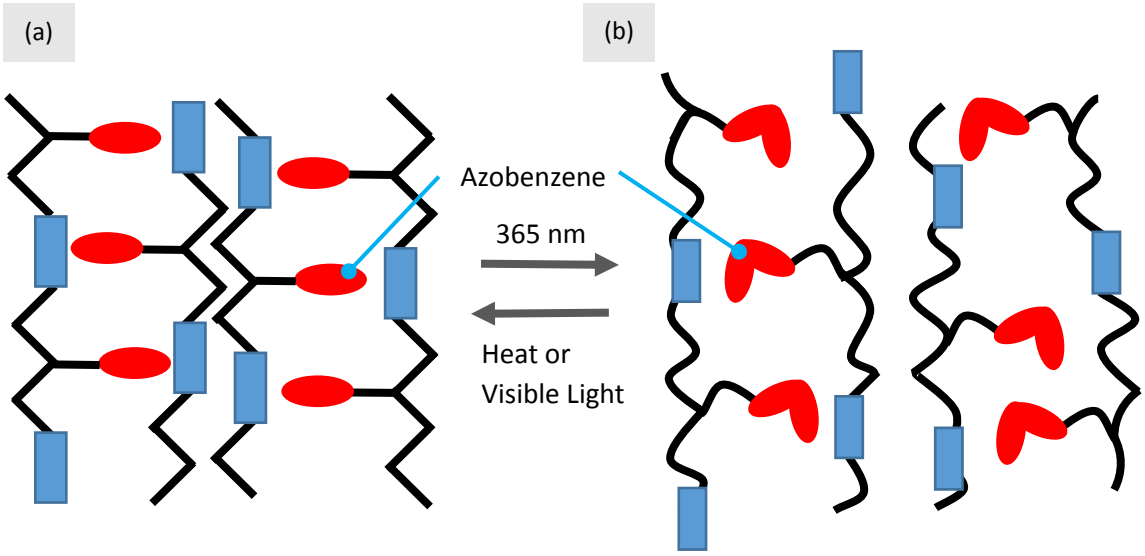

Figure 3- 3. Schematic of the volumetric change of an azobenzene shape changing polymer network that begins in an a) ordered liquid crystalline phase and b) transforms into a disordered conformation when exposed to UV light. The polymer is capable of returning to its original network structure when exposed to high temperatures or visible light.

Previously, researchers have synthesized a single polydomain LCE film that bends in controlled directions by altering the polarization angle of linearly polarized light . The polydomain consists of many micro-sized azobenzene liquid crystal moieties that are aligned in a single direction in each domain, but overall, the moieties are aligned randomly. During light activation, since there are moieties aligned in all random directions the linear polarized light only reacts with moieties aligned in its direction causing a trans-cis isomerization, which induces bending in the direction of linear light (Y. Yu et al., 2003) . The azobenzene moieties possess a strong absorption,

so the moieties on the surface of the film absorb a majority of the light, but the moieties below the surface do not react and cause a contraction on the surface that prompts the bending. One downside to this azobenzene LCE is that it needs to be heated above its T_g in order to actuate. The LCE film, measured at 4.5 mm x 3 mm x 7 µm, is placed onto a heated copper stage set at 85°C and illuminated with linear polarized 3.5 mW/cm^2, 366 nm UV light. The film bends in the direction of the linear polarized UV light in 10 seconds and can unbend when exposed to visible light in 10 seconds (24.2 mW/cm^2, 547 nm and 26.8 mW/cm^2 , 577 nm) (Figure 3-4). This methodology serves as a starting point for our azobenzene research and is discussed later in the article.

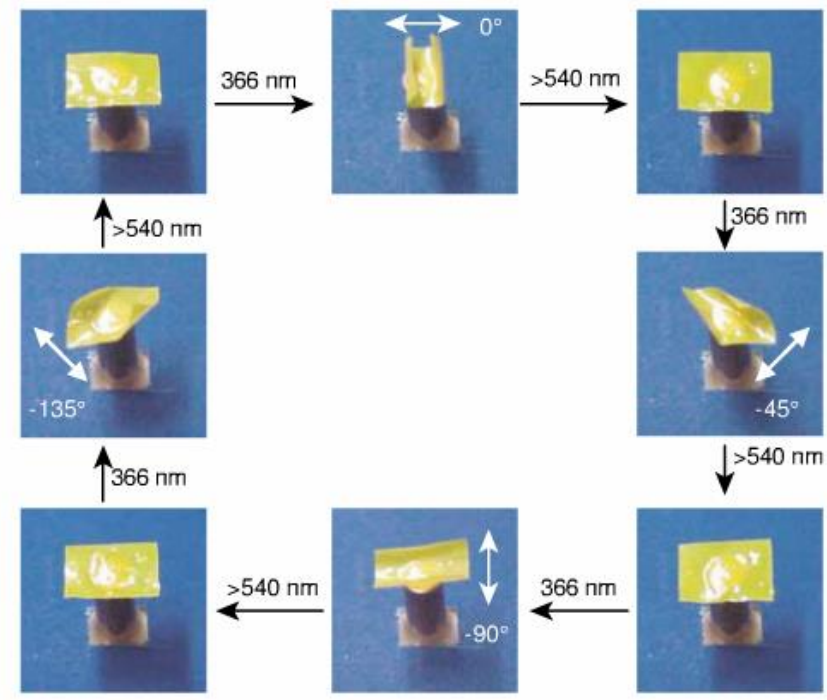

Figure 3- 4. Directional photobending test of a single polydomain LCE film. The film is placed onto a heated copper stage set at 85°C and exposed to different light sources. The film bends in the direction of the linearly polarized UV light (3.5 mW/cm^2, 366 nm) and unbends when exposed to visible light (24.2 mW/cm^2, 547 nm and 26.8 mW/cm^2, 577 nm). The bending takes 10 seconds and the unbending takes 10 seconds. *(Y. Yu et al., 2003)* . Adapted with permission from Nature, 425(6594), pp. 1, under Nature Publishing Group.

3.2.2 Results

The study of SCPs offered comprehension into the mechanism that these materials exhibit a photo-induced reversible shape change. However, one issue faced with the research was that current azobenzene SCPs were not compatible with our 3D-printing systems. Current SCPs consist of crosslinked elastomers that once cured lose most of their processing capabilities. They cannot be extruded into a filament or melt processed like standard thermoplastic polymers, which is necessary for some 3D printing systems such as FDM printers. This limitation has inspired us to design and synthesize a series of novel main-chain and side-chain azobenzene LC polymers (LCPs) for the goals of our project. Originally, an azobenzene PLA mixture would be synthesized and converted into a filament for FDM printing; however, it was discovered that there would be no photomechanical reaction due to the polymer backbone of PLA being too stiff. In the end, three different types of azobenzene SCPs were synthesized for the purpose of this project.

The first version of the azo SCP that would be used as an FDM printable material was based on *Yu et al.'s* work (Y. Yu et al., 2003) . Here, a LC monomer (Figure 3-5. (a)) and a diacrylate crosslinker (Figure 3-5. (b)) are prepared using thermal polymerization. Both of these molecules possess azobenzene moieties and possess different phase transitions when cooled from 95°C. During cooling, the LC monomer transitions from an isotropic phase to a nematic crystalline phase. The diacrylate crosslinker transitions from a crystalline phase to an isotropic phase when cooled to 98°C. The synthesis was successful, but there were issues with the film preparation because it required an oxygen-free environment. This caused the desired thin film to develop a mix of small particles that were less than ~5 mm in length and width.

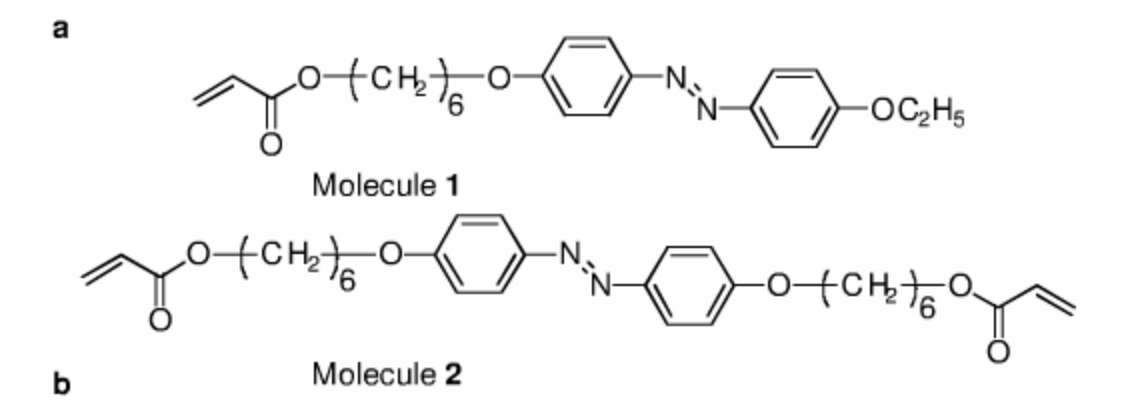

Figure 3- 5. The chemical structure of the a) liquid crystal monomer (molecule 1) and b) the crosslinker (molecule 2) that both contain azobenzene. *(Y. Yu et al., 2003)* Adapted with permission from Nature, 425(6594), pp. 1, under Nature Publishing Group.

Azobenzene SCP particles were photomechanically tested based on previous procedures that placed the film on a heated copper stage set above the film's glass transition temperature (85°C) (Figure 3-6. (a)) (Y. Yu et al., 2003) . Below the T_g, the SCP is stiff and prevents photomechanical bending, which is why the material needs to be heated. Next, a 366 nm UV LED with an intensity of 20-30 mW/cm^2 irradiates the azo SCP, which causes bending in ~10 seconds (Figure 3-6. (b)). The bent film returns to its flat state when the UV light is removed and visible light is used to irradiate the film. During the unbending tests, the process took around 150 seconds to return to its initial flat state (Figure 3-6. (c)). Overall, the photomechanical bending follows the same process as previous research; however, it was decided that the material would not fit our needs as a 3D printable material due to the required oxygen-free polymerization environment and required heating above T_g for photomechanical bending. In the end, a room temperature photomechanical bending azo SCP would be most suitable for the 4D printing needs.

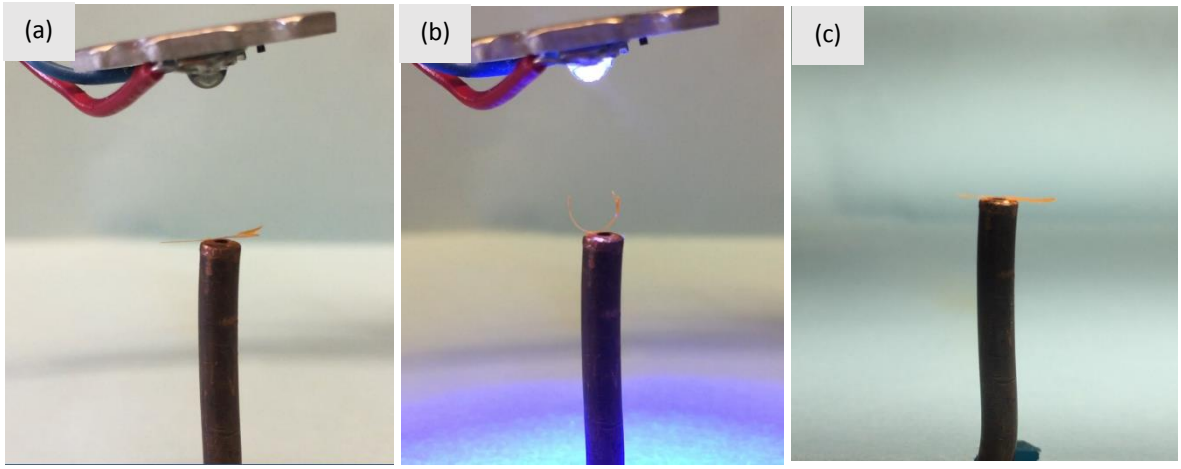

Figure 3- 6. An azobenzene SCP is heated on a copper stage set at 85°C and displays reversible shape change if light is turned on or off. a) The SCP begins in a flat shape and b) induces bending for 10 seconds when exposed to 366 nm light. c) The azobenzene SCP takes 150 seconds to return to flat shape when exposed to visible >455 nm light.

3.3 Synthesis and Conversion of an azobenzene poly(hydro- methylsiloxane) shape changing polymer into a solution for a syringe 3D printer

3.3.1 Synthesis and Experimental Setup of Azobenzene MeOABHx and DR1Hx Polymers

A second linear azobenzene SCP was synthesized that better suited our printing and photo activation needs. The polymer was capable photomechanical bending without the need for heat and the polymer was capable of being converted into a solution that was inserted into a syringe and 3D printed. A poly(hydro- methylsiloxane) (PHMS-g-MeOAB) was synthesized that grafts an azobenzene AB copolymer (Figure 3-7. molecule 1) onto a siloxane backbone to form a side-chain polymer (Figure 3-7. Molecule 2). The synthesis used a platinum catalyst (H_2PtCl_6) for Pt catalyzed

hydrosilylation. This final product, (E)-[-4-(hex-5-en-1-yloxy)phenyl](4-methoxyphenyl)diazene , also known as MeOABHx was synthesized using standard Williamson etherification settings. This photo polymer possessed a T_g below room temperature that removed the need for the SCP to be heated during light activation. The SCP also possessed the property of solubility in solvents, which allowed the SCP to be converted to a solution that was mixed with toluene for syringe printing. This printing method uses the concept of bilayer films, where the azo SCP acts as the active layer and a Kapton film acts as a passive layer. The mechanics of the light activation of bilayer films will be discussed later in the paper.

Finally, a third azobenzene SCP was synthesized using an azo dye N-Ethyl-N-(2-hydroxyethyl)-4-(4-nithrophenylazo)aniline, also called Disperse Red 1 (DR1Hx) (Figure 3-8. molecule 3). Potassium hydroxide and a phase transfer catalyst used in a hydrosilylation reaction synthesized the anticipated DR1Hx product. However, there were issues synthesizing DR1Hx using the same conditions as MeOABHx because the dye DR1Hx contains a basic tertiary amine that poisons the chloroplatinic acid during the hydrosilylation reaction. The synthesis of DR1Hx generated about 35% of polymer with an azobenzene grafting density of 0.69. This synthesis is much lower when compared to the MeOABHx synthesis, which yielded about 75% polymer and an azobenzene grafting density of 0.84.

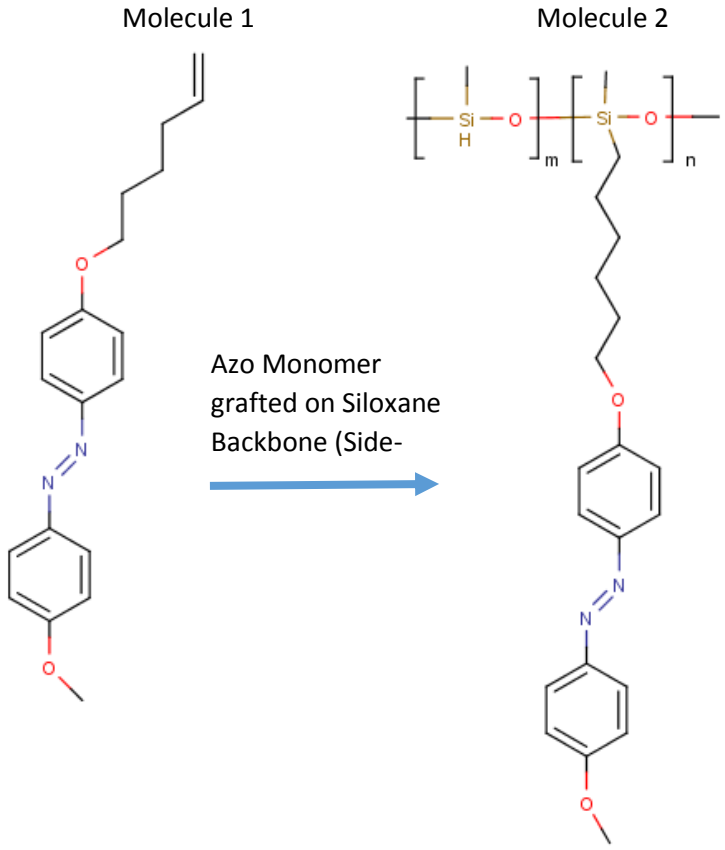

Figure 3- 7. The chemical structure of an azobenzene AB copolymer (molecule 1) that is grafted onto a polysiloxane backbone to form an azobenzene poly(hydro- methylsiloxane) (PHMS-g-MeOAB) (molecule 2).

Molecule 3

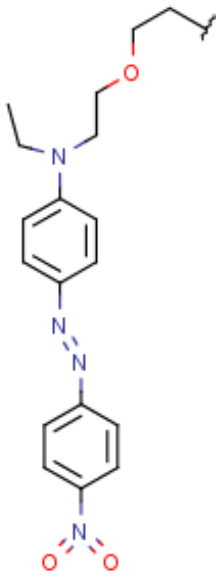

Figure 3- 8. The chemical structure of an azo dye N-Ethyl-N-(2 hydroxyethyl)-4-(4-nithrophenylazo)aniline, also known as Disperse Red 1 (DR1Hx) (molecule 3), which is used to synthesize a second azobenzene PHMS SCP.

3.3.2 Results

A 3D bioprinter (Tissue Scribe) from 3D Cultures was used to print a solution of the azobenzene PHMS-g-MeOAB. An 8 weight percent (% w/v) of azobenzene SCP toluene solution was loaded into a 10 ml syringe with a 25 gage nozzle tip. A rectangle, measuring 6.20 mm L x 20 mm W, was printed on a Kapton film that measured at 40 mm L x 10 mm W x 25.4 µm H. The printer speed was set to 200 mm/min and the height of the nozzle was measured manually at 0.25 mm above the Kapton film. The printer nozzle and substrate were set to room temperature 25°C. The designs were created using Creo Parametric 3.0 and converted to G-code. The printed rectangle acted as a hinge for the bilayer product and used for the photomechanical bending tests (Figure 3-

9. (a) & (b)). Similar methods were used for printing the DR1Hx polymer using 10 %w/v of the azobenzene SCP toluene solution. The DR1Hx solution did not mix as well with the toluene as compared to the MeOABHx polymer. The DR1Hx was also noticeably more viscous, but 3D printed very well.

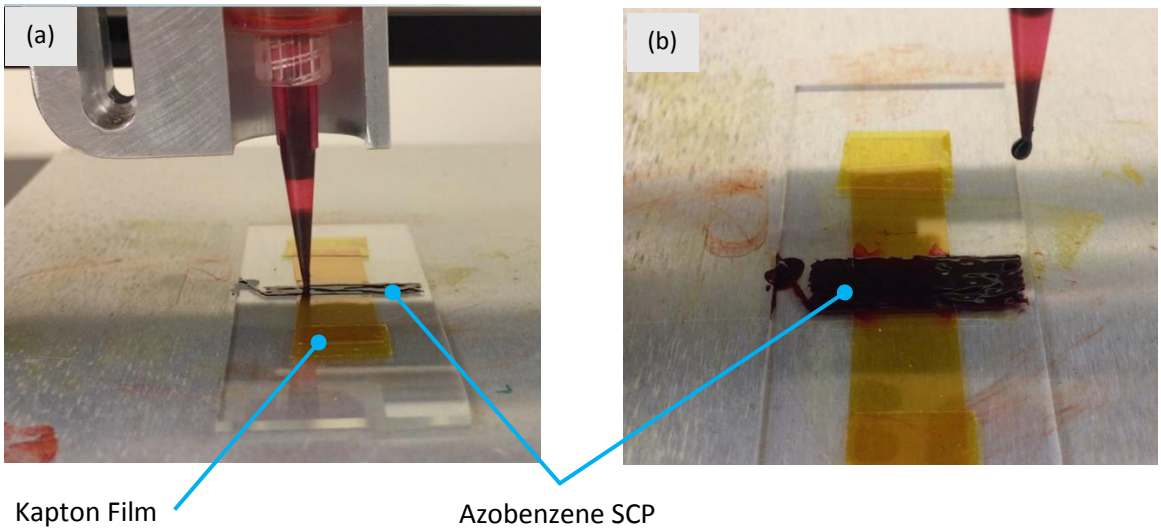

Figure 3- 9. (a) Experimental printing process of the azobenzene SCP hinge using a syringe 3D printer and (b) its final printing design after the azobenzene SCP has been bonded to the Kapton film. The passive Kapton film measures at 40 mm x 30 mm x 25.4 μm and the 3D printed azobenzene polymer hinge measures at 6.2 mm x 10 mm.

3.3.3 Outcomes

The outcomes of this aim offered knowledge on the design and synthesis, along with the concepts of azobenzene photoisomerization and azobenzene SCP 3D printability. The knowledge gained from this aim provided insight on what factors affect the photomechanical bending of azobenzene SCPs and what 3D printing techniques are possible for printing the azobenzene SCPs. Three different azobenzene SCPs have been synthesized for the purpose of this project. The first

SCP synthesized is an LCE film containing an azobenzene chromophore. It was successful in inducing photomechanical bending and unbending when exposed to UV and visible light. The small decrease in microscopic size and ordering of the LC components led to a substantial macroscopic volume contraction on the surface of the film that resulted in bending. This is caused by azobenzene moieties on the surface of the film reacting to the light, but the bulk of the material not absorbing the light energy, thus causing the anisotropic contraction on the surface of the film (Ikeda, Nakano, Yu, Tsutsumi, & Kanazawa, 2003) . However, the LCE film possessed difficulties with the synthesis and required heating above the film's T_g (85°C) during photoactivation. The difficult film fabrication and the material's high T_g for photomechanical bending were considered negatives for the material processing and stimuli activation. We wanted to remove the need for multiple stimuli activation for the material and focus on only requiring light to actuate the materials. A new approach to the 4D printing light activated polymer was addressed due to these needs.

An azobenzene monomer grafted to the backbone of a polysiloxane polymer was synthesized (MeOABHx). This polymer possessed a T_g below room temperature that allowed for photomechanical bending without heating, which simplified the behavior and design of the SCP products, since not all applications are compatible with temperatures up to 85°C. The polymer also possessed the ability to be combined with a solvent (toluene) that can be inserted into a syringe and 3D printed. These procedures allowed us to understand what 3D printing methods are best suited for our research. Next, another azobenzene SCP (DR1Hx) was synthesized to compare its printability and photomechanical behavior to the MeOABHx. This polymer was capable of 3D printability and shape change; however, it possessed difficulty with the synthesis process and lacked miscibility with the toluene solvent. Other solvents such as heptane could be used to test the miscibility of the DR1Hx for improved 3D printing. The physical properties of the two ideal polymers (MeOABHx and DR1Hx) will be discussed and compared later in this paper. In the

future, a different photoisomerable SCP could be synthesized, such as spiropyrans, to compare the printing and shape changing properties to azobenzene materials.

3.4 Characterizing of the Azobenzene Shape Changing Polymer (SCP) for the purpose of 3D printing and photomechanical actuation

3.4.1 Experimental Setup for the Characterization of the Azobenzene SCPs

After synthesis, the chemical composition, structure, molecular weight, crystallinity, absorbance, bending efficiency, reaction time, and mechanical strength of the polymers will be studied using a number of corresponding techniques: differential scanning calorimetry (DSC), thermogravimetric analysis (TGA), nuclear magnetic resonance spectroscopy (NMR), optical polarizing microscopy, X-Ray diffraction (XRD), attenuated total reflectance infrared spectroscopy (ATR-IR) and UV-Vis spectroscopy, cyclic photomechanical tests, and a dynamic mechanical analysis (DMA). DSC will be used extensively to examine the LC phases and T_g values of the resulting polymer. TGA and DSC will be employed to determine the thermal stability of the SCP. Optical polarizing microscopy will be used to confirm and help identify LC phases present in the material. NMR, XRD, and ATR-IR will be used together to determine structure and composition. Specifically, XRD will be used to study the crystal structure of the LCPs. The DMA will be used to study the photomechanical response and measure the generated stress when the polymer is exposed to different wavelengths of light and different passive layer thicknesses.

The molecular weight of the polymer will be evaluated using size exclusion chromatography (SEC) and NMR spectroscopy. The molecular weight is an important factor because the mechanical performance of the material can reduce significantly if the molecular

weight is too low. Also, the solubility and processing can affect the photomechanical performance if the molecular weight is too high. Synthesis conditions such as concentration, temperature, and monomer ratio can be controlled and tailored to obtain an appropriate molecular weight for different applications.

3.4.2 Results

The chemical composition of the final product azobenzene PHMS MeOABHx and DRH1x polymers were characterized using proton nuclear magnetic resonance (^{1}H NMR). The first ^{1}H NMR shows that the azobenzene AB copolymer possessing three methyl chains was successfully synthesized, noting peaks centering at 8.0 and 7.0 ppm that represent the azobenzene compound, the three methyl groups that center peaks around 2.25-1.25, and the double bond at the end of the methyl groups with peaks at 5.75 ppm and 5.25 ppm (Figure 3-10). Next, an ^{1}H NMR was performed on the azobenzene AB copolymer grafted to the siloxane backbone and proved that the synthesis of MeOABHx was successful (Figure 3-11). A reduction in the double bond (5.75 ppm and 5.25 ppm) shows that the azobenzene monomer was successfully grafted to the siloxane backbone and maintained the same concentration of azobenzene compounds in the polymer, ~250 at 8.0 and 7.0 ppm. ^{1}H NMR was used to characterize the final products of DR1Hx, which did not synthesize as well as the MeOABHx polymer by means of similar conditions (Figure 3-12). The typical yield of the final polymer was 75% that possessed a 0.84 azobenzene grafting density. The DR1Hx only yielded 35% of the final polymer with an azobenzene grafting density of 0.69. This shows that the synthesis of DR1Hx was not as efficient as the MeOABHx because DR1Hx contains a basic tertiary amine that poisons the chloroplatinic acid during the hydrosilation reaction and produces small amounts of crosslinking in the final product. The low yield of the DR1Hx polymer,

unsolicited side reactions, purification difficulties, and time consuming process made the DR1Hx polymer less desirable to use in our light reactive 4D printing experiments. Ergo, there was more focus on the MeOABHx polymer for use in our 3D printing and photomechanical testing experiments. In the future, different catalysts that do not poison the functional groups in the DR1Hx polymer could be used for synthesis.

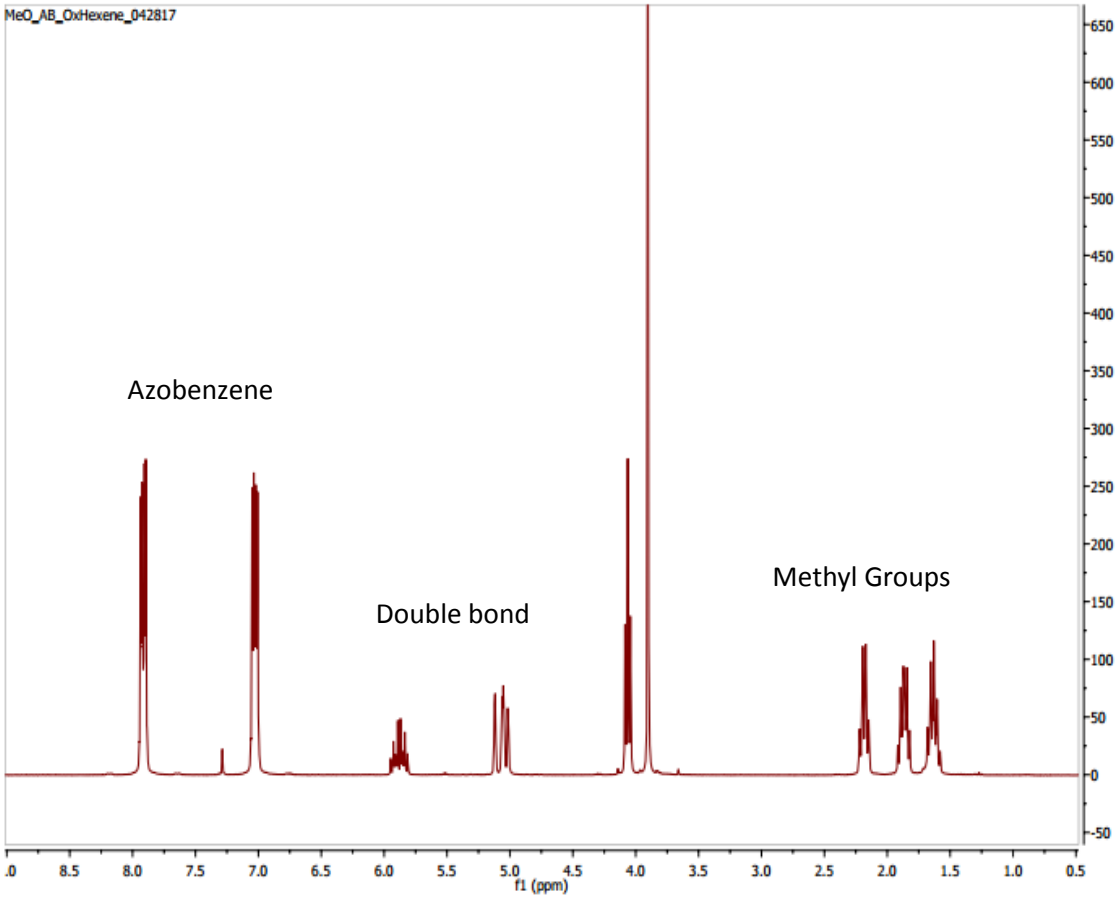

Figure 3- 10. The ^{1}H NMR for the synthesized azobenzene AB copolymer with three methyl groups and the double bond at the end of the methyl groups. The data presented was performed by Dr. Frank Ji's lab in the Chemistry Department. It has been adapted with permission by Dr. Frank Ji's lab in the Chemistry Department.

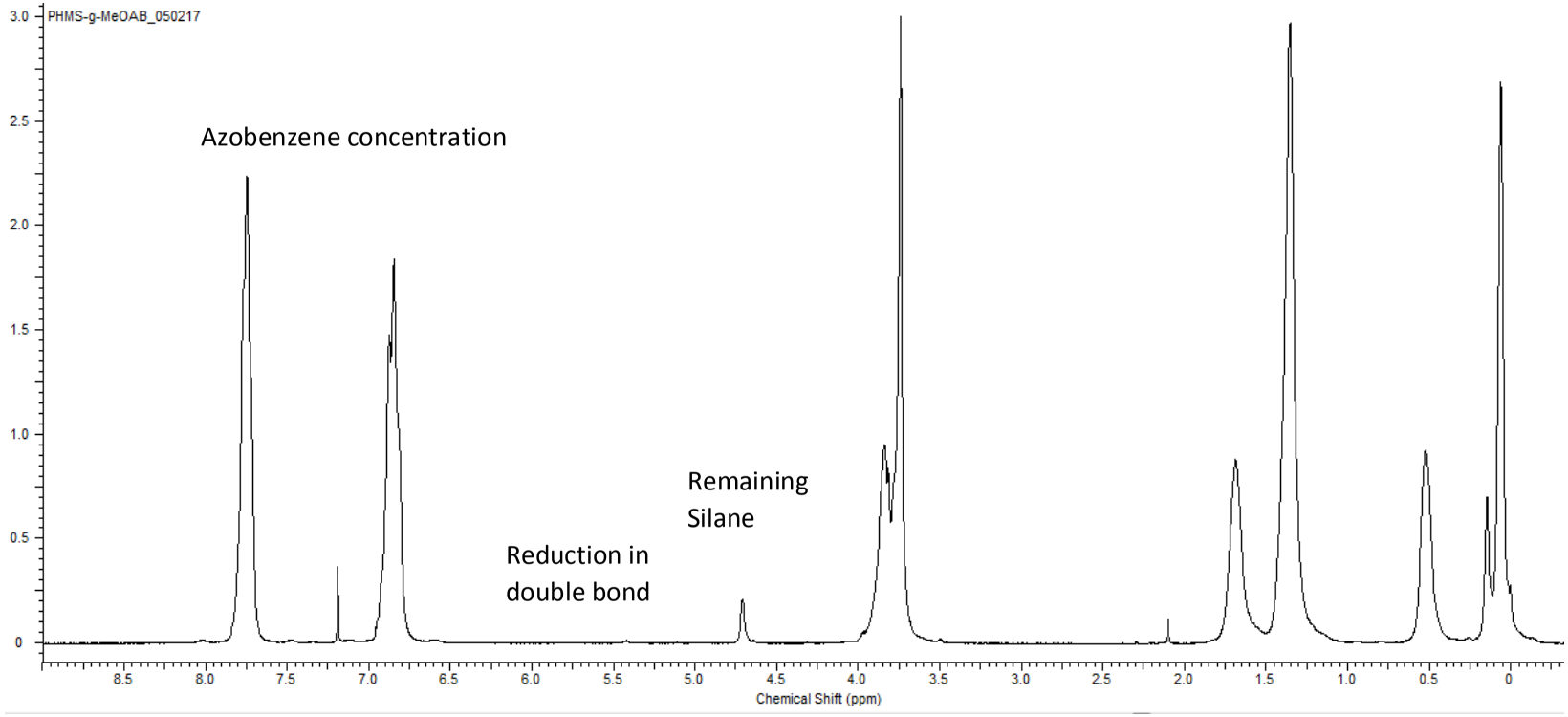

Figure 3- 11. a) The ^{1}H NMR for the synthesized azobenzene AB copolymer grafted to the polysiloxane backbone for the creation of MeOABHx. The data presented was performed by Dr. Frank Ji's lab in the Chemistry Department. It has been adapted with permission by Dr. Frank Ji's lab in the Chemistry Department.

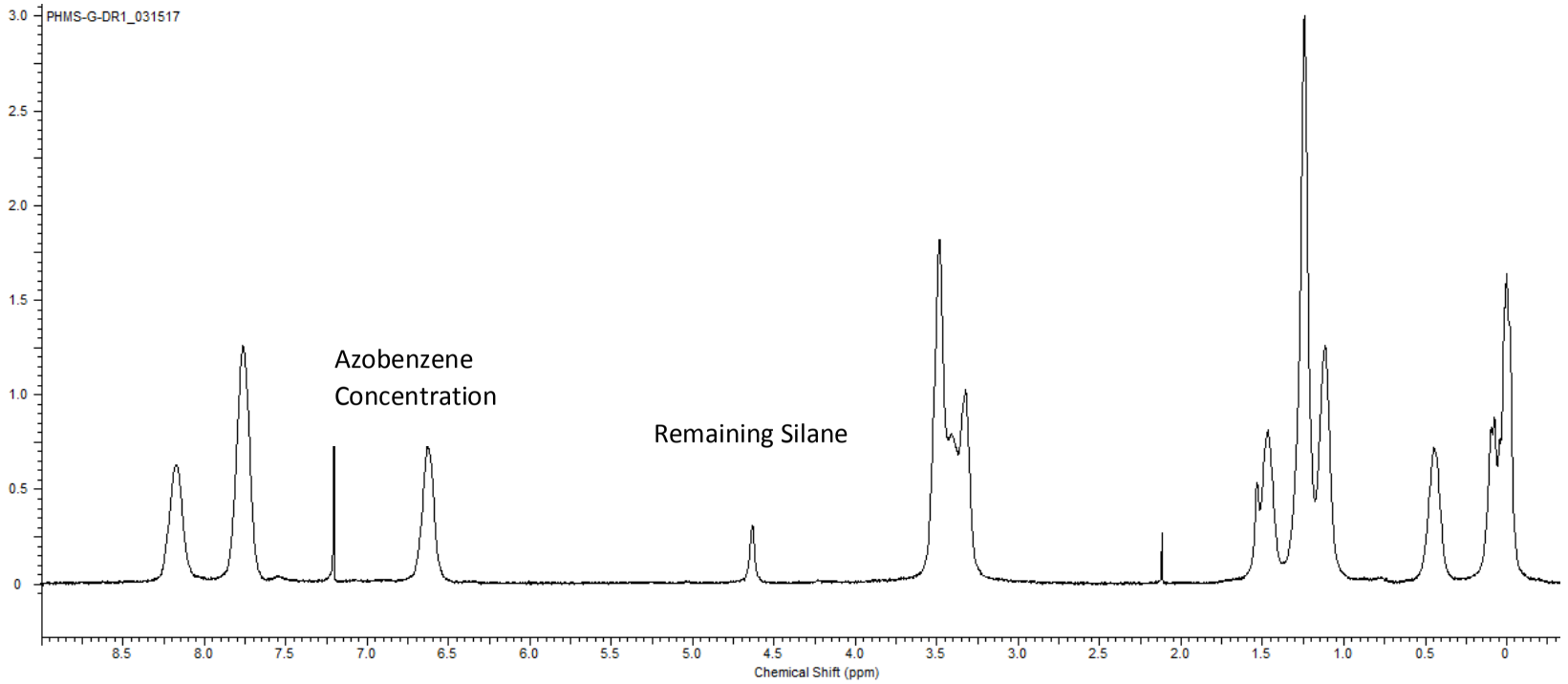

Figure 3- 12. ^{1}H NMR spectrum of the synthesized DR1Hx polymer where DR1 dye is grafted onto the backbone of the polysiloxane. The ratio between the silane peaks and the azobenzene peaks can be used to calculate the ratio of azobenzene in the final product. The data presented was performed by Dr. Frank Ji's lab in the Chemistry Department. It has been adapted with permission by Dr. Frank Ji's lab in the Chemistry Department.

UV-Vis spectroscopy was performed on the azobenzene MeOABHx SCP to observe the absorbance of the material when exposed to different wavelengths of light: UV (365 nm) and visible green light (520-535 nm). The polymer was exposed to the light sources for different exposure times, ranging from 10 s, 20 s, 30 s, and 60 s, to observe the absorbance of the azobenzene moieties. The large absorption peak is apparent, measuring ~1.2, for the *trans* isomer before irradiation (as deposited) at 360 nm (Figure 3-13. (a)). The lack of a peak near 450 nm suggests that the *cis* isomer concentration is reasonably low and may be near 0. When the polymer is exposed to 366 nm UV light for 10-60 seconds the absorption peak at 360 nm decreases, while the peak at 450 nm increases. The UV absorption plot follows the typical absorbance trend for azobenzene materials (K. Lee, Tabiryan, et al., 2011) . Next, the azobenzene MeOABHx SCP's absorbance when exposed to visible light was observed. The data shows that after the SCP is exposed to UV light the 450 nm wavelength has increased in absorbance. When the same material is exposed to visible green light, >450 nm, the 450 nm peak decreases with increased exposure time (Figure 3-13. (b)). Eventually, the 450 nm peak decreased to near 0 and the 360 nm peak increased to its original absorbance peak, ~1.2. The results suggested that the MeOABHx may be capable of shape change when exposed to UV light and shape recovery when exposed to visible light. Results showed that the ideal wavelength for *trans-cis* photoisomerization of MeOABHx would be 360 nm, but the material could be activated between 300-420 nm spectrums (Figure 3-15). The ideal wavelength for *trans-cis* isomerization for DR1Hx would be 420 nm (Figure 3-16)

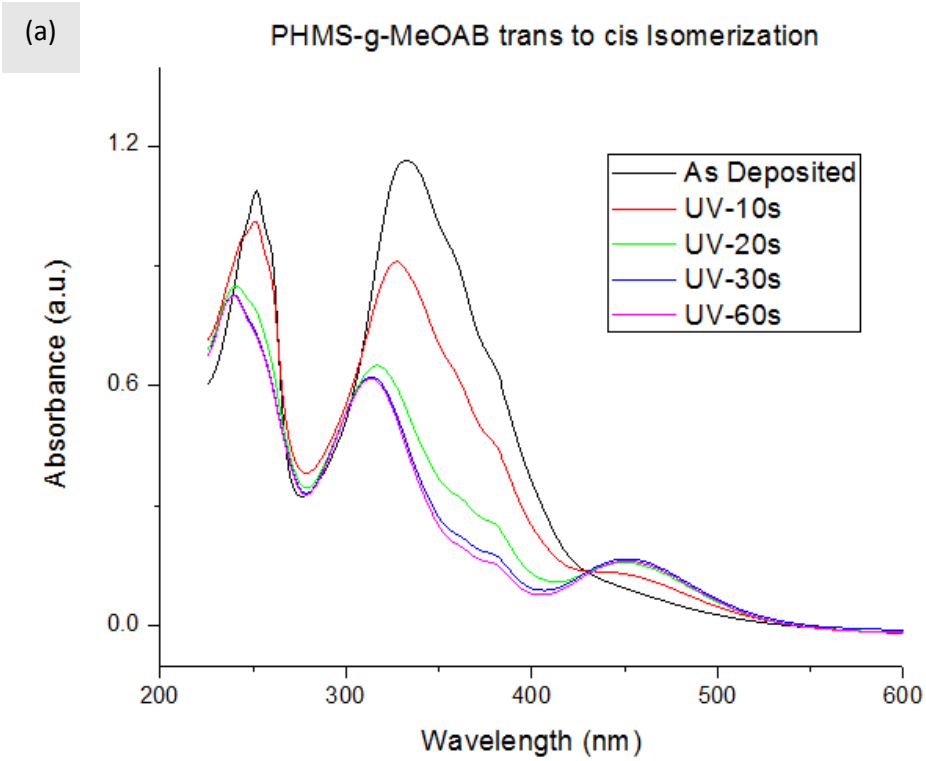

Figure 3- 13. UV-vis spectra of the azobenzene PHMS SCP exposed to (a) UV (365 nm) light for different exposure times: 10 s, 20 s, 30 s, and 60 s. The data presented was performed by Dr. Frank Ji's lab in the Chemistry Department. It has been adapted with permission by Dr. Frank Ji's lab in the Chemistry Department.

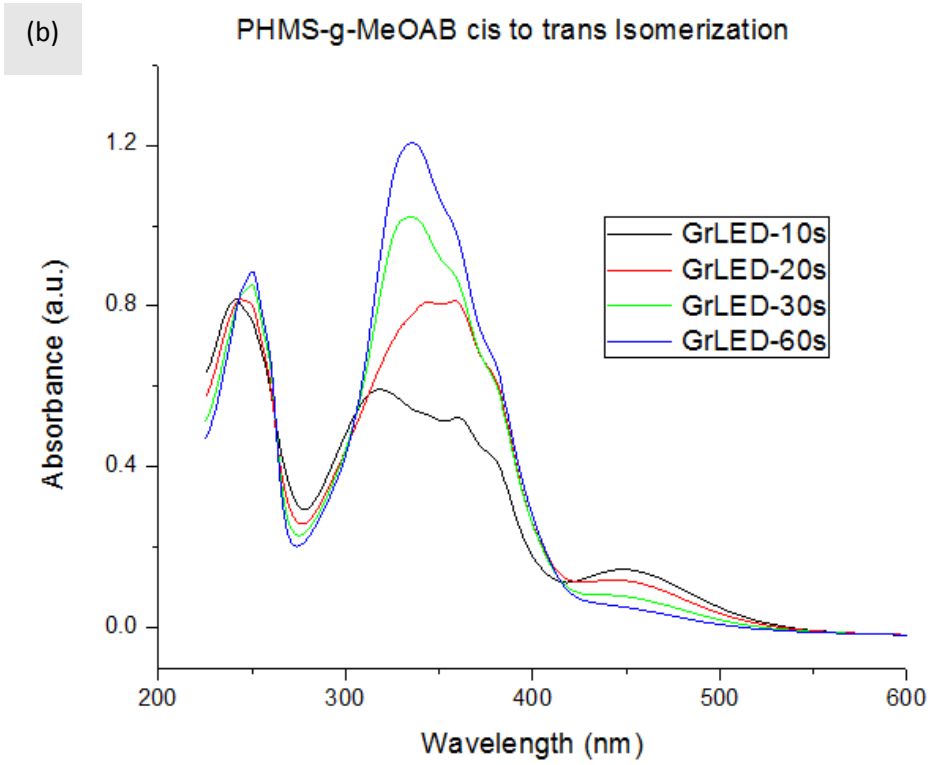

Figure 3- 14. UV-vis spectra of the azobenzene PHMS SCP exposed to visible green (520-535 nm) light for different exposure times: 10 s, 20 s, 30 s, and 60 s. The data presented was performed by Dr. Frank Ji's lab in the Chemistry Department. It has been adapted with permission by Dr. Frank Ji's lab in the Chemistry Department.

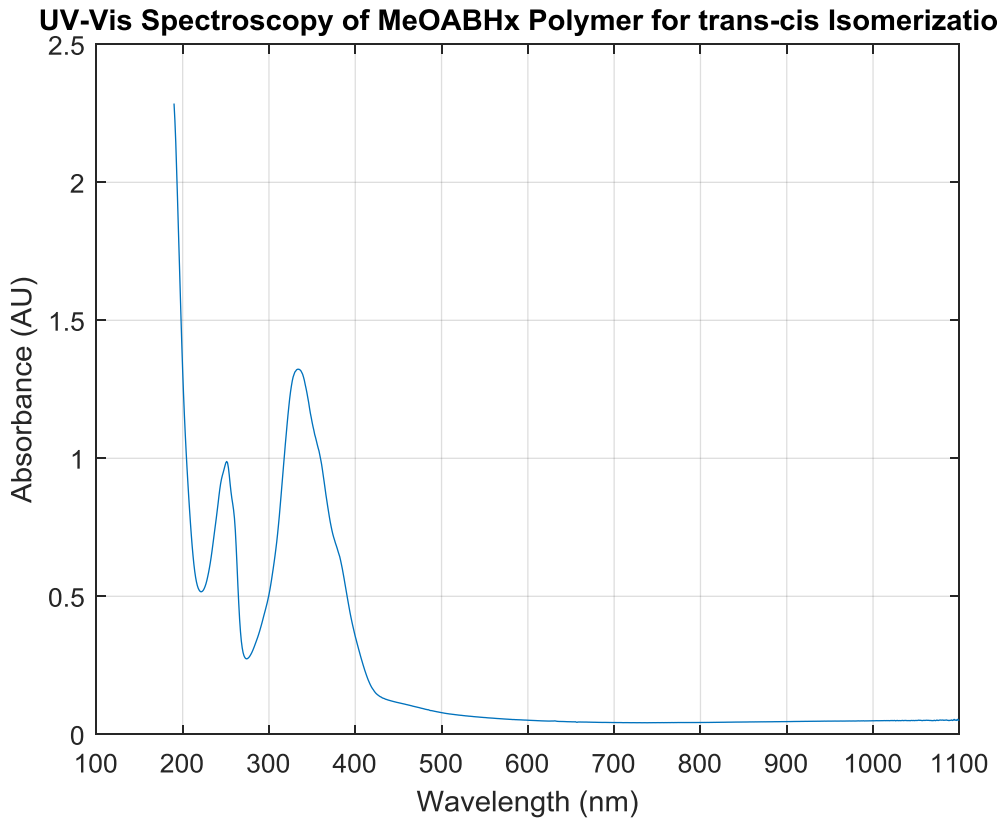

Figure 3- 15. UV-Vis spectroscopy of azobenzene MeOABHx Polymer to determine best wavelength for trans-cis isomerization. The optimal spectrum can be observed at the highest peak of 334 nm. The data presented was performed by Dr. Frank Ji's lab in the Chemistry Department. It has been adapted with permission by Dr. Frank Ji's lab in the Chemistry Department.

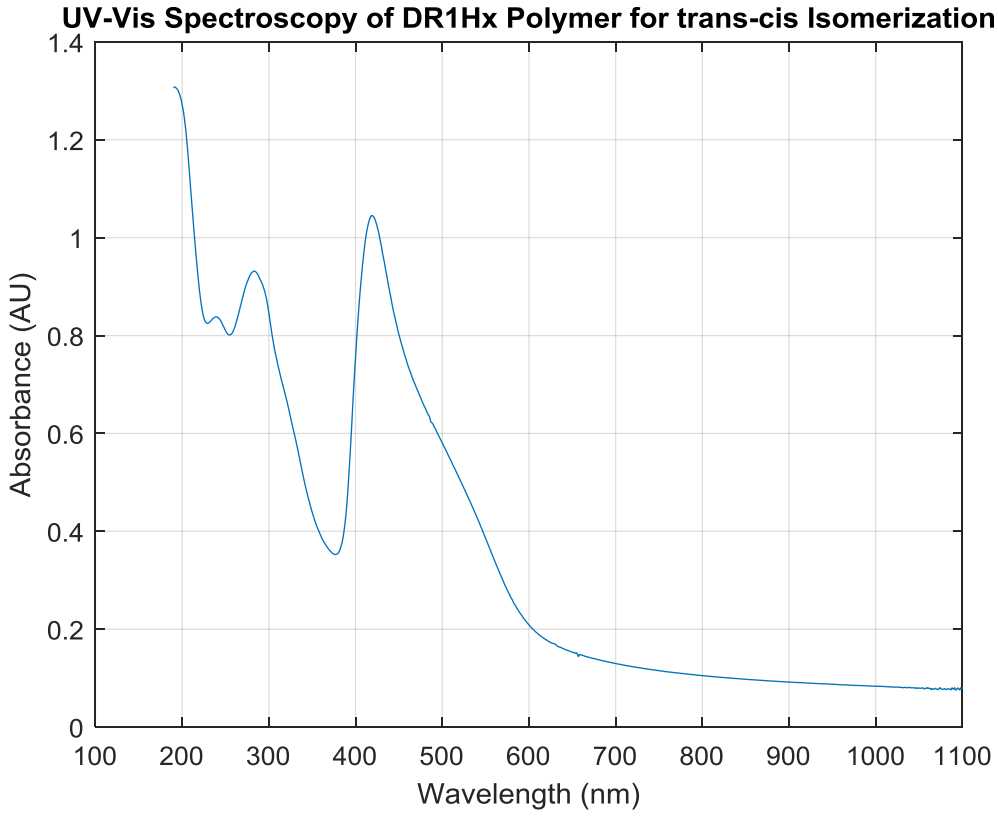

Figure 3- 16. UV-Vis spectroscopy of azobenzene DR1Hx Polymer to determine best wavelength for trans-cis isomerization. The optimal spectrum can be observed at the highest peak of 450 nm. The data presented was performed by Dr. Frank Ji's lab in the Chemistry Department. It has been adapted with permission by Dr. Frank Ji's lab in the Chemistry Department.

Next, Kinetics studies were performed on the two different polymers, MeOABHx and DR1Hx, to observe the absorption overtime while the polymers are exposed to different light sources. From the previous studies, it was determined that the ideal wavelength *trans-cis* isomerization for MeOABHx was 334 nm and the ideal wavelength of *trans-cis* isomerization for DR1Hx was 420 nm. The first experiment exposed MeOABHx to UV light (365 nm) and observe the absorbance at 334 nm. As observed, the average absorbance decreased over time because the *trans* isomers absorb energy in the 365 nm range (Figure 3-17). This causes the *trans* isomers to

isomerize into the *cis* isomer, which absorbs energy at a higher wavelength (>450 nm). As the *trans* isomer convert to the *cis* isomer, the absorbance in the visible light region increases (Figure 3-18).

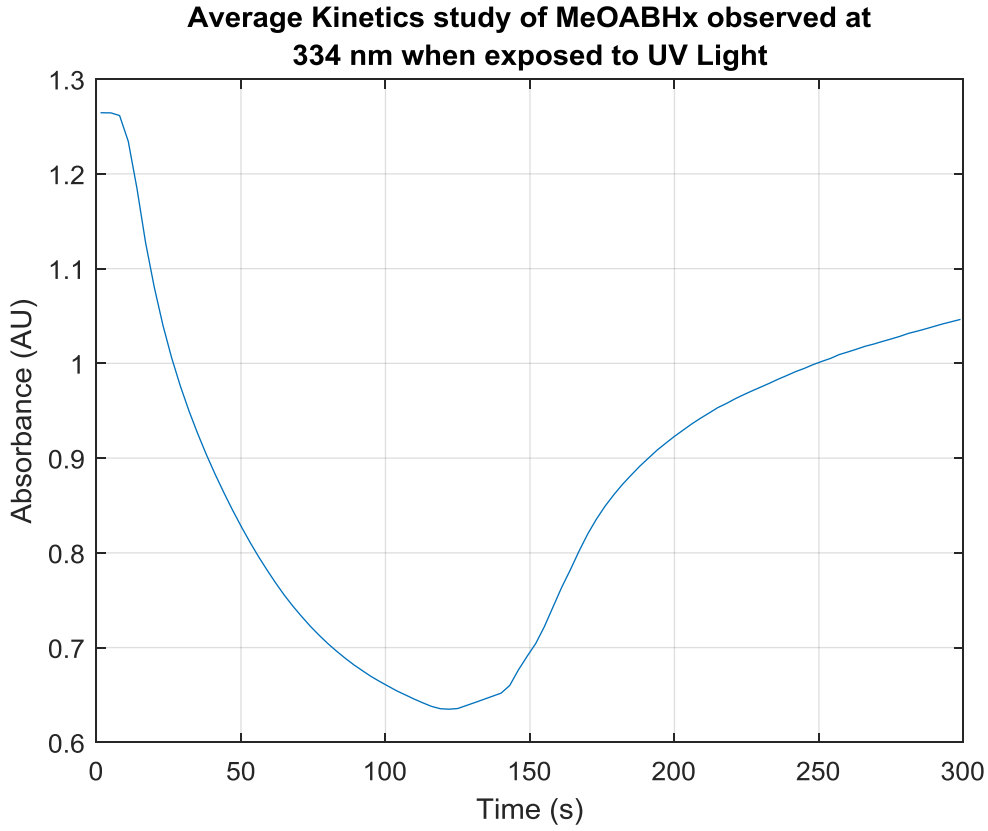

Figure 3- 17. Kinetics study of the MeOABHx polymer that displays the average absorbance observed at a wavelength of 334 nm when exposed to UV light (365 nm). The data presented was performed by Dr. Frank Ji's lab in the Chemistry Department. It has been adapted with permission by Dr. Frank Ji's lab in the Chemistry Department.

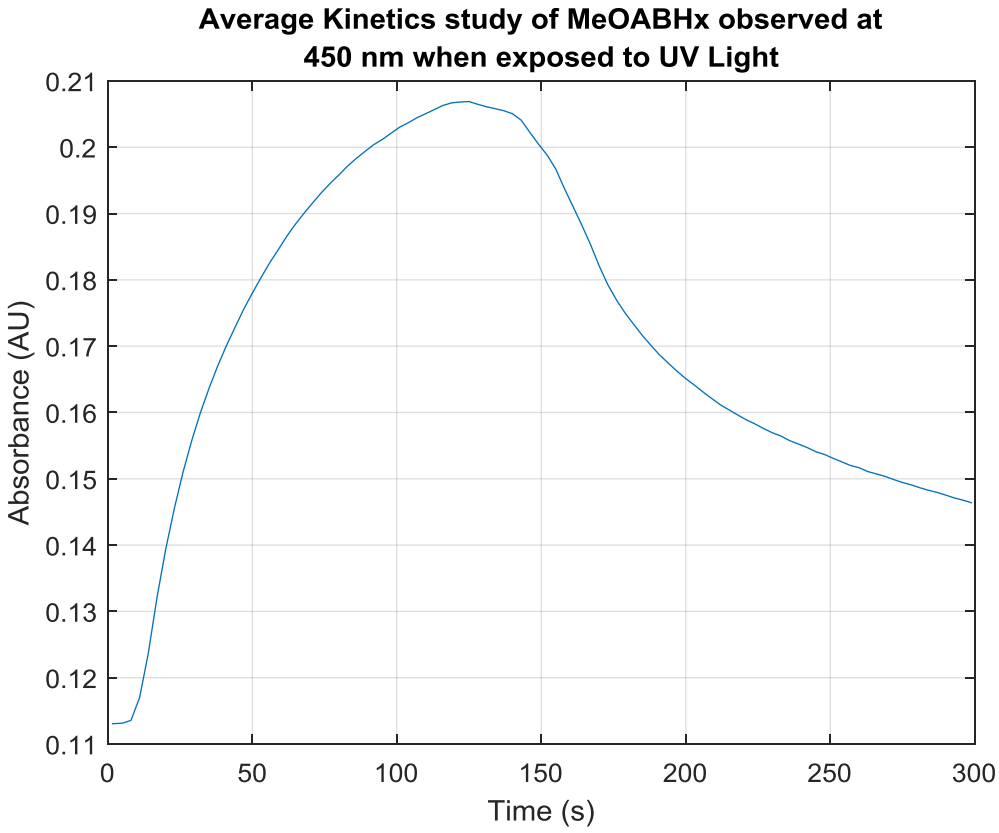

Figure 3- 18. Kinetics study of the MeOABHx polymer that displays the average absorbance observed at a wavelength of 450 nm when exposed to UV light (365 nm). The data presented was performed by Dr. Frank Ji's lab in the Chemistry Department. It has been adapted with permission by Dr. Frank Ji's lab in the Chemistry Department.

In a final test, similar kinetics studies were performed on DR1Hx. DR1Hx ideal wavelength for *trans-cis* isomerization was 420 nm. During the kinetics tests, the material was exposed to visible blue light (455 nm) and the absorbance was registered. It can be observed that the absorbance at 420 nm reduced because a majority of the *trans* isomers convert to the *cis* isomers (Figure 3-19). Reduction in absorption means a majority of the *trans* isomers have converted to *cis* isomer and cannot absorb within the 420 nm spectra. When observing the absorption in the 525 nm

spectra, the *trans-cis* isomerization can be confirmed because the absorbance in the 525 nm wavelength increases, which shows an increase in *cis* isomers (Figure 3-20).

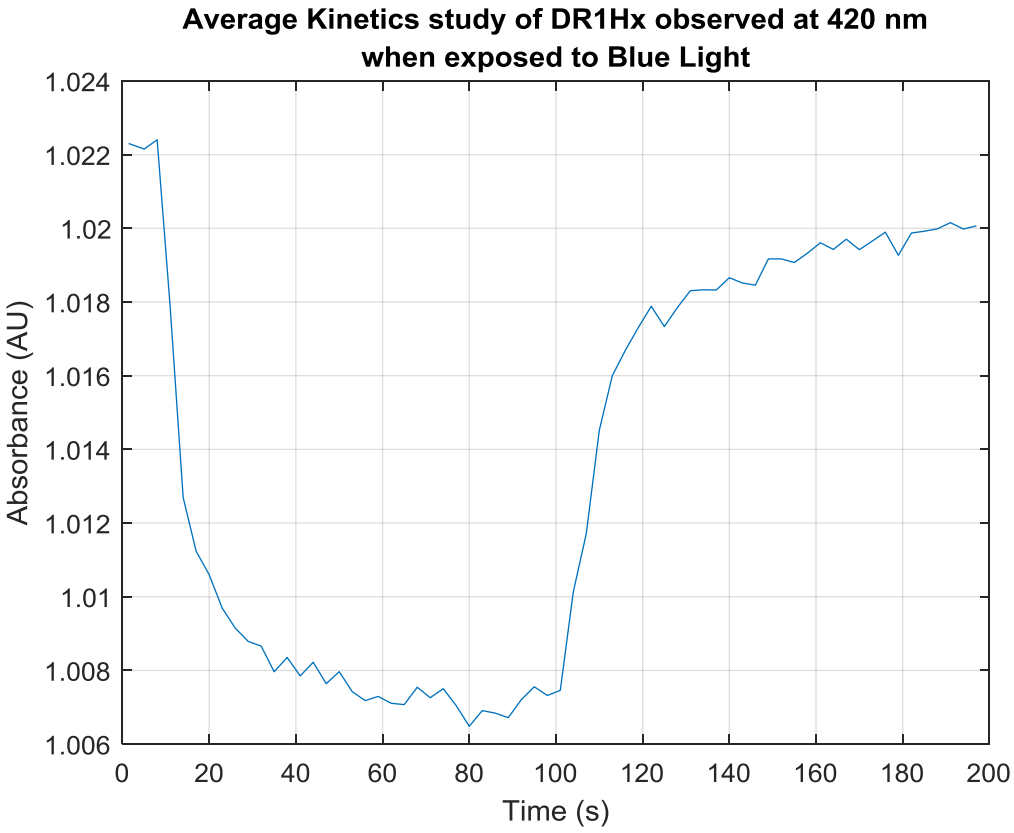

Figure 3- 19. Kinetics study of the DR1Hx polymer that displays the average absorbance observed at a wavelength of 420 nm when exposed to visible blue light (455 nm). The data presented was performed by Dr. Frank Ji's lab in the Chemistry Department. It has been adapted with permission by Dr. Frank Ji's lab in the Chemistry Department.

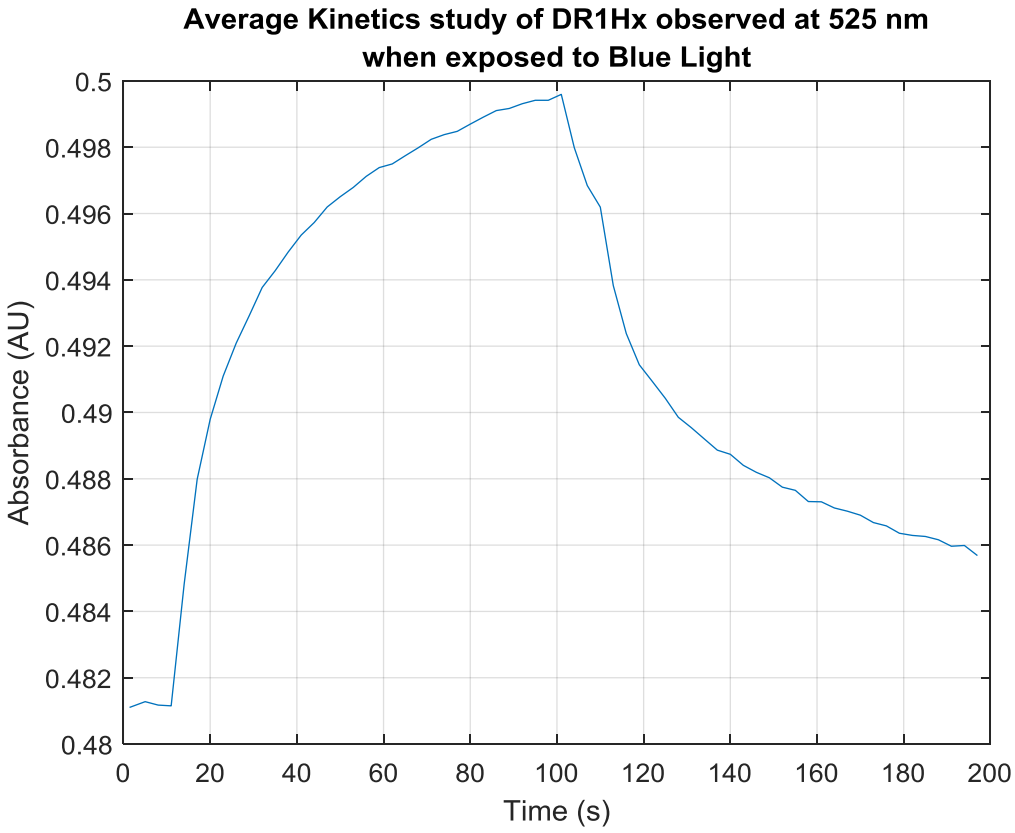

Figure 3- 20. Kinetics study of the DR1Hx polymer that displays the average absorbance observed at a wavelength of 525 nm when exposed to visible blue light (455 nm). The data presented was performed by Dr. Frank Ji's lab in the Chemistry Department. It has been adapted with permission by Dr. Frank Ji's lab in the Chemistry Department.

In our experiments, the synthesized polymers' thermal properties and crystalline properties were determined using differential scanning calorimetry (DSC). DSC is a thermoanalytical technique used to determine important thermal properties of materials such as the T_g, T_m, crystallinity temperature (T_c), and the percentage of crystallinity. All of these properties are important to determining the ideal printing environment of the polymers and the activation environment. Crystallinity of our materials may affect their mechanical strength and thermal properties, which may assist in determining what are the best methods for activating the shape

change of the polymers. Polymer MeOABHx displays two sharp peaks at 97°C and 115°C during the heating rate (Figure 3-15). The 97°C represents the material's T_m and the 115°C peak represents the material's LC phase. At temperatures above 115°C the interactions between the azobenzene moieties breakdown and the material transitions from an LC phase to an isotropic phase. However, the specific LC phase needs to be determined; whether the phase is nematic or smectic. Looking at the DSC curves, the T_g of MeOABHx could not be determined and had to be established through quenching, which revealed it was around 26°C. Next, the DSC of DR1Hx reveals a T_g of 8°C and a T_m of 60°C. The crystallization of the material occurs at 50°C during cooling; however, it is unclear if DR1Hx possesses an LC phase (Figure 3-16).

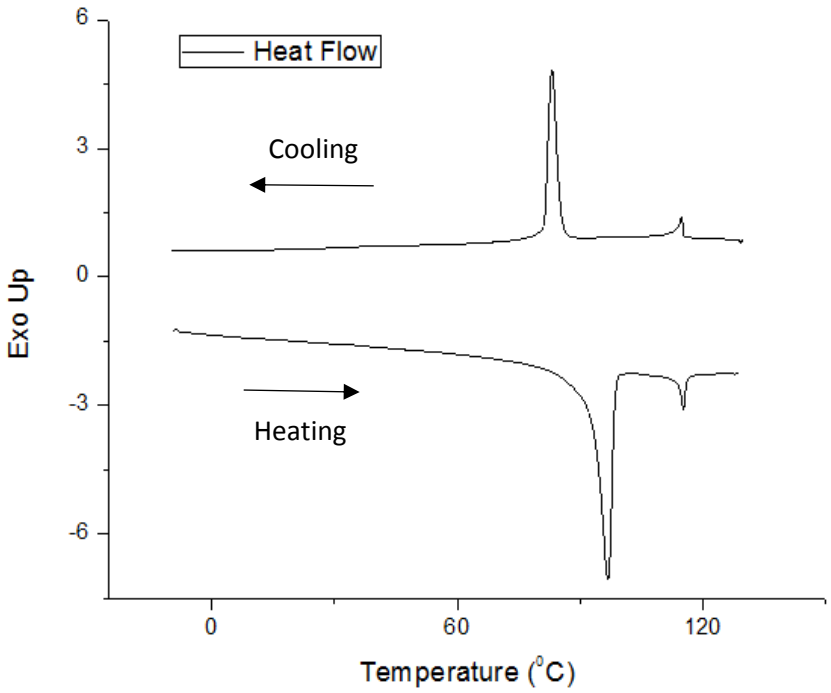

Figure 3- 21. The DSC curve of polymer MeOABHx that displays the material's melting temperature at 97°C and its crystallinity phase between 97°C and 115°C. The heating rate was 10°C per minute and the cooling rate was 5°C per minute. The data presented was performed by Dr.

Frank Ji's lab in the Chemistry Department. It has been adapted with permission by Dr. Frank Ji's lab in the Chemistry Department.

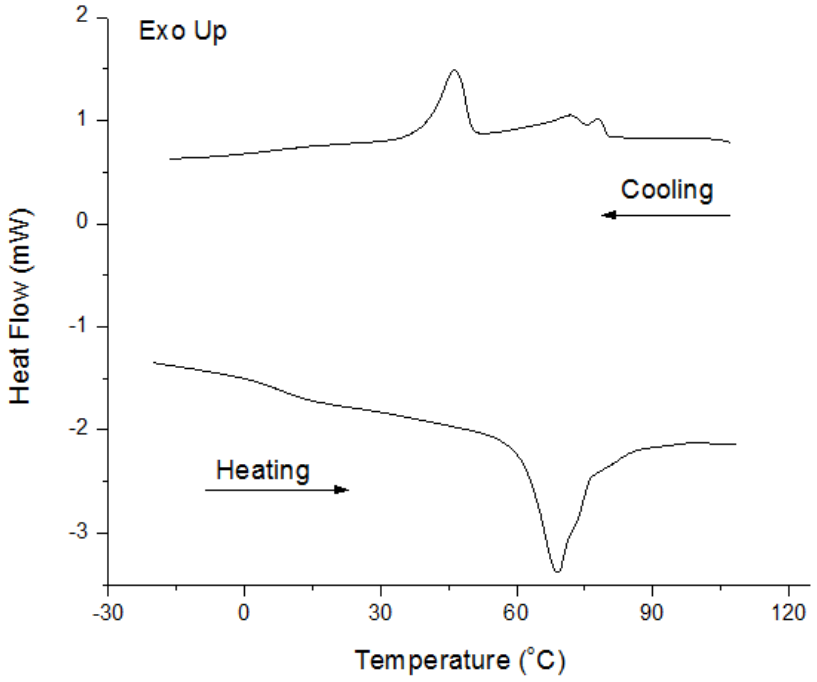

Figure 3- 22. The DSC curve of polymer DR1Hx that displays the material's glass transition temperature at 8°C and its melting temperature at 60°C. Note that the material's crystallinity phase is difficult to observe from the DSC curve and may not exist. The heating rate was 10°C per minute and the cooling rate was 5°C per minute. The data presented was performed by Dr. Frank Ji's lab in the Chemistry Department. It has been adapted with permission by Dr. Frank Ji's lab in the Chemistry Department.

3.4.3 Outcomes

The outcome from this aim aided in the identification of the chemical composition and structure of the synthesized azobenzene SCP. The characterization of the material help in the design of future polymers that possess better photomechanical properties or better printing capabilities. Chemical composition of the polymer was confirmed using the ^{1}H NMR spectroscopy and verified

that the final product corresponded with the desired materials. Two different azobenzene PHMS materials were analyzed. MeOABHx proved to be a much easier polymer to synthesize and provided higher concentrations of the final product. The second polymer, DR1Hx, proved to be more difficult to synthesize under similar conditions and provided limited concentrations of azobenzene and final product post synthesis. In the end, a different catalyst could be used for the synthesis of DR1Hx.

Absorbance of the polymer when exposed to different frequencies of light for different exposure times was performed to determine the ideal wavelengths of light to provoke photoisomerization in the polymer and explore its different methods of isomerization. The data revealed that the highest absorbance peak was around 360 nm, but the longer the exposure time to UV light reduced the peak size. This trend followed the *trans-cis* reaction where *trans* isomers, which absorbed 360 nm wavelength light, converted to *cis* isomers, which absorbed at 450 nm. Alternatively, a *cis-trans* reaction can be induced by exposing the material to visible green light, which increases the number of *trans* isomers, ergo, leading to an increase in absorbance in the 360 nm wavelength (Figure 3-14)). This means that after inducing a *trans-cis* reaction with UV light, a *cis-trans* reaction can be induced using visible light and force the SCP to revert back to its original state. This *cis-trans* isomerization can also be induced using heat, so this introduces two different activation methods for the azobenzene SCP. Next, other light sources such as royal blue (455 nm) light could be tested in the future since the polymer reacts to this wavelength.

A DSC was used to confirm the T_g, T_m, and crystallinity of the polymers MeOABHx and DR1Hx. These properties were important because they identified what temperatures should the polymers be 3D printed at and the ideal environmental temperature for photoactivation. The DSC also revealed the LC phase of the MeOABHx polymer, which may affect the light actuation efficiency. However, the DSC could not identify the LC phase for the DR1Hx polymer and a

separate test may need to be performed on the DR1Hx at different temperatures in order to determine the LC phase or if an LC phase exists. The results show that both polymers possess low glass transition temperatures that are below room temperature. This is a positive characteristic for use as a photoactive shape changing material since it can be activated at room temperature and require no heating, unlike the previous azobenzene LCE that possessed an azobenzene LC monomer and azobenzene crosslinker. There are many varieties of light activated shape changing LCEs, but the materials require simultaneous heating above their T_g and light activation. Typically, azobenzene LCEs possess T_g values higher than room temperature and the macroscale actuation is thoroughly restricted due to stiff polymer chains below T_g. Since MeOABHx and DR1Hx polymers both possess a T_g below room temperature, which measured at 26ºC and 8 ºC, respectively, this removes the need to heat the materials during light activation. The synthesis of these two new azobenzene SCPs simplified the design and testing process for our 4D printing research by reducing the number of concurrent activation methods.

3.5 Investigating the optical and mechanical properties of the azobenzene SCP to see how thickness, surfaces, and geometry affect the absorption of light and efficiency of the photoactive reaction

3.5.1 Investigations into the Photomechanical Bending of Azobenzene SCPs and Experimental Setup

The inspiration for our design comes from previous investigations where researchers managed to synthesize a light reactive azobenzene polysiloxane SCP and bond it with a passive layer, silk fibroin film (Figure 3-17. (a)). The theory is based on the bending of piezoelectric actuators, which are fabricated from a bonded piezoelectric sheet and an elastic sheet. The

deflection of these bilayer actuators is based on the theory that the deflection of bending is proportional to the transverse strain generated in the active layer, the thickness ratio between the two layers, and the Young's modulus of the two different materials. The bilayer structure amplifies the volume change of the active layer, azobenzene SCP, because the azobenzene SCP expands in volume during trans-cis isomerization to induce bending. The silk layer is unreactive to the UV light, but UV irradiation on the active azobenzene side causes the *trans* to *cis* isomerization of the azobenzene moieties and decreases the density of the material, which causes the increase in volume and shape change. The azobenzene moieties return to their original *trans* state when the UV light is turned off and causes the polymer to reduce in volume and unbend back to its original position. Overall, the azobenzene silk bilayer functioned very well as an actuator. The bilayer film displayed fast motions and high angle of bending, up to 115° (Figure 3-17. (b)). Unlike single layer azobenzene films that can bend bidirectionally depending on the location of the light source and polarity of light, the silk bilayer film bends in the direction opposite of the irradiation source if the active layer is facing the light source (Figure 3-17. (c)). If the passive layer is facing towards the irradiation source, then the bilayer film bends towards the irradiation source.

Wen et al. found that the intensity of the light source and the thickness of the passive layer affected the bending efficiency of the azobenzene silk bilayers, which may affect our bilayer materials also. As the intensity of the UV light increased, the final bending angle increased, but maxed out at 90° bending around 70-80 mW/cm^2. They also found the final bending angle decreased with increasing passive layer thickness, which reached a bending angle of 40° at 50 μm silk fibroin thickness. This is interesting design feature because the final bending position of the actuator could be controlled by using different thicknesses of passive film. In our research we tested the effects of using a passive Kapton layer with different thicknesses: 25.4 μm, 50.8 μm, and 125

μm. Both of these design parameters are required to be tested in our photomechanical tests to evaluate the bending efficiency of our azobenzene bilayer films.

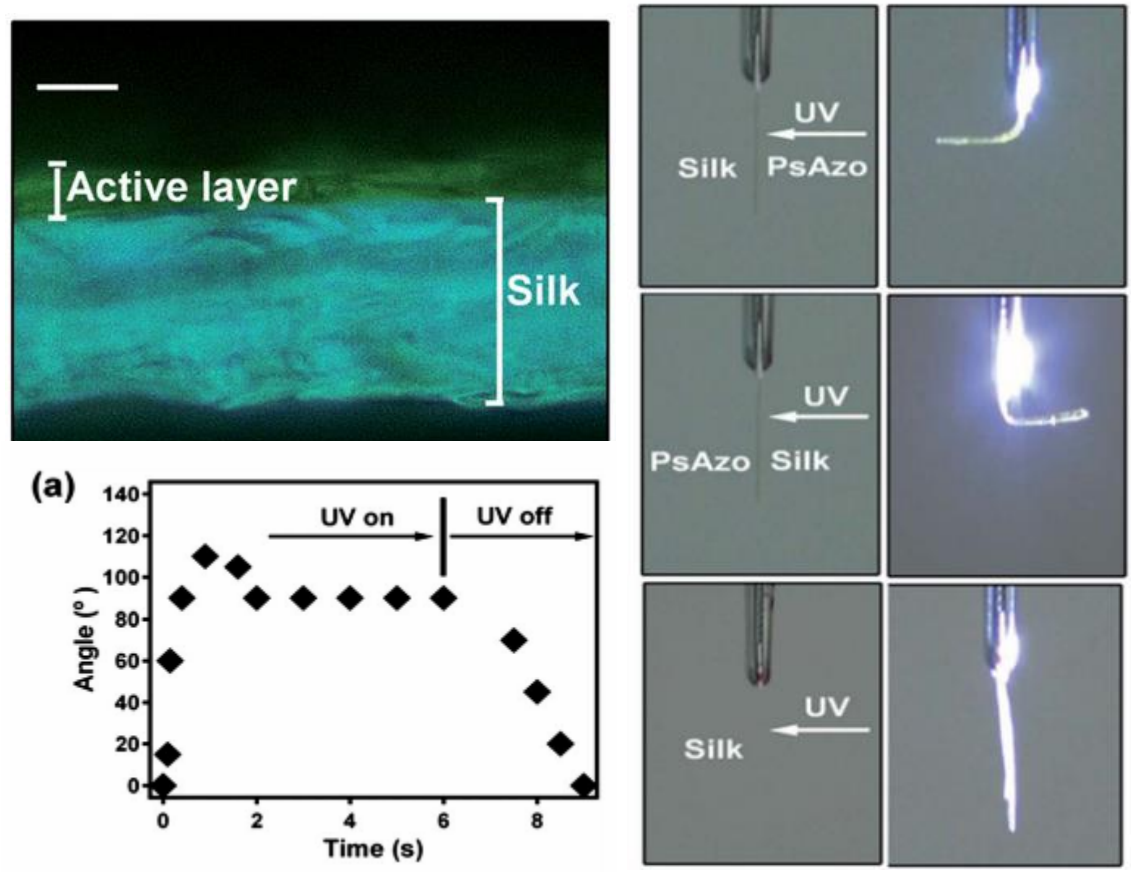

Figure 3- 23. (a) A cross-sectional optical microscope image of the bilayer film. The active layer represents the active linear azobenzene polymer and the silk is the passive layer. (b) A plot of the bending angles for the bilayer actuator when exposed to UV light at 365 nm, 70 mW/cm^2. (c) Images displaying the light activated motion of the silk bilayer film when exposed to UV light at 365 nm, 70 mW/cm^2. The film measures at 2mm x 12 mm x 16 μm. *(Wen et al., 2014)* . Adapted with permission from RSC Advances, 4(23), pp. 11778-11779, under Royal Society of Chemistry.

The silk azobenzene bilayer possessed a low T_g below room temperature, 19°C, similar to our synthesized azobenzene SCPs, which was ideal for our activation requirements. The silk

azobenzene bilayer activation method to induce *trans-cis* isomerization was a UV light (365 nm, 70 mW/cm^2). The passive layer was chosen as silk fibroin because of the material's transparent properties (>90% transmission in the visible light spectrum), exceptional mechanical toughness, and biocompatibility (Jiang et al., 2007; Jin et al., 2005; Lawrence et al., 2010; Lawrence, Cronin-Golomb, Georgakoudi, Kaplan, & Omenetto, 2008; Perry, Gopinath, Kaplan, Negro, & Omenetto, 2008) . The bilayer films were prepared by spin coating the azobenzene polymer onto the silk fibroin films, which means the entire passive layer is deposited with the active azobenzene polymer then custom shapes must be cut out of the bilayer film. Our research proposes to use additive manufacturing technology to dispense azobenzene SCP onto desired location onto the passive bilayer film, which saves waste of SCP material and permits the ability to create more complex and accurate designs. The table displays the mechanical and thermal properties of the previous researcher's azobenzene polymer, the silk fibroin (Nakamura, Magoshi, & Magoshi, 1994), and our Kapton film (Table 3-1).

Table 3- 1. Mechanical and thermal properties of linear azobenzene polymer, silk fibroin film, and Kapton films of different thicknesses tested in the experiments.

Material	**Ultimate Tensile Strength, σ (MPa)**	**Young's Modulus, E (MPa)**	**Glass Transition Temperature, T_g (°C)**	**Thickness, μm**
Linear Azobenzene Polymer	1.3	52.3	19	~2
Silk Fibroin	12.5	753.1	160-210	~12
Kapton Film, 1 mil	231	2500	360-410	25.4
Kapton Film, 2 mil	234	-	-	50
Kapton Film, 5 mil	231	-	-	125

Our proposed 4D printing light reactive material will be a multifunctional, interactive, and flexible material made from LC PHMS with a side chain azobenzene monomer. The light sensitivity, flexible nature, and bending mechanics can be regulated through the chemical composition of the polymer and the design of the passive layer. Other factors such as the melting temperature and viscosity of the material must be tailored for the printing purposes. After printing a prototype of the SCP, the mechanical properties and shape changing efficiencies must be tested.

AM machines are limited in their accuracy and resolution, although they are getting better each year. Current printers have a Z-axis resolution of 100 µm, which means the thinnest consistent thickness of the deposited azobenzene SCP material will be 100 µm. The bending speed and max bending angle of the actuator is determined by the thickness of the part and the intensity of the light. Different thicknesses of the actuator will be printed and exposed to different intensities of light to determine which features are most efficient. The maximum bending angle of each part will be measured along with the time it takes for the actuator to reach the final bending angle.

The bending and unbending position are fitted with an exponential curve using the following equations (Eq. 4 and Eq. 5) (Zhang et al. 2014):

$$\boldsymbol{\theta_b = \theta_0\left[1 - exp(-\frac{t}{\tau_b})\right]} \quad \textbf{(Eq. 4)}$$

$$\boldsymbol{\theta_u = \theta_0\left[exp(-\frac{t}{\tau_u})\right]} \quad \textbf{(Eq. 5)}$$

Here, θ_b represents the angle of bending during light activation, θ_u is the angle of bending during relaxation, θ_0 represents the max bending angle during light activation, τ_b is the actuation response

time constant during light activation, τ_u is the relaxation response time constant, and t is the time. The time constants differ because azobenzene SCPs tend to have a slower relaxation time when compared to their light activated response time. These values can change depending on the thickness of the passive material and the intensity of the light source. These equations will assist in the prediction of the angular position of the bilayer actuators when exposed to light and during relaxation when the light is turned off.

In our photomechanical bending tests, the bilayer films will be clamped on one end of the cantilever and free-standing on the other end. A light source (UV or visible light) is positioned facing the film's surface. A camera perpendicular to the film is used to record the testing process (Figure 3-18. (a)). The UV LED, by LED Engin, was purchased from Mouser Electronics and possessed a wavelength of 365 nm, 200 mW luminous flux, and a power rating of 3W was used for UV activation in the experiments. An ultramarine royal blue LED in the spectrum of 440-445 nm, a 520 mW radiant flux, and a power rating of 1.26 W was used for the visible blue light activation. During testing, the light source illuminates the film that causes actuation of the film and the camera records the light induced bending (Figure 3-18. (b)). The video is exported to a position tracking software, called Tracker, and the angular position of the free-standing end of the cantilever is recorded every 15 frames per 0.5 seconds. Next, the same mechanical tests will be performed, but with different frequencies of light and with different thicknesses of the passive film to define if these characteristics increase or decrease the mechanical efficiency. The tests will be performed on the same parts multiple times to test for consistency and mechanical degradation. Equation 2 will be utilized during measurement of the angular position for the cantilever bending tests of the azo bilayer films.

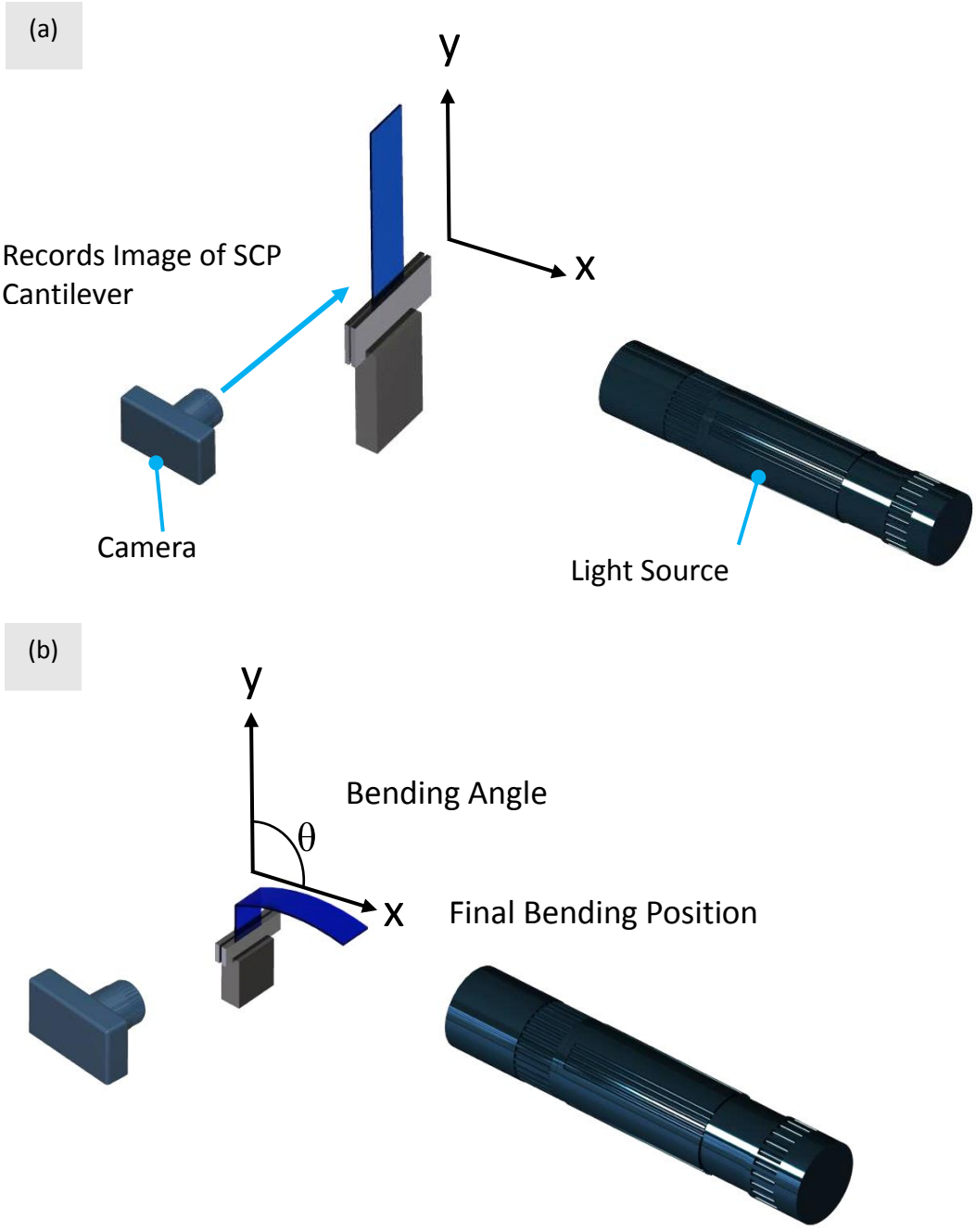

Figure 3- 24. Experimental setup for the photomechanical bending angle and reaction time measurements of the azobenzene bilayer films. (a) Before irradiation, the cantilever beam is fixed to a mount. A light source (UV or visible) is positioned perpendicular to the cantilever and a camera is positioned parallel to the cantilever for recording bending tests. (b) During irradiation, the light source illuminates the cantilever to induce bending and the camera records the cantilever's bending angle and position, which are exported and analyzed using Tracker, a position tracking software.

In order to quantify the shape memory and shape recovery properties of the smart materials, the cyclic mechanical tests using the dynamic mechanical analyzer (DMA) will be performed to calculate the strain recovery rate (R_r) of the materials. A DMA 2980 from TA Instruments was used to perform our photomechanical stress tests. The bilayer films measured at 7.5 mm x 30 mm with varying thickness of 25.4 µm, 50 µm, and 125 µm. The deposited azobenzene material on the Kapton film measured at 10 mm x 7.5 mm. The films were clamped on both ends in the DMA machine (Figure 3-19) and the materials were given an initial preload tension of 40 mN, a constant strain of 125%, and a sampling rate of 1 sec/point. The light source was placed perpendicular to the film at a distance of 10 mm from the film's surface. Once the films were subject to constant strain and stress, the films were allowed to reach equilibrium and then the light source was turned on. The illumination times were different for the different light sources to reduce any thermal stress or expansion on the films. The UV light was turned on for 10 seconds and the blue light was turned on for 20 seconds. The stress, strain, and displacement of the films were all measured using the DSC. The R_r quantifies the materials' ability to return the mechanical deformation of the permanent shape, $\varepsilon_p(N)$, after administering mechanical strain (ε_m) (Eq. 6). The ratio between the strain during the programming stage ($\varepsilon_m - \varepsilon_p(N-1)$) is compared to the strain during the recovery stage ($\varepsilon_m - \varepsilon_p(N)$). The total strain recovery rate ($R_{r,tot}(N)$) is defined as the final strain recovery after a number of cycles (N) in comparison to the original ε_m of the material (Eq. 7). It should be noted that the ideal value for all of the equations should be 100%.

$$\boldsymbol{R_r(N) = \frac{\varepsilon_m - \varepsilon_p(N)}{\varepsilon_m - \varepsilon_p(N-1)}\, x\, 100\%} \qquad \textbf{(Eq. 6)}$$

$$R_{r,tot}(N) = \frac{\varepsilon_m - \varepsilon_p(N)}{\varepsilon_m} \quad \textbf{(Eq. 7)}$$

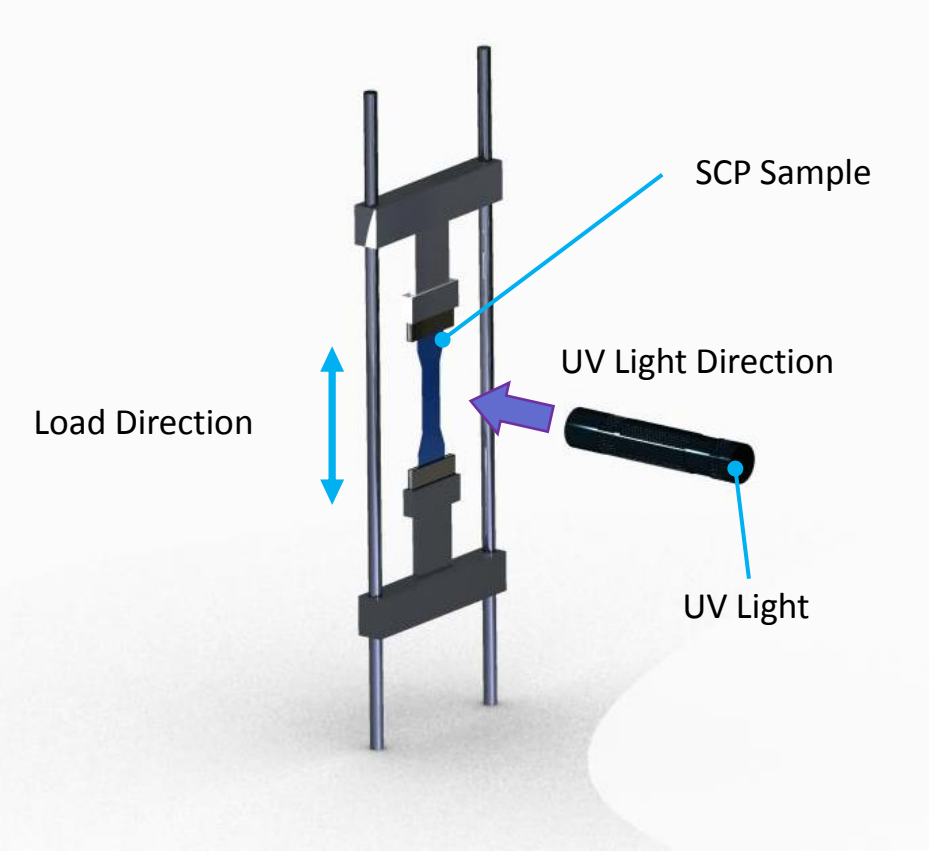

Figure 3- 25. Experimental setup for measuring the photomechanical stress using a dynamic mechanical analyzer (DMA). The bilayer films are placed in tension in the DMA and the light source is illuminated on the sample. Next, the stress is generated from the light is measured.

The anisotropic nature of the printed azobenzene SCP should be explored, since a 3D printer dispenses the material in a line and layer-by-layer pattern, the direction of printing may affect the configuration of the azobenzene moieties. The configuration of the moieties may determine bending efficiency and direction of the material. After printing, some samples were

annealed in an oven set at 120ºC then slowly cooled to room temperature. This process induced crystallization in the MeOABHx polymer that may affect the bending efficiency and bending direction. In future tests, Kapton films were placed on a hot plate with a temperature of 80-100ºC and the azobenzene material was dispensed onto the films. After extrusion, the bilayer films were allowed to cool to room temperature to induce the crystallization phase. During the cooling phase the films formed a random bending and contracted shape. This phenomenon will be discussed later in the paper.

3.5.2 Results

Different styles of Kapton films and azobenzene PHMS Kapton Bilayer films were tested in different light sources. The angular bending position (°, degrees) were recorded when the films were exposed to UV light and visible blue light. Both light sources were maintained at an input power of 4.0 V and 1.0 Amps. The Kapton films measured 10 mm in width, 40 mm in length, and 0.0254 mm in thickness. Some of the Kapton films were annealed in an oven at 120°C for 24 hours, while others were unannealed for initial testing. The azobenzene PHMS material was deposited onto the top layer of the Kapton film using a syringe 3D printer (Figure 3-20).

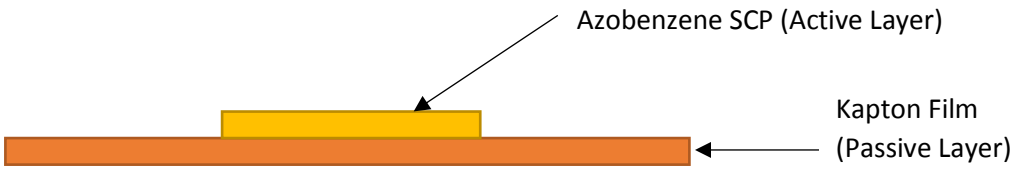

Figure 3- 26. Schematic of the azobenzene PHMS and Kapton bilayer films

When the azobenzene polymer is exposed to light, it causes the polymer to increase in volume due to the azobenzene moieties in the polymer structure (side-chain group), but the volume expansion is restricted by the Kapton substrate (Figure 3-21. (a)). During light activation, the azobenzene SCP applies a stress onto the Kapton film because of the volume expansion (Figure 3-21. (b)), which induces bending of the bilayer, similar to the mechanism used by Wen et al.

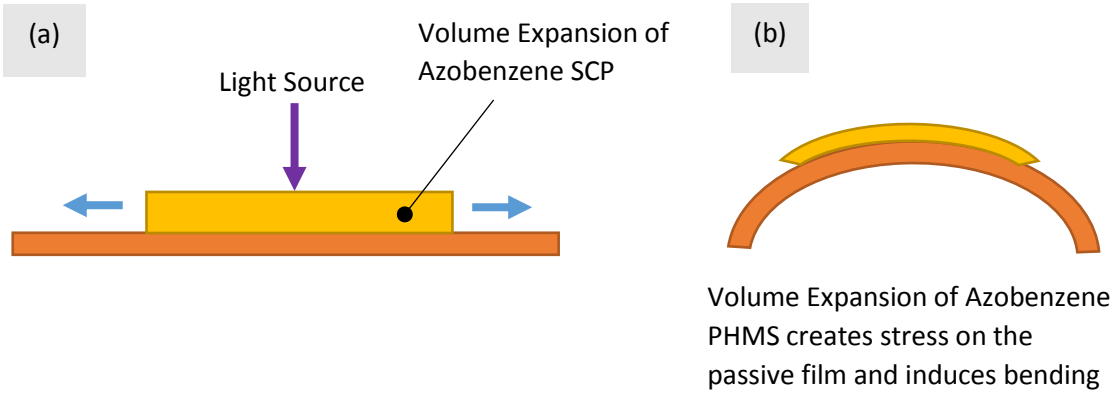

Figure 3- 27. Schematic of the photomechanical mechanism causing bending in the bilayer films. a) The azobenzene PHMS shape changing polymer expands in volume when exposed to a light source. b) The stress generated from the volume expansion in the azobenzene SCP causes the bilayer film to bend.

The angular position is recorded to test the photomechanical bending of the films. During the initial tests, the cantilever was positioned horizontally. Next, the angular position is recorded from its initial point and through its bending behavior when the light source is turned on and off (Figure 3-22. (a) & (b)). During illumination, the free-standing end of the cantilever quickly moved downward, within tens of seconds. When the light is turned off the cantilever bends up and returns to its initial position. It can be seen that the cantilever displays significant bending when exposed

to UV (365 nm) and visible royal blue (455 nm) light by comparing its starting and final bending position. During experiments the cantilevers were illuminated for 20~30 seconds and the bending movement was recorded. The video was exported and the position of the cantilever was tracked. The angular position of the cantilevers were plotted to show any differences in the bending efficiency of the samples.

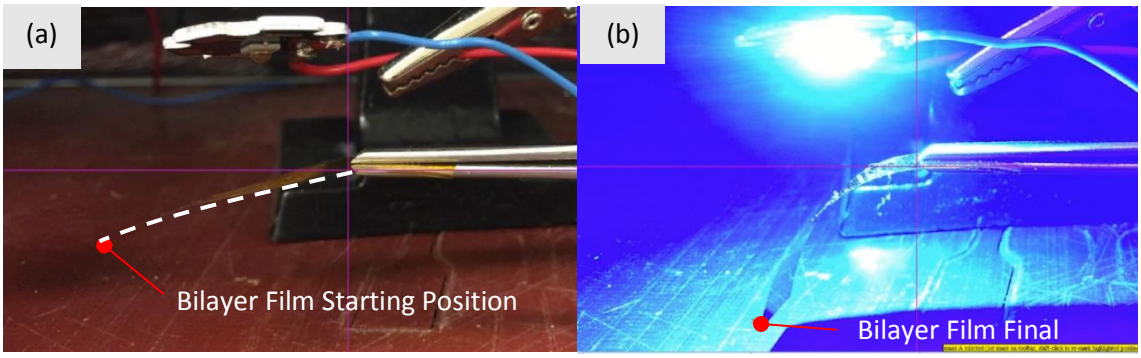

Figure 3- 28. (a) Initial angular position of the azobenzene PHMS and Kapton bilayer film before light exposure. (b) The final bending position of the bilayer film when exposed to 455 nm blue light. The bending process takes less than 10 seconds to reach its final bending position.

Looking at Figures 3-23 and 3-24, it was discovered that Kapton film without any azobenzene PHMS does possess some small shape changing properties due to thermal expansion when exposed to heat from the light sources. The thermal coefficient of expansion for a Type HN film, 25.4 μm in thickness, is 17 ppm/°C for temperatures ranges in 30-100°C. The temperatures of the UV LED and the visible blue light were measured at different distances to understand if temperature from the light sources would affect the shape change of the Kapton material. In general, the blue light possessed lower temperatures, ranging from 25°C to 58°C on average. However, the UV light possessed higher temperatures at different distances, which ranged from 25°C to 82°C on

average (Figure 3-25 & 3-26). After prolong exposure to light, the material was within range of the temperatures for thermal expansion. The amount of shape change is small compared to the bilayer films that possessed azobenzene SCP. The highest angle of bending in blank Kapton films was around 2.60°. However, higher angles of bending can be observed when Kapton film is combined with azobenzene SCP. Bending angles for azobenzene bilayer films ranged from 15°-30°. The highest bending was observed for annealed bilayer films with azobenzene on top of the film in both UV and blue light. Also note, close to 100% shape recovery can be seen for bilayer films exposed to blue light; however, bilayer films exposed to UV light show discrepancies in their final shape recovery. This occurrence may be an effect of a majority of the azobenzene moieties isomerizing from the *trans* state to the *cis* state. Since, there is a higher concentration of *cis* azobenzene moieties post illumination, it may take longer for the moieties to return to the *trans* state, which causes slower shape recovery as a result.

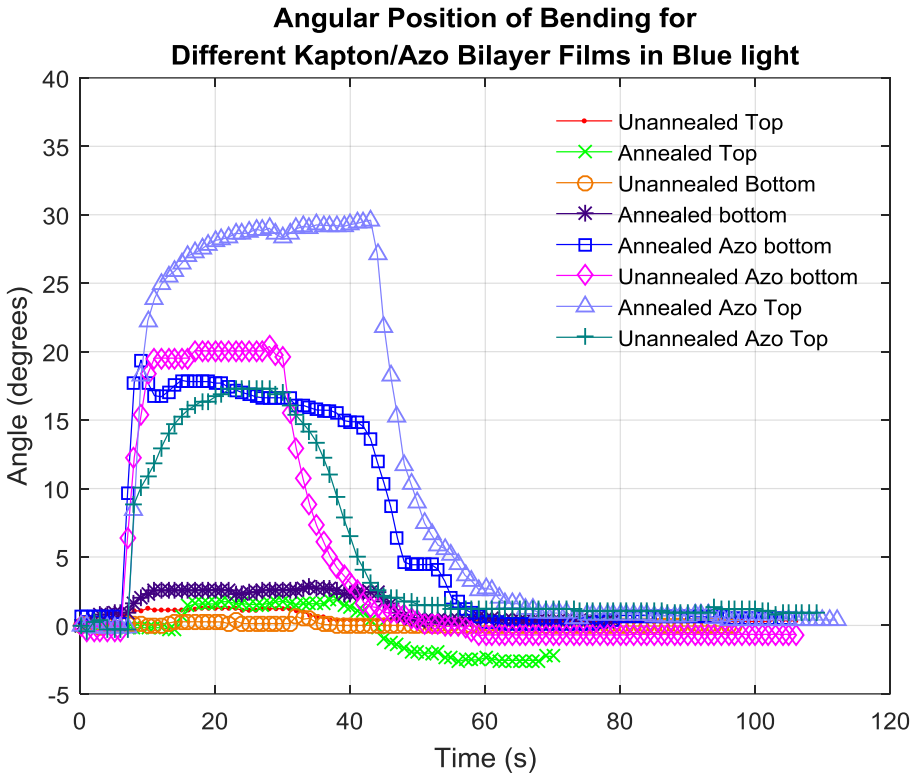

Figure 3- 29. The bending angle for Kapton films and bilayer azobenzene films when exposed to visible blue light (455 nm). A combination of annealed and unannealed Kapton films were used in the test. The bending was measured for films with the azobenzene material on top of the film or on the bottom of the bilayer film. It can be observed that Kapton films possess some thermal shape change, but not as high as bilayer films with azobenzene.

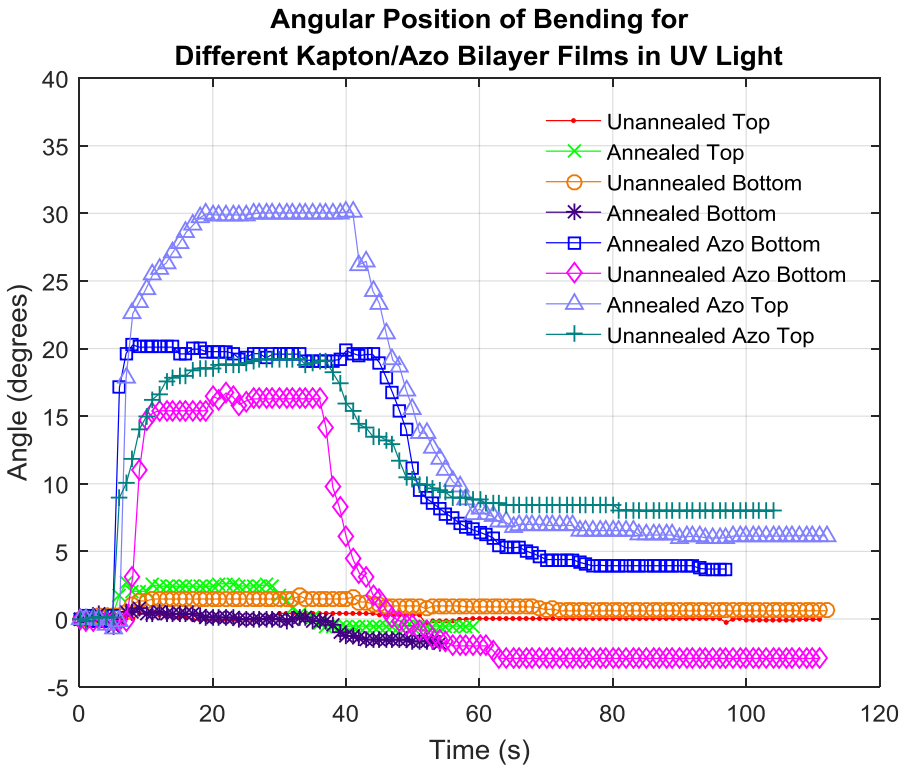

Figure 3- 30. The bending angle for Kapton films and bilayer azobenzene films when exposed to UV light (365 nm). A combination of annealed and unannealed Kapton films were used in the test. The bending was measured for films with the azobenzene material on top of the film or on the bottom of the bilayer film. It can be observed that Kapton films possess some thermal shape change, but not as high as bilayer films with azobenzene.

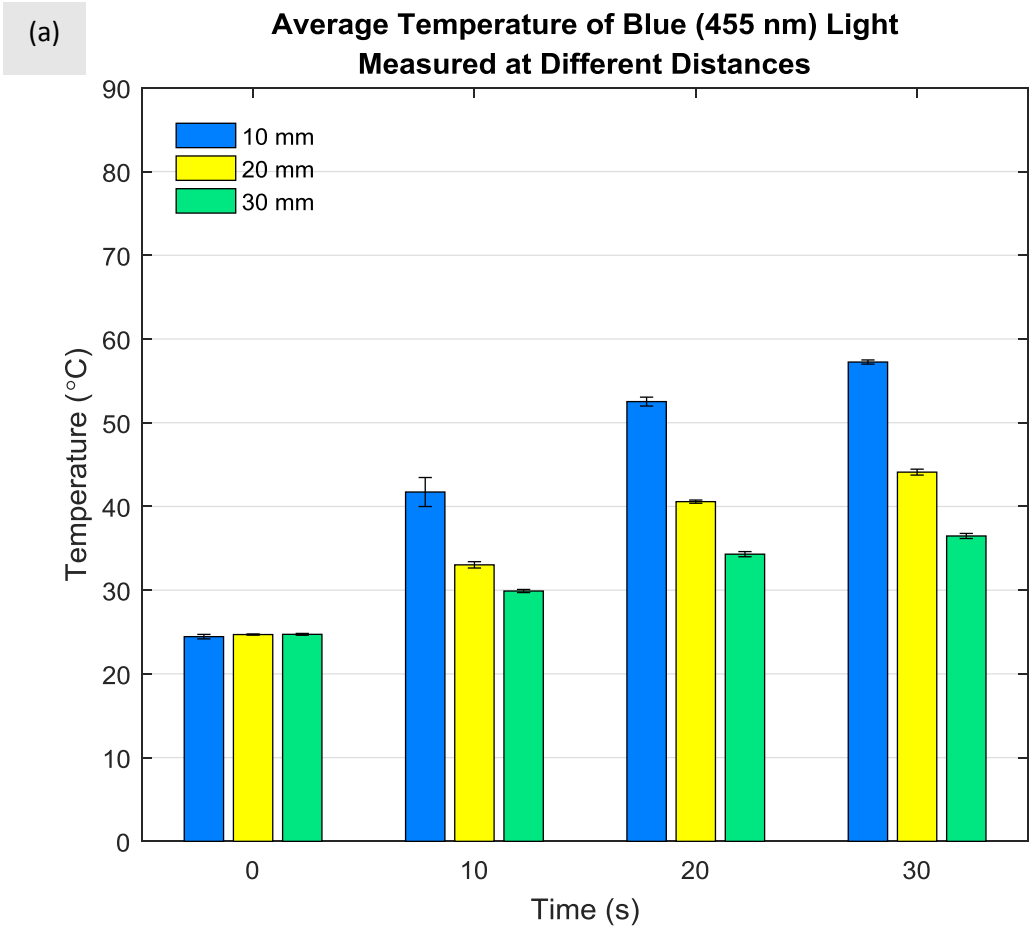

Figure 3- 31. The average temperatures for 455 nm light measured at distances of 10 mm, 20 mm, and 30 mm. The averages are plotted with their standard deviations.

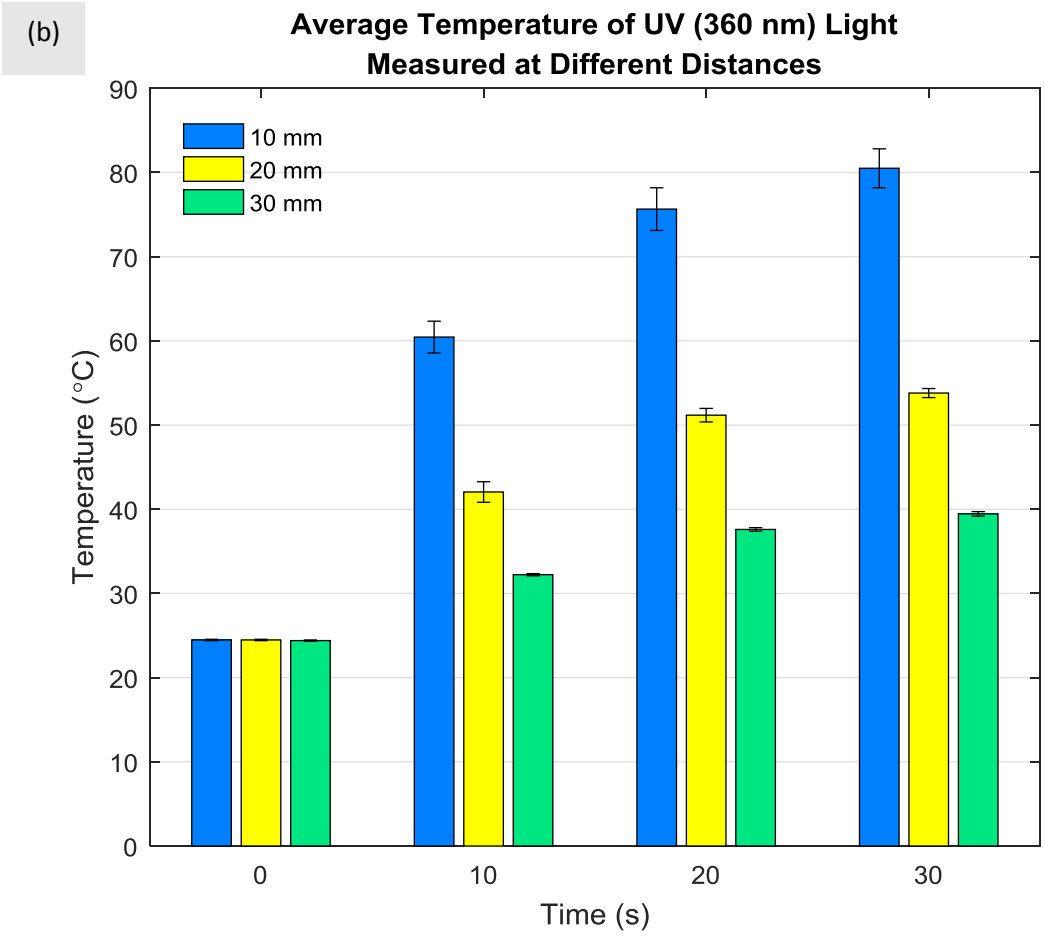

Figure 3- 32. The average temperatures for 360 nm light measured at distances of 10 mm, 20 mm, and 30 mm. The averages are plotted with their standard deviations.

After measuring the temperatures emanated from the light sources, it can be observed that a large amount of power is lost due to heat. Next, the amount of power that is used as light energy was observed using a Newport optical power meter, model 1916-C, which measures the light intensity at different wavelengths. Multiple light sources were measured using the optical power meter: a 365 nm LED with a heatsink, 365 nm LED without heatsink, 465 nm LED, and 530 nm LED. All light sources had a input power of 4.1 V and 0.98 Amps. The intensity was measured at

different distances, measured at 10 mm, 20 mm, and 30 mm away from the optical power meter. A heatsink was applied to the 365 nm LED because it produces the most heat out of all of the LEDs due to the inefficiency of the semiconductor where 60-95% of the power can be lost as heat. It can be observed that there is a significant increase in light intensity when the heatsink is applied to the UV LED (Figure D-1). However, the 455 nm LED is slightly more powerful than the 365 nm LED without the heatsink. Finally, the 530 nm LED had the lowest intensity for all trials when compared to the other LED light sources.

Next, the focus was placed on predicting the angle of bending for the bilayer films. The average angle of bending for a bilayer azobenzene film with a passive film thickness of 1 mil and exposed to blue light (455 nm) at a distance of 10 mm from the light source was 33.79° (Figure 3-27). The bilayer film was exposed to blue light for 20 seconds and turned off for 40 seconds to allow for the bilayer film to return to its original flat state. It takes about 5 seconds for the cantilever to reach its max bending angle, but takes about 30 seconds for the film to return to its original state. Two models were used to predict the light actuation; one model used to predict the angle of bending during light activation, θ_b (Equation 3) and the second model was used to predict the angle of relaxation when the light is turned off, θ_u (Equation 4). The max bending angle, θ_0, for equations 3 and 4 was taken from the empirical data as 33.79°. The actuation response time constant, τ_b, during light activation was noted as 1.56 s and the relaxation response time constant, τ_u , was noted as 5.55 s. Both models seem to fit the actual data very closely. In order to confirm the fit, a correlation between the actual data and the models shows a close relation with an R^2 value of 0.99 (Figure 3-28). It can be seen that the model fits very closely to the actual bending position, which proves that it could be used for future predictions if users can determine their max angle of bending during light activation and their response time. However, the max bending angle, activation

response time, and relaxation response time would be different depending on the thickness of materials, the type of azobenzene SCP, the type of passive material, and the light intensity.

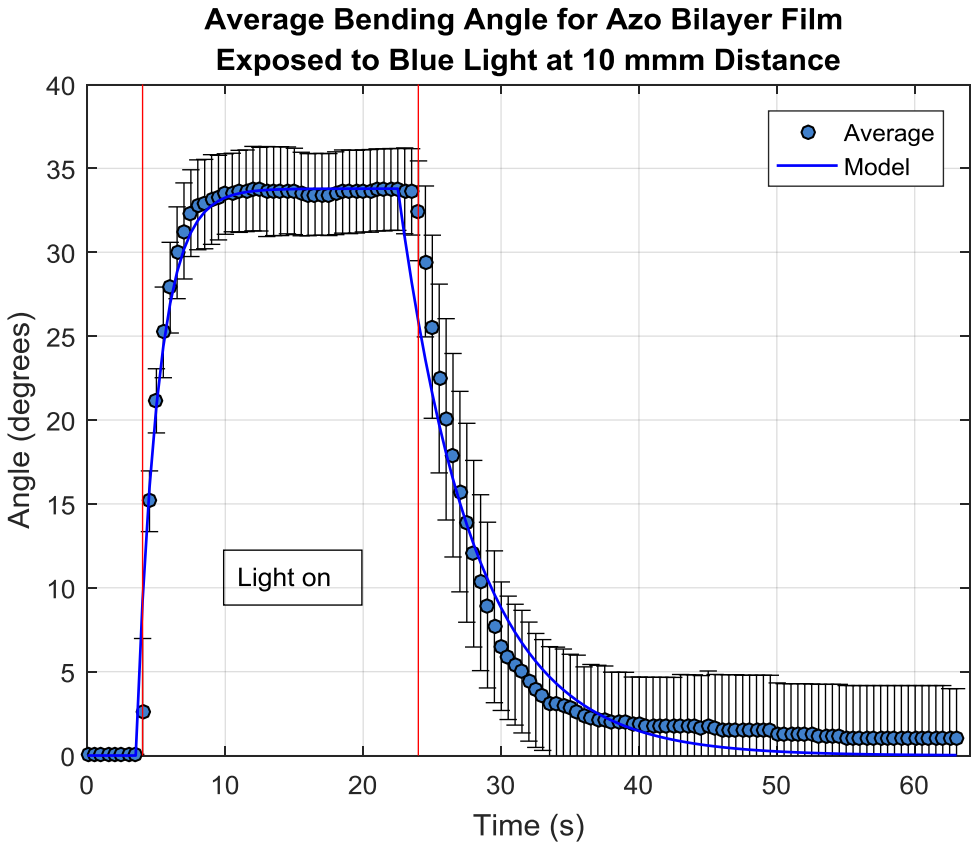

Figure 3- 33. Average bending angle as a function of time for an azobenzene bilayer film exposed to blue light (455 nm) at a distance of 10 mm from the light source. The light is turned on at 3 seconds and off at 23 seconds. Circle points represent the average and standard deviation for 4 trials and the smooth blue line represents the exponential fit.

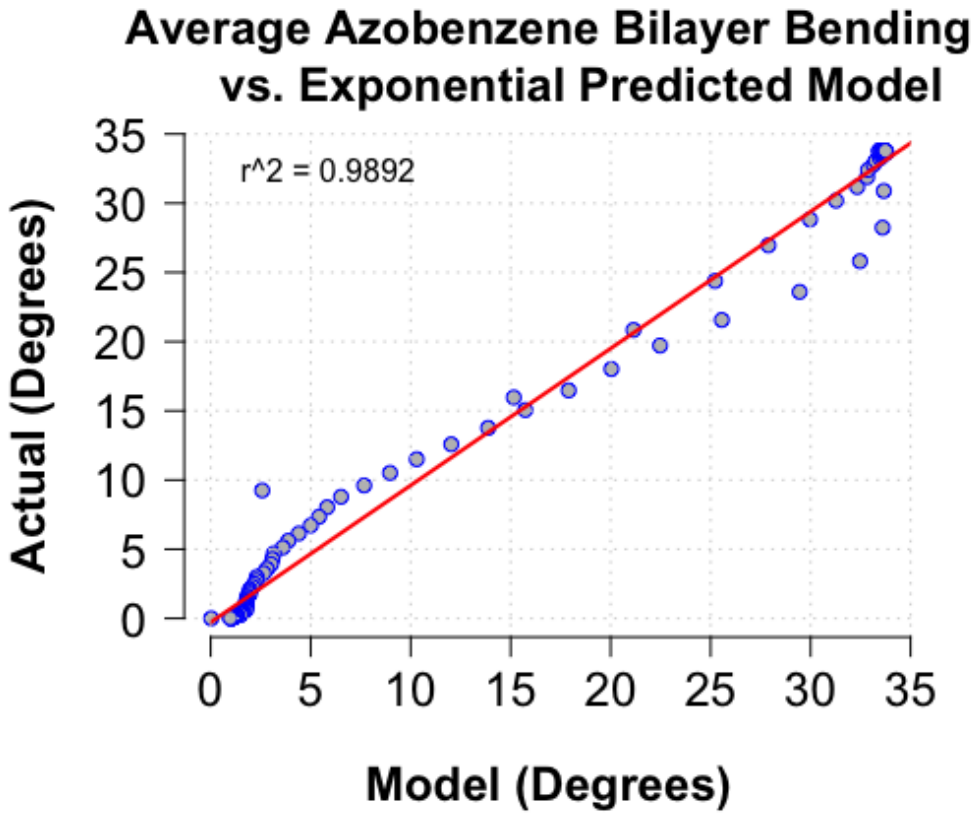

Figure 3- 34. Correlation plot of the actual angular bending position of the bilayer azobenzene film and the exponential models for bending and unbending of the film. The bilayer film possesses a 25.4 µm passive film thickness, exposed to blue light (455 nm) at a distance of 10 mm for 20 seconds.

A repeatability test was performed on a sample of the azobenzene MeOABHx bilayer film, which presented very little degradation (Figure 3-29). The sample was exposed to visible blue (455 nm) light at a distance of 10 mm for 10 seconds then the light was turned off for 20 seconds. During light activation, the cantilever would bend away from the light source. When the light was removed, the cantilever would slowly return to its original position. The process was repeated 9 times and showed little fatigue or decay. The cantilever reached a max bending angle above 35° during light activation in each case. The cantilever did not return to its original 0° flat state when the light was

turned off for the 20 seconds cool down period. The cantilever consistently reached a relaxation angle of ~4° during the relaxation time. However, on the final unbending process the cantilever gradually approaches 0°. It is assumed that the cantilever would reach 0° after a longer relaxation period.

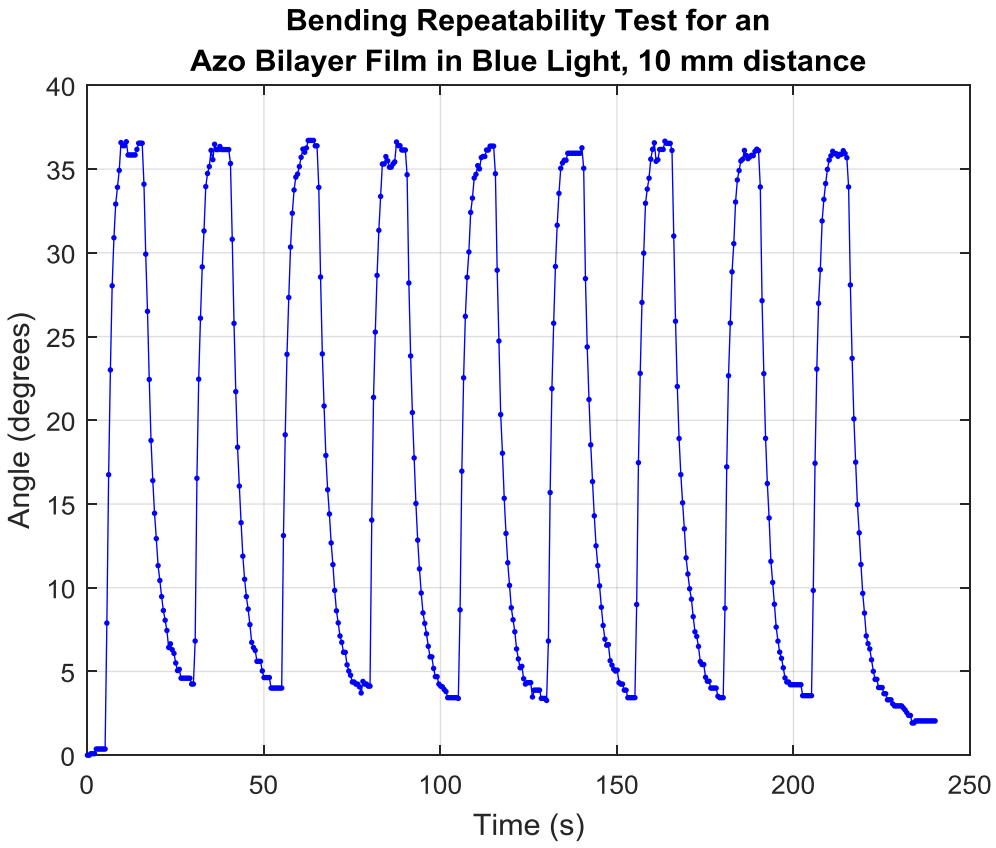

Figure 3- 35. Bending and unbending repeatability test for azobenzene bilayer film exposed to blue light (455 nm) at a distance of 10 mm from the light source.

The next test was to measure the photo-generated stress and strain during light activation using a DMA machine. The photo-generated stress was measured for blank Kapton films of

different thicknesses, MeOABHx bilayers with different thicknesses, and 1 mil DR1Hx bilayer films in UV light (Figure 3-30) and visible blue light (Figure 3-31). The blank Kapton films displayed some form of photo-generated stress due to some produced thermal expansion in the films with heating from the light sources (both UV and visible blue light). The stress was much higher than expected for the blank films, which ranged from 0.82 to 1.02 MPa for UV light and 0.97 to 0.56 MPa in blue light. This may be due to the high pretension on the films before testing. There were some interesting phenomena when observing the stress data for the 2 mil azobenzene bilayer films. The 2 mil azobenzene bilayer films seem to display similar results as the blank Kapton films, with a max stress of 0.89 MPa. However, the 2 mil bilayer films displayed higher photo-generated stress than the blank Kapton films when exposed to blue light that possessed a max stress of 1.31 MPa. This stress is very similar to 1 mil bilayer film with MeOABHx, which exhibited a stress of 1.29 MPa in UV light and a stress of 1.36 MPa in visible blue light. Overall, the DR1Hx bilayer displayed higher photo-generated stress, with a max stress of 1.99 MPa in UV light and 1.60 MPa in blue light. The 1 mil bilayer samples displayed consistent large photo-generated stress for both the DR1Hx and MeOABHx polymers.

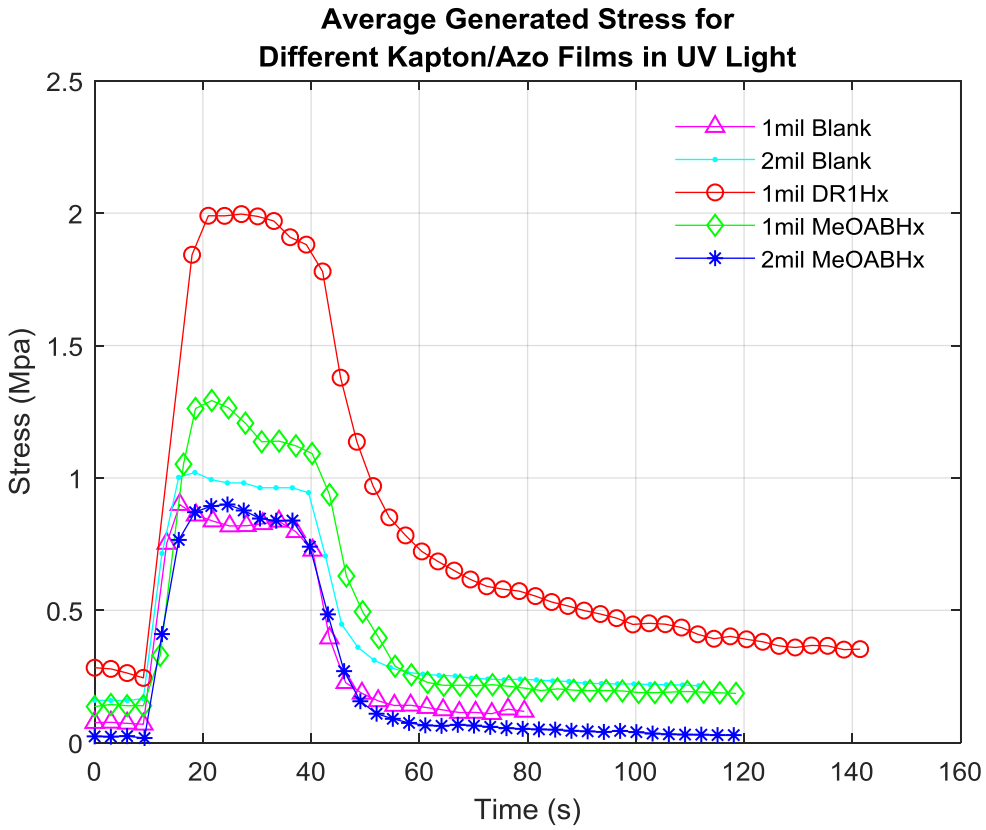

Figure 3- 36. Plot of the average photo-generated stress for different samples of blank Kapton films of different thicknesses (1 mil and 2 mil) and different azobenzene polymers (MeOABHx and DR1Hx) when exposed to UV light (365 nm) at a distance of 10 mm. Individual plots of the test samples with their averages and standard deviations for 4 different trials is posted in Appendix A of the literature.

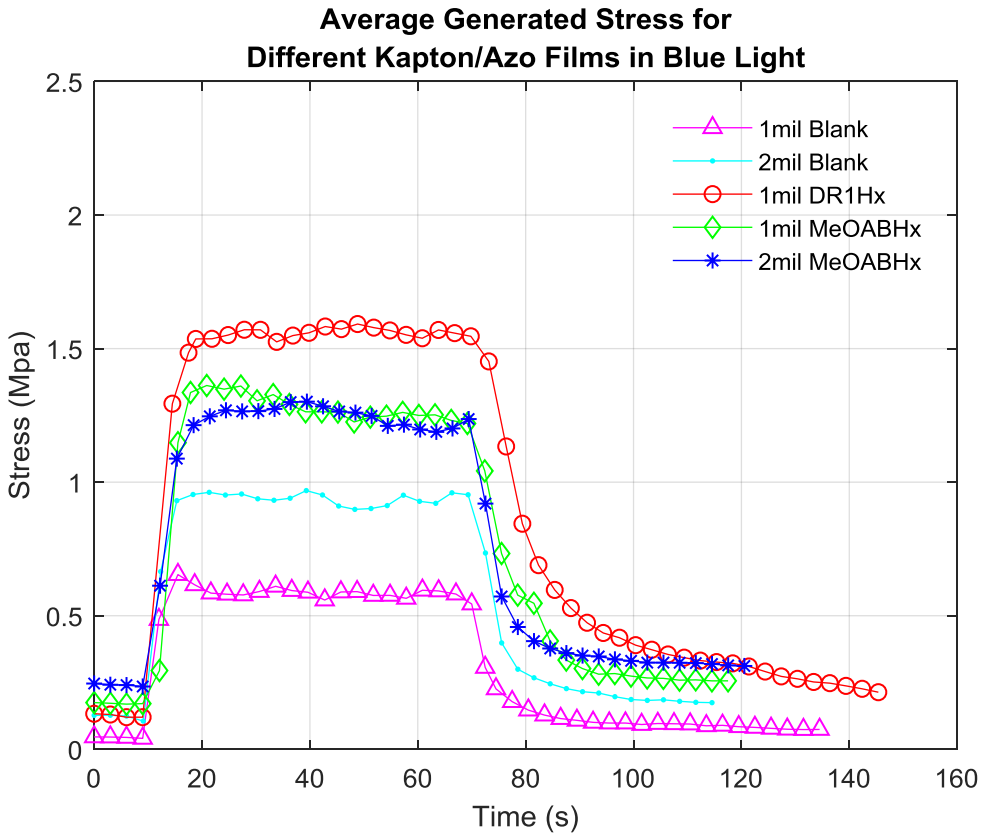

Figure 3- 37. Plot of the average photo-generated stress for different samples of blank Kapton films of different thicknesses (1 mil and 2 mil) and different azobenzene polymers (MeOABHx and DR1Hx) when exposed to visible blue light (455 nm) at a distance of 10 mm. Individual plots of the test samples with their averages and standard deviations for 4 different trials is posted in Appendix A of the literature.

The stress generated by combining the azobenzene polymers with the Kapton films was established by finding the difference between the average max stress generated by the blank Kapton films and stress generated by the bilayer films. In this case, the DR1Hx displayed higher photogenerated stress with UV light (916.61 KPa) than in blue light (868.39 KPa). Conversely, the MeOABHx polymer bilayers presented higher photogenerated stress in blue light (565.50 KPa) than in UV light (290.61 KPa). The 2 mil MeOABHx bilayers had higher photogenerated stress in blue light (189.15 KPa), but the UV light displayed significantly lower photogenerated stress at

1.26 KPa. Overall, the DR1Hx bilayers generated higher stress during illumination; however, both polymers bilayers with 1 mil thick passive layers make promising candidates as actuators (Table 3-2).

Table 3- 2. The average photo-generated stress for different bilayer polymer films when exposed to different wavelengths of light.

Sample	Average Stress Generated in UV Light (kPa)	Average Stress Generated in Blue Light (kPa)
DR1Hx, 1 mil	916.61	868.39
MeOABHx, 1 mil	290.61	565.50
MeOABHx, 2 mil	1.26	189.15

The samples tested in the DMA machine displayed interesting shape recovery characteristics. Each sample was tested four times and the shape recovery of the first trial displayed much lower values than the succeeding trials for a majority of the samples. The only sample that did not display lower shape recovery values in the initial test was the 2 mil blank Kapton exposed to blue light (95.44%). In the succeeding trials, even the blank Kapton films demonstrated high average shape recovery. This high shape recovery may be due to the blank films possessing lower deflections than the azobenzene bilayers and also lower photogenerated stress than the bilayers. Also, no pattern can be observed for possessing higher shape recovery in UV or blue light. The MeOABHx possessed high shape recovery ranging from 71.92% in blue light to 95.57% in UV light for a 2 mil thick passive bilayer film. Overall, the 2 mil thick bilayers displayed higher shape recovery, but this may be due to them possessing lower deflection than the 1 mil samples and lower photogenerated stress. The DR1Hx bilayer materials possessed fairly high shape recovery in both UV light (77.17%) and blue light (79.14%). The initial shape recovery and average shape recovery can be observed in Table 3-3.

Table 3- 3. The shape initial shape recovery and average shape recovery of Kapton and bilayer samples tested in the DMA machine when exposed to UV light and blue light at a distance of 10 mm. Some bilayer samples possessed different passive layer thicknesses: 1 mi and 2 mil. Initial shape recovery tends to be lower for the majority of the samples, while the average shape recovery was much higher.

Sample	Initial shape recovery (%)	Average shape recovery (%)
Kapton, 1mil, UV	56.92	84.27
Kapton, 1mil, Blue	33.84	76.98
Kapton, 2mil, UV	43.09	82.66
Kapton, 2mil, Blue	95.44	90.24
MeOABHx, 1mil, UV	56.12	82.34
MeOABHx, 1mil, Blue	32.34	71.92
MeOABHx, 2mil, UV	89.88	95.57
MeOABHx, 2mil, Blue	53.99	85.31
DR1Hx, 1mil, UV	37.93	77.17
DR1Hx, 1mil, Blue	11.73	79.14

In a separate experiment, the passive Kapton films were heated during the 3D printing process because it was witnessed that the bilayer films would spontaneously bend and contract when heated. Due to this observed feature, the amount of contraction was measured for the MeOABHx bilayer polymer with different passive layer thicknesses (1 mil, 2 mil, and 5 mil) and four samples of each were tested. As predicted, the thicker films displayed lower contraction angles. The 5 mil thick passive films only exhibited an average angle of contraction of 4.19° (Figure 3-32. (a)). The 2 mil thick passive films possessed a contraction angle of 29.90° (Figure 3-32. (b)) and the 1 mil thick films reached 88.50° (Figure 3-32. (c)). Quantitative data on the polymerization contraction angle of the different film thicknesses can be seen in figure 3-33.

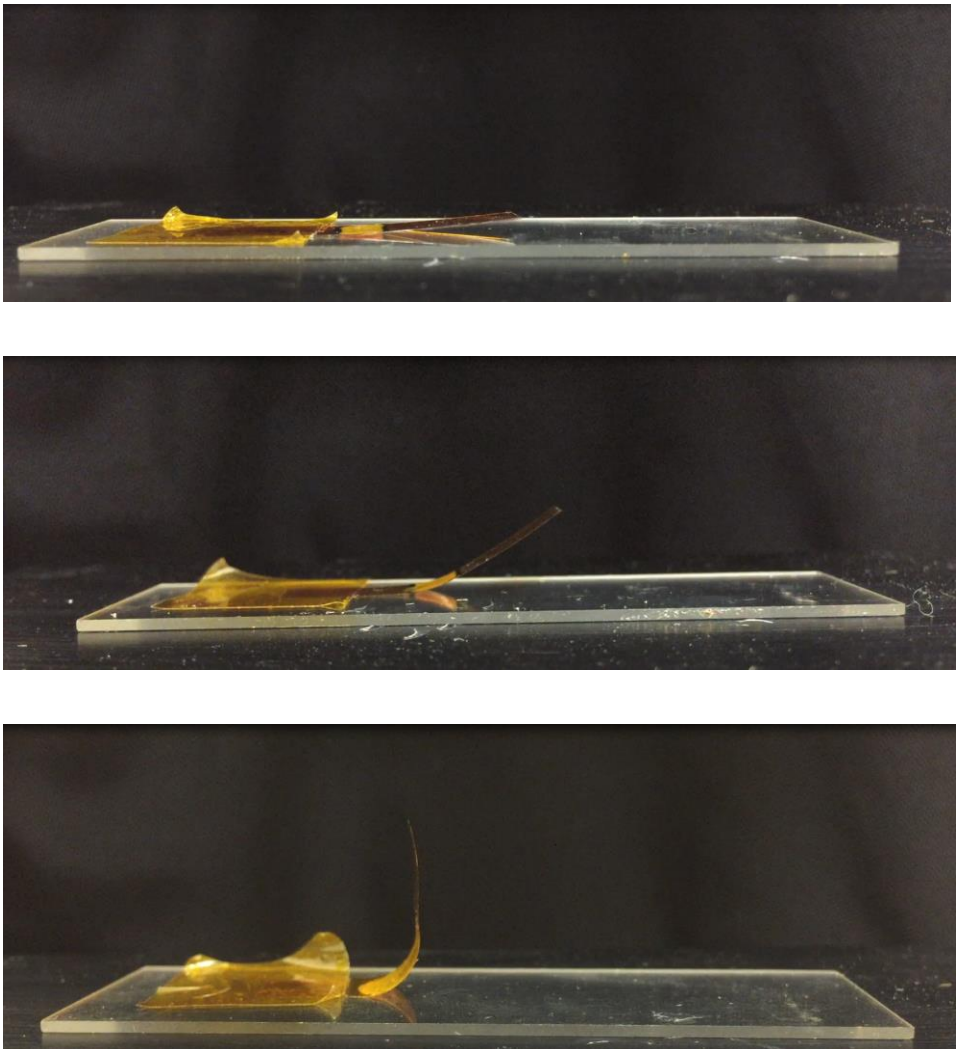

Figure 3- 38. The polymerization contraction angles of different MeOABHx bilayer films that possess different thicknesses of the passive layer: (a) 5 mil, (b) 2 mil, and (c) 1 mil. The films are heated to 80~100°C then cooled to room temperature to induce the contraction.

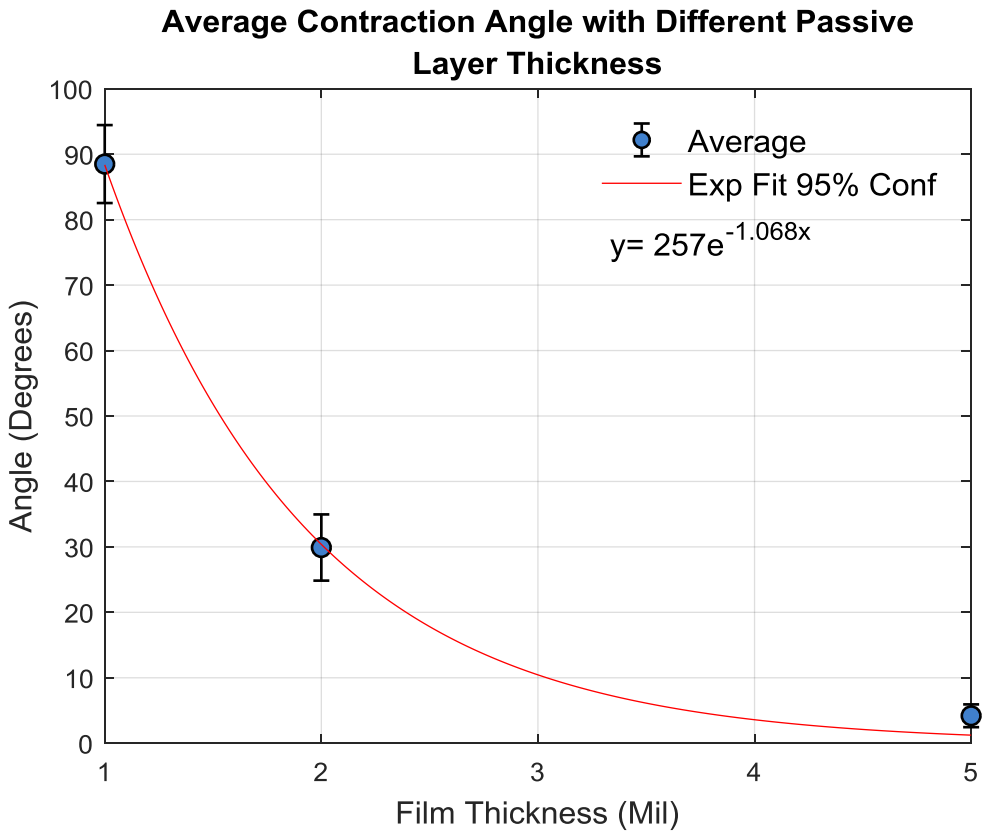

Figure 3- 39. The average contraction angle of different passive layer thickness when MeOABHx is deposited on the film surface then allowed to cool. After cooling the bilayer forms a random bending position due to contraction of the MeOABHx material. Four samples of each thicknesses were tested.

The photomechanical bending of the different thickness bilayer films after their annealing and have contracted was measured when exposed to different light sources. The bilayer films were exposed to 455 nm and 365 nm light at a distance of 10 mm. When exposed to the light sources, the films bent away from the incident light and when the light was turned off the films returned to their original position. Generally, the films possessed lower bending angles than their contraction angles and blue light induced larger bending angles than the UV light (Figure 3-34). The 5 mil bilayers possessed very tiny bending that maxed out at 0.54° for UV light and 1.03° in blue light.

2 mil bilayers demonstrated bending angles of 10.49° in UV light and 14.90° in blue light. Finally, 1 mil bilayers displayed the highest angle of bending with 37.48° in UV light and 44.29° in blue light. In both light sources there is an exponential decrease in photomechanical bending angle as the passive layer increases.

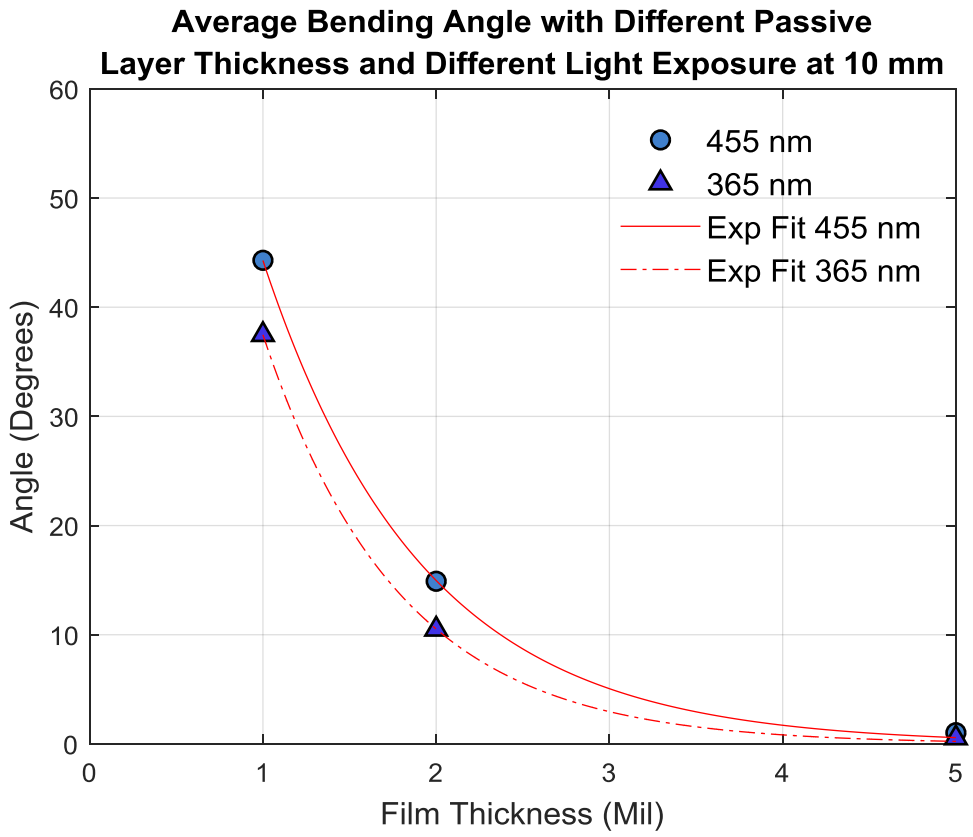

Figure 3- 40. The average angle of bending for MeOABHx bilayer films that possessed a Kapton passive film with thicknesses of 1 mil, 2 mil, 5 mil. The films were exposed to 455 nm light at a distance of 10 mm.

3.5.3 Outcome

Outcomes of this aim helped quantify the photomechanical behavior of two different azobenzene SCPs when exposed to different light sources and different thicknesses of the passive layer. It was discovered that adding azobenzene SCPs to Kapton film for the creation of bilayer films created significant observable photomechanical bending and had potential to be used as a light activated actuator. In earlier experiments, the azobenzene MeOABHx bilayer films were tested to confirm if the bilayer films possessed light activated shape changing properties. The azobenzene bilayer films demonstrated similar bending results when exposed to both UV and visible blue light, but the bilayer film did not return to its original state with UV light as quickly as the blue light. This property might be due to more azobenzene moieties isomerizing from *trans* to *cis* state because the wavelength of highest absorption was in the 365 nm spectrum, as presented in section 2.3 of this literature. The transition from *cis* to *trans* takes much longer, so it may take longer for the UV illuminated bilayer to return to their original state.

One concern about the photomechanical testing was the effect of heating from the LEDs. It seemed that Kapton film did possess some form of shape change due to thermal expansion, but the overall angle of bending was much smaller when compared to the bilayer films. The 455 nm and the 365 nm LED temperatures were measured at different distances and the 455 nm blue light possessed lower temperatures than the UV light. This is a positive find because the blue light seemed to induce higher angles of bending than the UV light. This confirms that temperature was not a significant activation method that induced the higher bending angles and that the isomerization of the azobenzene moieties had a larger effect on the photomechanical bending. The higher bending because of the blue light may be due to the 455 nm light possessing a higher intensity than the UV light. Light intensity measurements were performed to confirm this theory.

It was found that 365 nm LED with a heatsink possessed the highest light intensity because less of the power is lost as heat due to the inefficient semiconductor. However, the 455 nm LED possessed slightly higher intensity than the 365 nm LED without the heatsink. Also, life cycle test of the photomechanical bending was performed and the samples exhibited very little photomechanical degradation. The bilayer films could be used as actuators for long term purposes.

The photogenerated stress and strain that was measured using the DMA machine provided insight into the amount of stress the films generate when illuminated by a light source (UV or visible blue light). In some cases, this stress may be caused by the heat generated from the light or through photoisomerization of the azobenzene moieties. The DMA results showed that the blank Kapton films exhibited stress generated by thermal expansion from the light. The amount of stress was much higher than expected and may have been caused by the large pretension placed on the film before testing. The difference between the stress of the blank Kapton films and the bilayer films could be used to find the amount of photogenerated stress is caused by the azobenzene SCP. The majority of the samples possessed photogenerated stress above 200 kPa, which is the amount of stress generated by skeletal muscles (Ikeda, Mamiya, & Yu, 2007; Naciri et al., 2003; Yoshino et al., 2010) . DR1Hx bilayers exhibited the highest stress at 916.61 kPa and 868.39 kPa for UV light and blue light, respectively. The MeOABHx bilayers that possessed a passive layer thickness of 290.61 kPa and 595.50 kPa for UV light and blue light, respectively. The data shows that both the DR1Hx and the MeOABHx bilayers have the potential to be used as light-activated artificial muscles. These artificial muscles could be combined with many more azobenzene films or fibers to generate higher stresses and wirelessly activated using a light source.

In separate experiments, the MeOABHx bilayer films were placed onto a hotplate set to temperatures ranging from 80-100°C to test for liquid crystallization and alignment of the moieties after MeOABHx had been 3D printed. At elevated temperatures, the MeOABHx polymer begins

to enter its isotropic phase and as it is cooled to room temperature the polymer reaches a nematic phase. In the isotropic phase, the molecules possess random alignment in all directions, but in the nematic phase the molecules are ordered in the same direction. After the annealing process, the films spontaneously bend in the location of the SCP on the Kapton film. The largest bending angle occurs when the polymerization temperature is much higher than the operation temperature. The amount of contraction can be observed visually (Figure 3-32), but the video analysis provided insight on just how much bending was induced for each film thickness (Figure 3-33). The degree of bending is dependent on the thickness of the passive layer. Only three different thicknesses of Kapton film (1 mil, 2 mil, and 5 mil) were tested for the contraction experiments, but the data shows that there is an exponential decrease in the contraction angle as the Kapton film's thickness increased. It was predicted that the thicker materials would induce lower photomechanical bending angles because of their small contraction angles.

The contraction experiments are interesting because it shows that the MeOABHx polymer possesses an LC phase that affects the photomechanical bending when transitioning from a nematic phase to an isotropic phase. These phase transitions cause density and volume change of the polymer, which induces bending on the passive layer. These contraction angle results will aid in the design of light activated actuators and shape changing products. Designers may choose different thicknesses of the passive layers if their products requires different final bending angles. The location of the polymer the bilayer films during annealing may affect the final shape of the product after it has cooled and may induce different shapes and motions during photoactivation. This will become important in the design of light activated SCPs to ensure different components do interfere with each other during the shape changing process. This methodology will be discussed in later sections 3.3.

The photomechanical bending of the MeOABHx bilayer films after they have contracted was performed to determine if the contraction angle affects the photomechanical bending of the films. Thinner films had significantly higher angles of bending in both light sources (365 nm and 455 nm) when compared to thicker films. However, the bilayer films only reached a max photomechanical bending angle that was less than ~50% of their contraction angle. The bending angle could be increased if the intensity of the light source was increased or the area of the polymer being illuminated by the light was increased. In each trial, the distance between the light source and the film was at 10 mm. During one of the experiments using the MeOABHx 1 mil bilayer, the visible blue LED was moved closer to the film's surface. As the light moved closer, the photomechanical bending angle increased. There is the possibility that the photomechanical bending angle's final bending angle could reach values equitable to the contraction angles if the distance between the light and the film was increased or if the light intensity was increased. However, to remain consistent, the testing distance between the light and the film was maintained at 10 mm.

Overall, the photomechanical bending and properties for two different azobenzene SCPs have been quantified. The photomechanical bending of these azobenzene SCPs have not been reported for bilayer materials that include Kapton film as a passive layer. It has been shown how the increasing thickness of the passive layer can have an exponential decline for the contraction angle and photomechanical bending angle of the bilayers. However, this should not be considered a negative feature, but rather a design tool for 3D printed shape changing materials. The ability to bend the films up to 90° would be desired, but it is predicted that the bending angle could be increased with a higher light intensity. Different passive layer materials should also be considered and tested. So far, the Kapton film presented in this study and *Wu et al's* silk fibroin layer are the only azobenzene bilayer materials reported. Also, it was observed that the cantilever bends in the

opposite direction of the active layer. In order to induce bidirectional bending, azobenzene SCP would have to be deposited on both sides of the film. DMA provided better insight on the force generated by the photomechanical bending of the Azo SCP. Increasing thickness of the passive layer showed a reduction in the photomechanical efficiency of the bilayer actuators.

Chapter 4. Applications for a 4D Printed Actuator

4.1 Introduction into the Potential Applications of Light Activated Actuating Smart Materials

AM machines are mainly used for rapid prototyping and manufacturing, providing users the ability to observe how their parts will fit with tolerances and physical dimensions. New material and process development increases the advancements in AM applications. Current 3D printing materials prevent movement in printed parts since they are rigid and static. Adding SCPs to the 3D printed material allows the materials to move when exposed to external energies. This is an advantage in the additive manufacturing sector because this potentially reduces the number of moving parts in a product, which should reduce the amount of material and further reduce the costs and wastes of materials. Flexible light activated materials show promising applications in soft robotics, artificial muscles, and flexible actuators (Garcia-Amorós, Piñol, Finkelmann, & Velasco, 2011; Garcia-Amorós & Velasco, 2012; Li, Keller, Li, Wang, & Brunet, 2003; Niu et al., 2016; Wen et al., 2014) . Light activated materials show advantages over other SCP materials because light allows for activation to be wireless, automated, clean, and controlled. The actuator would have SCP material printed on both sides of the arm, which allows the actuator to bend bidirectionally

depending on the location of the light source or location of the active material (Figure 4-3. (a) & (b)).

Currently, there is a focus in the research on the functional applications of light activated shape changing polymers. Azobenzene polymers may be considered contenders for micro-robotics and light activated robotics because of their fast reacting motions, reversible motions, large mechanical actuation, and efficient mechanical motion. All of these motions can be accomplished without the need for onboard batteries, sensors, wires, processors, and moving parts. The use of smart polymers in micro-robotics is advantageous because polymers possess easy fabrication, bulk fabrication, relatively low weight compared to metals, low cost, and low environmental impact (Bar-Cohen, 2004; Mirfakhrai, Madden, & Baughman, 2007) . There have been demonstrations of light activated micro-robots using inchworm-like mobility. In one example, an azobenzene crosslinked liquid crystalline polymer (CLCP) was laminated onto a flexible polyethylene (PE) sheet Yamada, Kondo, Miyasato, et al., 2008 . CLCPs are a distinctive class of material because it possesses the characteristics of liquid crystalline materials and elastomers. The PE sheet possesses a sharp edge that remains stationary during UV light (366 nm, 240 mW/cm^2) activation that causes expansion of the film and it possesses a flat edge that slides during the expansion. The sharp edge drags during visible light (540 nm, 120 mW/cm^2) activation, while the flat edge remains stationary. In another example, a light-responsive LCE using a DR1 doped into the polymer network. The design of the light activated inchworm has PVA that is rubbed in a single direction and covered with a Teflon adhesive tape. Then the LCE is spin coated onto the adhesive layer and the desired shape is cutout of the film. The cutout shape is initially flat, but when it is annealed in an oven at 50°C, the cutout randomly forms a triple curl shape due to the material releasing internal stress between the surfaces of the LCE and PVA film. The curled film became flat when exposed to visible light (488 nm, 220 mW/cm^2) and had an average step length of 0.25 mm. It should be noted

that the step length changed depending on the surface material it was walking on. For example, the film had a max step length of 2.7 mm on a grating surface (Figure 4-1. (b)), but only possessed a step length of 0.8 mm on paper (Figure 4-1. (a)). The use of visible light in the activation of these locomotive light reactive materials is a desirable feature because most biological organisms can be harmed by UV light. These examples show that azobenzene materials can be used to simulate biological organisms and serve as suitable use in biomimicry research.

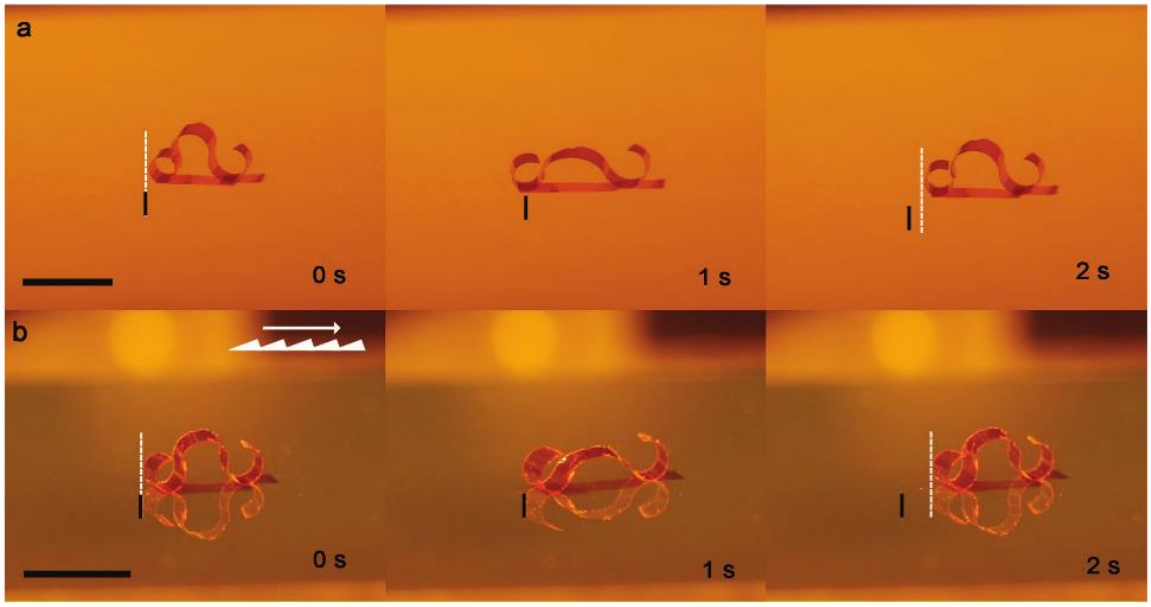

Figure 4- 1. The light driven movement of a DR1 LCE on different surfaces when exposed to visible light. (a) The images show the LCE sliding across the surface of paper when exposed to visible light (488 nm) with an intensity of 150 mW/cm^2. (b) The LCE slides across a grating surface when exposed to 488 nm light with an intensity of 200 mW/ cm^2. The grating direction is shown in the first image. The horizontal scale bars represent a length of 5 mm. the vertical black bars represent the starting position of the materials and the dashed white bar represents the final position after illumination. *(Zeng, Wani, Wasylczyk, & Priimagi, 2017)* . Adapted with permission by Macromolecular Rapid Communications, pp. 5, under John Wiley and Sons.

Another example of photo reactive azobenzene smart material application is the creation of a light induced self-regulating ocular iris based on a LCE. Researchers created a photoresponsive

material that opens and closes (dilates) in response to increasing and decreasing intensities of light. The material is an LCE, which is an anisotropic material that possesses a loosely crosslinked network of LC moieties that exhibit uniform molecular alignment. The moieties were aligned using photo alignment of radial-polarized incident light. The material was polymerized at 45°C and cooled to room temperature, where it remained flat. The material was cut into a disc that measured at 14.00 mm in diameter and twelve fin segments were cut out of the disc (Figure 4-2. (a)). Next, the disc was annealed at 50°C and cooled to room temperature, which caused the fins to spontaneously curl due to the relaxation of internal stress (Figure 4-2. (b)). The gap between the open fins was ~10 mm. Upon exposure to 470 nm light with an illumination area of 12.00 mm in diameter, the fins uncurled inward and closed the gap of the iris (Figure 4-2. (c)). The closure time of the fins could be controlled by the amount of intensity of the light source. In 230 mW/cm^2 light exposure, the film took 30 seconds to fully close, but only took 5 seconds to fully close in 300 mW/cm^2 light. Here, the materials could dilate and reduce the amount of absorbed light as the intensity of the light source increased, similar to an actual iris. This research is a great example of self-sensing and self-regulating soft materials that detect changes in their stimuli and react to them.

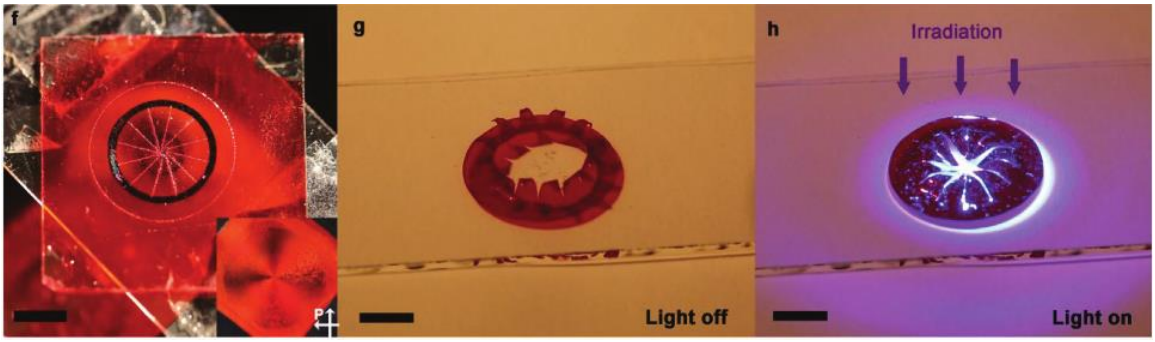

Figure 4- 2. (a) Image of the polymerized DR1 LCE with the 14.00 mm disc and the 12 fins cut out. (b) Image of the disc after it has been annealed at 50°C and cooled to room temperature in order to induce random curling in the fins. (c) The fins of the iris uncurl inward upon exposure to polarized 470 nm light at 250 mW/cm^2. Scale bars represent 5 mm. *(Zeng, Wani, Wasylczyk, & Priimagi, 2017)* . Adapted with permission by Advanced Materials, 29(30), pp. 4, under John Wiley and Sons.

Another issue with 3D printing is the limited build volume or build space of AM machines; if a user wants to print an object larger than the provided build stage then they must buy a larger printer or print two separate parts and combine them in post printing. Light activated SCPs would be useful in areas of advanced manufacturing, textiles, buildings, and structures. Parts are printed in flat compact shapes that efficiently use the print volume of parts that may be too large for the print bed. Those parts may be able to expand or unfold into their final stage after being exposed to light (Figure 4-4. (a) & (b)). These materials can be transported to their final destination and activated to unfold into their final shape. The products have the potential of being automated and transform at their final locations without human interaction. The light activated actuation and motions (expansion, contraction, bending, and twisting) of the azobenzene materials can be translated to real world applications by using careful design. The designs presented in this literature are proof-of-concept that light reactive materials are proficient of producing pertinent work.

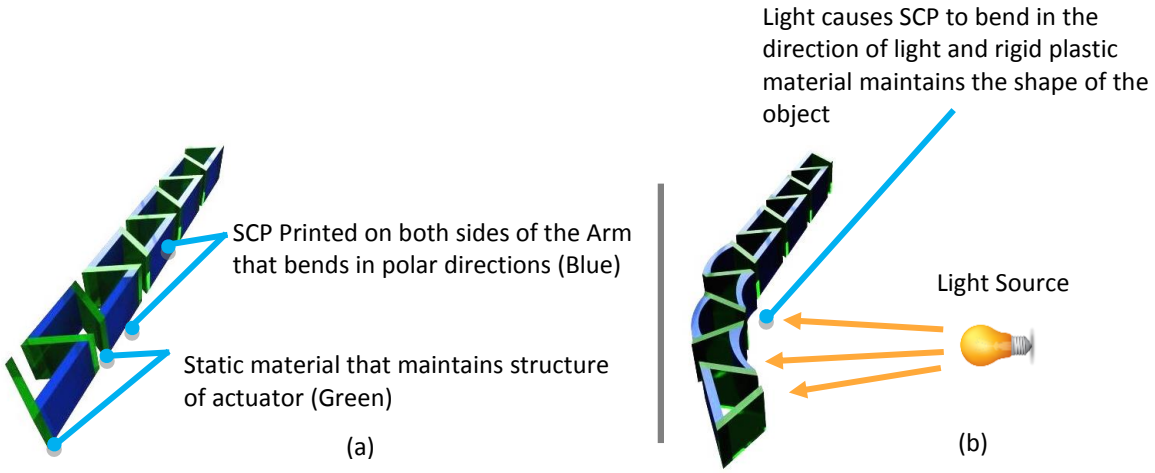

Figure 4- 3. (a) Photoactivated SCP is 3D printed on both sides (blue) of the arm for reversible bending. (b) Light activated SCP arm bends in the direction of the light source for use as a flexible actuator and artificial muscles.

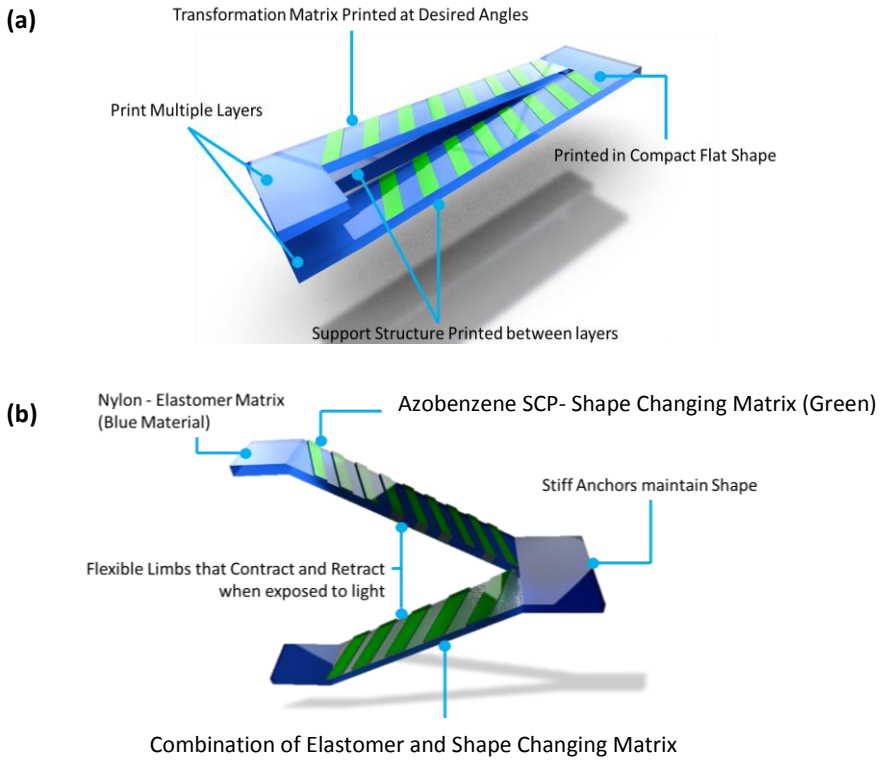

Figure 4- 4. (a) SCP actuator that can be printed in a flat structure to save space on the printing bed and (b) extends in vertical position when the light is projected onto the actuator.

4.2 Results

The photomechanical tests from section 3.2 provided a lot of insight into the design and mechanisms of the azobenzene bilayer films. The first aspect was the polymerization contraction angles generated when the azobenzene SCP is deposited onto heated passive layer, Kapton films. It was deciphered that the thinner passive film would induce a larger contraction angle, therefore, causing a larger photomechanical bending angle. A 1 mil thick passive layer was used in the applications experiments because it prompted the largest bending angle. The azobenzene SCP used in the experiments was MeOABHx due to the difficult synthesis of the DR1Hx SCP. Part of the design process was to take advantage of the polymerization contraction and use it as a design tool. As previously discussed, a 1 mil passive layer could exhibit a contraction angle up to ~90° and the photomechanical bending could be in the range of 35-45°. The actuation and bending of these films could be activated from the SCP side of the film or the passive layer of the film. This shows that the location of the light source does not determine the bending direction, but rather the location of the SCP on the bilayer film.

In the first example, a 1 mil Kapton film was annealed into a curved shape. The films measured at 30 mm x 7 mm, and an arc length of 14.14 mm (Figure 4-5. (a)). Since, the polymerization of the MeOABHx on heated Kapton caused contraction of the film, depositing MeOABHx on the top of the curvature would cause a contraction at the top of the film, ergo, causing the film to form a straight shape (Figure 4-5. (b)). Conversely, depositing the polymer onto

the bottom of the curved film would cause contraction along the bottom of the film, thus causing the film to induce further bending. In one test, the initial flat film was exposed to visible blue light (455 nm) at a distance of 10 mm. During the exposure, the film deflected upward at a distance of 2.33 mm in 2.5 seconds (Figure 4-5. (c)). The film was capable of maintaining this deflection until the light was turned off, which caused the film to return to its initial flat shape in the span of 5 seconds.

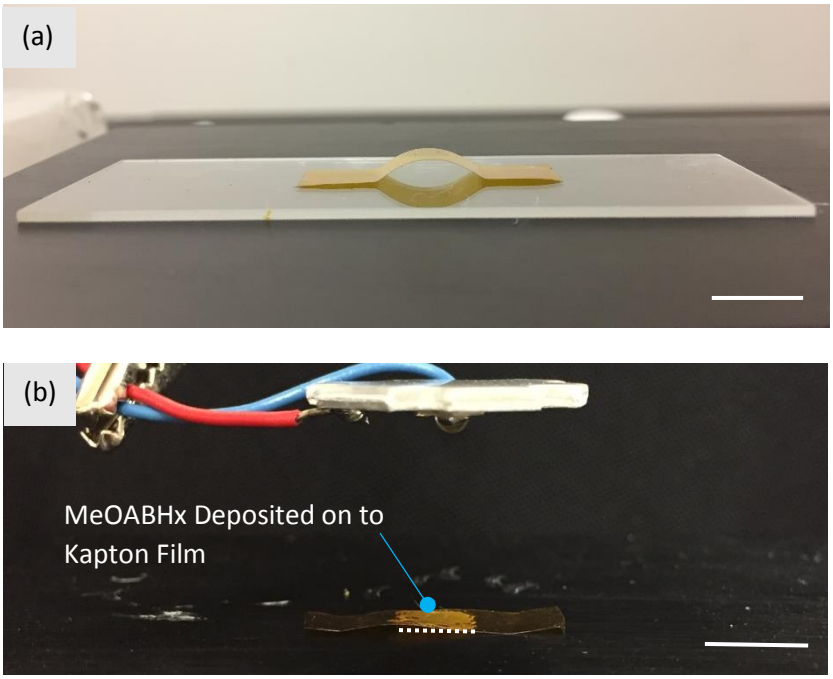

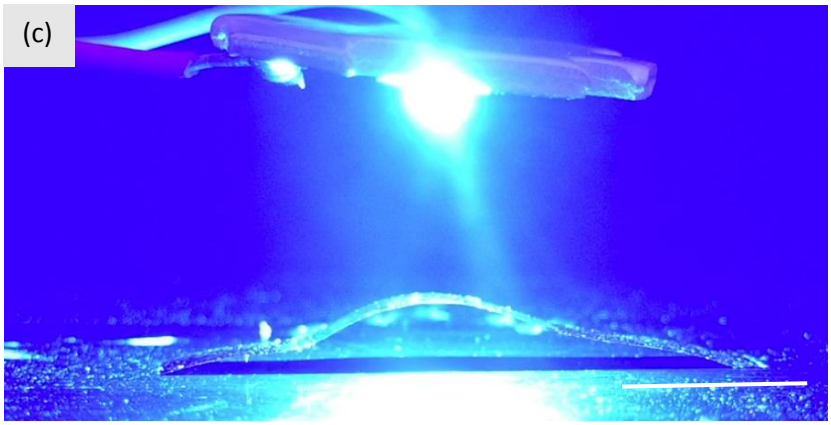

Figure 4- 5. (a) A curved 1 mil Kapton film after annealing in an oven for 24 hours at 120ºC. (b) Deposition of the azobenzene MeOABHx polymer on top of the passive Kapton film causes the film to contract and form a straight shape. (c) When activated by blue light (455 nm), the film rises by 2.33 mm. Solid white bars represent a scale bar of 10 mm in length.

The next step in testing of applications involved the process of sequential folding and multi-hinge materials. In this design, azobenzene SCP was deposited onto multiple areas of the Kapton film. In one example, 2 sections of the Kapton film had azobenzene MeOABHx deposited onto the film, which caused polymerization contraction bending in only those sections. In another example, three sections of the Kapton film had MeOABHx deposited onto the film, which caused contraction bending in those portions. The idea is that during light activation the areas with azobenzene polymer only react to the light and induce bending in those sections. The Kapton film is inert to the light, except for minor thermal expansion due to the heat from the light source. This design allows users to control which areas of their material they want to activate and produce complex bending motions.

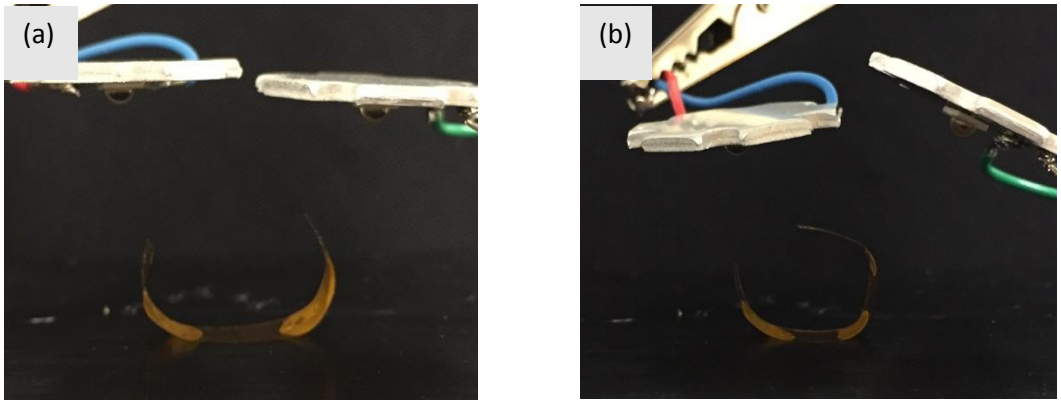

Figure 4- 6. (a) Azobenzene MeOABHx deposited on two sections of the film that induces almost 90º contraction angle at the two points of deposition. (b) In this image, three sections of the Kapton film have MeOABHx polymer deposited onto it, which causes ~90º contraction at those points.

Next, the multi-hinge films were exposed to royal blue light (455 nm) to test if specific areas of the films can be activated or if the entire film can be activated at once. During the dual hinge photomechanical testing, two blue lights are positioned 20 mm away from the azobenzene SCP hinges. Initially, the hinges are bent at ~90°, but the hinges quickly unbend to ~120° when the blue light is turned on (Figure 4-7. (a & b)). The hinges were capable of unbending in 6.5 seconds when exposed to the light and relaxed to their initial bent state in 6.5 seconds. Individual hinges could be controlled by controlling which lights were turned on. The quicker shape recovery may be due to the greater distance between the lights and the azobenzene SCP, which means a reduction in the light intensity. Less intensity would be mean less azobenzene moieties are isomerizing to the *cis* state. Next, a triple hinge film was activated using similar methods (Figure 4-8. (a)). The first blue light was positioned to the right of the triple hinge film that would activate hinge 1. The second blue light was positioned above the film that would activate hinges 2 and 3. The lights were turned

on sequentially, the first light was turned on that activated hinge 1 causing it to unbend and reveal access to the bottom hinges, 2 and 3 (Figure 4-8. (b)). The second light was activated once the first hinge reached its maximum bending angle. The second caused hinges 2 and 3 to further unbend (Figure 8. (c)). The hinges returned to their initial positions when the light sources were turned off.

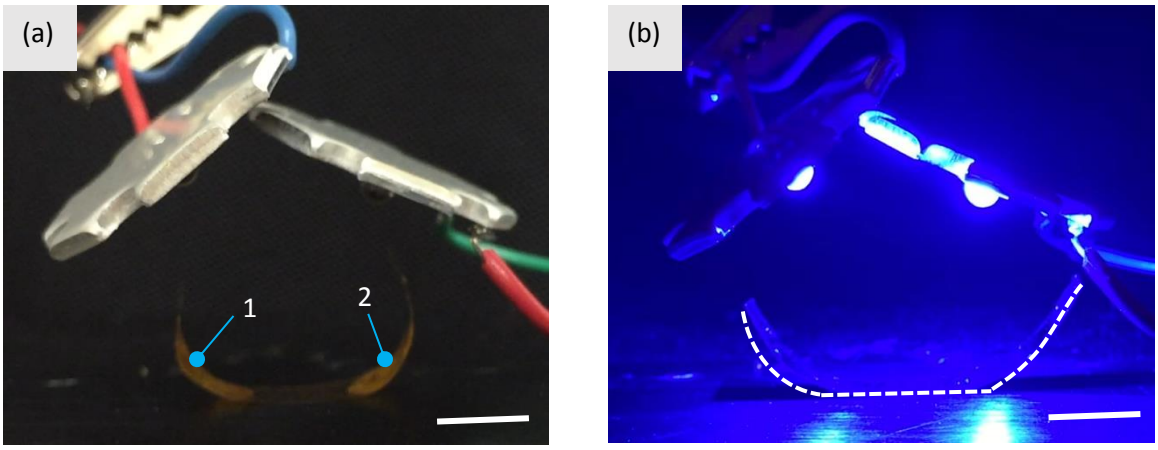

Figure 4- 7. Photomechanical Bending tests of a dual bending hinge. (a) Initially, the hinges are bent at ~90°. (b) When light activated, the hinges unbend to ~120°. Hinges were activated using two visible blue lights (455 nm). The dashed white line highlights the angle of bending of the bilayer film due to low visibility. Solid white bars represent a scale of 6.5 mm.

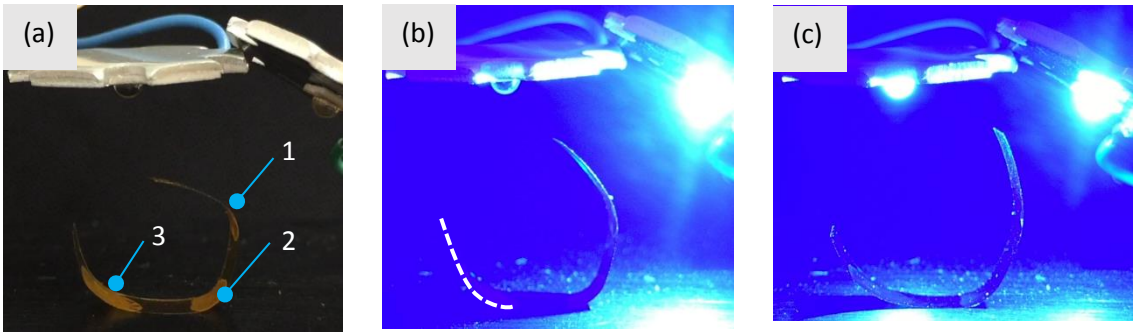

Figure 4- 8. Photomechanical bending tests of triple bending hinge. (a) The hinges are bent at ~90° in areas that possess azobenzene polymer. The hinges are identified as hinge 1, 2, and 3. (b) When activated with blue blight (455 nm) from the left side, the hinge 1 unbends and allows access to the two bottom hinges. (c) The second light is turned on and activates hinges 2 and 3, which causes them to unbend further. The dashed white line highlights the angle of bending of the bilayer film due to low visibility.

The next step of the applications testing was to investigate if different mechanisms and shapes can be generated using light activated materials. As previously stated, Kapton film can be annealed into different shapes. A sinusoidal shape with 3 curvatures was annealed at 120°C for 24 hours. After annealing, the Kapton film was capable of maintaining this shape. Next, the azobenzene polymer was deposited on top of the curvatures. Deposition on top of the curvatures caused the curves to become straight due to the azobenzene polymer contracting during polymerization (Figure 4-9. (a)). During photomechanical testing, different hinges could be activated one at a time, which caused controlled, selectable, and sequential shape change of the film (Figure 4-9. (b-d)). However, users could activate multiple sections of the films using multiple light sources. Two sections of the film formed curvatures when two light sources illuminated two different azobenzene polymer sections (Figure 4-9. (d)).

Alternatively, a switch was designed to test if two different motions could be generated from the same Kapton film. A film that possessed two fins, one fin that was in the flat state and a second fin that was bent upward, was annealed at 120°. Next, the azobenzene polymer was deposited on the fixed end of each fin. During polymerization, contraction of the polymer caused the flat fin to bend upwards and caused the bent fin to bend downward to a flat state (Figure 4-10. (a)). Upon light activation, the bent fin (fin 1) unbent in a downward motion and the flat fin (fin 2) bent upward (Figure 4-10. (b)). This shows that two different motions can be activated on the same material using the same light source.

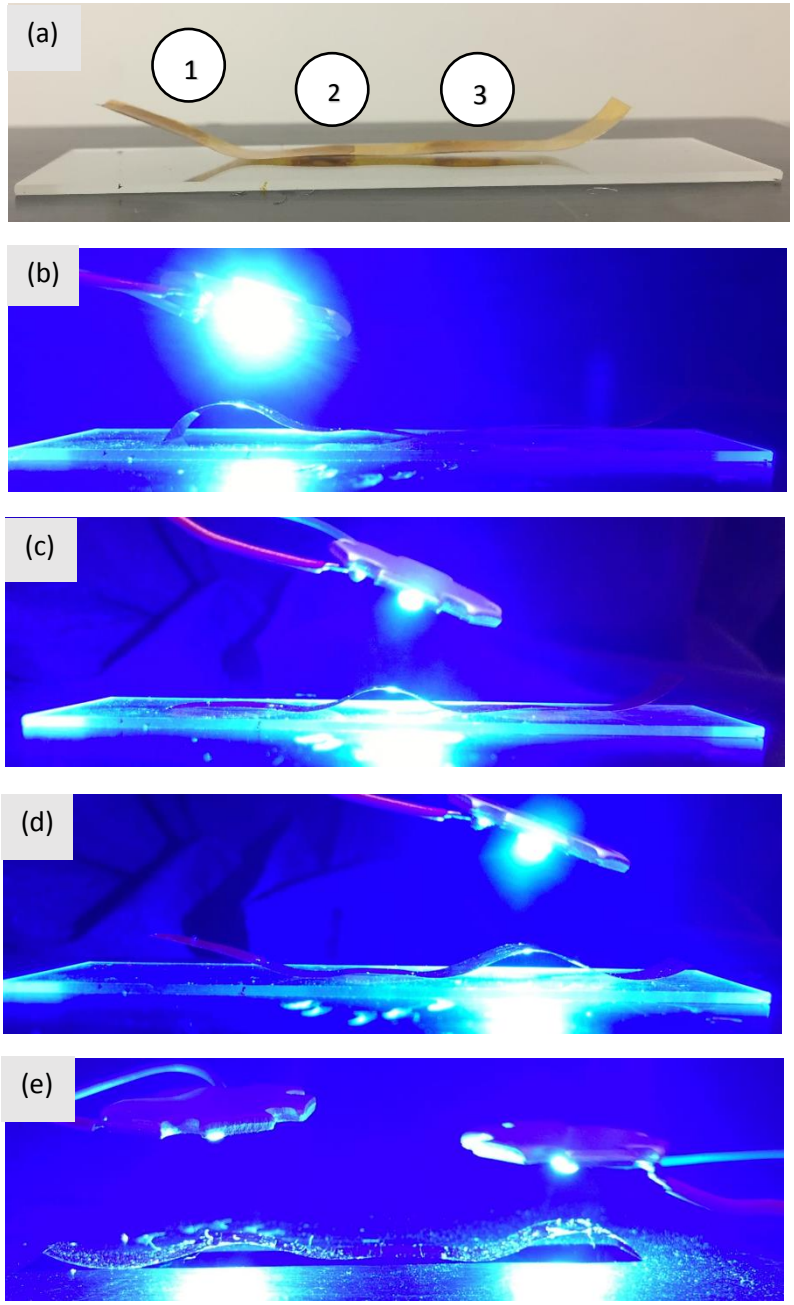

Figure 4- 9. (a) The initial shape of a triple segment azobenzene bilayer film. Originally, the film possesses three curvatures, but the contraction of the azobenzene polymer causes the curvatures to straighten. Next, sequential light activation of the bilayer film shows how the bending and shape transformation can be controlled by illuminated (b) segment 1, (c) segment 2, and (d) segment 3. (e) Multiple segments can be activated at once. Removal of the light source causes the hinges to return to their original shape.

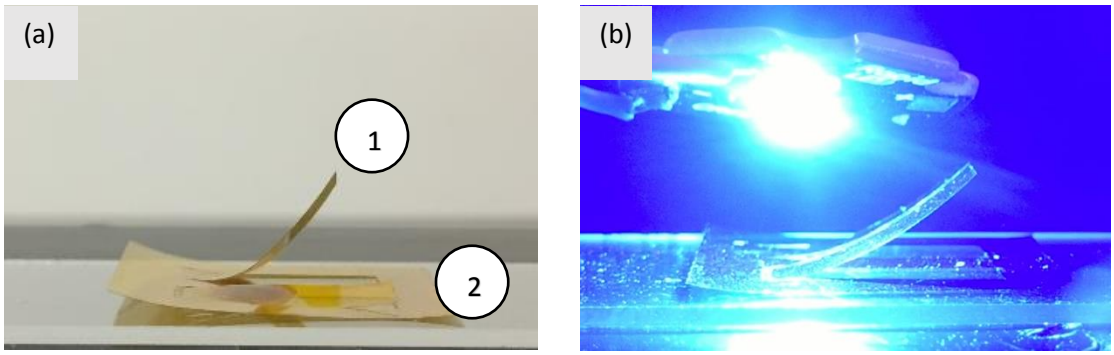

Figure 4- 10. A 4D printed azobenzene switch that allows cantilever 1 to lower during light activation and cantilever 2 to rise during light activation. (a) The final contraction angle of the cantilevers after deposition of the azobenzene polymer onto the 1 mil thick Kapton film. (b) The bending positions of the cantilevers during light activation using 455 nm light. The light activation causes cantilever 1 to lower and cantilever 2 to rise.

4.3 Outcomes

The outcomes of this aim set a baseline for designing and producing 4D printed photoisomerable products. Users can create complex actuators because of the accuracy and precision of current AM technology. The actuators could be used as micro-robotic arms, hands, and fingers for grasping different objects. Also, the actuators could serve as switches or sensors without the need for onboard electromechanical sensors, processors, actuators, and power storage. Light as an activation method is advantageous because it is wireless, abundant, and can be focused on specified points. The use of sequential folding allows users to control the bending motions of the film by focusing light on specific areas of the product.

The transformation and control of complex shapes during light actuation was successful throughout the applications experiments. The bending direction was capable of being controlled depending on the location of the azobenzene polymer on the passive layer. However, the direction

of the light source did not change the direction of bending. Also, the contraction angle due to the polymerization of MeOABHx could be used as a design mechanism. The bilayer films would induce a random bending angle if the azobenzene polymer was deposited on heated (80-100ºC) Kapton films. After the deposition and during the cooling process, the bilayer films would form random bending positions. Flat films would form almost 90° bending angles during the polymerization contraction for 1 mil thick Kapton films. Users could take advantage of this knowledge in order to design complex shape changing products.

Since, the films produced a contraction angle during polymerization, the technique could be used for films that are already pre-bent or annealed into different complex shapes. In one example, pre-bent films would become straight during contraction when the polymer was deposited on the top of the curvature. Deposition of the azobenzene polymer on the bottom of the curved films would cause the film to further contract, thus forming a larger curvature of the film. This proves that the location of the azobenzene polymer on the passive film plays a large role in the final actuation and shape of the bilayer actuators. In this case, an actuator can move in an upward direction. This type of actuator could be used to make a switch or a pump. Also, different actions can occur using the same type and shape of annealed Kapton film by changing which side of the film has azobenzene deposited on it. This could reduce the amount of required materials that are needed to create an actuator that performs different movements because facilities would need to manufacture one shape and print polymer on different sides of the film.

It was also discovered that multi-hinge actuators could be created by depositing azobenzene polymer on multiple areas of the passive film. As an example, two different Kapton films had two and three sections deposited with azobenzene SCP. Bending only occurred in the areas with SCP. This shows that the actuating structures can only be created in specific sections by 3D printing SCP in specific areas of the bilayer actuators. Sequential folding is a special research

area that takes into account the distinct design of the shape changing hinge, so that the actuating parts move in a specific order, at a specific rate, possess different final bending positions, and ensure that actuating parts do not interfere with each other. In this case, the order of the hinge activation can be controlled by focusing the light on the desired azobenzene SCP hinge and only activating that hinge.

In order to induce complex shapes, the Kapton film has to be annealed first. In these experiments, different shapes can be formed such as a spiral, a curvature, and a sinusoidal shape. These different shapes can perform different motions when azobenzene SCP is deposited onto the films. The different shapes can be used for different applications such as transportation, opening and closing, and sensing and connecting switches. Overall, the design method is fairly simple; however, an elimination for the need to anneal the films into different shapes would be ideal. The process of 3D printing the azobenzene SCP onto the films would better streamline the manufacturing process, but the need to anneal and heat the materials after just adds another step. In the future, different materials could take the place of the passive film. The Kapton film is ideal for the proof-of-concept experiments because it is mechanical robust and does not react to most solvents, which allows many different solutions to be extruded onto it. Other materials may prove to possess other properties that are better than Kapton such as lower Young's modulus for better bending photomechanics. Also, the idea plan would use a passive material that can be converted into solution and 3D printed into different shapes. Next, the azobenzene SCP could be 3D printed on top of the passive films, producing a fully 3D printed product. Alternatively, a new azobenzene SCP could be used, such as 3D printing of an LCE or LCN. This method may eliminate the need for a passive layer.

In the end, the 3D printed azobenzene bilayers were capable of actuation and changing shape; however, the materials were unable of performing complex tasks such as gripping objects.

The amount of stress generated by the films was around 200 kPa, which was comparable to skeletal muscle fiber but not powerful enough to grip objects. Although macroscale applications of the light reactive 4D printed material may not be realistic, the materials may find applications in the micro-scale areas such as micropumps, switches, and actuators. The materials have simplified the design and manufacturing of actuating parts that use light as a power source.

Chapter 5. Summary of Work

Overall, multiple 4D printing techniques were observed in this research. Both FDM and syringe printing techniques were used for 3D printing of the smart materials. FDM printing was used to test thermomechanical shape memory polymers and their combination with nylon materials for the creation of smart textiles. The concept of using a 4D printed PLA as a shape memory material has been demonstrated. The shape memory recovery of different thicknesses of post printed PLA exposed to different temperatures has been quantified. As predicted, thicker materials perform slower than thinner materials. Results showed that thicker materials display less shape recovery as thinner materials. The activation temperature increases the shape recovery efficiency at higher temperatures above the material's T_g. Finally, a proof-of-concept process of combining 3D printed PLA with nylon fabric for the creation of 4D printed smart textiles was established.

A second activation method for 4D printing was investigated. Two different azobenzene SCPs were synthesized and photomechanically tested. It was determined that an azobenzene SCP with a main-chain azobenzene moiety required heating during light activation and an oxygen-free environment during polymerization. The second synthesized polymer, an azobenzene PHMS MeOABHx chemical composition was analyzed and confirmed that it is the correct composition using ^{1}H NMR. UV-Vis spectroscopy was performed to observe the material's absorption in

different light sources (UV and visible green), which proves the material exhibits a *trans-cis* and *cis-trans* isomerization process. The UV-Vis spectroscopy provided what were the ideal wavelengths for activating the *trans* isomer and the *cis* isomer was 360 nm and 450 nm, respectively. Finally, a third azobenzene SCP using DR1 dye was synthesized to compare its properties to MeOABHx. The chemical compositions, UV-Vis spectroscopy, and thermal properties were analyzed for DR1Hx using similar techniques as MeOABHx for consistency. The glass transition temperature and melting temperature was determined for MeOABHx, which was below room temperature, making it ideal for light activation without the need for simultaneous heating. DR1Hx melting temperature was determined, but the glass transition temperature was unobservable.

The azobenzene SCPs (MeOABHx and DR1Hx) were 3D printed with a syringe printer onto Kapton films, which created photoactive bilayer films. The results proved that azobenzene could be used as a 4D printable material. The films were tested for photomechanical bending in UV (365 nm) and visible blue (455 nm) light. It was observed that blank Kapton film possessed some thermal shape changing properties, but not comparable to the azobenzene bilayer films. The photomechanical bending was quantified and analyzed for different passive layer thicknesses and different wavelengths of light. The repeatability of the photomechanical bending was tested and showed little degradation.

The MeOABHx and DR1Hx bilayers films' photogenerated stress was measured using a DMA machine. The photogenerated stress of different passive layer thicknesses and different light activation wavelengths were measured for the two different polymers. DR1Hx, surprisingly, possessed much higher photogenerated stress than MeOABHx. Overall, thinner films were more ideal for higher photogenerated stress, which was over ~200 kPa and similar to the stress generated

by skeletal muscle fibers. In the end, further studies were focused on polymer MeOABHx because DR1Hx proved to be difficult to synthesize and faced issues of delamination from the passive layer.

The polymerization contraction angle was measured for polymer MeOABHx when deposited onto heated passive films of different thickness. Passive films with thicker layers possessed less contraction angle during polymerization. The amount of contraction angle seem to correlate with the photomechanical bending angle during light activation. Bilayers that possessed higher contraction angles seem to possess higher photomechanical bending. Thinner materials may be ideal for designing actuators that possesses the highest amount of bending. However, the design of products that possess different bending rates and final bending positions can be utilized by altering the thickness of the passive layer. This testing aided in the testing and design of applications.

Proof-of-concept designs were tested in the applications division of the research. It was determined that the direction of light does not affect the bending direction of the cantilever films. The location of the polymer on the film determines the bending motion when the films are activated by light. This means that placement of the polymer onto films must be taken into account when designing 4D printed actuators. Also, after contraction polymerization tests were performed, it was determined that the materials could form 3D shapes after cooling to room temperature from a higher temperature (80-100°C) due to contraction of the polymer on the film surface as it transitions from a isotropic molecular structure to a nematic structure. The contraction can be taken advantage of and used in the design of actuators. Different shapes of the blank Kapton film were created and annealed. A curved arc film, a sinusoidal shape with a peak-to-peak amplitude of 3, a dual switch that possessed two cantilevers (cantilever 1 is bent upwards and cantilever 2 is in a flat state), a dual hinged cantilever, and a triple hinged cantilever. The tests showed that users can control which areas of the films are activated by light, induce fast reaction, induce reversible shape change, and

activate multiple sections using multiple light sources. Applications testing showed that different shapes can be formed very quickly using light activation without the need for heavy onboard sensors, batteries, processors, and multi-part hinges.

Chapter 6. Conclusion and Future Work

6.1 Conclusion

Additive manufacturing remains a growing industry that is reaching more and more markets. New printing methods, software, machinery, and materials are continually being advanced and improved, which makes 4D printing a more realistic and accessible industry. 4D printing may promote the use of 3D printers for creating final products instead of prototypes. 4D printing has introduced new design techniques that may reduce the amount energy, materials, time, and money to create actuating products. The point of 4D printing is to simplify the design and manufacturing process that allows for complicated designs and actuated products to be created from the base materials alone.

The concepts presented in this report have aided in the research area of 4D printing and smart materials. It has been shown that common 3D printing material, PLA, displays shape memory properties after being 3D printed in a FDM printer. Thermomechanical shape memory 4D printed products can be designed to actuate at different rates or possess different final bending positions depending on the thickness of the materials and the temperature of the environment. These properties may prove to be important for a process called sequential folding, where design of the actuating hinges is important for creating 3D objects from 2D bodies to prevent moving parts from interfering with each other. Different mechanisms can be designed for different applications such

as a spline that can act as spring, components that can fold into compact shapes for easy packaging, or grippers that can grasp small objects.

3D printing PLA onto nylon materials is described as a form of 4D printing smart textiles. The smart textiles can be formed into custom shapes when heat treated and return to their original flat shapes when heated above their glass transition temperature. This allows for custom shapes and aesthetics for clothing, or the encapsulation and release of materials when activated by their environments. This research describes current 3D printing materials that can be used for 4D printing technology and lead to faster development of 4D printing applications in areas of biomedical devices, smart textiles, and advanced manufacturing.

Light-reactive 3D printable smart materials may be the future of 4D printing technology; specifically, photoisomerable reactions and not temperature reaction due to light, which possess the ability for fast reactions and reverse shape change. This research proved that light reactive or photoisomerable materials can be used as 4D printable materials, but it was revealed that not all azobenzene SCPs are suitable for 3D printing or they are only suitable for specific printing processes. Multiple azobenzene polymers were synthesized for different purposes. A main-chain azobenzene SCP was not suitable for the purposes of this research, but may find applications in high temperature (above 85°C) environments. Two different side-chain azobenzene PHMS were synthesized that were capable of actuating when combined with a passive layer (Kapton film) for the creation of photoisomerable bilayer films that can bend and unbend with minimal degradation. The azobenzene PHMS was capable of being accurately and precisely 3D printed onto Kapton films after being designed in 3D modelling software. Complex design could be created and specific areas of a product can be specified as light reactive and other material can be static by using 3D printers. Only specific areas of a product would actuate when exposed entirely to light or light reactive areas can actuate in sequence using a focused beam. Light reactive materials would prove

to be beneficial to many applications because light is wireless, easily controllable, clean, and fast reacting. Azobenzene research is constantly being pursued; azobenzene materials could react to different wavelengths of light, such as sunlight, depending on the synthesis of the of azobenzene polymers.

In the future, light reactive 4D printable materials could be used to create lightweight, flexible, and fast reacting actuating parts such as soft robotics. The future of 4D printing lies in the controllability of the movement, assembly, and disassembly of printed products, automating the reactions of 4D printing products (removing the human interaction), expanding the activation stimuli for 4D printable smart materials, and creating software that models and simulates shape change behavior. Once these challenges are solved, this exciting and new technology will, hopefully, simplify and support many people's lives in many different applications and industries.

6.2 Major Contributions

The contributions of this research are summarized below:

1. PLA is a very common FDM thermoplastic, but its shape memory properties after 3D printing has not been reported. The research shows that PLA can be used as a 4D printed shape memory material post printing. The shape memory and shape recovery of the material was quantified depending on the 3D printed material's thickness and the activation environment temperature.
2. The combination of PLA and textiles by 3D printing PLA onto nylon mesh fabric in order to explore the area of smart textiles. It was discovered that the nylon mesh fabric could retain shape memory properties post 3D printing. The materials could then be fixed into customized shapes and retain these shapes at room temperature.

The materials recovered their original shape when reheated above its glass transition temperature. The materials could also be used to encapsulate components and release them when it reacts to the environmental temperature.

3. There are many different azobenzene SCPs, but the materials have not been 3D printed before. Typically, materials are spin coated or casted then cut out into desired shapes. In this research, two different azobenzene polysiloxane SCPs were synthesized that can be used as 3D printing materials. The materials were loaded into a bioprinter and printed onto Kapton films for the creation of light reactive bilayers. Users can take advantage of 3D printers' fast and accurate printing process to create complex 2D designs using the azobenzene SCP.
4. After 3D printing, the material's photomechanical bending was quantified through cantilever bending tests during light activation. Photomechanical bending was measured in accordance to the passive film's thickness, the light sources wavelength, and the light sources intensity. Also, properties were measured for the two different azobenzene SCPs (MeOABHx and DR1Hx). The relationships will aid researchers in material selection of SCPs and passive films, and light activation sources.
5. Random contraction of the bilayer films occurred during deposition of the azobenzene SCP onto the Kapton film. This occurrence was caused by the polymer network transforming from a random isotropic structure to an ordered nematic structure during polymerization. A relation between the contraction angle, azobenzene polymer, and film thickness was established. Next, a relation between the contraction angle and the photoactivated bending angle was formed.

6. Although the azobenzene bilayer films display large amount of deflection during light activation, the stress generated during light activation needed to be measured. The photogenerated stress for the MeOABHx and DR1x polymers were measured for different thicknesses of Kapton film and different light activation sources. It was discovered the materials exert stresses above 200 kPa when exposed to light, which is higher than skeletal muscle fibers. The experiment shows that the materials may be better suited for microfabrication applications and applications that require small amounts of stress. The films could be bundled together, just like muscle fibers, in order to generate larger stresses.
7. Different designs of the 3D printed azobenzene bilayer films were tested. This contribution serves as a proof-of-concept and how different designs can be created for different applications. It was shown that 3D printed single hinged bilayer films can actuate when exposed to different wavelengths of light. Multi-hinged/multi-segment azobenzene materials can be activated using a single light sources or multiple light sources.

6.3 Future Work

The work performed in this thesis explores the feasibility and development of using a current thermosensitive 3D printable material and a new innovative light reactive shape changing polymer as 4D printable materials. Although much development has been made in these areas, there is still much that can be improved. Beginning with the thermosensitive material (PLA). PLA proved to be a credible 4D printable FDM material that reacts to high temperatures; however, a material that reacts to lower temperatures would be desired. The future of biological devices may lie in

additive manufacturing because the technique allows for the ability to tailor devices to individuals. Biomedical devices such as stents could be 3D printed for different arteries in the body and expand automatically by reacting to the internal body temperature (37ºC). The use of a shape changing polymer in the body may allow for the devices to degrade over time, which would remove the need for future surgeries to modify or remove parts. Currently, there are limited low melting 3D printable materials. One method to reduce the T_g of these materials is to blend them with other low melting or low T_g materials such as polyurethane. However, one negative with blending low T_g materials is the loss of mechanical strength and shape memory efficiency. The area of smart textiles was explored in this research by 3D printing PLA onto nylon fabrics. The technique proved to be successful, but different textiles were not tested. In the future, different fabrics can be 3D printed on and test their shape memory capabilities. Also, if low T_g materials are developed, then the development of materials that dynamically react to the wearer's body temperature or the surrounding environment that cools the person or keeps them warmer may become a reality.

The next portion of this research was to synthesize a light reactive photoisomerable shape changing polymer and explore its possibility as a 4D printable material. Overall, the research proved that is possible to create a photoisomerable 4D printing material, but the concept to prototype was not perfect. In the end, a bilayer design had to be used in order to generate actuation from our material. Different passive layer materials that possess lower Young's moduli than Kapton film could be used that may generate better shape changing properties during light activation. Also, a passive layer that could be converted into a solution and loaded into a syringe for 4D printing could be developed. Previously, Polydimethylsiloxane (PDMS) and polyurethane were converted into a solution for 3D printing. The solutions were capable of being deposited, but the thickness of the passive films were very thick (>1 mm) and inconsistent. Next, azobenzene SCP was deposited onto the passive films, but the SCP did not adhere to the PDMS and the toluene solution used in

the SCP deteriorated the polyurethane. In the future, different materials for the passive layer could be explored that can be 3D printed and produce better light activated shape change efficiency.

In this research, azobenzene side-chain shape changing polymers were synthesized. Extensive photomechanical testing and material property testing was performed in this research, but further testing is always desired. One theory about the photomechanical bending efficiency was postulated that the molecular alignment and liquid-crystalline structure of the polymer network may affect the bending effectiveness. The molecular alignment was never observed in this research. In the future, an X-ray diffraction or polarized-optical microscope could be used to analyze the alignment when the material is in different phases. This will confirm how much of an effect the molecular alignment has on the photomechanical bending. Also, the thickness of the azobenzene polymer deposited on the films was never quantified. A light-profile microscope or high-powered optical microscope could be used to measure the thickness of the SCP. Then photomechanical tests can be performed that measure the bending angle or photo-generated stress of the bilayer films with different thickness of the SCP. Photomechanical tests were not performed for different widths and lengths of deposited SCP on the bilayer films. Again, the photomechanical efficiency could be quantified depending on the geometry and location of the deposited SCP onto passive films.

For future research, different azobenzene SCPs such as LCEs and/or LCNs could be synthesized. The type of SCP used in the research was limited by the 3D printing methodology. Ideally, polyjet printing would be used because it can print highly detailed and accurate parts from a solution. However, polyjet printers tend to be expensive and the UV curing of the materials during the printing process may interfere with the azobenzene moieties. Azobenzene materials that display the highest photomechanical efficiency are typically crosslinked in some way. LCNs display properties of shape change when exposed to UV light and shape memory when exposed to visible light. A material that possesses shape change and shape memory properties would have increased

access to more applications because customized shapes could be formed post 3D printing. Light reactive 4D printing faces many different design challenges and leaves room for product development. This research presented a proof-of-concept for 4D printing of light actuation materials.

Appendix A: Individual Kinetics Studies for MeOABHx and DR1Hx Polymers when exposed to different Wavelengths of Light

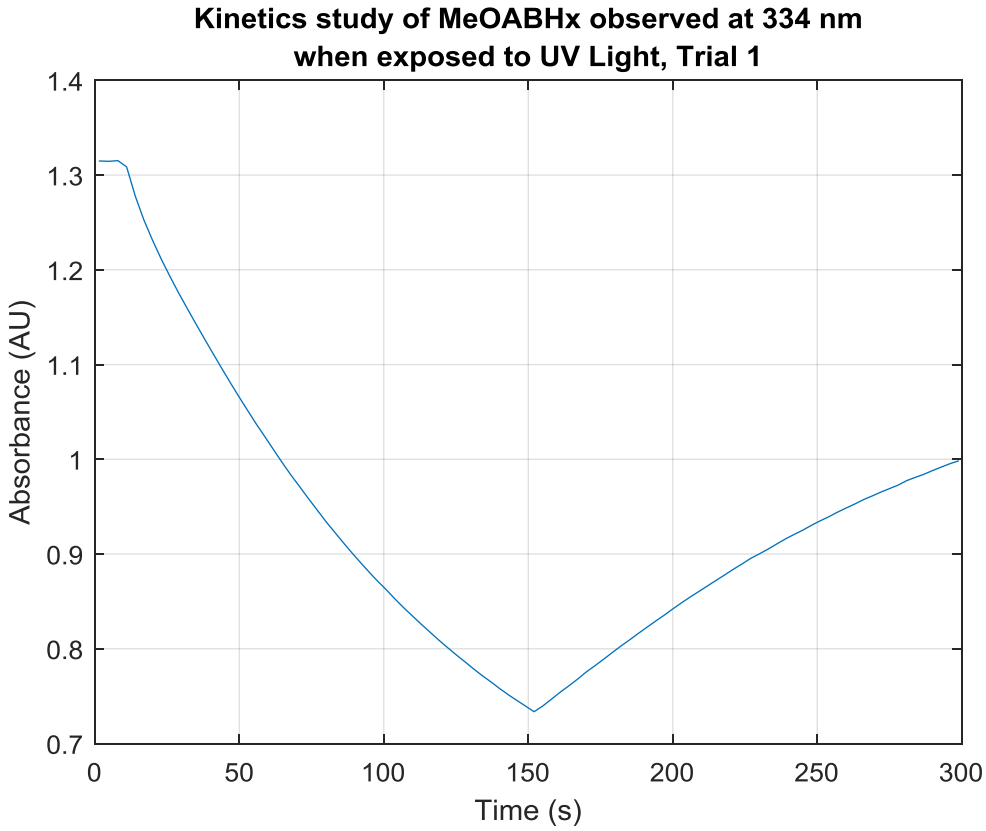

Figure A- 1. Trial 1 of the Kinetics Study for MeOABHx observed at 334 nm when exposed to UV Light (365 nm). The data presented was performed by Dr. Frank Ji's lab in the Chemistry Department. It has been adapted with permission by Dr. Frank Ji's lab in the Chemistry Department.

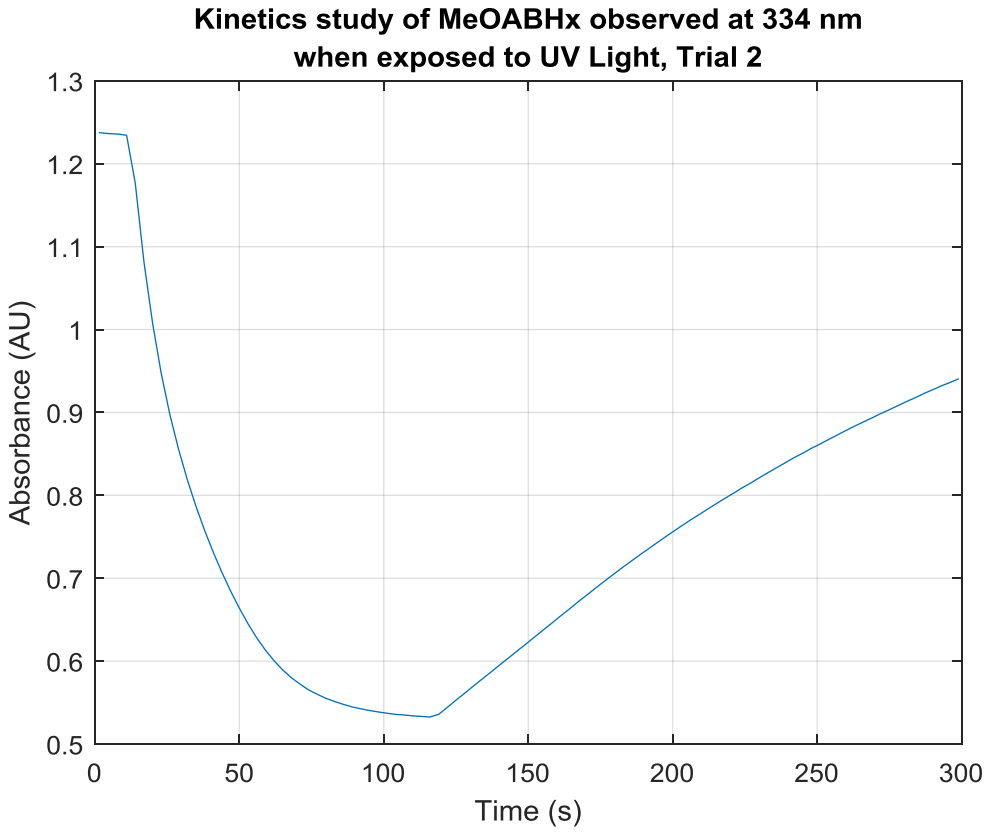

Figure A- 2. Trial 2 of the Kinetics Study for MeOABHx observed at 334 nm when exposed to UV Light (365 nm). The data presented was performed by Dr. Frank Ji's lab in the Chemistry Department. It has been adapted with permission by Dr. Frank Ji's lab in the Chemistry Department.

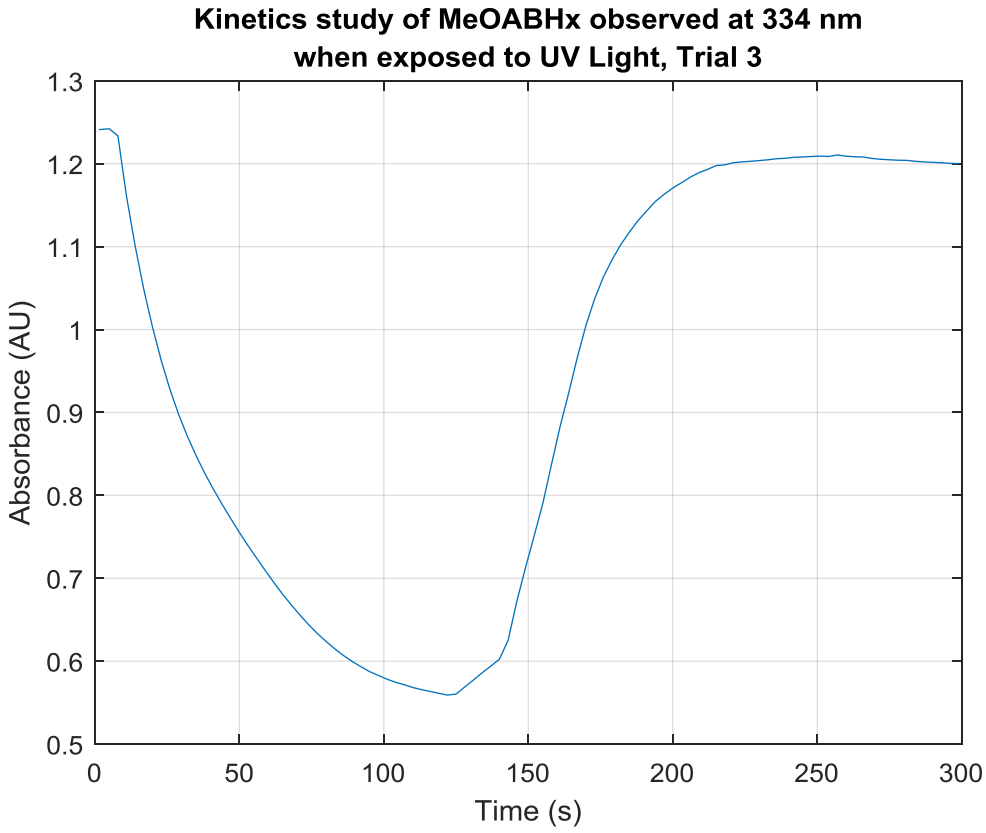

Figure A- 3. Trial 3 of the Kinetics Study for MeOABHx observed at 334 nm when exposed to UV Light (365 nm). The data presented was performed by Dr. Frank Ji's lab in the Chemistry Department. It has been adapted with permission by Dr. Frank Ji's lab in the Chemistry Department.

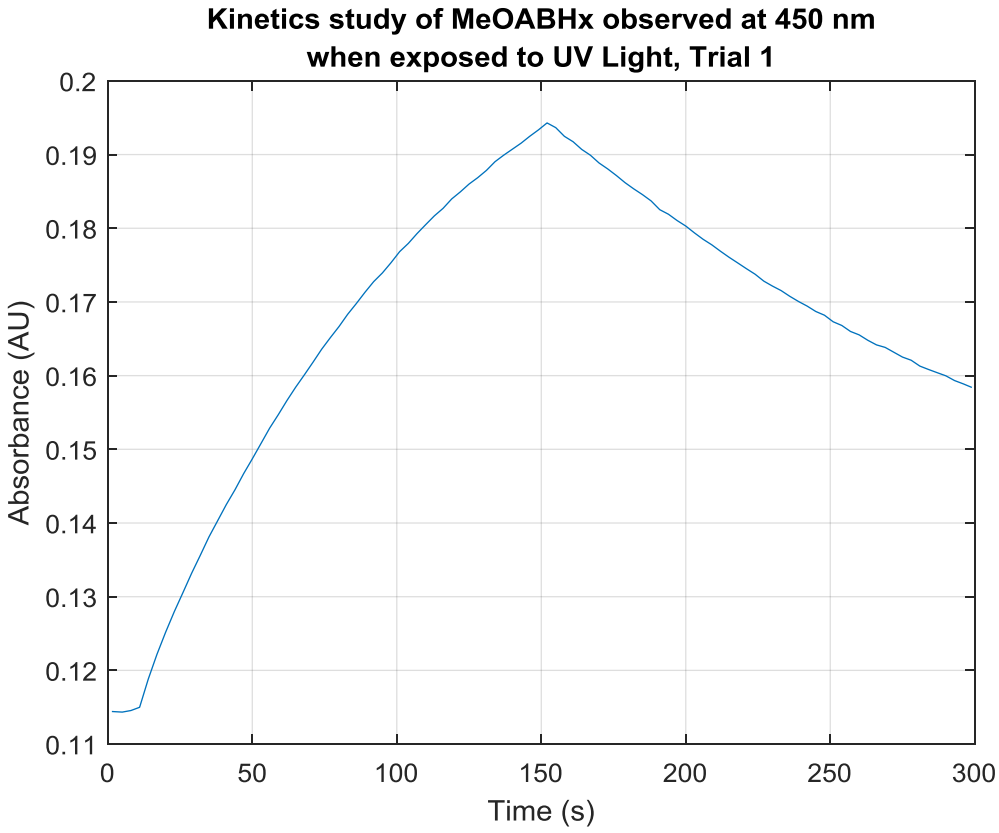

Figure A- 4. Trial 1 of the Kinetics Study for MeOABHx observed at 450 nm when exposed to UV Light (365 nm). The data presented was performed by Dr. Frank Ji's lab in the Chemistry Department. It has been adapted with permission by Dr. Frank Ji's lab in the Chemistry Department.

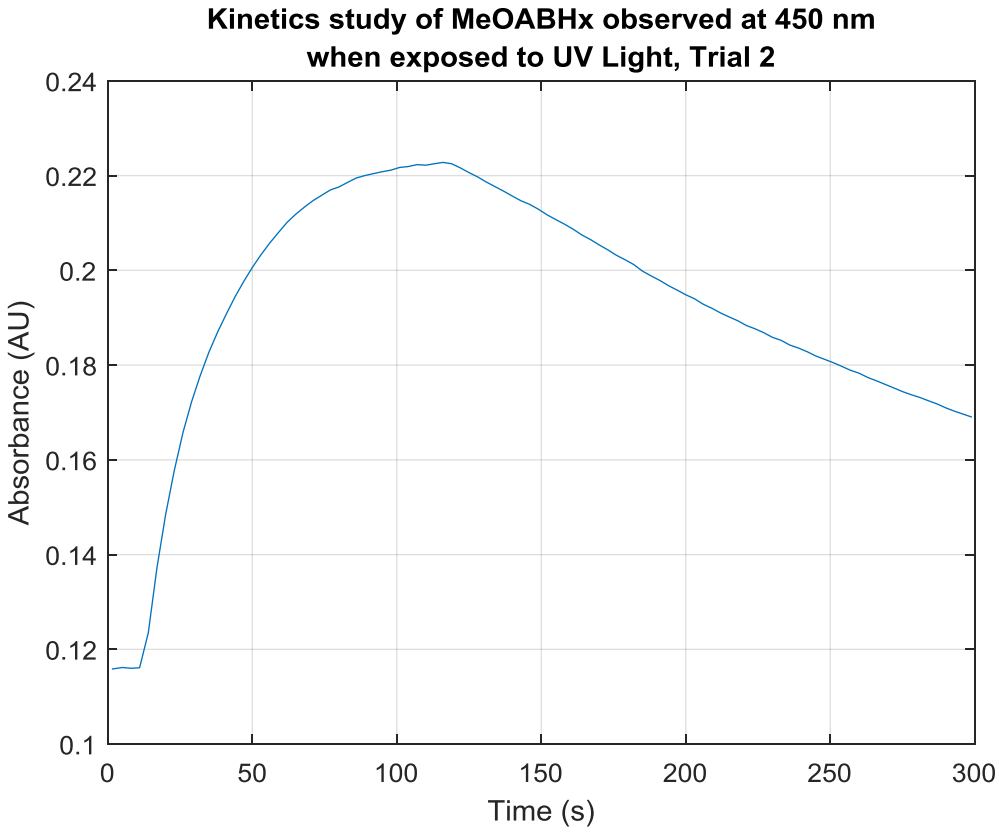

Figure A- 5. Trial 2 of the Kinetics Study for MeOABHx observed at 450 nm when exposed to UV Light (365 nm). The data presented was performed by Dr. Frank Ji's lab in the Chemistry Department. It has been adapted with permission by Dr. Frank Ji's lab in the Chemistry Department.

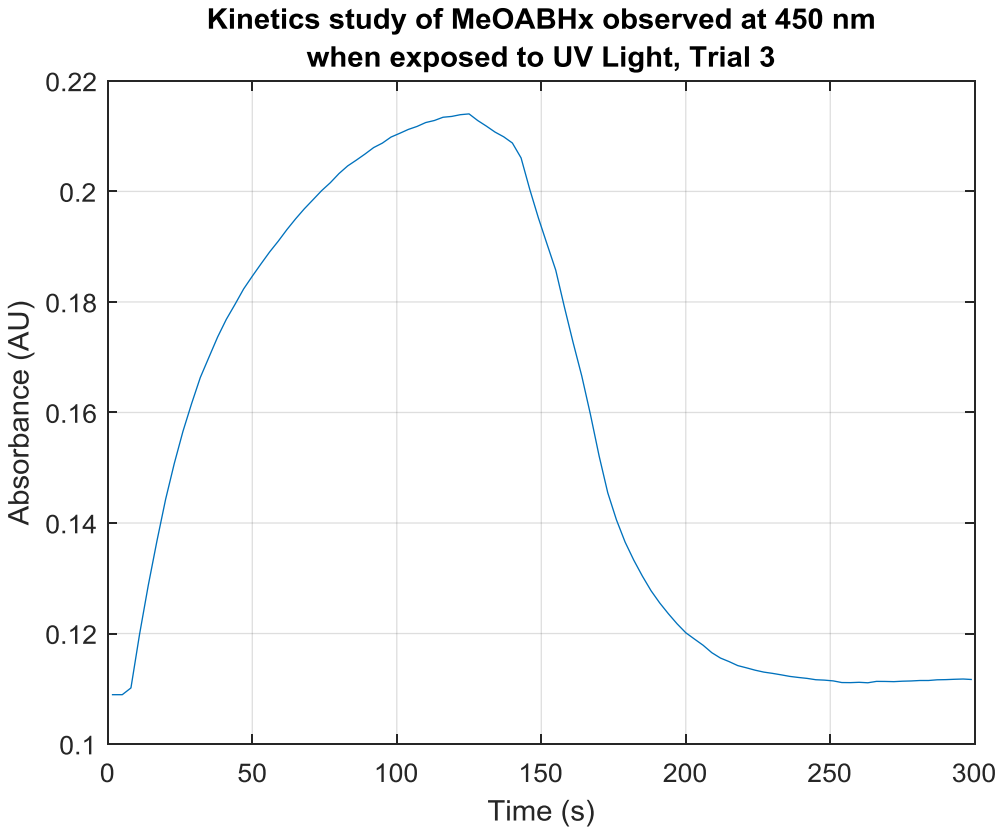

Figure A- 6. Trial 3 of the Kinetics Study for MeOABHx observed at 450 nm when exposed to UV Light (365 nm). The data presented was performed by Dr. Frank Ji's lab in the Chemistry Department. It has been adapted with permission by Dr. Frank Ji's lab in the Chemistry Department.

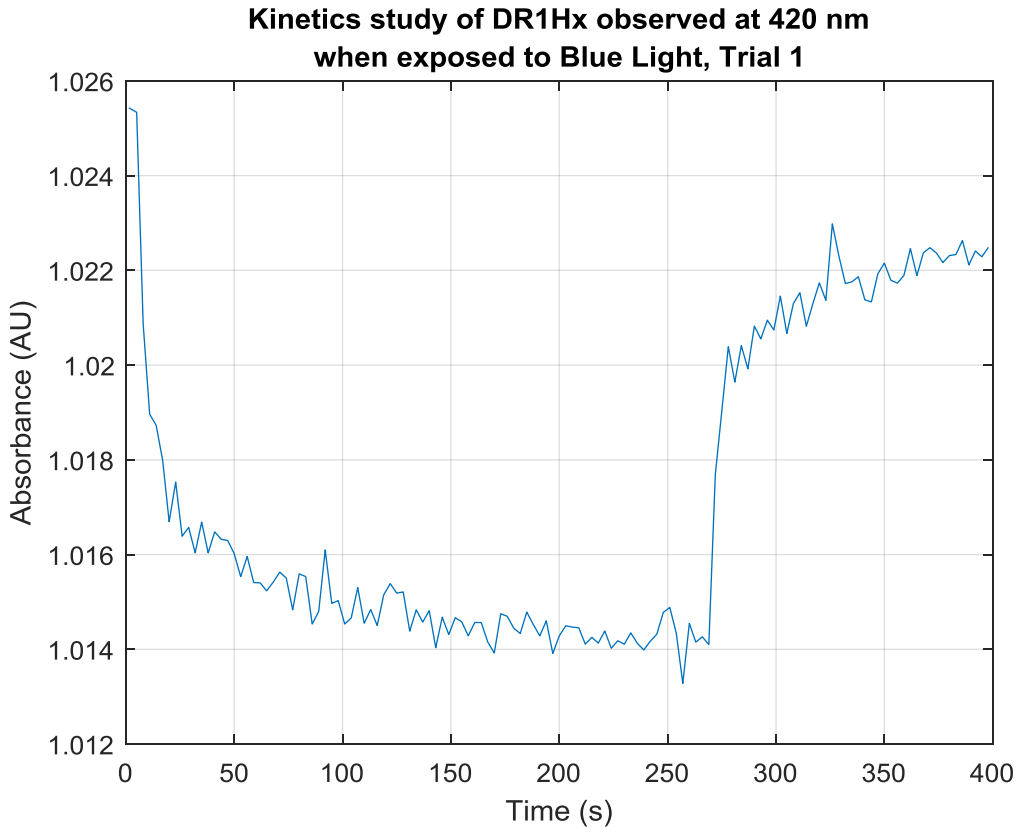

Figure A- 7. Trial 1 of the Kinetics Study for MeOABHx observed at 420 nm when exposed to Visible Blue Light (455 nm). The data presented was performed by Dr. Frank Ji's lab in the Chemistry Department. It has been adapted with permission by Dr. Frank Ji's lab in the Chemistry Department.

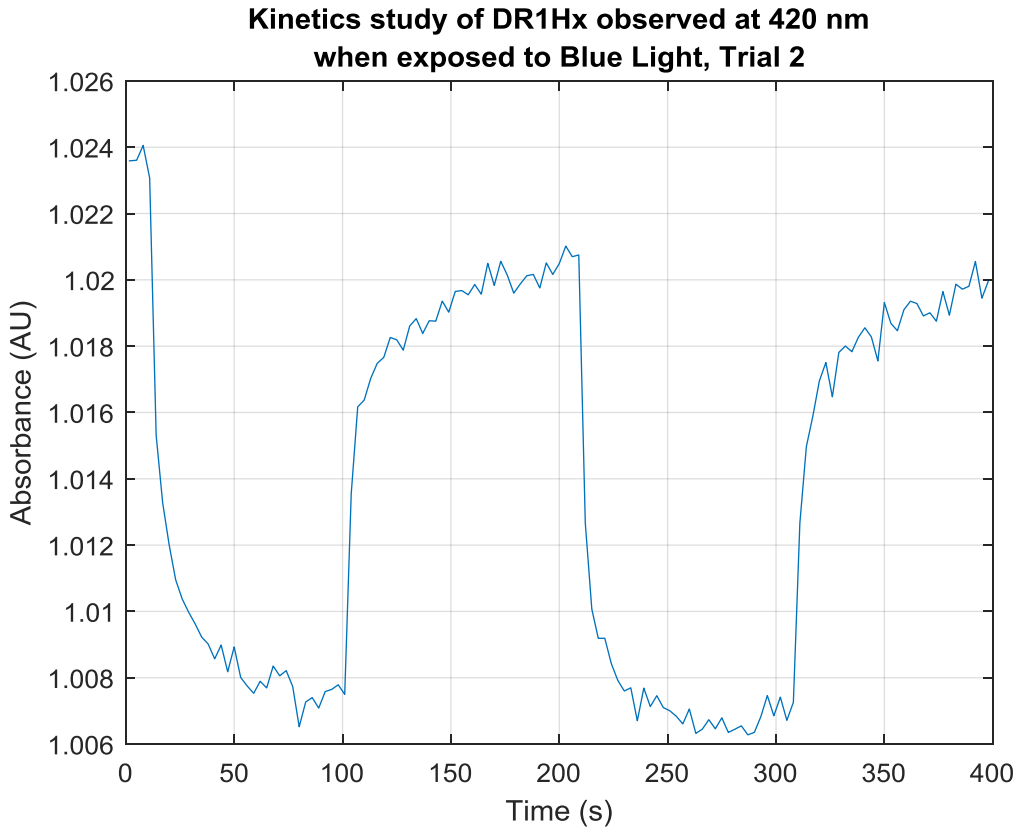

Figure A- 8. Trial 2 of the Kinetics Study for MeOABHx observed at 420 nm when exposed to Visible Blue Light (455 nm). The data presented was performed by Dr. Frank Ji's lab in the Chemistry Department. It has been adapted with permission by Dr. Frank Ji's lab in the Chemistry Department.

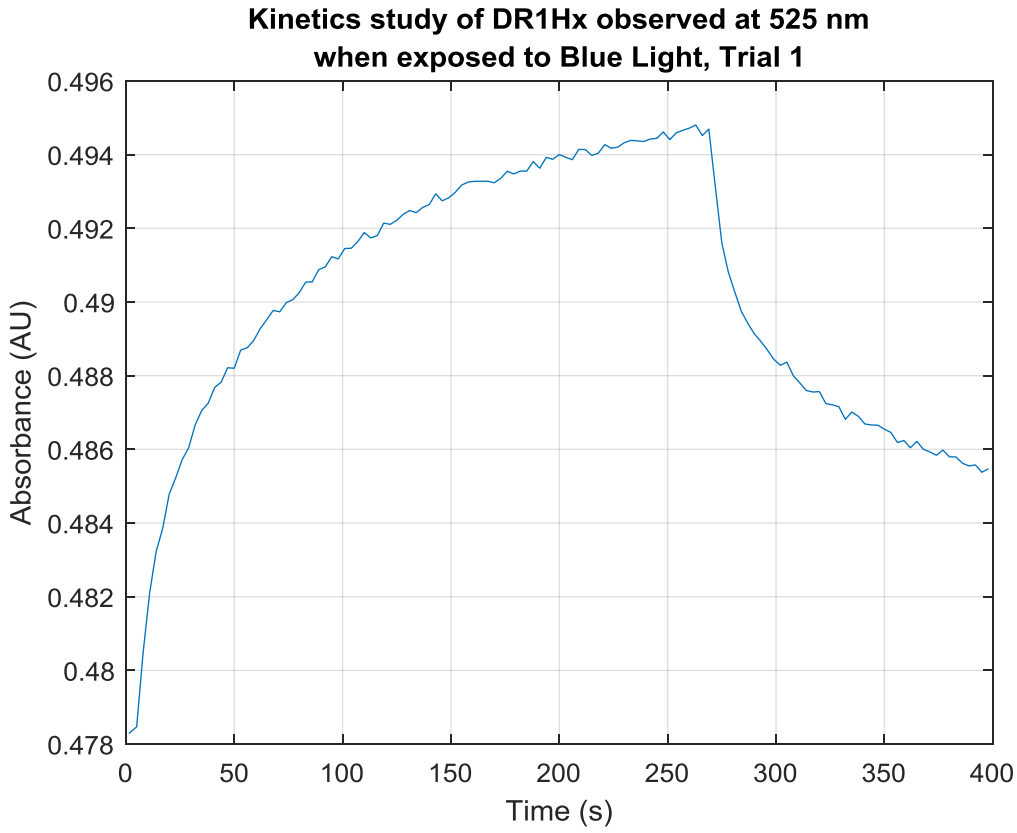

Figure A- 9. Trial 1 of the Kinetics Study for MeOABHx observed at 525 nm when exposed to Visible Blue Light (455 nm). The data presented was performed by Dr. Frank Ji's lab in the Chemistry Department. It has been adapted with permission by Dr. Frank Ji's lab in the Chemistry Department.

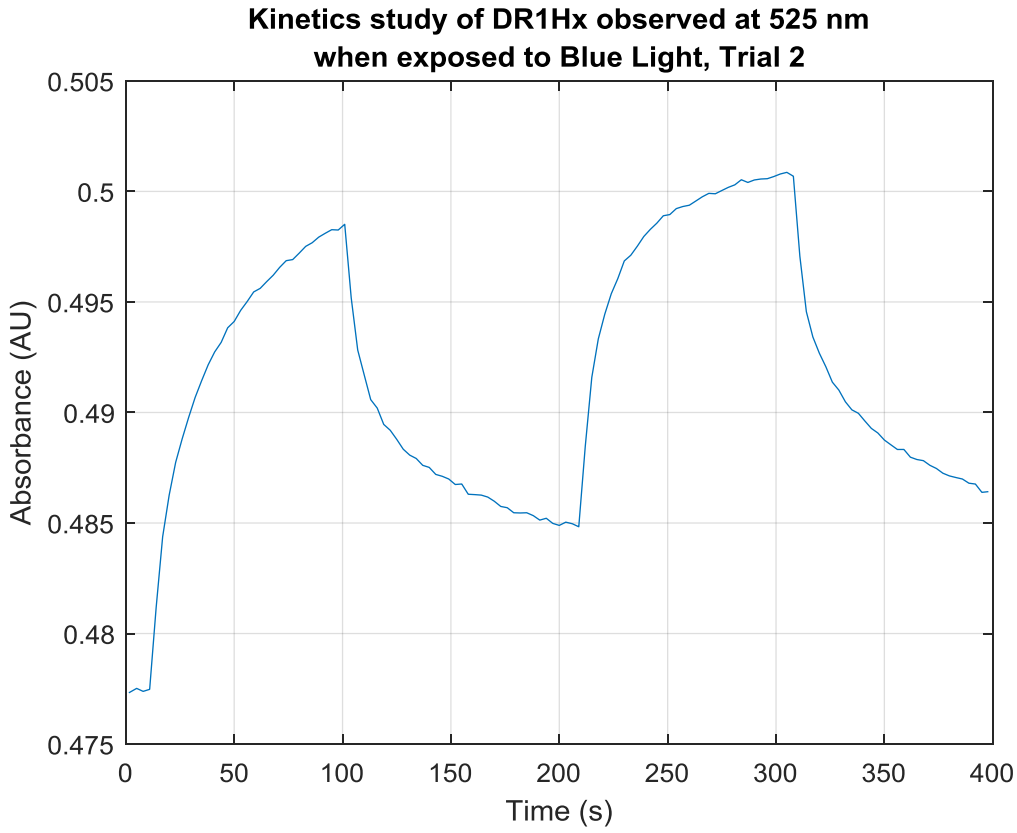

Figure A- 10. Trial 2 of the Kinetics Study for MeOABHx observed at 525 nm when exposed to Visible Blue Light (455 nm). The data presented was performed by Dr. Frank Ji's lab in the Chemistry Department. It has been adapted with permission by Dr. Frank Ji's lab in the Chemistry Department.

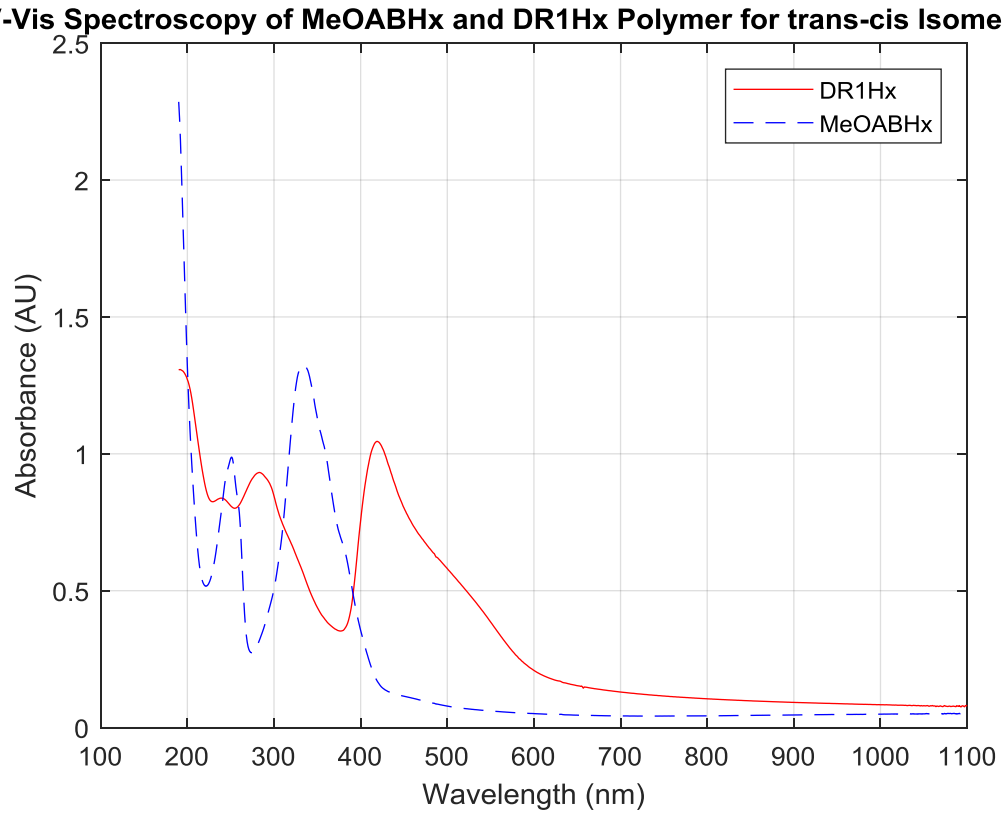

Figure A- 11. Combined UV-Vis spectroscopy comparison of DR1Hx and MeOABHx polymer that displays their peak absorptions. The data presented was performed by Dr. Frank Ji's lab in the Chemistry Department. It has been adapted with permission by Dr. Frank Ji's lab in the Chemistry Department.

Appendix B: Dynamic Mechanical Analysis of Blank Kapton Films and Kapton/Azobenzene Bilayer Films

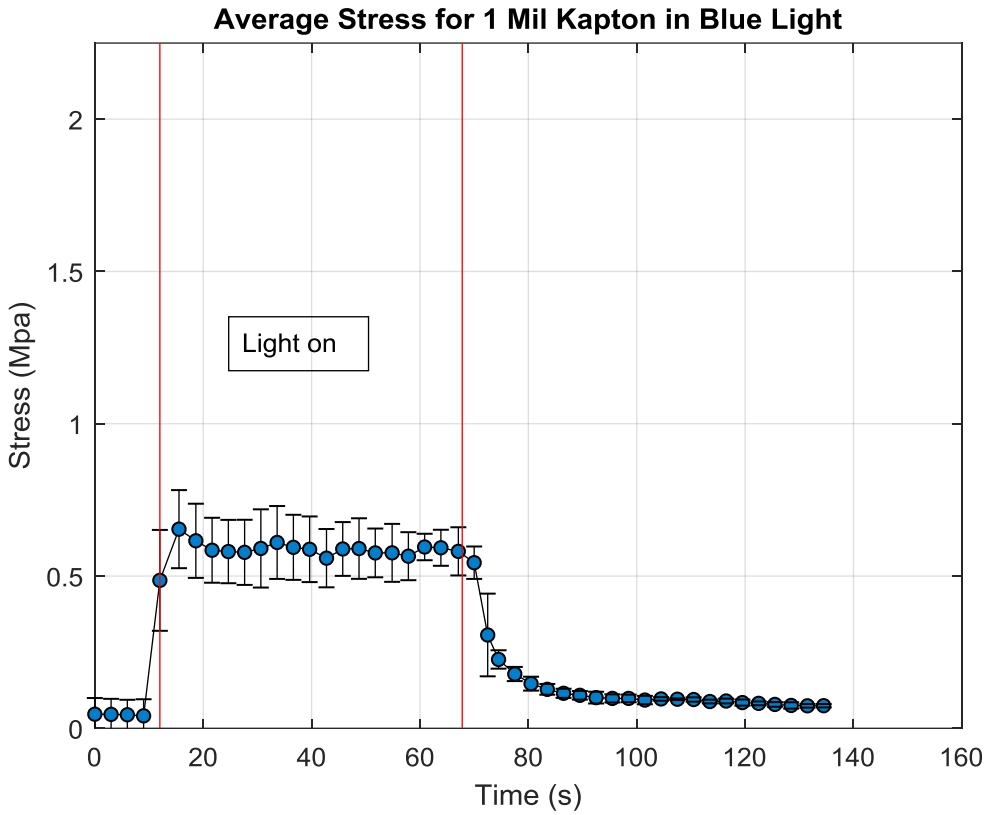

Figure B- 1. Average photomechanical stress generated for blank 1 mil thick Kapton film when exposed to blue light (455 nm) at a distance of 10 mm. Red lines represent the time when the film is exposed to the light source, ~60 seconds. Average values are shown with their standard deviation.

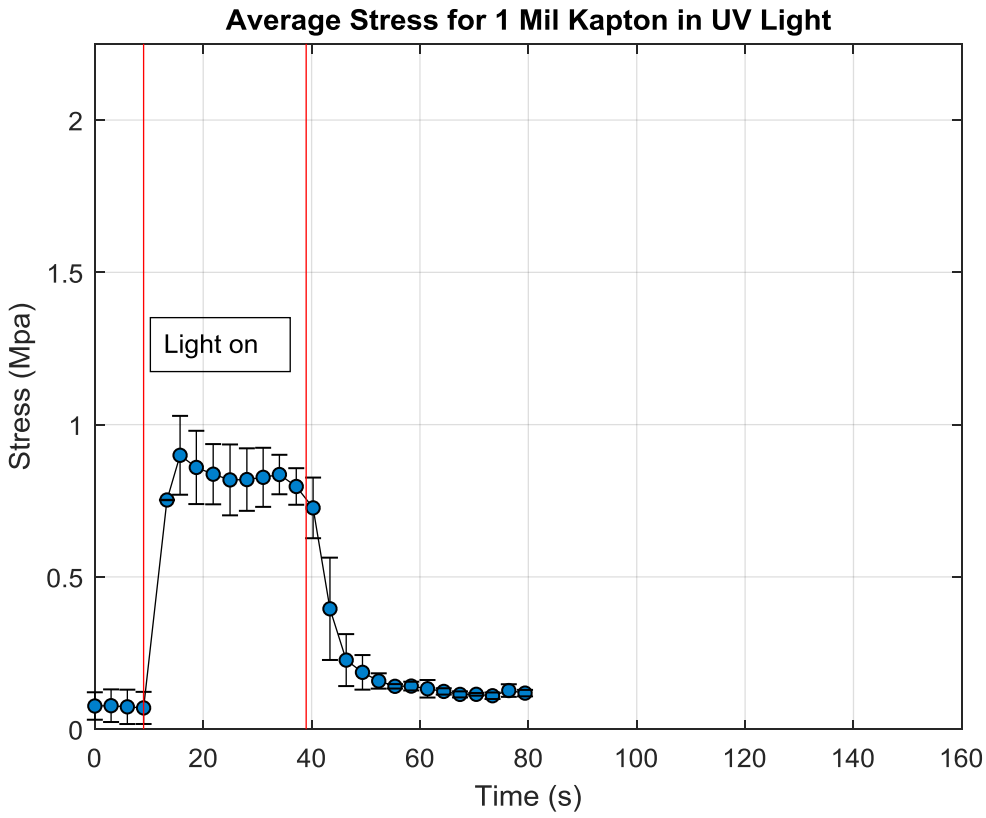

Figure B- 2. Average photomechanical stress generated for blank 1 mil thick Kapton film when exposed to UV light (365 nm) at a distance of 10 mm. Red lines represent the time when the film is exposed to the light source, ~30 seconds. Average values are shown with their standard deviation.

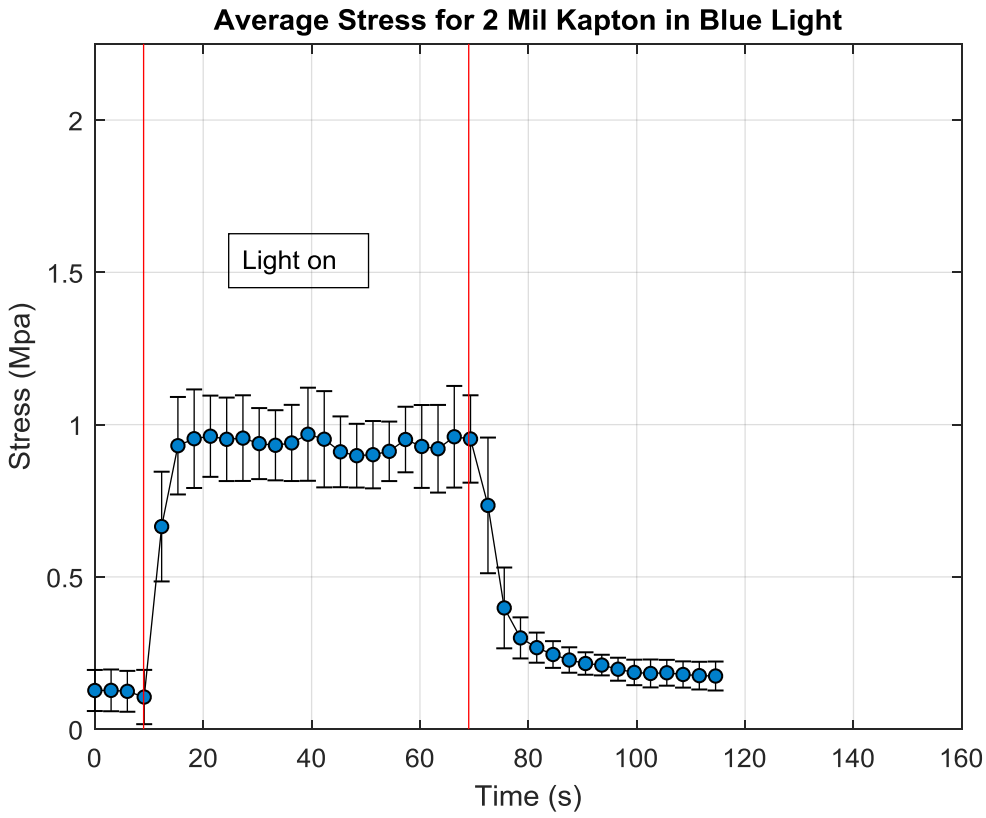

Figure B- 3. Average photomechanical stress generated for blank 2 mil thick Kapton film when exposed to blue light (455 nm) at a distance of 10 mm. Red lines represent the time when the film is exposed to the light source, ~60 seconds. Average values are shown with their standard deviation.

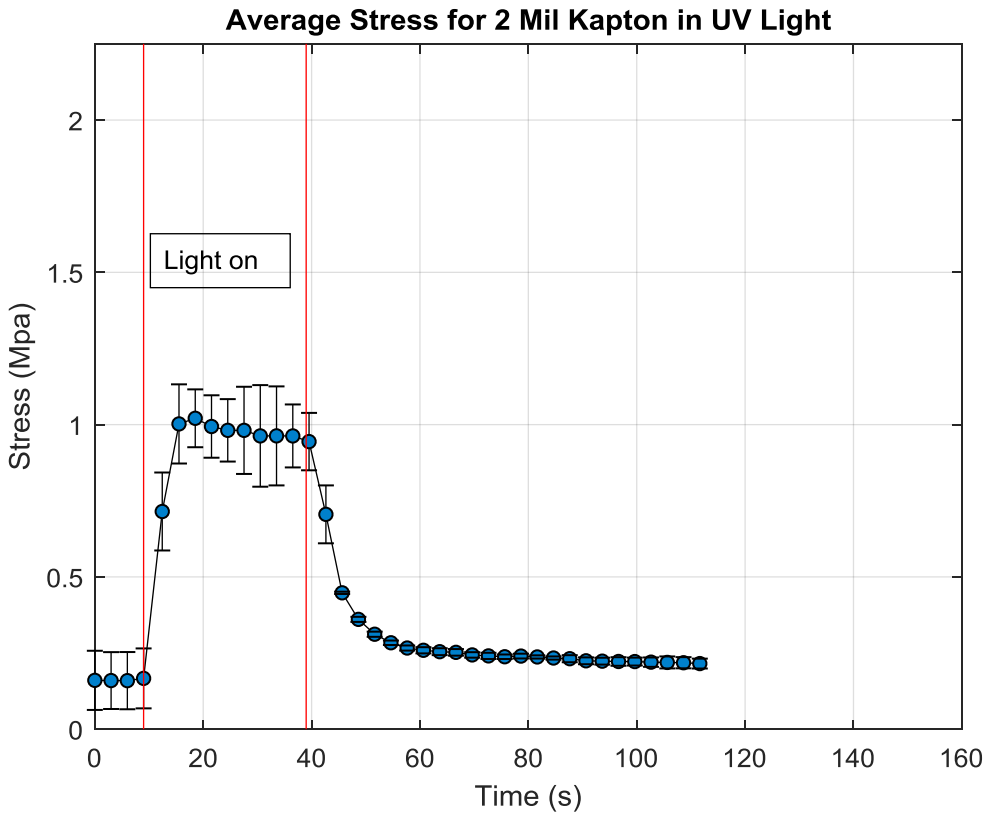

Figure B- 4. Average photomechanical stress generated for blank 2 mil thick Kapton film when exposed to UV light (365 nm) at a distance of 10 mm. Red lines represent the time when the film is exposed to the light source, ~30 seconds. Average values are shown with their standard deviation.

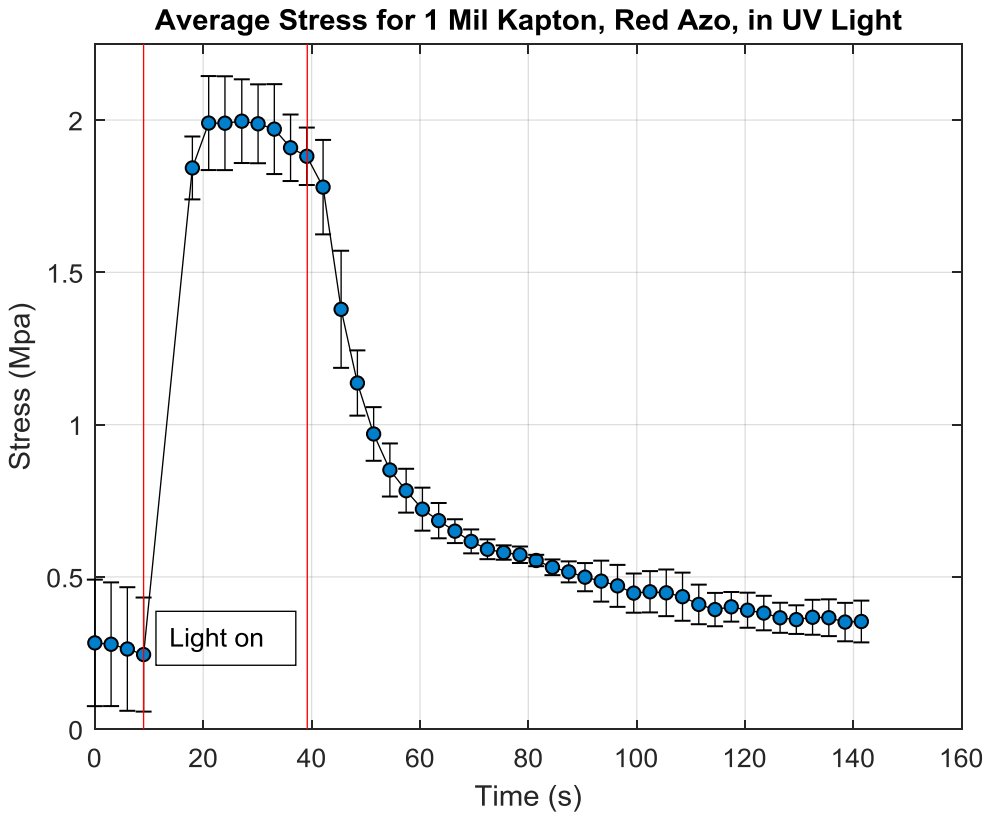

Figure B- 5. Average photomechanical stress generated for DR1Hx bilayer film with a 1 mil thick Kapton film when exposed to UV light (365 nm) at a distance of 10 mm. Red lines represent the time when the film is exposed to the light source, ~30 seconds. Average values are shown with their standard deviation.

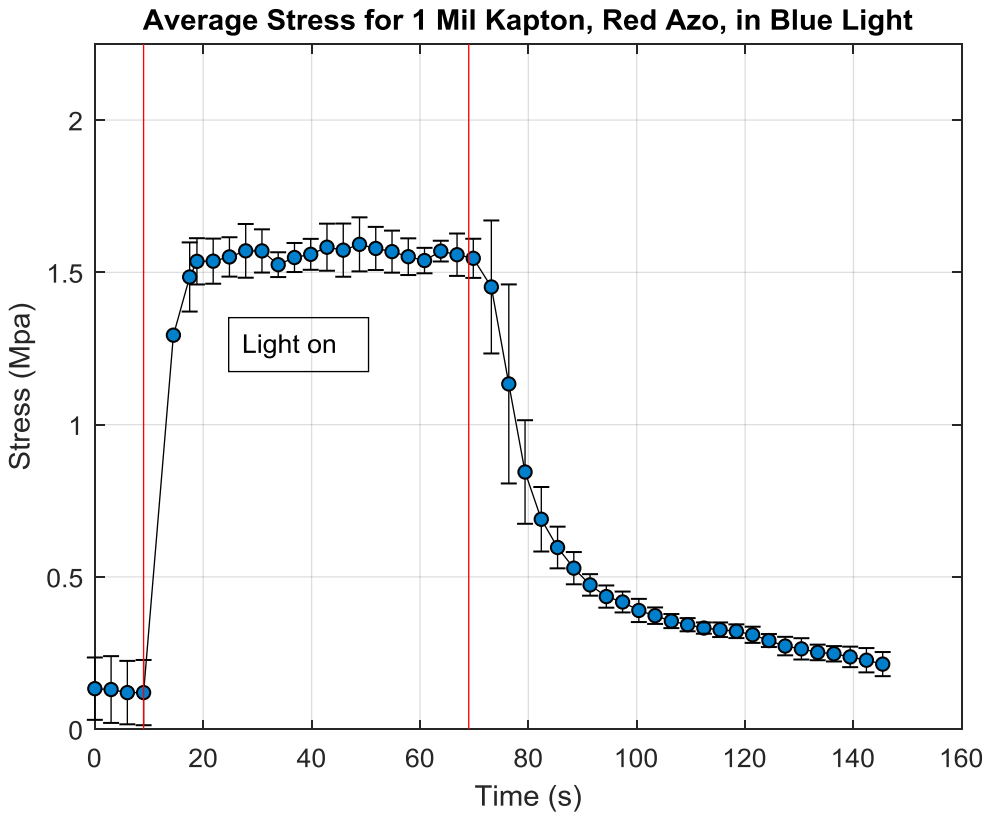

Figure B- 6. Average photomechanical stress generated for DR1Hx bilayer film with a 1 mil thick Kapton film when exposed to blue light (455 nm) at a distance of 10 mm. Red lines represent the time when the film is exposed to the light source, ~60 seconds. Average values are shown with their standard deviation.

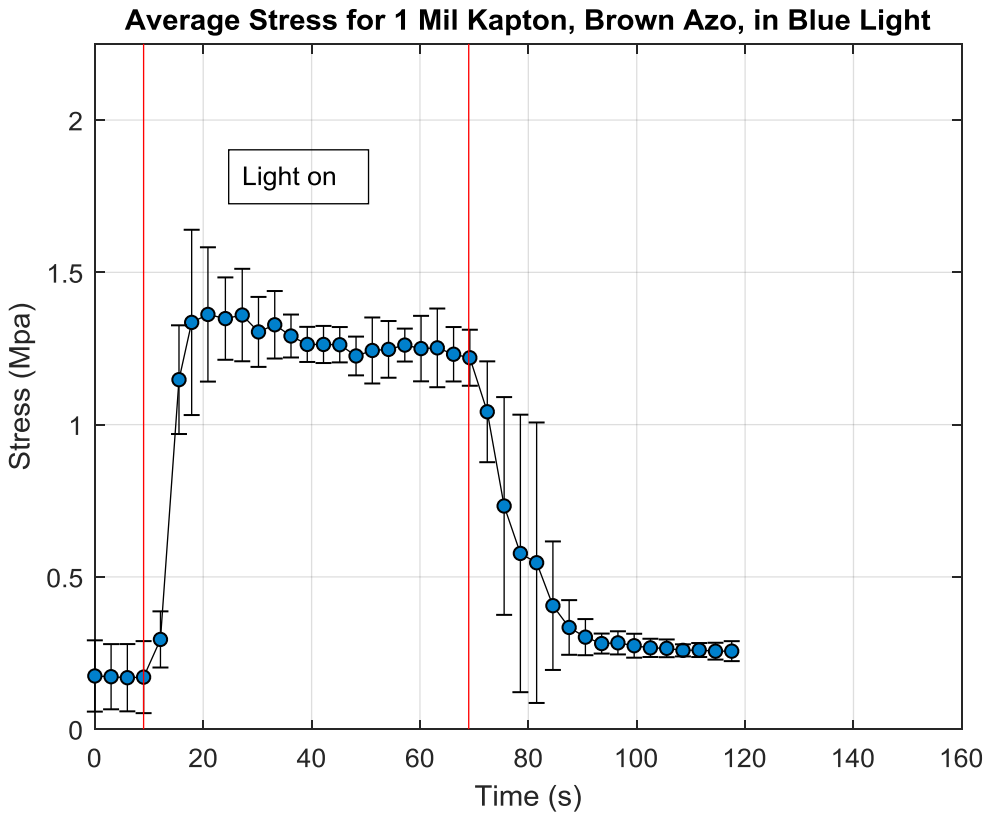

Figure B- 7. Average photomechanical stress generated for MeOABHx bilayer film with a 1 mil thick Kapton film when exposed to blue light (455 nm) at a distance of 10 mm. Red lines represent the time when the film is exposed to the light source, ~60 seconds. Average values are shown with their standard deviation.

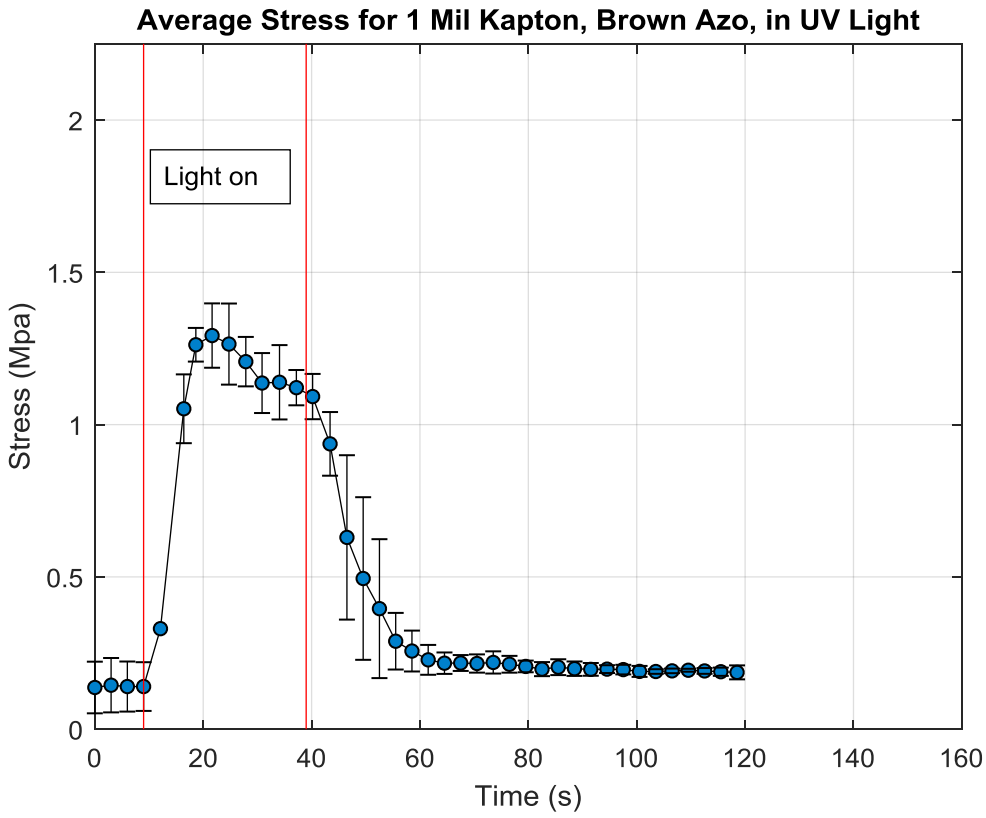

Figure B- 8. Average photomechanical stress generated for MeOABHx bilayer film with a 1 mil thick Kapton film when exposed to UV light (365 nm) at a distance of 10 mm. Red lines represent the time when the film is exposed to the light source, ~30 seconds. Average values are shown with their standard deviation.

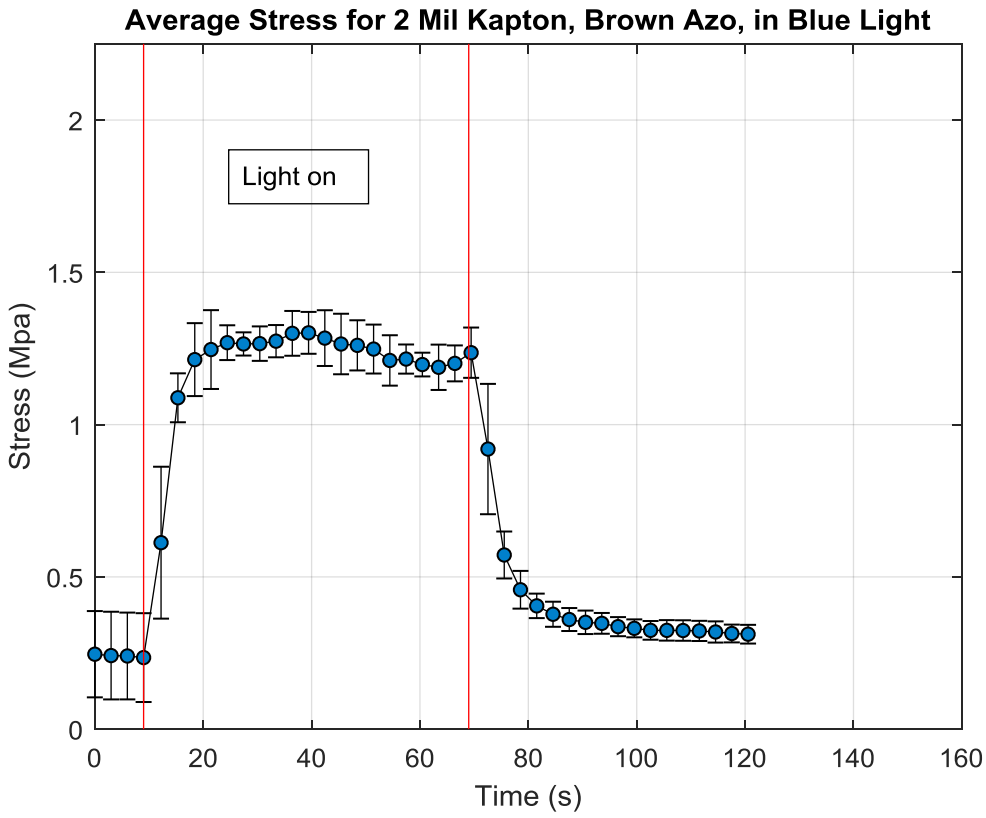

Figure B- 9. Average photomechanical stress generated for MeOABHx bilayer film with a 2 mil thick Kapton film when exposed to blue light (455 nm) at a distance of 10 mm. Red lines represent the time when the film is exposed to the light source, ~60 seconds. Average values are shown with their standard deviation.

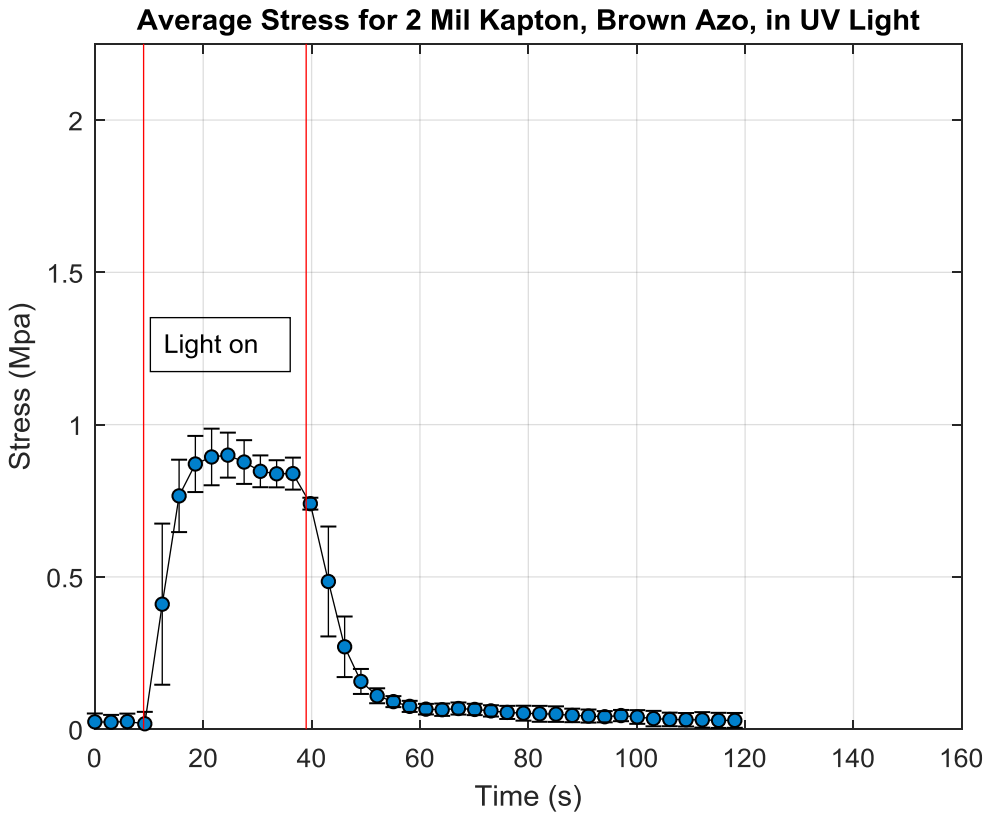

Figure B- 10. Average photomechanical stress generated for MeOABHx bilayer film with a 1 mil thick Kapton film when exposed to UV light (365 nm) at a distance of 10 mm. Red lines represent the time when the film is exposed to the light source, ~30 seconds. Average values are shown with their standard deviation.

Appendix C: Polymerization angle of contraction and photomechanical bending analysis for Kapton and Azobenzene Bilayer Films

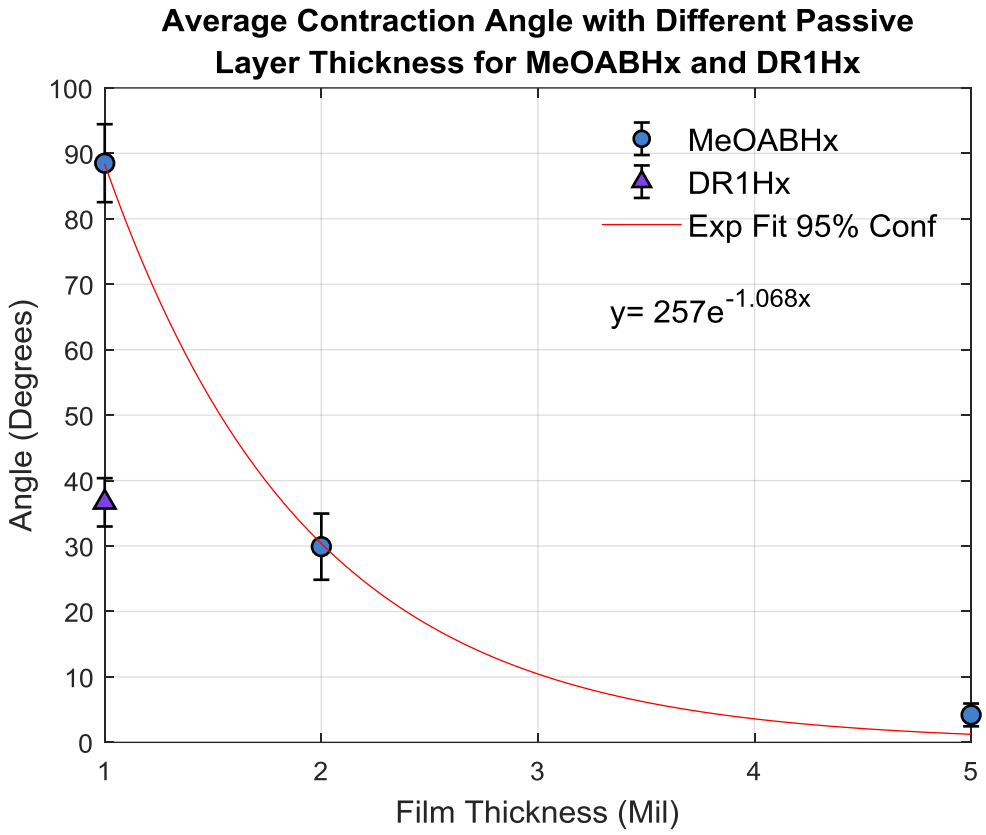

Figure C- 1. Plot of the average contraction angle during polymerization with different passive layer thicknesses ranging from 1 mil, 2 mil, and 5 mil Kapton thickness. MeOABHx polymer is represented by circles and DR1Hx is represented by triangle symbols. The average contraction angle, standard deviation, and exponential curve fit are plotted.

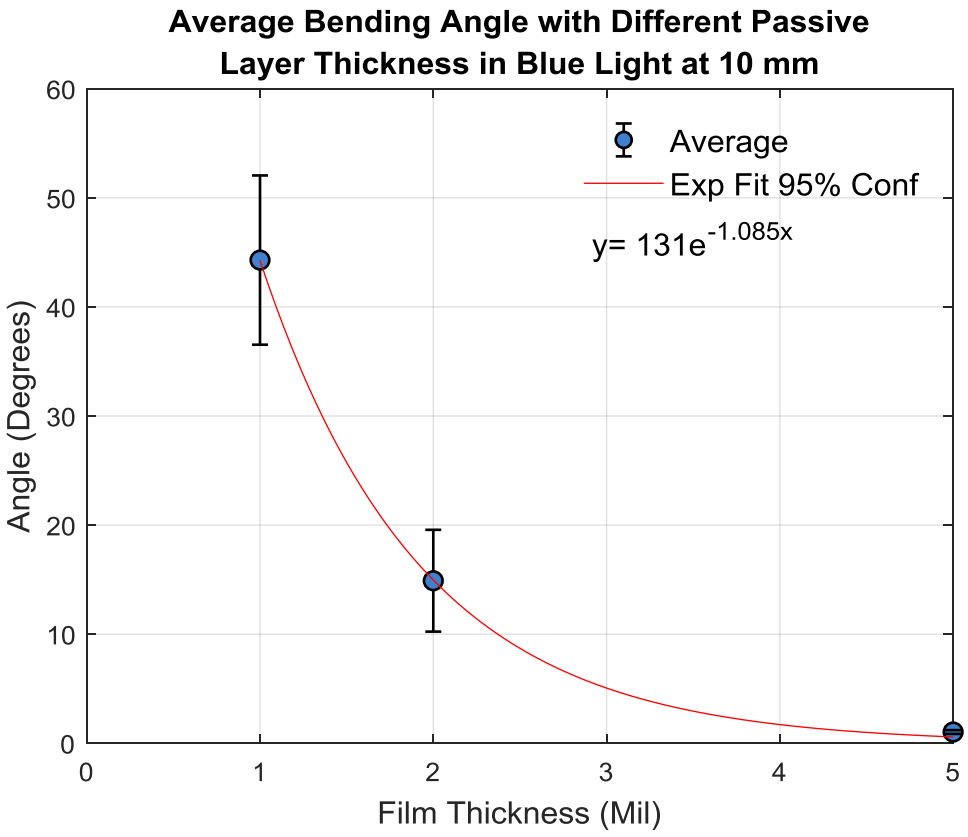

Figure C- 2. Plot of the average contraction angle during the azobenzene MeOABHx polymerization when deposited onto different thicknesses of the passive layer, which ranged from 1 mil, 2 mil, and 5 mil. The average contraction angle, standard deviation, and exponential curve fit are plotted.

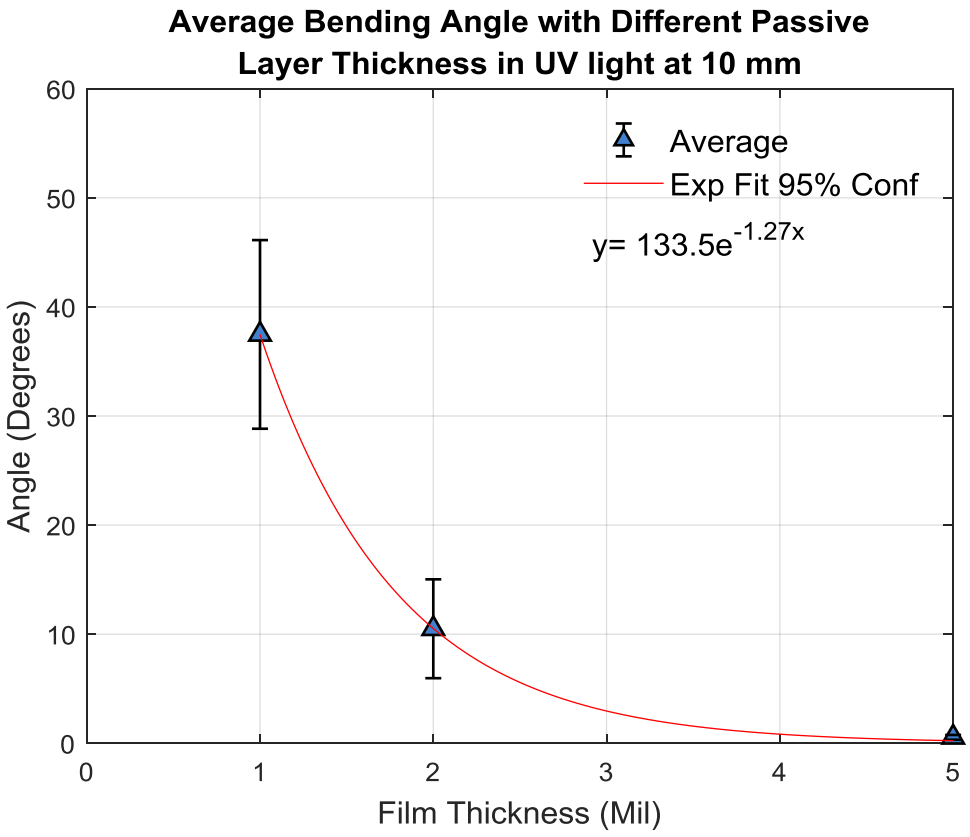

Figure C- 3. Plot of the average bending angle of the azobenzene bilayer films with different passive layer thicknesses ranging from 1 mil, 2 mil, and 5 mil. The averages of the bending angles, their standard deviations, and an exponential curve fit is plotted.

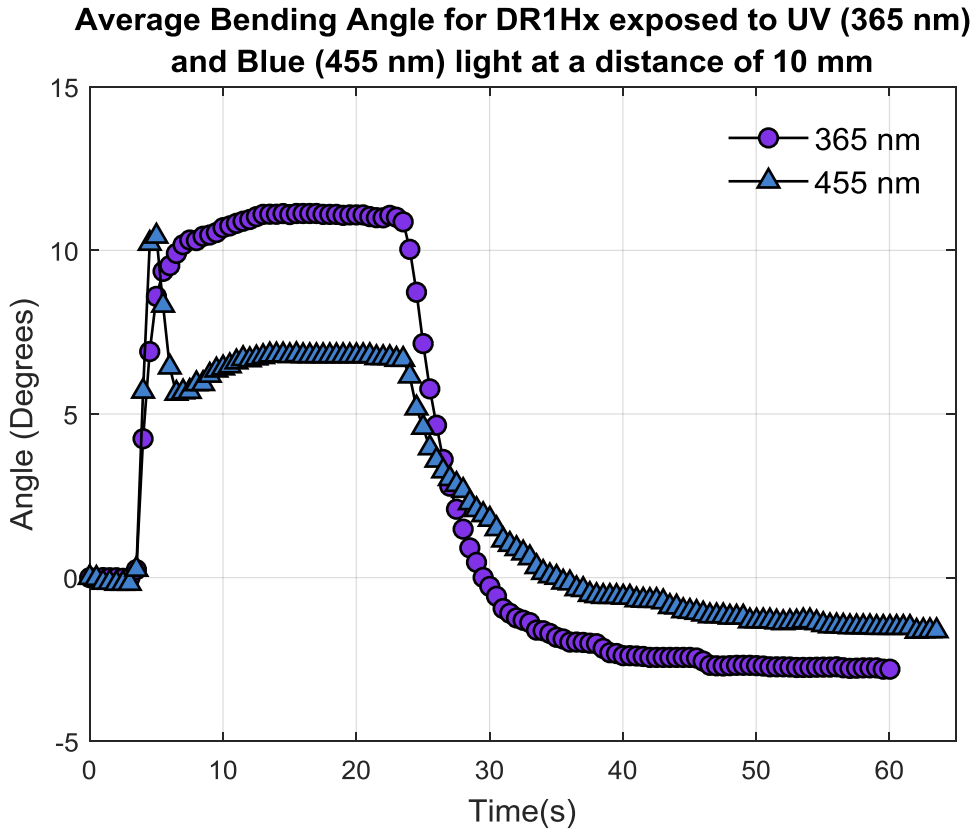

Figure C- 4. Plot of the average bending angle of the azobenzene DR1Hx bilayer films with 1 mil passive layer thicknesses when exposed to 365 nm and 455 nm light for 20 seconds. The averages of the bending angles are plotted.

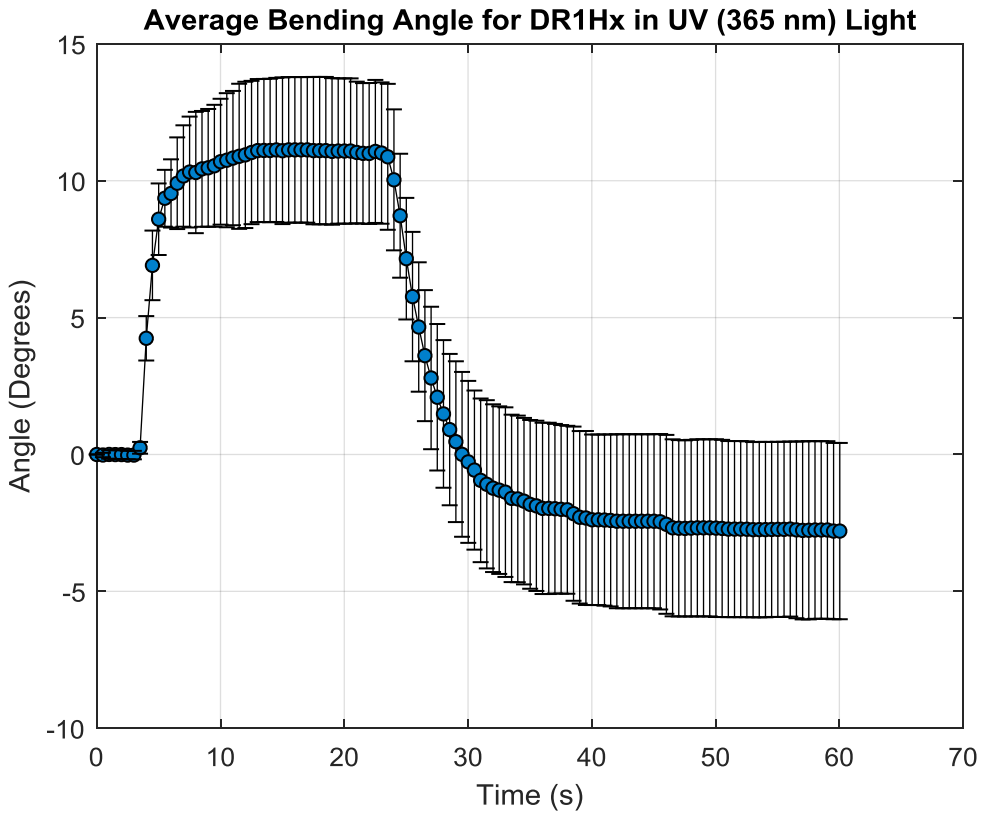

Figure C- 5. Plot of the average bending angle of the azobenzene DR1Hx bilayer films with 1 mil passive layer thicknesses when exposed to 365 nm light for 20 seconds. The averages of the bending angles and standard deviations are plotted.

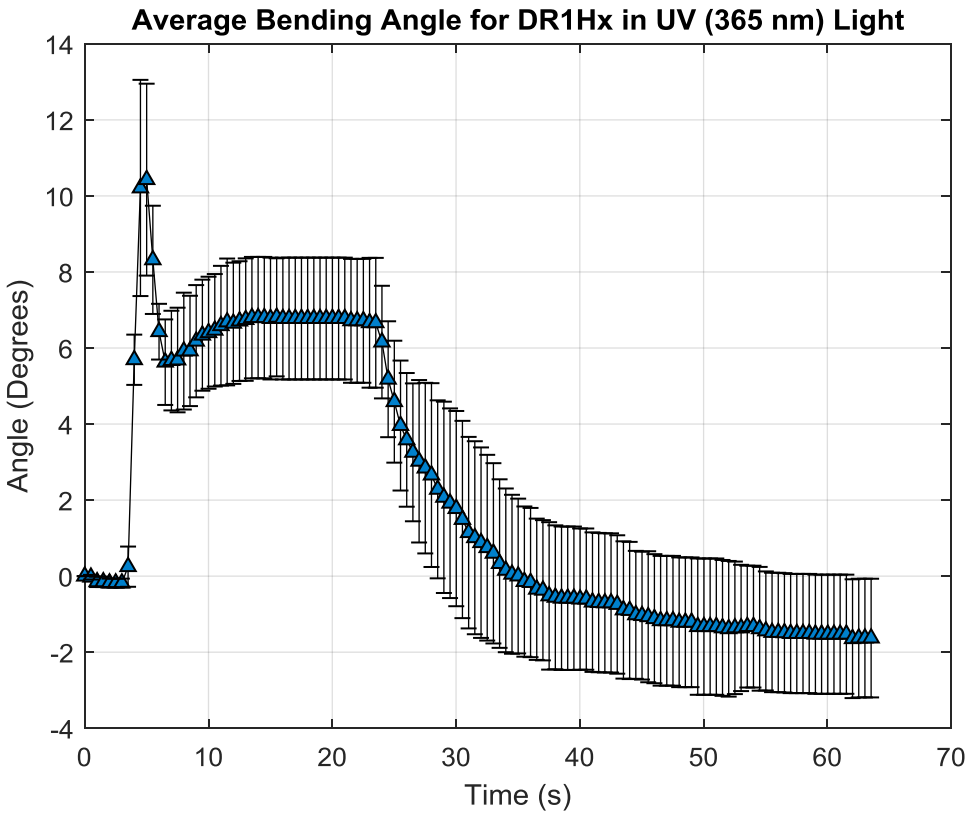

Figure C- 6. Plot of the average bending angle of the azobenzene DR1Hx bilayer films with 1 mil passive layer thicknesses when exposed to 455 nm light for 20 seconds. The averages of the bending angles and standard deviations are plotted.

Appendix D: Light intensity measurements for different light sources used to activate the azobenzene shape changing polymers.

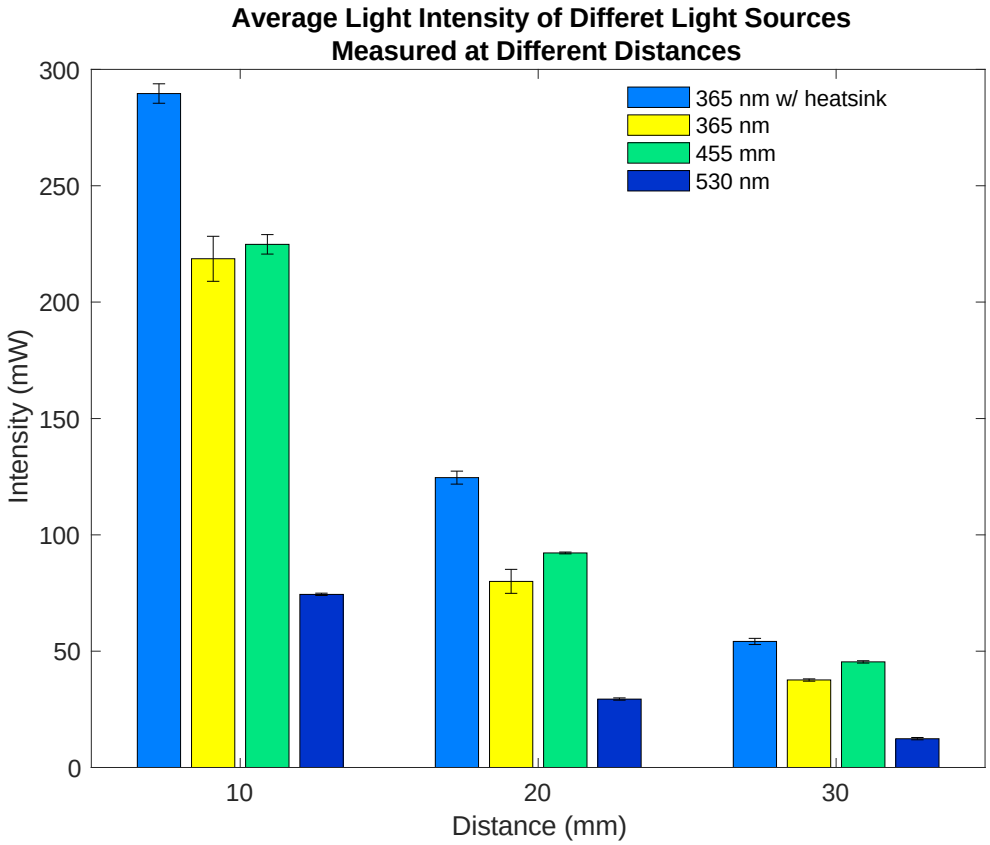

Figure D- 1. Plot of the average light intensity of different light sources (365 nm with a heatsink, 365 nm without heatsink, 455 nm, and 530 nm) measured at varied distances (10 mm, 20 mm, and 30 mm). The averages of the bending angles and standard deviations are plotted.

References

Ahmad, M., Luo, J., & Miraftab, M. (2016). Feasibility study of polyurethane shape-memory polymer actuators for pressure bandage application. *Science and Technology of Advanced Materials*, *13*(1), 015006. doi:10.1088/1468-6996/13/1/015006

Auricchio, Scalet, & Urbano. (n.d.). A Numerical/Experimental Study of Nitinol Actuator Springs. doi:10.1007/s11665-014-0883-1

Bar-Cohen, Y. (2004). Electroactive polymer (EAP) actuators as artificial muscles: reality, potential, and challenges, *136*.

Barrett, C., Mamiya, J., Yager, K., & Ikeda, T. (2007). Photo-mechanical effects in azobenzene-containing soft materials. *Soft Matter*, *3*(10), 1249–1261. doi:10.1039/B705619B

Behl, M., & Lendlein, A. (2007). Shape-memory polymers. *Materials Today*, *10*(4), 20–28.

Berg, GJ, McBride, MK, Wang, C, & Bowman, CN. (2014). New directions in the chemistry of shape memory polymers. *Polymer*. Retrieved from http://www.sciencedirect.com/science/article/pii/S0032386114006612

Berman, B. (2012). 3-D printing: The new industrial revolution. *Business horizons*. Retrieved from http://www.sciencedirect.com/science/article/pii/S0007681311001790

Brinson, Bekker, & Hwang. (1996). Deformation of shape memory alloys due to thermo-induced transformation.

Bublitz, Helgert, Fleck, Wenke, Hvilsted, & Ramanujam, P. S. (2000). Photoinduced deformation of azobenzene polyester films. *Applied Physics B*, *70*(6), 863–865. doi:10.1007/PL00021146

Burgert, I., & Fratzl, P. (2009). Actuation systems in plants as prototypes for bioinspired devices. *Philosophical Transactions of the Royal Society of London A: Mathematical, Physical and Engineering Sciences*, *367*(1893), 1541–1557. doi:10.1098/rsta.2009.0003

Camacho-Lopez, M., Finkelmann, H., Palffy-Muhoray, P., & Shelley, M. (2004). Fast liquid-crystal elastomer swims into the dark. *Nature materials*, *3*(5), 307–10. doi:10.1038/nmat1118

Chan Vili, Y. Y. F. (2007). Investigating smart textiles based on shape memory materials. *Textile Research Journal*, *77*(5), 290–300. doi:10.1177/0040517507078794

Cheng, F., Yin, R., Zhang, Y., Yen, C.-C., & Yu, Y. (2010). Fully plastic microrobots which manipulate objects using only visible light. *Soft Matter*, *6*(15), 3447–3449. doi:10.1039/c0sm00012d

Cheng, L., Torres, Y., Lee, K., McClung, A., Baur, J., White, T., & Oates, W. (2012). Photomechanical bending mechanics of polydomain azobenzene liquid crystal polymer network films. *Journal of Applied Physics*, *112*(1), 013513. doi:10.1063/1.4729771

Cianchetti, M., Licofonte, A., Follador, M., Rogai, F., & Laschi, C. (2014). Bioinspired Soft Actuation System Using Shape Memory Alloys. *Actuators*, *3*(3), 226–244. doi:10.3390/act3030226

Dunn, M., & Maute, K. (2009). Photomechanics of blanket and patterned liquid crystal elastomer films. *Mechanics of Materials*, *41*(10), 1083–1089. doi:10.1016/j.mechmat.2009.06.004

Ercole, F., Davis, T., & Evans, R. (2009). Photo-responsive systems and biomaterials: photochromic polymers , light-triggered self-assembly , surface modification, fluorescence modulation and beyond. *Polymer Chemistry*, *1*(1), 37–54. doi:10.1039/B9PY00300B

Garcia-Amorós, J., Piñol, A., Finkelmann, H., & Velasco, D. (2011). Azophenol-based liquid-crystalline elastomers for light-driven actuators. *Organic letters*, *13*(9), 2282–5. doi:10.1021/ol200546q

Garcia-Amorós, & Velasco. (2012). Polysiloxane side-chain azobenzene-containing liquid single crystal elastomers for photo-active artificial muscle-Like actuators.

Ge, Q., Dunn, C., Qi, J., & Dunn, M. (2014). Active origami by 4D printing. *Smart Materials and Structures*, *23*(9), 094007. doi:10.1088/0964-1726/23/9/094007

Ge, Q., Qi, J., & Dunn, M. (2013). Active materials by four-dimension printing. *Applied Physics Letters*, *103*(13), 131901. doi:10.1063/1.4819837

Ge, Q., Sakhaei, A., Lee, H., Dunn, C., Fang, N., & Dunn, M. (2016). Multimaterial 4D Printing with Tailorable Shape Memory Polymers. *Scientific Reports*, *6*(1), 31110. doi:10.1038/srep31110

Gebler, M., Uiterkamp, A., & Visser, C. (2014). A global sustainability perspective on 3D printing technologies. *Energy Policy*, *74*, 158–167. doi:10.1016/j.enpol.2014.08.033

Gladman, S., Matsumoto, E., Nuzzo, R., Mahadevan, & Lewis, J. (2016). Biomimetic 4D printing. *Nature Materials*, *15*(4), 413–418. doi:10.1038/nmat4544

Gross, B., Erkal, J., Lockwood, S., Chen, C., & Spence, D. (2014). Evaluation of 3D Printing and Its Potential Impact on Biotechnology and the Chemical Sciences. *Analytical Chemistry*, *86*(7), 3240–3253. doi:10.1021/ac403397r

Habault, D., Zhang, H., & Zhao, Y. (2013). Light-triggered self-healing and shape-memory polymers. *Chemical Society Reviews*, *42*(17), 7244–7256. doi:10.1039/C3CS35489J

Hager, M. D., Bode, S., Weber, C., & Schubert, U. S. (2015). Shape memory polymers: Past, present and future developments. *Progress in Polymer Science*, *49*(50), 3–33.

Hager, M., Greil, P., Leyens, C., van der Zwaag, S., & Schubert, U. (2010). Self-healing materials. *Advanced materials (Deerfield Beach, Fla.)*, *22*(47), 5424–30. doi:10.1002/adma.201003036

Hu, J, Meng, H, Li, G, & Ibekwe, SI. (2012). A review of stimuli-responsive polymers for smart textile applications. *Smart Materials and Structures*. Retrieved from http://iopscience.iop.org/article/10.1088/0964-1726/21/5/053001/meta

Huang, C., Lv, J., Tian, X., Wang, Y., Yu, Y., & Liu, J. (2015). Miniaturized Swimming Soft Robot with Complex Movement Actuated and Controlled by Remote Light Signals. *Scientific Reports*, *5*, 17414. doi:10.1038/srep17414

Huang, S., Liu, P., Mokasdar, A., & Hou, L. (2013). Additive manufacturing and its societal impact: a literature review. *The International Journal of Advanced Manufacturing Technology*, *67*(5-8), 1191–1203. doi:10.1007/s00170-012-4558-5

Hudson, S. E. (2014). Printing Teddy Bears: A Technique for 3D Printing of Soft Interactive Objects. *ACM*.

Humbeeck, J. (1999). Non-medical applications of shape memory alloys. *Materials Science and Engineering: A*, *273*, 134–148. doi:10.1016/S0921-5093(99)00293-2

Ikeda, Nakano, Yu, Tsutsumi, & Kanazawa. (2003). Anisotropic Bending and Unbending Behavior of Azobenzene Liquid-Crystalline Gels by Light Exposure. *Advanced Materials*, *15*(3), 201–205. doi:10.1002/adma.200390045

Ikeda, T., Mamiya, J., & Yu, Y. (2007). Photomechanics of Liquid-Crystalline Elastomers and Other Polymers. *Angewandte Chemie International Edition*, *46*(4), 506–528. doi:10.1002/anie.200602372

Ikeda, T., & Tsutsumi, O. (1995). Optical Switching and Image Storage by Means of Azobenzene Liquid-Crystal Films. *Science*, *268*(5219), 1873–1875. doi:10.1126/science.268.5219.1873

Iqbal, D., & Samiullah, M. (2013). Photo-Responsive Shape-Memory and Shape-Changing Liquid-Crystal Polymer Networks. *Materials*, *6*(1), 116142. doi:10.3390/ma6010116

Jani, J., Leary, M., & Subic, A. (2014). Shape Memory Alloys in Automotive Applications. *Applied Mechanics & Materials*, (663).

Jani, J., Leary, M., Subic, A., & Gibson, M. (2013). A review of shape memory alloy research, applications and opportunities. *Materials & Design*, *56*. doi:10.1016/j.matdes.2013.11.084

Jiang, Wang, Gunawidjaja, Lin, Y. -H., Gupta, Kaplan, … Tsukruk. (2007). Mechanical Properties of Robust Ultrathin Silk Fibroin Films. *Advanced Functional Materials*, *17*(13), 2229–2237. doi:10.1002/adfm.200601136

Jin, H. -J., Park, Karageorgiou, Kim, U. -J., Valluzzi, Cebe, & Kaplan. (2005). Water-Stable Silk Films with Reduced β-Sheet Content. *Advanced Functional Materials*, *15*(8), 1241–1247. doi:10.1002/adfm.200400405

Jing, X., Mi, H., Peng, X., & Turng, L. (2015). The morphology, properties, and shape memory behavior of polylactic acid/thermoplastic polyurethane blends. *Polymer Engineering & Science*, *55*(1), 70–80. doi:10.1002/pen.23873

Khoo, Z., Teoh, J., Liu, Y., Chua, C., Yang, S., An, J., … Yeong, W. (2015). 3D printing of smart materials: A review on recent progresses in 4D printing. *Virtual and Physical Prototyping*, *10*(3), 103–122. doi:10.1080/17452759.2015.1097054

Kietzmann, J., Pitt, L., & Berthon, P. (2015). Disruptions, decisions, and destinations: Enter the age of 3-D printing and additive manufacturing. *Business Horizons*, *58*(2), 209–215. doi:10.1016/j.bushor.2014.11.005

Laschi, C., & Cianchetti, M. (2014). Soft Robotics: New Perspectives for Robot Bodyware and Control. *Frontiers in Bioengineering and Biotechnology*, *2*. doi:10.3389/fbioe.2014.00003

Lawrence, B., Cronin-Golomb, M., Georgakoudi, I., Kaplan, D., & Omenetto, F. (2008). Bioactive Silk Protein Biomaterial Systems for Optical Devices. *Biomacromolecules*, *9*(4), 1214–1220. doi:10.1021/bm701235f

Lawrence, B., Wharram, S., Kluge, J., Leisk, G., Omenetto, F., Rosenblatt, M., & Kaplan, D. (2010). Effect of Hydration on Silk Film Material Properties. *Macromolecular Bioscience*, *10*(4), 393–403. doi:10.1002/mabi.200900294

Lee, K., Bunning, T., & White, T. (2012). Autonomous, Hands-Free Shape Memory in Glassy, Liquid Crystalline Polymer Networks. *Advanced Materials*, *24*(21), 28392843. doi:10.1002/adma.201200374

Lee, K., Koerner, H., Vaia, R. A., Bunning, T. J., & White, T. J. (2011a). Light-activated shape memory of glassy, azobenzene liquid crystalline polymer networks. *Soft Matter*, *7*(9), 4318–4324. doi:10.1039/C1SM00004G

Lee, K., Koerner, H., Vaia, R., Bunning, T., & White, T. (2010). Relationship between the Photomechanical Response and the Thermomechanical Properties of Azobenzene Liquid Crystalline Polymer Networks. *Macromolecules*, *43*(19), 8185–8190. doi:10.1021/ma1014758

Lee, K., Koerner, H., Vaia, R., Bunning, T., & White, T. (2011b). Light-activated shape memory of glassy, azobenzene liquid crystalline polymer networks. *Soft Matter*, *7*(9), 4318–4324. doi:10.1039/C1SM00004G

Lee, K., Tabiryan, N., Bunning, T., & White, T. (2011). Photomechanical mechanism and structure-property considerations in the generation of photomechanical work in glassy, azobenzene liquid crystal polymer networks. *Journal of Materials Chemistry*, *22*(2), 691–698. doi:10.1039/C1JM14017E

Lee, Y., Lee, H., Hwang, T., Lee, J.-G., & Cho, M. (2015). Sequential Folding using Light-activated Polystyrene Sheet. *Scientific Reports*, *5*, 16544. doi:10.1038/srep16544

Leist, S., Gao, D., Chiou, R., & Zhou, J. (2017). Investigating the shape memory properties of 4D printed polylactic acid (PLA) and the concept of 4D printing onto nylon fabrics for the creation of smart textiles. *Virtual and Physical Prototyping*, 1–11. doi:10.1080/17452759.2017.1341815

Leist, S., Kunkle, C., Chong, P., & Zhou, J. (2015). Dual chamber shape memory alloy unplugging and mixing system coupled to a high pressure optical cell for biophysical studies. *Smart Materials and Structures*, *24*(3), 035014. doi:10.1088/0964-1726/24/3/035014

Leist, S., & Zhou, J. (2016). Current status of 4D printing technology and the potential of light-reactive smart materials as 4D printable materials. *Virtual and Physical Prototyping*, 1–14. doi:10.1080/17452759.2016.1198630

Lendlein, A. (2010). Progress in actively moving polymers. *Journal of Materials Chemistry*, *20*. doi:10.1039/c004361n

Lendlein, A., Jiang, H., Jünger, O., & Langer, R. (2005). Light-induced shape-memory polymers. *Nature*, *434*(7035), 879–882. doi:10.1038/nature03496

Lendlein, A., Kelch, S., Lendlein, A., & Kelch, S. (2002). Shape-Memory Polymers. *Angewandte Chemie International Edition*, *41*, 2034–2057. doi:10.1002/1521-3773(20020617)41:12<2034::AID-ANIE2034>3.0.CO;2-M

Leng, J., Lan, X., Liu, Y., & Du, S. (2011). Shape-memory polymers and their composites: Stimulus methods and applications. *Progress in Materials Science*, *56*. doi:10.1016/j.pmatsci.2011.03.001

Li, M. -H., Keller, Li, Wang, & Brunet. (2003). Light-Driven Side-On Nematic Elastomer Actuators. *Advanced Materials*, *15*(7-8), 569–572. doi:10.1002/adma.200304552

Liu, Y, Genzer, J, & Dickey, MD. (2016). "2D or not 2D": Shape-programming polymer sheets. *Progress in Polymer Science*. Retrieved from http://www.sciencedirect.com/science/article/pii/S0079670015001021

Liu, Qin, & Mather. (2007). Review of progress in shape-memory polymers. *Journal of Materials Chemistry*, *17*(16), 1543–1558. doi:10.1039/B615954K

Liu, Y., Boyles, J., Genzer, J., & Dickey, M. (2011). Self-folding of polymer sheets using local light absorption. *Soft Matter*, *8*(6), 1764–1769. doi:10.1039/C1SM06564E

Lu, B., Li, D., & Tian, X. (2015). Development Trends in Additive Manufacturing and 3D Printing. *Engineering*, *1*(1), 085–089. doi:10.15302/J-ENG-2015012

Mahimwalla, Z, Yager, KG, Mamiya, J, & Shishido, A. (2012). Azobenzene photomechanics: prospects and potential applications. *Polymer bulletin*. doi:10.1007/s00289-012-0792-0

Mao, Y., Yu, K., Isakov, M., Wu, J., Dunn, M., & Qi, J. (2015). Sequential Self-Folding Structures by 3D Printed Digital Shape Memory Polymers. *Scientific Reports*, *5*, 13616. doi:10.1038/srep13616

Martin, & Avérous. (2001). Poly(lactic acid): plasticization and properties of biodegradable multiphase systems. *Polymer*, *42*(14), 6209–6219. doi:10.1016/S0032-3861(01)00086-6

Mazzolai, Margheri, Cianchetti, Dario, & Laschi. (2012). Soft-robotic arm inspired by the octopus: II. From artificial requirements to innovative technological solutions. *Bioinspiration & Biomimetics*, *7*(2), 025005. doi:10.1088/1748-3182/7/2/025005

Milam, K., O'Malley, G., Kim, N., Golovaty, D., & Kyu, T. (2010). Swimming photochromic azobenzene single crystals in triacrylate solution. *The journal of physical chemistry. B*, *114*(23), 7791–6. doi:10.1021/jp1033454

Mirfakhrai, T., Madden, J., & Baughman, R. (2007). Polymer artificial muscles. *Materials Today*, *10*(4), 30–38. doi:10.1016/S1369-7021(07)70048-2

Morgan, N. . (2004). Medical shape memory alloy applications—the market and its products. *Materials Science and Engineering: A*, *378*(1-2), 16–23. doi:10.1016/j.msea.2003.10.326

Naciri, J., Srinivasan, A., Jeon, H., Nikolov, N., Keller, P., & Ratna, B. (2003). Nematic Elastomer Fiber Actuator. *Macromolecules*, *36*(22), 8499–8505. doi:10.1021/ma034921g

Nakamura, S., Magoshi, J., & Magoshi, Y. (1994). Thermal properties of silk proteins in silkworms. *Silk Polymers*, *544*, 211–221. doi:10.1021/bk-1994-0544.ch019

Niu, D., Jiang, W., Liu, H., Zhao, T., Lei, B., Li, Y., … Lu, B. (2016). Reversible Bending Behaviors of Photomechanical Soft Actuators Based on Graphene Nanocomposites. *Scientific Reports*, *6*(1), 27366. doi:10.1038/srep27366

Perry, H., Gopinath, A., Kaplan, D., Negro, L., & Omenetto, F. (2008). Nano- and Micropatterning of Optically Transparent, Mechanically Robust, Biocompatible Silk Fibroin Films. *Advanced Materials*, *20*(16), 3070–3072. doi:10.1002/adma.200800011

Qin, C., Feng, Y., Luo, W., Cao, C., Hu, W., & Feng, W. (2015). A supramolecular assembly of cross-linked azobenzene/polymers for a high-performance light-driven actuator. *Journal of Materials Chemistry A*, *3*(32), 16453–16460. doi:10.1039/C5TA01543J

Qiu, Y., & Park, K. (2012). Environment-sensitive hydrogels for drug delivery. *Advanced Drug Delivery Reviews*, *64*, 49–60.

Radjabian, Kish, & Mohammadi. (2012). Structure–property relationship for poly(lactic acid) (PLA) filaments: physical, thermomechanical and shape memory characterization. *Journal of Polymer Research*, *19*(6). doi:10.1007/s10965-012-9870-0

Ramuz, M., Tee, B., Tok, J., & Bao, Z. (2012). Transparent, Optical, Pressure-Sensitive Artificial Skin for Large-Area Stretchable Electronics. *Advanced Materials*, *24*(24), 3223–3227. doi:10.1002/adma.201200523

Raviv, D., Zhao, W., McKnelly, C., Papadopoulou, A., Kadambi, A., Shi, B., … Tibbits, S. (2014). Active Printed Materials for Complex Self-Evolving Deformations. *Scientific Reports*, *4*, 7422. doi:10.1038/srep07422

Rayna, T., & Striukova, L. (2016). From rapid prototyping to home fabrication: How 3D printing is changing business model innovation. *Technological Forecasting and Social Change*, *102*, 214–224. doi:10.1016/j.techfore.2015.07.023

Saphiannikova, M, & Toshchevikov, V. (2010). Photoinduced deformations in azobenzene polymer films. *Nonlinear Opt.* Retrieved from http://www.academia.edu/download/41677277/saphiannikova-toshchevikov-ilnytskyi_noqo.pdf

Spaggiari. (2013). Modelling, Simulation and Testing of Shape Memory Alloy Negator Springs As Long-Stroke Constant-Force Actuators.
Srivastava, V., Chester, S., Ames, N., & Anand, L. (2010). A thermo-mechanically-coupled large-deformation theory for amorphous polymers in a temperature range which spans their glass transition. *International Journal of Plasticity*, *26*. doi:10.1016/j.ijplas.2010.01.004

Stylios, G. K., & Wan, T. (2007). Shape memory training for smart fabrics. *Transactions of the Institute of Measurement and Control*, *29*(3-4), 321–336. Retrieved from http://journals.sagepub.com/doi/abs/10.1177/0142331207069479

Tabiryan, N., Serak, S., Dai, X.-M., & Bunning, T. (2005). Polymer film with optically controlled form and actuation. *Optics Express*, *13*(19), 7442. doi:10.1364/OPEX.13.007442

Takashima, Y., Hatanaka, S., Otsubo, M., Nakahata, M., Kakuta, T., Hashidzume, A., … Harada, A. (2012). Expansion-contraction of photoresponsive artificial muscle regulated by host-guest interactions. *Nature communications*, *3*, 1270. doi:10.1038/ncomms2280

Tee, B., Wang, C., Allen, R., & Bao, Z. (2012). An electrically and mechanically self-healing composite with pressure- and flexion-sensitive properties for electronic skin applications. *Nature Nanotechnology*, *7*(12), 825–832. doi:10.1038/nnano.2012.192

Tibbits, S. (2014). 4D Printing: Multi-Material Shape Change. *Architectural Design*, *84*. doi:10.1002/ad.1710

Tibbits, S., & Cheung, K. (2012). Programmable materials for architectural assembly and automation. *Assembly Automation*, *Volume 32*(Issue 3), 216–225. doi:10.1108/01445151211244348

Utela. (2008). Development and Application of New Material Systems for Three Dimensional Printing (3DP).

Van Oosten, C., Bastiaansen, C., & Broer, D. (2009). Printed artificial cilia from liquid-crystal network actuators modularly driven by light. *Nature Materials*. doi:10.1038/nmat2487

Wang, W., Ping, P., Chen, X., & Jing, X. (2006). Polylactide-based polyurethane and its shape-memory behavior. *European Polymer Journal*, *42*(6), 1240–1249. doi:10.1016/j.eurpolymj.2005.11.029

Ware, T., McConney, M., Wie, J., Tondiglia, V., & White, T. (2015). Voxelated liquid crystal elastomers. *Science*, *347*(6225), 982–984. doi:10.1126/science.1261019

Wen, H., Zhang, W., Weng, Y., & Hu, Z. (2014). Photomechanical bending of linear azobenzene polymer. *RSC Advances*, *4*(23), 11776–11781. doi:10.1039/C3RA48035F

White, T. (2012). Light to work transduction and shape memory in glassy, photoresponsive macromolecular systems: Trends and opportunities. *Journal of Polymer Science Part B: Polymer Physics*, *50*(13), 877880. doi:10.1002/polb.23079

White, T., & Broer, D. (2015). Programmable and adaptive mechanics with liquid crystal polymer networks and elastomers. *Nature Materials*, *14*(11), 1087–1098. doi:10.1038/nmat4433

White, T., Serak, S., Tabiryan, N., Vaia, R., & Bunning, T. (2008). Polarization-controlled, photodriven bending in monodomain liquid crystal elastomer cantilevers. *Journal of Materials Chemistry*, *19*(8), 1080–1085. doi:10.1039/B818457G

White, T., Tabiryan, N., Serak, S., Hrozhyk, U., Tondiglia, V., Koerner, H., … Bunning, T. (2008). A high frequency photodriven polymer oscillator. *Soft Matter*, *4*(9), 1796–1798. doi:10.1039/B805434G

Wu, & Schetky. (2000). Industrial applications for shape memory alloys.

Yamada, M., Kondo, M., Mamiya, J., Yu, Y., Kinoshita, M., Barrett, C., & Ikeda, T. (2008). Photomobile Polymer Materials: Towards Light-Driven Plastic Motors. *Angewandte Chemie*, *120*(27), 5064–5066. doi:10.1002/ange.200800760

Yamada, M., Kondo, M., Miyasato, R., Naka, Y., Mamiya, J., Kinoshita, M., … Ikeda, T. (2008). Photomobile polymer materials—various three-dimensional movements. *Journal of Materials Chemistry*, *19*(1), 60–62. doi:10.1039/B815289F

Yang, WG, Lu, H, Huang, WM, Qi, HJ, Wu, XL, & Sun, KY. (2014). Advanced shape memory technology to reshape product design, manufacturing and recycling. *Polymers*.

Yang, Huang, W. M., Li, & Li. (2006). Effects of moisture on the thermomechanical properties of a polyurethane shape memory polymer. *Polymer*, *47*(4), 1348–1356. doi:10.1016/j.polymer.2005.12.051

Yang, W., Lu, H., Huang, W., Qi, H., Wu, X., & Sun, K. (2014). Advanced Shape Memory Technology to Reshape Product Design, Manufacturing and Recycling. *Polymers*, *6*(8), 2287–2308. doi:10.3390/polym6082287

Yoshino, T., Kondo, M., Mamiya, J., Kinoshita, M., Yu, Y., & Ikeda, T. (2010). Three-dimensional photomobility of crosslinked azobenzene liquid-crystalline polymer fibers. *Advanced materials (Deerfield Beach, Fla.)*, *22*(12), 1361–3. doi:10.1002/adma.200902879

Yu, K., Ritchie, A., Mao, Y., Dunn, M., & Qi, J. (2015). Controlled Sequential Shape Changing Components by 3D Printing of Shape Memory Polymer Multimaterials. *Procedia IUTAM*, *12*, 193–203. doi:10.1016/j.piutam.2014.12.021

Yu, Y., & Ikeda, T. (2004). Alignment modulation of azobenzene-containing liquid crystal systems by photochemical reactions. *Journal of Photochemistry and Photobiology C: Photochemistry Reviews*, *5*(3), 247–265. doi:10.1016/j.jphotochemrev.2004.10.004

Yu, Y., & Ikeda, T. (2006). Soft Actuators Based on Liquid-Crystalline Elastomers. *Angewandte Chemie International Edition*, *45*(33), 5416–5418. doi:10.1002/anie.200601760

Yu, Y., Nakano, M., & Ikeda, T. (2003). Photomechanics: directed bending of a polymer film by light. *Nature*, *425*(6954), 145–145. doi:10.1038/425145a

Zarek, M., Layani, M., Cooperstein, I., Sachyani, E., Cohn, D., & Magdassi, S. (2016). 3D Printing of Shape Memory Polymers for Flexible Electronic Devices. *Advanced Materials*, *28*(22), 4449–4454. doi:10.1002/adma.201503132

Zeng, H., Wani, O., Wasylczyk, P., Kaczmarek, R., & Priimagi, A. (2017). Self-Regulating Iris Based on Light-Actuated Liquid Crystal Elastomer. *Advanced Materials*, *29*(30), 1701814. doi:10.1002/adma.201701814

Zeng, H., Wani, O., Wasylczyk, P., & Priimagi, A. (2017). Light-Driven, Caterpillar-Inspired Miniature Inching Robot. *Macromolecular Rapid Communications*, 1700224. doi:10.1002/marc.201700224

Zhang, Q., Yan, D., Zhang, K., & Hu, G. (2015). Pattern transformation of heat-shrinkable polymer by three-dimensional (3D) printing technique. *Scientific reports*, *5*, 8936. doi:10.1038/srep08936

Zhang, Q., Zhang, K., & Hu, G. (2016). Smart three-dimensional lightweight structure triggered from a thin composite sheet via 3D printing technique. *Scientific reports*, *6*, 22431. doi:10.1038/srep22431

Zhang, W., Chen, L., & Zhang, Y. (2009). Surprising shape-memory effect of polylactide resulted from toughening by polyamide elastomer. *Polymer*, *50*(5), 1311–1315. doi:10.1016/j.polymer.2009.01.032

Zhang, X., Yu, Z., Wang, C., Zarrouk, D., Seo, J.-W., Cheng, J., … Javey, A. (2014). Photoactuators and motors based on carbon nanotubes with selective chirality distributions. *Nature communications*, *5*, 2983. doi:10.1038/ncomms3983

Zhang, X., Zhou, Q., Liu, H., & Liu, H. (2014). UV light induced plasticization and light activated shape memory of spiropyran doped ethylene-vinyl acetate copolymers. *Soft Matter*, *10*(21), 3748–3754. doi:10.1039/C4SM00218K

Zhao, Q., Behl, M., & Lendlein, A. (2012). Shape-memory polymers with multiple transitions: complex actively moving polymers. *Soft Matter*, *9*(6), 1744–1755. doi:10.1039/c2sm27077c

Zhao, Q., Qi, H. J., & Xie, T. (2015). Recent progress in shape memory polymer: New behavior, enabling materials, and mechanistic understanding. *Progress in Polymer Science*, *49*(50), 79–120.

Vita

Steven K. Leist

Education

Ph.D., Mechanical Engineering, Design and Manufacturing, Drexel University, 2017

M.S.., Mechanical Engineering, Design and Manufacturing, Drexel University, 2013

B.S., Mechanical Engineering, Design and Manufacturing, Drexel University, 2010

Professional Experience

- **Research Assistant**, Dr. Jack Zhou, Drexel University, Design of a 4D Printing System that uses Thermosensitive and Light Reactive Smart Materials. 2013-2017
- **Research Assistant**, Dr. Jack Zhou, Drexel University, Design and Implementation of a Dual Chamber Shape Memory Alloy Actuating and Mixing System for a High Pressure Optical Cell. 2010-2013
- **Teaching Assistant**, Drexel University. 2011-2017
- **Co-op Internship**, STV Incorporated. 2009
- **Co-op Internship**, Allen-Sherman-Hoff Company. 2008
- **Co-op Internship**, Philadelphia Streets Department. 2007

Publications

Leist, S. K., Gao, D., Chiou, R., & Zhou, J. (2017). Investigating the shape memory properties of 4D printed polylactic acid (PLA) and the concept of 4D printing onto nylon fabrics for the creation of smart textiles. *Virtual and Physical Prototyping*, *12*(4), 290-300.

Bartolo, P., Chua, C. K., Zhou, J. G., & Leist, S. (2017). Editorial Part I: Editorial of VPP Volume 12 Issue 1; Part II: Guest Editorial on Special Issue of 4D Printing.

Leist, S. K., & Zhou, J. (2016). Current status of 4D printing technology and the potential of light-reactive smart materials as 4D printable materials. Virtual and Physical Prototyping, 1-14. doi:10.1080/17452759.2016.1198630

Leist, S. K., Kunkle, C., Chong, P. L., & Zhou, J. (2015). Dual chamber shape memory alloy unplugging and mixing system coupled to a high pressure optical cell for biophysical studies. Smart Mater. Struct. Smart Materials and Structures, 24(3), 035014. doi:10.1088/0964-1726/24/3/035014

Grants

Zhou, J.G., Ji, H. (2015). 4D printing with photoactive shape-changing polymer. Manufacturing Machines & Equip, National Science Foundation (NSF). Award Number: 1538318